

Seabed Pockmarks and Subsurface Fluid Migration at Multiple Scales

Investigations using Hydroacoustic and Seismic Data

A thesis
submitted in partial fulfilment
of the requirements for the degree of
Doctor of Philosophy
at the University of Otago, Dunedin, New Zealand,
by
Jasper Justus Lutz Hoffmann

27.08.2020

Abstract

Fluid migration from deep sedimentary basins towards Earth's surface has various implications for hydrocarbon accumulations and influences slope stability, climate and ecological systems. Fluids seeping from the seafloor can give insight into deep crustal and tectonic processes and can significantly change the seafloor morphology as well as the chemical composition of the overlying ocean.

The timing of fluid migration in many sedimentary basins is often poorly constrained and the composition of fluids involved in the formation of migration pathways and seafloor venting structures is difficult to determine. Likewise, the effect of upward migrating fluids on the surrounding host sediments and their diagenetic processes is an under-investigated field. Although gas bubbles venting from the seafloor are well constrained and easily identified in hydroacoustic data, the detection of submarine groundwater discharge sites often relies on oral traditions and visual reports from fishermen who recognize anomalies (schlieren/streaks) on the sea-surface. In many regions (e.g. organic muds, hydrothermal fields), submarine groundwater discharge is accompanied by gas venting. However, the processes involved in simultaneous gas and water discharge, as well as their relative contributions to geomorphological structures, are generally not well understood.

Decreasing acoustic resolution with depth requires a multi-scale approach to gain a better understanding of the various fluids and migration processes involved at different depths. Using different hydroacoustic systems and frequencies, I examine fluid migration pathways in the subsurface and various morphological expressions that seeping fluids create on the surface during discharge. I integrate well logs, surface sediment grab samples, as well as sediment cores and geochemical porewater analysis to validate and ground truth the hydroacoustic and seismic observations. I apply these methods to datasets from two study areas: the Canterbury Basin, east of New Zealand's South Island, and Eckernförde Bay in the Baltic Sea of Northern Germany.

In the Canterbury Basin, my analyses reveal a wide variety of subsurface migration pathways as well as surface structures related to fluid migration. I show how diagenetic processes of fine-grained sediments are dramatically changed in a 2 km

radial distance around a conduit feeding a sediment volcano. This change manifests itself in the suppression of polygonal faulting, and is a result of either 1) a significant change in differential stress induced by buoyant upward migrating fluids that accumulate at depth, or 2) permeable stringers intruding into the surroundings of the feeding pipe and therefore facilitating the dewatering of the enclosing sediments. On the surface of the Oligocene Marshall Paraconformity, I find pockmarks as well as discharged sediments emplaced by sediment volcanism. While the pockmarks appear to be related to dewatering mechanisms of the underlying strata, the sediments emplaced on the same surface seem to be sourced from Cretaceous strata. Several sediment intrusions into Paleocene sediments are similarly sourced from Cretaceous lithologies and affect the overlying fault orientation.

Also, I find that recent fluid migration pathways are likely to be responsible for shallow gas accumulations on the continental slope of the Canterbury Basin. On the present-day seafloor, there are numerous pockmarks on the shelf and slope that have been modified by currents. The pockmarks form as a result of gas and/or groundwater seepage, but the contribution of gas versus offshore groundwater could not be unequivocally determined for the Canterbury Basin.

In Eckernförde Bay, in contrast to the Canterbury Basin, I was able to hydroacoustically distinguish areas of submarine groundwater discharge and areas additionally affected by gas seepage. Using very high-resolution multibeam data and sub-bottom profiling, I observed and characterised a new type of pockmark that is associated with submarine groundwater and gas discharge. I determined that, in gaseous muddy sediments, submarine groundwater discharge results in unusually consistent and exceptionally shallow free gas that can even be detected with high-frequency 400 kHz multibeam systems.

Acknowledgements

First and foremost, I would like to thank my PhD supervisors Andrew Gorman and Gareth Crutchley for giving me the fantastic opportunity to come to Otago. I am very grateful for their sustained help and supportive advice, especially for Gareth sometimes during ungodly hours.

I'm especially grateful to Jens Schneider von Deimling whose continuous and invaluable advice, encouragement and most of all his positive attitude accompanied me throughout my early studies and made this dream possible. I also want to thank Sebastian Clar, Felix Gross and Phillip Held for the great rants, ideas and their friendship.

I gratefully acknowledge New Zealand Oil and Gas (NZOG), in particular Bernice Herd, for the provision of seismic data and their ongoing efforts, comments and contributions. I additionally thank Anadarko NZ Ltd, Origin Energy, and the National Institute of Water and Atmospheric Research (NIWA) for the provision of data used during this research.

This study was funded by New Zealand's Ministry of Business, Innovation and Employment (MBIE) as part of the GNS Science-led programme "Understanding petroleum source rocks, fluids, and plumbing systems in New Zealand basins: a critical basis for future oil and gas discoveries" (Contract C05X1507). Thanks also to the crew of the RV Polaris II for their help and support during data acquisition. Seismic and multibeam processing and analysis were undertaken through academic licences for GLOBE Claritas, CGG's HampsonRussell, IHS Markit's Kingdom, QPS Qimera and Fledermaus software.

I am thankful for onboard coring and sediment sampling assistance by Mats Ippach and the chemical analyses conducted by A. Bodenbinder, A. Bleyer, and B. Domeyer. Thanks also to Ercan Erkul and the crew of the R/V Littorina, R/V Alkor, and R/V Elisabeth Mann Borgese for their help and support during data acquisition.

I also thank the University of Otago for providing me with a PhD scholarship and the German Academic Exchange Service (DAAD) for their additional research grant. I also want to thank the University of Kiel and especially the Marine Hydroacoustics research group for hosting me during my stay in Germany.

The Department of Geology at the University of Otago has been a wonderful home and I want to thank the great staff, especially Hamish Bowman and Bill Dickson for their support in the field, Stephen Read for his mapping knowledge and Damian Walls for putting up with me.

I want to thank the J-Squad and Tom as well as the Fowlers and Tippers for the welcome distractions in the water and on the pitch. Thanks to the wonders of technology, my friends in Germany such as Felix, Enno, Volker, Kapi, Hinzer, Judith and Christoph never seemed far away and I'm grateful for their support. I also want to thank Hannah James for putting up- and being locked-down with me in the final stages of this work and distracting me in the mountains whenever necessary.

Finally, for their continuous support and invaluable advice I would like to thank my amazing family back home. This is for them.

Table of Contents

Chapter 1 Introduction	1
1.1 Motivation	1
1.2 Structure of the thesis.....	3
1.3 Thesis Aims.....	4
1.4 Structures associated with fluid migration.....	6
1.4.1 Pockmarks.....	6
1.4.2 Chimneys and pipes.....	9
1.4.3 Sediment volcanoes.....	11
1.4.4 Polygonal faults.....	12
Chapter 2 Study areas.....	15
2.1 Canterbury Basin.....	15
2.1.1 Stratigraphy.....	17
2.1.2 Marshall Paraconformity.....	21
2.1.3 Oceanography.....	22
2.1.4 Volcanic activity.....	24
2.1.5 Fluid flow in the Canterbury Basin.....	24
2.1.6 Data used.....	26
2.2 Eckernförde Bay.....	27
2.2.1 Evolution of the Baltic Sea.....	27
2.2.2 Sedimentary setting of Eckernförde Bay.....	29
2.2.3 Hydrogeology of the Eckernförde region.....	30
2.2.4 Fluid flow in Eckernförde Bay.....	31
2.2.5 Data used.....	33
Chapter 3 Fluid migration on the Canterbury Shelf and Slope.....	35
3.1 Introduction.....	35
3.2 Methods.....	37
3.2.1 Seismic data.....	39
3.2.2 Multibeam data.....	41
3.2.3 Sediment grab.....	42
3.3 Results.....	42
3.3.1 Bathymetry.....	42
3.3.2 Backscatter.....	45
3.3.3 Seismic data.....	48
3.3.4 Water column imaging.....	52
3.4 Discussion.....	52
3.4.1 Formation of Canterbury Shelf pockmarks.....	52
3.4.2 Modification and distribution of Canterbury Shelf pockmarks...57	
3.4.3 Activity and age of Canterbury Shelf pockmarks.....	60

3.5	Conclusions	62
-----	-------------------	----

Chapter 4 Seismic evidence for repeated vertical fluid flow through polygonally faulted strata in the Canterbury Basin, New Zealand ..63

4.1	Introduction.....	63
4.2	Data	66
4.2.1	Waka 3D seismic data	68
4.2.2	Endurance 3D seismic data.....	68
4.2.3	Boomer 2D seismic data	68
4.3	Methods.....	69
4.3.1	Velocity analysis.....	69
4.3.2	AVA analysis	70
4.3.3	Interpretation.....	73
4.4	Results.....	74
4.4.1	Polygonal faults	74
4.4.2	Surface of the Marshall Paraconformity	76
4.4.3	Mounded structures associated with radial faults	77
4.4.4	Seismic character of cylindrical faults.....	80
4.4.5	Shallow bright spots / chimneys	82
4.4.6	Velocity structure	84
4.4.7	Angle stacks	86
4.5	Discussion.....	88
4.5.1	Formation mechanisms of the cylindrical anomaly.....	88
4.5.2	Cylindrical and radial faults.....	89
4.5.3	Lack of polygonal faults within the cylindrical feature.....	91
4.5.4	Recent fluid migration	93
4.5.5	Timing of fluid migration.....	94
4.6	Conclusions	97

Chapter 5 Complex eyed pockmarks and submarine groundwater discharge revealed by acoustic data and sediment cores in Eckernförde Bay, SW Baltic Sea99

5.1	Introduction.....	99
5.2	Data	102
5.2.1	Multibeam echo sounder	102
5.2.2	Subbottom profiler.....	103
5.2.3	Sediment cores	103
5.2.4	EK60.....	104
5.2.5	CTD.....	105
5.3	Results.....	105
5.3.1	Bathymetry	105
5.3.2	Backscatter.....	110
5.3.3	Subbottom profiling.....	112
5.3.4	Sediment cores	115
5.3.5	CTD.....	118
5.4	Discussion.....	119

5.4.1	Characterisation of Eckernförde Bay pockmarks	119
5.4.2	Formation and modification processes of the intra-pockmarks.....	120
5.4.3	Enhanced backscatter signals of intra-pockmarks.....	121
5.4.4	Acoustic indicators for groundwater	124
5.5	Conclusions	128
Chapter 6 Conclusions.....		131
6.1	Main findings.....	131
6.2	Final concluding remarks.....	136
6.3	Recommendations for future work	136
6.3.1	Pockmark formation processes	136
6.3.2	Submarine groundwater discharge.....	138
6.3.3	Temporal variations of Eckernförde Bay pockmarks	138
References		139
Appendix.....		183
Appendix A: Cruise reports.....		183
Appendix B1: Publications		187
Appendix B2: Conference presentations		221

List of Figures

Figure 1.1: Example of complex pockmarks forming on the Chatham Rise.....	7
Figure 1.2: Example of the seismic manifestation of gas migration.	10
Figure 1.3: Various different surface morphologies of mud volcanoes.....	12
Figure 1.4: Time slice through a 3D seismic attribute volume	13
Figure 1.5: Diagram of relationship between pockmarks and polygonal faults .	14
Figure 2.1: Bathymetric overview map of New Zealand	16
Figure 2.2: Stratigraphic cross-section of the main groups and formations	19
Figure 2.3: Overview of the ice cover and coastline variance	20
Figure 2.4: Satellite sea-surface temperature data around New Zealand	23
Figure 2.5: Formation mechanism for the Canterbury Slope pockmarks	26
Figure 2.6: Overview of the Baltic Sea area with the glacial extent.	28
Figure 2.7: Overview of Eckernförde Bay	30
Figure 2.8: Seasonal temperature cycle	32
Figure 3.1: Overview of the Canterbury Basin pockmarks.....	36
Figure 3.2: Overview of the Canterbury Shelf seismic data	38
Figure 3.3: Overview of the datasets used in the study.	40
Figure 3.4: Pockmarks on the shelf and slope.	43
Figure 3.5: Pockmark distribution on the shelf	44
Figure 3.6: Multibeam backscatter data on top of the regional lithology	46
Figure 3.7: Bathymetric slope and multibeam backscatter data.....	47
Figure 3.8: Seismic section imaging Miocene volcanic cones.....	49
Figure 3.9: Seismic cross-section of the Canterbury Shelf	50
Figure 3.10: Seismic line on the Canterbury Shelf	51
Figure 3.11: Distribution of mud on the shelf.....	58
Figure 3.12: Comparison of pockmarks on the shelf and slope.....	60
Figure 4.1: Bathymetric overview map of the Otago margin.....	65
Figure 4.2: Composite seismic tie line to the Clipper-1 well.....	67
Figure 4.3: Possible AVA responses of a gas-charged sand with overlying shale	72
Figure 4.4: Overview of the three tiers of polygonal faults	75

Figure 4.5: Horizon slice of the similarity seismic attribute	76
Figure 4.6: Comparison of A) present-day submarine canyon system.....	77
Figure 4.7: Seismic cross-section through mounded structures.....	79
Figure 4.8: Map view and seismic cross-sections of the cylindrical feature	81
Figure 4.9: Layer thickness between horizons.....	82
Figure 4.10: AVA-Product (Intercept x Gradient)	83
Figure 4.11: Seismic velocity structure of the Canterbury Basin.....	85
Figure 4.12: Seismic velocities around the shallow bright spots.....	86
Figure 4.13: The near angle stack (5°-14°) and far angle stack (32°-41°).....	87
Figure 4.14: Comparison between present-day seafloor pockmarks.....	95
Figure 4.15: Schematic summary of mud and fluid migration in Canterbury	96
Figure 5.1: Overview bathymetric map of Eckernförde Bay.....	102
Figure 5.2: Bathymetric overview of the eastern Mittelgrund pockmark	106
Figure 5.3: Bathymetry of A) 2014, B) 2017, and C) 2019.	108
Figure 5.4: Bathymetrical changes over time	109
Figure 5.5: Backscatter image of the western Mittelgrund pockmark.....	110
Figure 5.6: Backscatter changes over time	111
Figure 5.7: Innomar subbottom profiler data across Mittelgrund pockmarks.	113
Figure 5.8: North-South profile through the pockmarks.....	114
Figure 5.9: Porewater methane, chloride and sulfate concentrations.	116
Figure 5.10: Voids in the sediment cores.....	117
Figure 5.11: EK60 single beam operated at 70 kHz	126
Figure 6.1: Backscatter patterns on the Canterbury Shelf.....	137

Chapter 1

Introduction

1.1 Motivation

Fluid venting/seeping from the seafloor is a widespread and common phenomenon in a wide variety of oceanographic settings, e.g. coastal environments, the continental shelf and slope and in the deep ocean. Fluid migration has important consequences for the seabed and sub-seabed geomorphology as well as for marine ecological systems, the ocean geochemistry and even the world's climate and is a critical factor in determining the movement of hydrocarbons within a sedimentary basin.

Fluids naturally migrating towards the Earth's surface have been known for thousands of years in various parts of the world. Onshore hydrocarbon seeps have been described and used for various purposes by different indigenous communities (Judd and Hovland, 2009). Since the nineteenth century, such seepage has attracted a lot of attention due to its indications of deeper hydrocarbon reservoirs. For example, Link (1952) reported that most petroleum reservoirs proven by 1952 were discovered by drilling near or on seeps. Consequently, the discovery of offshore submarine hydrothermal vents in the 1960s and seafloor morphological structures associated with fluid venting attracted much attention. In addition to commercial interests (the hydrocarbon industry), natural seepage has been investigated widely to gain insight into various science disciplines, including the influence of fluid seepage on slope stability, climate and seafloor ecology, and also

the insight seeping fluids provide into deeper crustal and tectonic processes (Elger et al., 2018; Kastner et al., 2014; Langmuir et al., 1997; Solomon et al., 2009; Werne et al., 2004). To understand present-day fluid accumulation and seepage, we must also consider past fluid distributions and migration pathways. By examining paleo-surfaces we can identify buried morphologies as well as structural indications for past fluid migration.

The impacts on our oceans of both hydrocarbon seepage and submarine groundwater discharge (SGD) are significant but often poorly understood. Kvenvolden and Cooper (2003) reported that between 0.2 and 2.0×10^6 (best estimate 0.6×10^6) tonnes of crude oil seep naturally into the marine environment every year. This accounted for 47% of all the crude oil entering the marine environment in 2009; humans are responsible for the rest (Judd and Hovland, 2009). SGD has been valued as a resource for agriculture, fishing, bathing, tourism as well as for fresh drinking water, for thousands of years (Moosdorf and Oehler, 2017). Although SGD potentially supplies as many nutrients into the oceans as rivers do (Cho et al., 2018), and therefore can contribute to algal blooms (Lapointe et al., 1990), SGD is still often overlooked as an important geological process. Escalating water demand in coastal areas and the effects on coastal environments have significantly increased scientific interest in SGD over the last decade. With increased groundwater extraction in coastal areas, sea-level rise and an increased frequency of storm surges (IPCC, 2014; Seager et al., 2007), coastal aquifers are becoming increasingly vulnerable to pollution and seawater intrusions (Ferguson and Gleeson, 2012; Pellikka et al., 2018; Wong et al., 2014). The advent of anthropogenic climate change and an expected increased frequency of global droughts (IPCC, 2014; Seager et al., 2007), has led to increased traction of research into offshore groundwater reserves as a possible source of drinking water and for agriculture. The global estimates of potential offshore groundwater reserves, between 3×10^5 (Cohen et al., 2010) and $4.5 \times 10^6 \text{ km}^3$ (Adkins et al., 2002), highlight the potential for offshore aquifers to become a future water resource (globally, only 4500 km^3 of water has been extracted from onshore reservoirs since 1900 (Konikow, 2011)). It is also important to understand the influence of offshore groundwater flow on seafloor morphology and ecology.

Identifying locations of seeping groundwater and other fluids, including hydrocarbons, is therefore a crucial part of future resource management. The recognition and understanding of different seafloor morphologies created by the seepage of different fluids are crucial for mapping out different fluid seepage types with confidence and over large areas.

1.2 Structure of the thesis

My thesis includes the contents of two peer-reviewed publications and another one in preparation, that I bring together by providing a general introduction into the research field and a final discussion of how the three chapters relate to each other with integrated concluding remarks. Although this thesis is written in the first person various other people contributed to the different chapters as indicated below each chapter.

Chapter 1 – *Introduction*

In this chapter, I provide a broad overview of the studies undertaken. I specify the aims of this thesis and introduce a number of geological structures and processes that will be built upon within the thesis.

Chapter 2 – *Study Areas*

I introduce two geologically different study areas and consider their respective geological contexts with regard to fluid migration processes. I also briefly describe the different scientific methods used in each study area which are in detail described at the beginning of each chapter.

Chapter 3 – *The shallow plumbing system and fluid migration on the Canterbury Shelf and Slope, New Zealand*

In this chapter, I present results of an investigation of shallow plumbing systems in the Canterbury Basin and discuss their implications for present-day seafloor pockmarks. The pockmarks are further analysed in terms of their distribution, their formation processes and their morphological modification by seafloor currents.

Contributors: Aaron Micallef, Tanita Averages, Joshu Mountjoy, Susi Woelz, Gareth Crutchley, Andrew Gorman, Rachel Worthington and Tayla Hill

Chapter 4 – *Seismic evidence for repeated vertical fluid flow through polygonally faulted strata in the Canterbury Basin, New Zealand*

I describe and examine deeper fluid migration pathways in the Canterbury Basin, interpreted from two 3D seismic datasets. Buried pockmarks, sediment volcanoes and polygonal fault systems are evaluated and discussed. Contents of this chapter are published in Hoffmann et al. (2019).

Contributors: Andrew Gorman, Gareth Crutchley and Bernice Herd

Chapter 5 – *Complex eyed pockmarks and submarine groundwater discharge revealed by acoustic data and sediment cores in Eckernförde Bay, SW Baltic Sea*

In this chapter, I discuss the different fluids involved in pockmark formation in Eckernförde Bay. I use a porewater geochemical approach to groundtruth hydroacoustic data for an integrated interpretation of the geological processes involved. Contents of this chapter are published in Hoffmann et al. (2020).

Contributors: Jens Schneider von Deimling, Jan Schröder, Mark Schmidt, Phillip Held, Gareth Crutchley, Jan Scholten and Andrew Gorman

Chapter 6 – *Conclusions and outlook*

The interpretations of the three individual studies are combined and the implications of the findings from Eckernförde Bay for the Canterbury Basin are discussed. I give an integrated conclusion of the different studies and discuss potential areas of future research.

1.3 Thesis Aims

Pockmark formation and modification processes are often poorly constrained and are strongly influenced by the subsurface geology and oceanographic conditions (Berndt, 2005; Hillman et al., 2018). I aim to improve the understanding of subsurface fluid flow and pockmark formation by characterising and comparing seismic and hydroacoustic manifestations of the processes across different geological settings, fluid migration systems, and fluid types.

The specific objectives of the thesis are to:

- constrain the timing of focused fluid migration as well as basin-wide fluid expulsion through polygonal faults, and determine their role in the formation of buried and present-day seafloor depressions in the Canterbury Basin
- constrain the fluids involved in pockmark formation in the Canterbury Basin
- evaluate how focused fluid migration affects diagenetic processes of the surrounding strata
- determine if there are relationships between sediment grain size distribution on the Canterbury Shelf and pockmark occurrence, and thereby investigate possible grain size range limits required for pockmark formation
- develop a conceptual integrated model for fluid migration in the Canterbury Basin
- define and characterise acoustic indications for submarine groundwater discharge (SGD)
- evaluate the effects of shallow gas on high-frequency multibeam backscatter data, to improve the understanding of how multibeam systems can be used to investigate seepage processes
- constrain the influence of SGD on pockmark formation and shallow gas distribution in the muddy sediments of Eckernförde Bay
- acoustically constrain the contribution of different fluid types in the formation of pockmarks

1.4 Structures associated with fluid migration

A wide variety of geological structures within the sub-seafloor and on the seafloor can be indicative of active and past fluid migration. These structures include pockmarks, pipes and chimneys, faults, sills, dikes or sediment volcanoes. The advances of hydroacoustic methods like side-scan sonar and multibeam echosounder systems have resulted in the detection of a large number of these structures on the seafloor associated with fluid venting (Bohrmann et al., 2003; Dimitrov and Woodside, 2003; Hovland, 1982; Nelson and Healy, 1984; Nikolovska et al., 2008). Lower frequency seismic imaging methods are frequently used to detect fluids and their associated migration pathways in the sub-seafloor (Berndt, 2005; Karstens and Berndt, 2015; Løseth et al., 2011).

Geomorphological structures associated with seepage from the seabed are affected by various factors, including the physical properties of the extruded material, the fluid flux, the seafloor material (e.g. composition, grain size, cohesion, sedimentation rate) and oceanographic conditions (Talukder, 2012).

1.4.1 Pockmarks

Pockmarks are circular to elongated seafloor depressions caused by venting fluids through the seafloor and are probably the most common seabed geomorphological expression of fluid escape (Judd and Hovland (2009), Figure 1.1). They are erosive in nature, with the eroding agent coming from beneath the seabed (Judd and Hovland, 2009). Although the exact mechanism of their formation is, in many places, poorly constrained, they are found in various geologic settings e.g. coastal environments, fjords, continental shelves and slopes, the deep sea, and even lakes all over the world (e.g. Bussmann et al., 2013; Dimitrov and Woodside, 2003; Kelley et al., 1994; Reusch et al., 2015; Webb et al., 2009; Whitticar and Werner, 1981). Fluid discharge can occur in a singular event, periodically or constantly, and pockmarks can form during both rapid discharges or slowly over time (Hovland et al., 2002; Hovland and Sommerville, 1985; Krämer et al., 2017). Although pockmarks are thought to initially form a circular morphology, many elongated and complex shapes have been reported (Brothers et al., 2011b, 2011a; Hillman et al., 2018; Pilcher and Argent, 2007; Schattner et al., 2016; Waghorn et al., 2017). While

some of these irregularly shaped pockmarks are thought to form as a coalescence of individual pockmarks, many such modifications from the original circular form are attributed to bottom currents reshaping the pockmark. Scouring of pockmarks due to currents after their initial formation has been postulated, as well as elongation or preservation due to seafloor current-pockmark interaction inducing rotational flows, upwelling within the pockmarks or eddy currents (Brothers et al., 2011b; Hammer et al., 2009; Hillman et al., 2018; Manley et al., 2004).

The most commonly described formation process in the literature is the suspension and removal of seabed material by fluids venting from the seafloor. In some cases though, pockmarks have been interpreted to result from the collapse of sub-seabed material as a result of gas hydrate dissociation (Imbert and Ho, 2012; Riboulot et al., 2016; Sultan et al., 2010; Taleb et al., 2020).

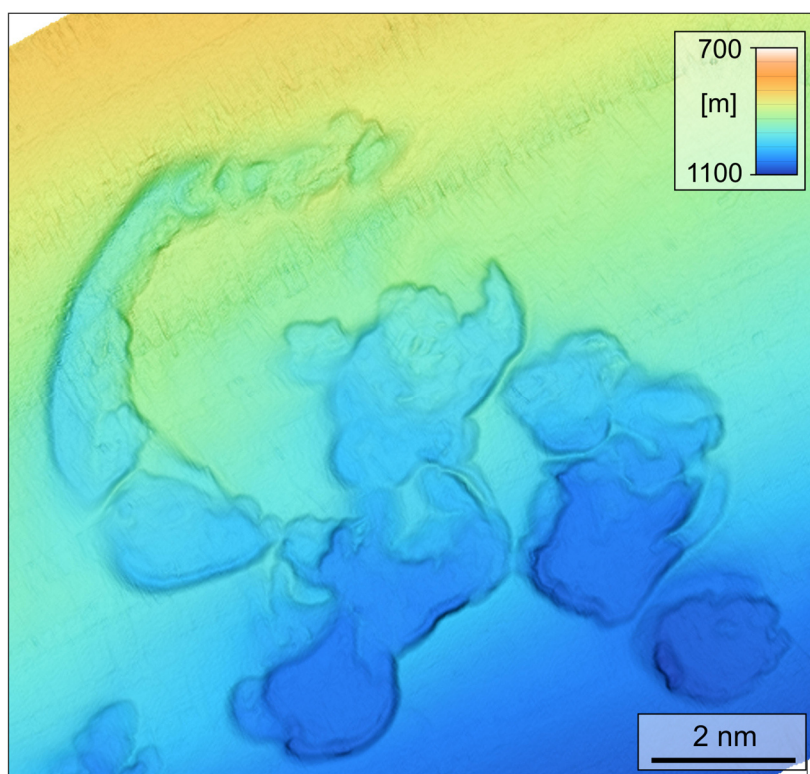


Figure 1.1: Example of complex pockmarks forming on the Chatham Rise (data sourced from Hoffmann (2013)).

Seafloor depressions also occur as a result of other processes, e.g. glacial processes like iceberg scouring and kettle holes (Hill et al., 2008; Solheim and Elverhøi, 1993; Stewart, 1999), calderas and volcanic intrusions (Branney, 1995; Wright and Gamble, 1999), impact craters (Ormö and Lindström, 2000; Roddy,

1977), current scours (Fildani et al., 2006; Heiniö and Davies, 2009), biological activity (Mueller, 2015), or dissolution of carbonates, limestones or evaporites by groundwater and subsequent collapse (Hardage et al., 1996; Jennings, 1971; Stewart, 1999). I do not consider these forms of seafloor depressions to be pockmarks though, due to their non-erosive nature or the lack of an eroding agent from the subsurface (following the definition from Judd and Hovland (2009)).

Pockmarks occur in various shapes and sizes. Hovland et al. (2002) classified pockmarks into six classes according to their morphological expression and acoustic reflectivity.

'Normal pockmarks' are circular in shape, between 10 and 700 m wide, and 1-45 m deep (King and MacLean, 1970; Loncke et al., 2004; Mazzini, 2009; Paull et al., 2008; Stott et al., 2019)

'Unit pockmarks' are smaller (1-10 m wide and up to 0.5 m deep) and often associated with one-time expulsion events (Hovland et al., 2010; Nelson et al., 1979; Szpak et al., 2015)

'Elongated pockmarks' show one longer axis and are often modified by strong bottom currents (Andresen et al., 2008; Hillman et al., 2018; Schattner et al., 2016)

'Strings of pockmarks' are aligned along one line due to faults or salt diapirism (Ho et al., 2018b; Maia et al., 2016; Michel et al., 2017)

'Complex pockmarks' occur as a combination, or cluster, of normal pockmarks or were otherwise modified (Hovland et al., 2005; Klauke et al., 2018; Mazzini et al., 2016)

'Eyed pockmarks' show a characteristic acoustically highly reflective object (e.g. shells or skeleton remains, authigenic carbonates which precipitated due to fluid expulsion, or coarse-grained seafloor material left behind after erosion by escaping fluids) at their bases (Böttner et al., 2019; Dandapath et al., 2010; García-García et al., 2004; Hovland and Judd, 1988; Hovland and Thomsen, 1989)

Others have classified pockmarks according to their seismic infill facies or the fluid origin (Albert et al., 1998; Andresen et al., 2008)

1.4.2 Chimneys and pipes

Fluid transportation through focused flow systems is a widespread phenomenon in sedimentary basins. Fluid migration pathways are frequently correlated to vertical or subvertical clustered amplitude anomalies in seismic data - so called chimneys or pipes (Figure 1.2) - which often form pockmarks at their upper termination (Berndt, 2005). According to Cartwright and Santamarina (2015), these fluid conduits form due to overpressured sequences and subsequent:

- hydraulic fracturing of the overburden rock (Andresen and Huuse, 2011; Cartwright et al., 2007; Hustoft et al., 2010; Karstens and Berndt, 2015; Løseth et al., 2011)
- capillary invasion when gas is forced into the pores of the capillary seal (Cathles et al., 2010; Cevatoglu et al., 2015; Clayton and Hay, 1994)
- erosive fluidization of granular material by seepage (Brown, 1990; Neramoen et al., 2010)
- syn-sedimentary sustained flows (Cartwright and Santamarina, 2015)
- dissolution and localized subsurface volume loss (Sun et al., 2013).

The terms chimney and pipe are often used interchangeably in the literature for the seismic expression of subsurface fluid conduits. I follow the convention of Andresen (2012) who defines a chimney as a wide or narrow vertical zone of distorted seismic reflections while defining a pipe as a narrow vertical zone of stacked high-amplitude anomalies.

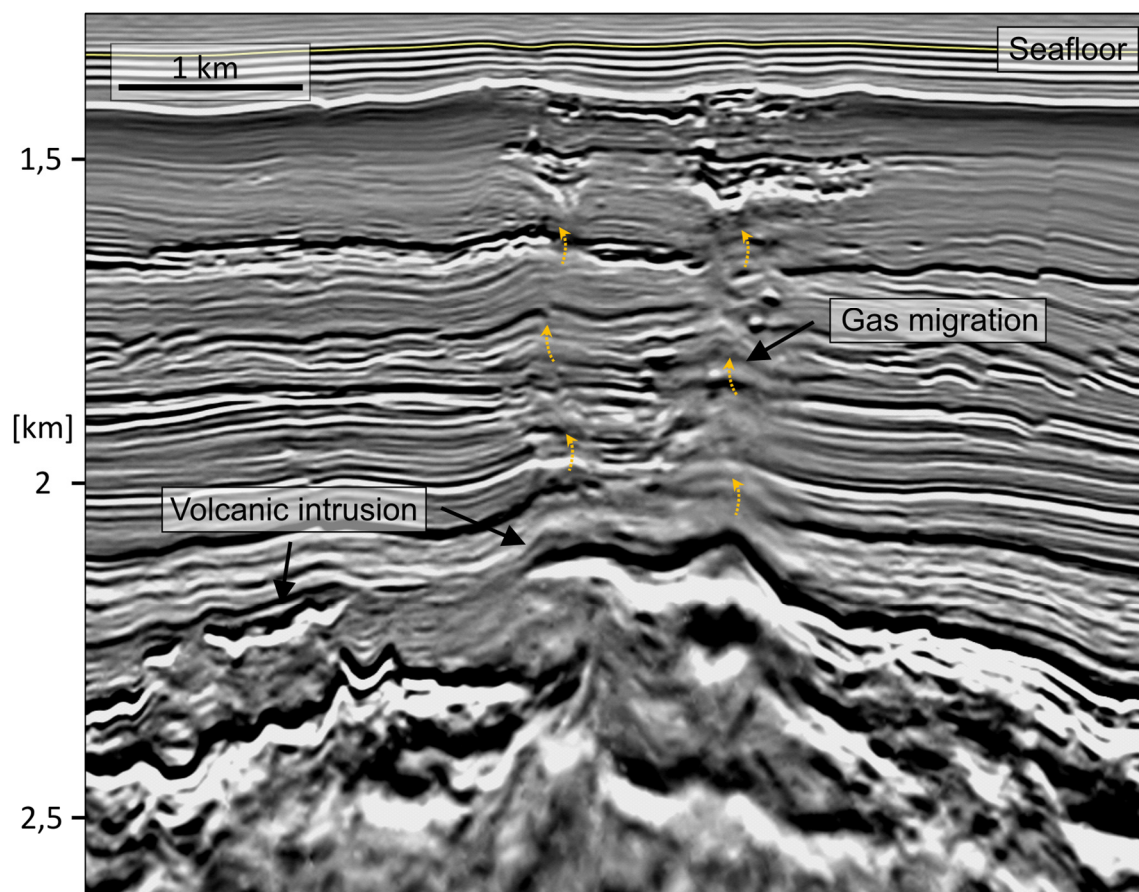


Figure 1.2: Example of the seismic manifestation of gas migration above a sill complex in the Norwegian North Sea (data sourced from Planke et al. (2017)).

Chimneys and pipes manifest themselves in seismic data by a variety of different amplitude anomalies. Distorted and strong chaotic reflections in chimneys are often attributed to the strong impedance contrasts between gas-bearing and water-saturated sediments. This effect may occur when there is as little as 1% of gas present (Judd and Hovland, 1992). It is common for reflections in gas-affected profiles to exhibit “push-down” effects, where reflections are deflected downwards by the decrease in acoustic velocity in gas-bearing zones (Ho et al., 2016; Hustoft et al., 2007; Plaza-Faverola et al., 2010). Ascending fluids that disturb or destroy otherwise parallel geological layers can result in locally “pulled-up” or “bent-up” seismic reflections. Alternatively, pulled-up reflections can be velocity artefacts due to anomalously high seismic velocities associated with, for example, gas hydrates or authigenic carbonate cement within the fluid-escape conduit (Ecker et al., 1998; Ho et al., 2012; Hustoft et al., 2010, 2007). Additionally, gas hydrate in pore spaces may reduce impedance contrasts between geologic layers causing acoustic blanking (Fraser et al., 2016; Lee et al., 1996; Lee and Collett, 2001; Westbrook et al., 2008).

Acoustic turbidity zones in seismic data are often caused by the reflection of a high proportion of the acoustic energy by gas-charged sediments or by some other overlying highly-reflective material (Judd and Hovland, 1992).

1.4.3 Sediment volcanoes

Sediment volcanoes represent a specific surface expression of natural oil and gas migration. Sediment volcanoes are often categorised in terms of the grain size of the material they eject on the surface (e.g. sand or mud volcanoes). Due to the same driving process behind both sand and mud volcanoes, I herein refer to them as sediment volcanoes.

In hydrocarbon-bearing sedimentary basins, sediment volcanoes form as the result of overpressure build-up and subsequent hydrofracturing (Mazzini, 2009). In contrast to most fluid escape structures, sediment volcanoes represent the surface expression of a discharge of at least a three-phase system (gas, water, sediment and occasionally oil) (Mazzini and Etiope, 2017). The high pore-fluid pressure required predominantly results from disequilibrium compaction (often referred to as undercompaction), kerogen maturation and gas formation, mineral dehydration and tectonic compressional forces (Kopf, 2002). The high gas and water content make the sediment semi-liquid, allowing it to flow upwards through long openings and fissures in the Earth's crust (Dimitrov, 2002). In most cases the gas is methane although in some cases (e.g. close to subducting slabs, in areas of high thermal gradients or in the final stages of gas generation) gas can be mainly CO₂ or N₂ (Baciu et al., 2007; Etiope et al., 2011; Motyka et al., 1989). In active sediment volcanoes, episodic, often catastrophic, eruptions alternate with dormant phases – the time where overpressure is generated at depth before it overcomes the seal strength in the conduit (Planke et al., 2003). The fluids, sediments and the overpressure necessary to form sediment volcanoes can be sourced from different stratigraphic levels along the feeder pipe.

Although many sediment volcanoes exhibit the characteristic volcanic cone shape, the extruded sediments on the surface can build up a wide variety of different shapes of various sizes (Figure 1.3). The edifices range from widths of a couple metres to up to 12 km. Sediment volcanoes occur on land (e.g. Mazzini and Etiope,

2017; Odonne et al., 2020; Planke et al., 2003) as well as on the seafloor (e.g. Bohrmann et al., 2003, 2002; Dupuis et al., 2019; López-Rodríguez et al., 2019; Medialdea et al., 2009), although the majority of studies focus on the comparatively well accessible onshore examples. They mainly form in areas of recent tectonic activity (especially compressional), strong sedimentary or tectonic loading and active or continuous hydrocarbon generating basins (Dimitrov, 2002). In New Zealand sediment volcanism mainly occurs in the northeast of New Zealand's North Island along the Hikurangi margin (Pettinga, 2003; Ridd, 1970).

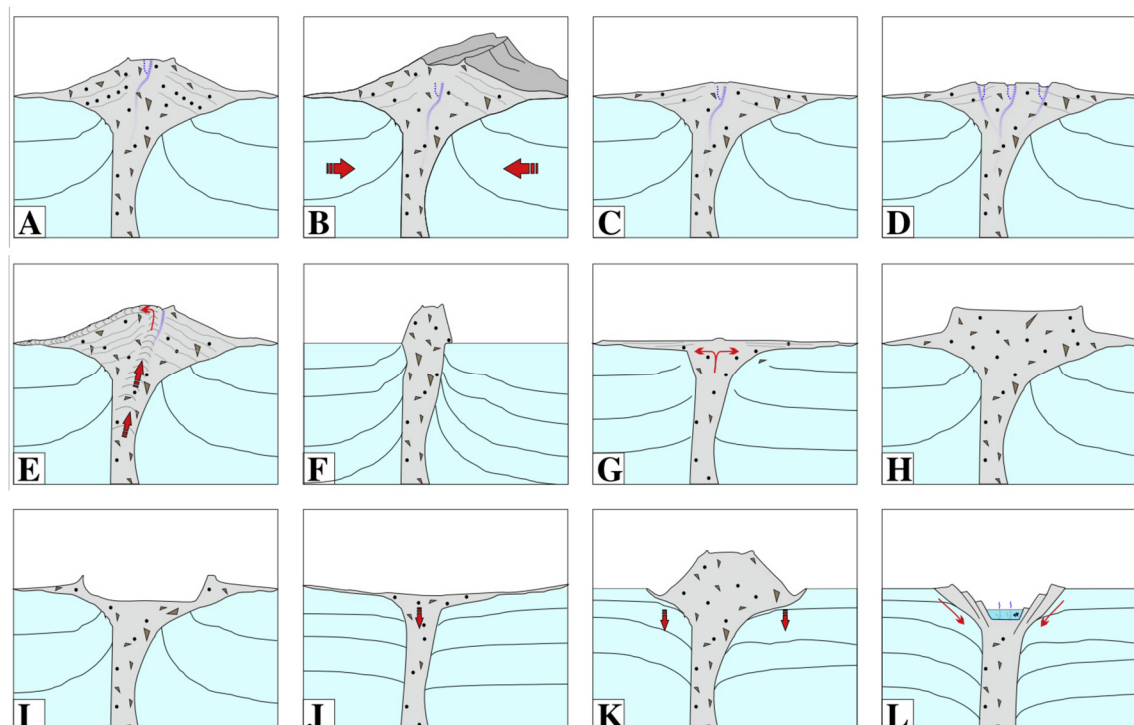


Figure 1.3: Various different surface morphologies of mud volcanoes (A) conical, (B) elongated, (C) pie-shaped, (D) multicrater, (E) growing diapir-like, (F) stiff-neck, (G) swamp-like, (H) plateau-like, (I) impact crater-like, (J) subsiding structure, (K) subsiding flanks, (L) sink-hole type (adopted from Mazzini and Etiope (2017)).

1.4.4 Polygonal faults

Polygonal faults are a layer bound, non-tectonic class of faults which don't exhibit any preferred large-scale strike direction (Figure 1.4). Polygonal faults, in general, form during the early burial history of their host sediments (Berndt et al., 2012; Cartwright et al., 2007, 2003; Cartwright and Lonergan, 1996; Gay et al., 2004). Pockmark formation above and within polygonal fault systems due to porewater expulsion and sediment compaction would therefore be expected to be

contemporaneous with the faulting (Andresen and Huuse, 2011; Gay et al., 2004; Maia et al., 2016). In some cases, pipes or chimneys form above polygonal fault systems, channelling the fluids and episodically releasing the fluids to form pockmarks above (Berndt et al., 2003; Gay and Berndt, 2007).

Polygonal faults only form in fine-grained sediments and display a polygonal pattern in plan view. After the landmark paper of Cartwright (1994), who was the first to describe the polygonal pattern of these faults in the North Sea basins, this type of faulting has been recognised in basins worldwide (Laurent et al., 2012). The polygonal planform can be modified by a local or regional horizontal stress anisotropy (Ho et al., 2013; Li et al., 2020; Morgan et al., 2015).

Cartwright & Dewhurst (1998) attributed the development of these regionally extensive faulted tiers to sediment compaction and dewatering processes during early burial history. Since polygonal faults have only been reported in packages composed of fine to very fine-grained sediments, Cartwright & Dewhurst (1998) and Dewhurst et al. (1999) introduced the process of syneresis as the formation mechanism. This poorly understood but widely appreciated process (especially in other disciplines, e.g. chemical engineering) describes a spontaneous contraction of a gel without evaporation (Cartwright et al., 2003). Well

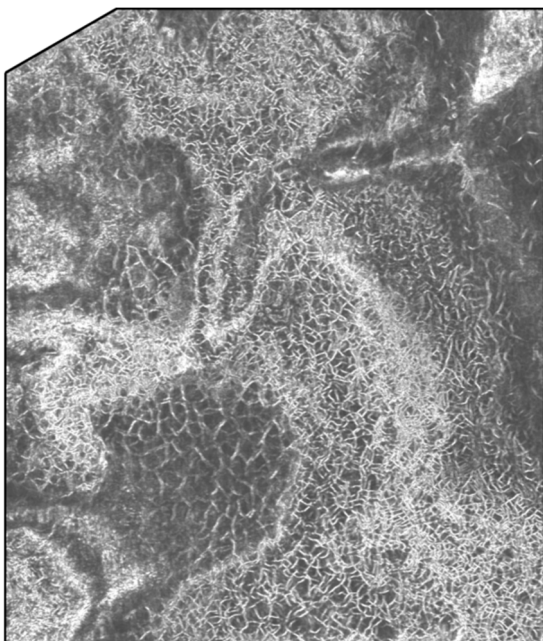


Figure 1.4: Time slice through a 3D seismic attribute volume highlighting discontinuities/polygonal faults in white. Data from the Canterbury Basin.

analysis conducted by Dewhurst et al. (1999) showed that the amount of shrinkage in colloidal sediments increases as the grain size decreases. Due to contraction, the syneresis cannot proceed without pore fluids being expelled from the sediments. The polygonal faults are therefore thought to form because they are required to act as fluid migration pathways for fluids expelled in localized regions of syneresis. Other formation mechanisms like density inversion and associated hydrofracturing (Henriet et al., 1991; Watterson et al.,

1.4 Structures associated with fluid migration

2000), gravitational downslope movement (Clausen et al., 1999), smectite-rich clays causing residual friction at low burial depth (Gouly, 2008, 2001a) and particle scale volume contraction by mineral dissolution leading to internally-driven shear failure (Cartwright, 2011; Shin et al., 2008) have since been suggested.

All of these mechanisms involve dewatering processes during burial. A 3D modelling approach by (Verschuren, 1992) suggests that the volume of expelled fluids might be as much as 60%, making polygonal fault systems a major source of fluids in sedimentary basins. Since fault throw accumulates mainly due to dewatering of the sediment, displacement rates of polygonal faults are as much as three magnitudes lower than tectonic faults (King and Cartwright, 2020). Pipe structures in the overburden of polygonal fault systems show that polygonal fault systems can act as a long term source for fluid flow (Berndt et al., 2003) as well as pathways for upward fluid migration from deeper strata (Gay et al., 2004) (Figure 1.5).

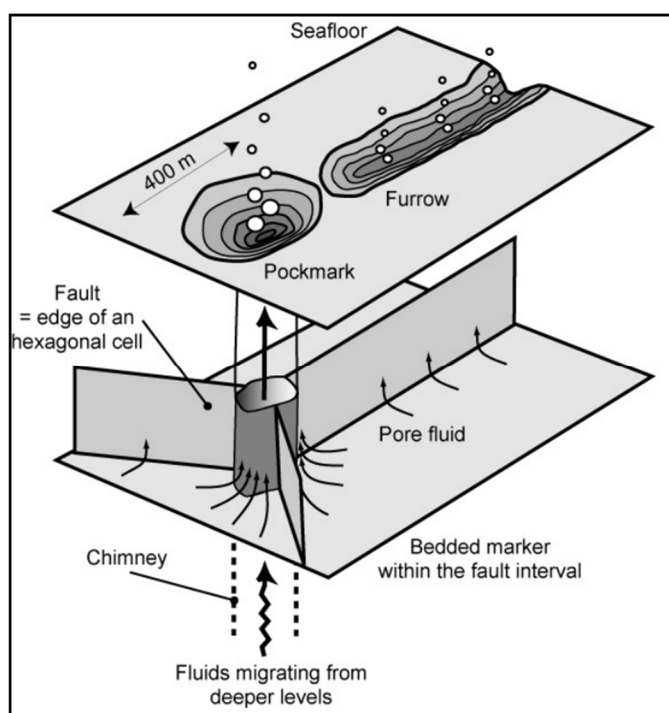


Figure 1.5: Schematic diagram illustrating the relationship of pockmarks to polygonal faults and fluid migration (adopted from Gay et al. (2004)).

Chapter 2

Study areas

Two geologically distinct study areas are considered in this thesis. By using similar techniques in the Baltic Sea and on the Canterbury Shelf, I aim to be able to compare freshwater and/or gas reservoirs and recharge characteristics. By comparing the pockmark formation mechanisms of the Baltic Sea to formation mechanisms on continental shelves, I aim to improve the understanding of the underlying controls.

2.1 Canterbury Basin

The Canterbury Basin is located on the eastern passive continental margin of New Zealand's South Island and covers an area of ~360,000 km². It is bounded to the north by the Chatham Rise and in the south by the Great South Basin (Figure 2.1). Most of the basin (that I will focus on) is presently submerged, but an eroded succession is exposed onshore. The present-day passive continental margin off the Canterbury/Otago coast is characterised by a variable shelf width of 10-90 km. The shelf exhibits low slope gradients of 0.0016° and extends out into water depths ~140 m. The margin slope in this region is incised by numerous canyons and gullies, which are larger and more significant features to the southeast than they are to the northwest of the Waitaki Canyon. Northwest of the Waitaki Canyon the slope is gradually less incised by gullies, which, in this area, show a straighter and narrower shape. The gradient of

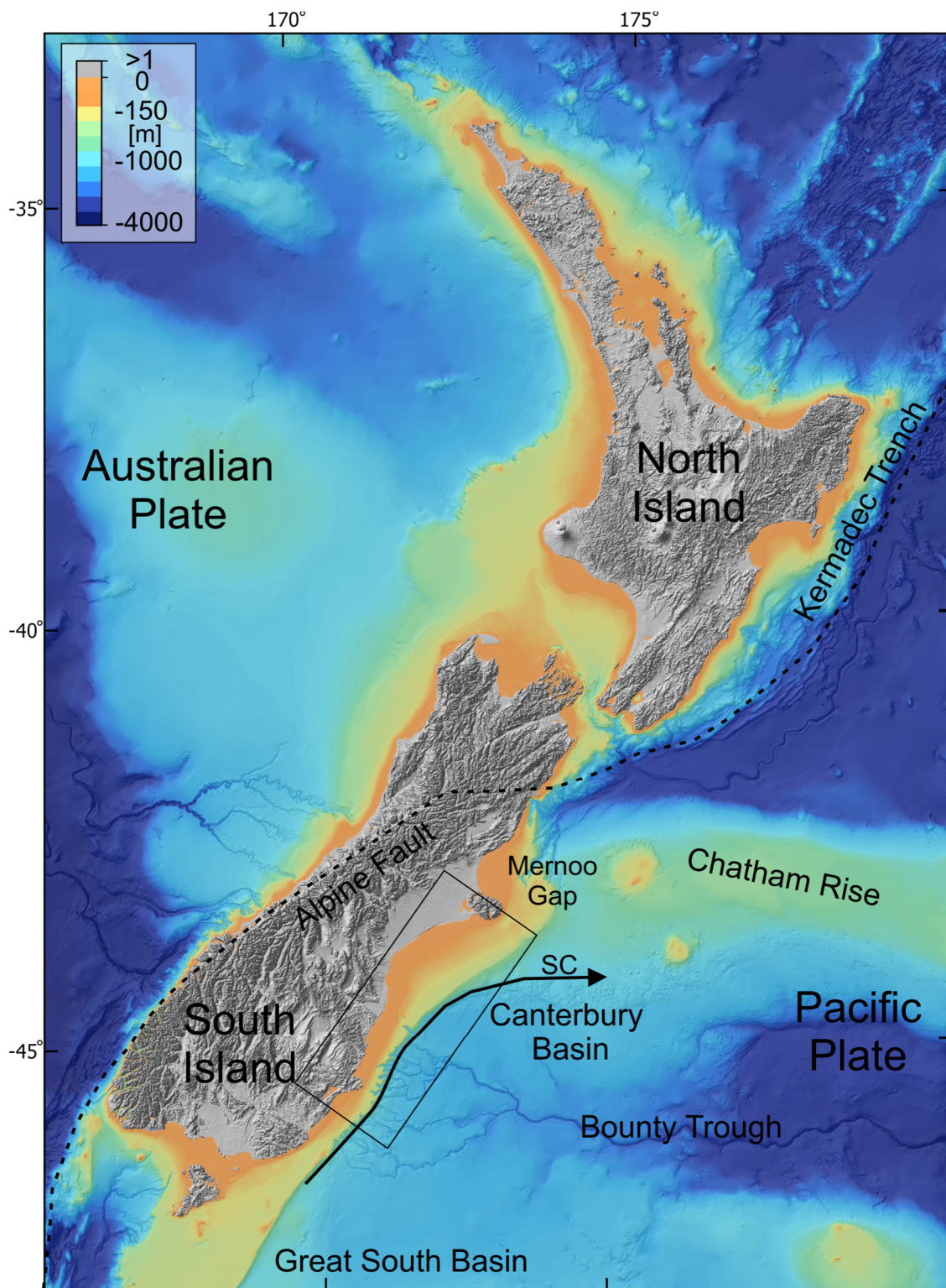


Figure 2.1: Bathymetric overview map of New Zealand (bathymetric data sourced from Mitchell et al. (2012)). The study area is outlined by the black rectangle.

the slope decreases from $>5^\circ$ in the south to $<2^\circ$ in the north of the basin towards the Mernoo Gap.

The margin began to rift from Antarctica at about 105 Ma during Gondwanaland breakup (Strogen et al., 2017) and is now located ~ 200 km to the east of the Alpine Fault (the plate boundary between the Australian and Pacific plates). It has experienced one large-scale tectonically controlled transgressive-regressive cycle during the Cretaceous to Recent, with a peak transgression during the Oligocene (Fulthorpe and Carter, 1989). The tectonically forced sea-level cycle has been overprinted by shorter-term eustatic sea-level changes. The region has been relatively stable tectonically since rifting, with faulting only occurring close to shore, mainly associated with local igneous intrusions of late Eocene-Oligocene and Miocene ages (Coombs et al., 1986; Milne, 1975). Generally, volcanism in the basin is of variable age (Cretaceous – Pliocene).

The dextral strike-slip motion of the Alpine Fault shear zone has led to a displacement of 440-470 km since earliest Miocene (23 Ma) (Kamp, 1987; King, 2000; Sutherland, 1999). The last ~ 10 Ma correspond to a phase of oblique compression leading to the uplift of the Southern Alps by about 11 km (Browne and Field, 1988; Browne and Naish, 2003; Carter and Norris, 1976). This uplift has been matched by average erosion rates of ~ 2 m/ky, supplying a significant amount of sediment into the subsiding (0.2-0.5 m/ky) Canterbury Basin (Browne and Naish, 2003; Kamp and Tippett, 1993).

2.1.1 Stratigraphy

The large-scale transgressive-regressive cycle in the Canterbury Basin has resulted in the deposition of three main stratigraphic units: the transgressive sequences of the Onekakara Group, a sea-level highstand unit (Kekenodon Group) and a regressive unit (Otakou Group) (Carter, 1988) (Figure 2.2). Post-rift thermal subsidence after the breakup of eastern Gondwana resulted in the initiation of the transgressional phase in the Late Cretaceous that continued until the mid-late Oligocene when flooding of the land mass was at a maximum (Carter, 1985). This mainly terrigenous, transgressive Onekakara Group (late Cretaceous-Oligocene) (Carter, 1985; Fulthorpe et al., 2010) is characterised in seismic

reflection data by mainly continuous horizontal reflections of moderate amplitude. Overlying Paleocene and Eocene sediments are well stratified and show at least three intense tiers of polygonal faults that developed in clay-rich mudstone (Sahoo et al., 2014). At the end of this transgressive phase, reduced terrigenous influx resulted in the deposition of the Amuri Limestone (Fulthorpe et al., 2010).

The regional Marshall Paraconformity separates the Onekakara Group from the blanket-like glauconitic and bioclastic sediments of the Concord Formation, a basal facies of the pelagic to hemipelagic bioclastic Weka Pass Limestone Formation which together build the Kekenodon Group (Late Oligocene-Miocene) (Fulthorpe and Carter, 1989). The Kekenodon Group is characterised by strong and discontinuous reflections in regions proximal to the emerging landmass to the west, whereas distal reflections are characterised by sub-parallel, horizontal and more consistent amplitudes. Increased sediment supply due to initiation of movement on the plate-bounding Alpine Fault and corresponding uplift of the Southern Alps induced a phase of regression in the region from late Oligocene to early Miocene (Carter and Norris, 1976; Fulthorpe and Carter, 1989). During this phase of regression, the prograding clinoforms of the Otakou Group (Miocene-Recent) were deposited. The Otakou Group mainly consists of fine quartzose sand and terrigenous siltstone that built the modern continental shelf (Carter et al., 1990). The clinoforms consist of onlapping and toplapping events indicating erosional and prograding stages (Lu et al., 2003; Marsaglia and Nolasco, 2016).

Clinofoms are intersected by various sediment drift bodies which together build up the Otakou Group (Carter et al., 2004a). These drifts have formed by a northward flowing current analogous to the present-day Southland Current (Lu et al., 2003).

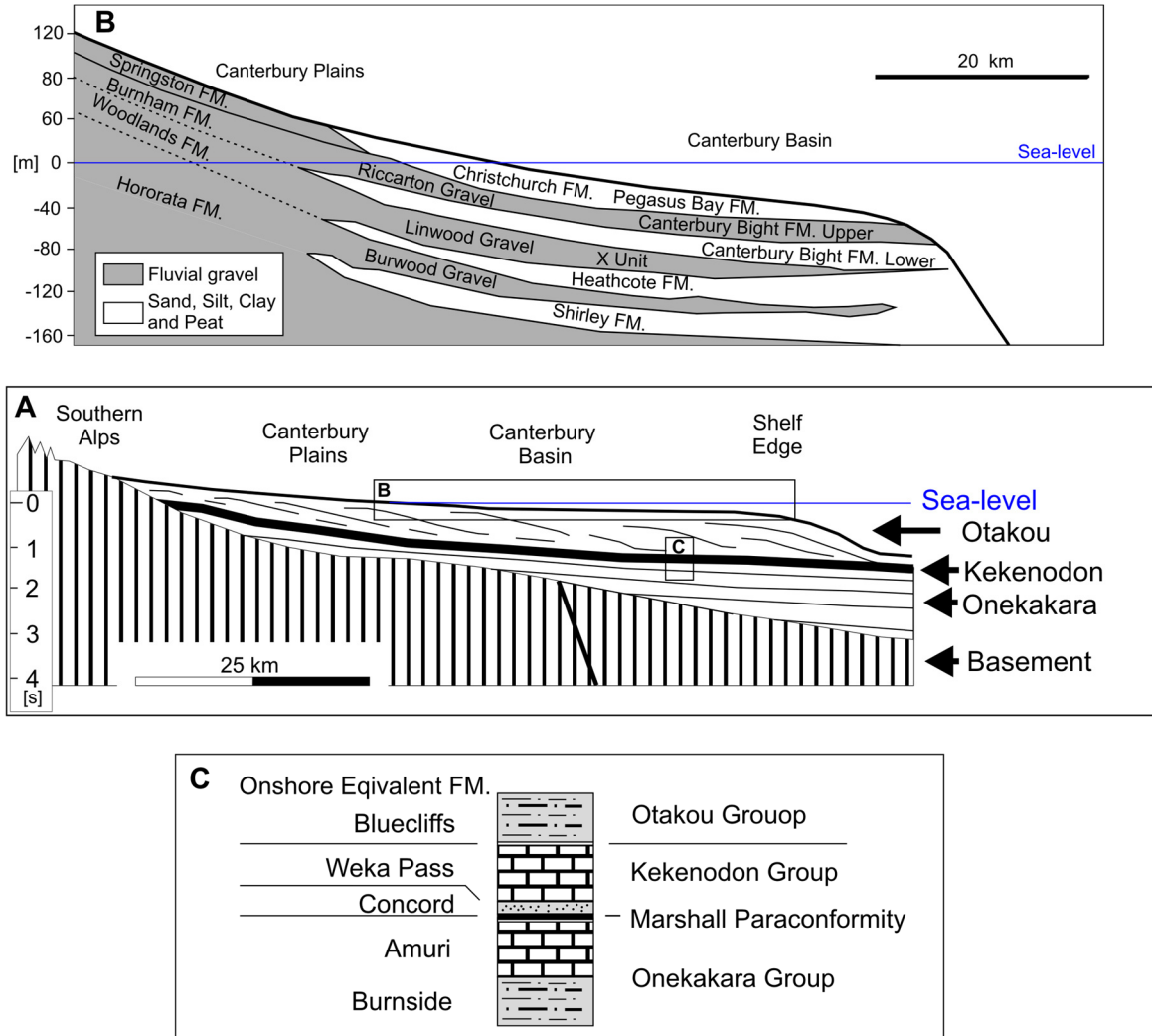


Figure 2.2: Stratigraphic cross-section of the main groups and formations in the Canterbury Basin. A) Schematic profile from the Southern Alps to the continental rise showing the three main geologic groups of the basin (modified from Fulthorpe and Carter (1989)). B) Schematic cross-section of the shallow fluvial gravels and sandy and silty units (modified from Browne and Naish (2003)). C) Onshore formations corresponding to the offshore groups after Fulthorpe et al. (1996).

2.1 Canterbury Basin

The present-day seafloor and shelf are strongly influenced by eustatic sea-level changes. Large coarse-grained braided rivers have shed significant amounts of sediment from the Southern Alps into the Canterbury Basin. During sea-level low stands, these braided rivers extended out onto the present-day shelf and lead to widespread aggradation of braided plains during glacial maxima. These are accompanied here by enhanced sediment supply due to glacial erosional processes and subsequently lead to a stratigraphy of alternating low stand fluvial gravels and sands and high stand sands, silts, and clays (Figure 2.2 and Figure 2.3). The present-day seafloor consists of the Pegasus Bay and Canterbury Bight formations (discussed in detail by Herzer (1981)), which show gravelly deposits in the north of the basin close to shore whereas sands and muds dominate the greater part of the outer shelf (Bostock et al., 2019a).

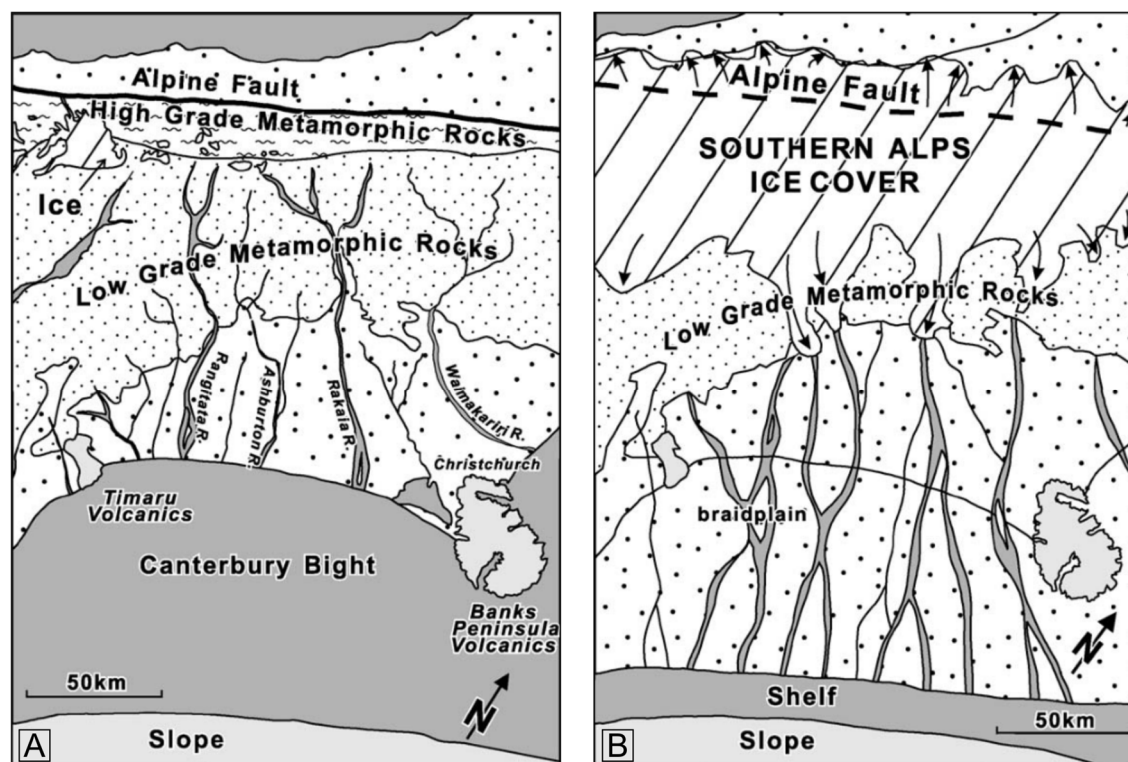


Figure 2.3: Overview of the ice cover and coastline variance during A) interglacial and B) glacial periods (adopted from *Browne and Naish (2003)*)

2.1.2 Marshall Paraconformity

Oligocene strata in the Canterbury Basin contain several discontinuities that have been referred to collectively as the Marshall Paraconformity (Carter and Landis, 1982, 1972; Findlay, 1980; Lever, 2007; Piekarski, 2020). The Marshall Paraconformity is a regional unconformity in the Canterbury Basin separating the transgressive Onekakara Group from the glauconitic Kekenodon Group. The unconformity is considered to be coeval with the initiation of thermohaline circulation following the separation of Australia and Antarctica ~33.7 Ma (Carter, 1985; Fulthorpe et al., 2010). It caps the widespread Amuri Limestone and is overlain by greensand and calcarenite limestone (Field et al., 1989).

Lewis and Belliss (1984) noted that the term paraconformity is misleading; the surface of the unconformity is observed in seismic data to be not only conspicuous and complex, but also angular, and therefore does not fit the definition of a paraconformity as introduced by Dunbar and Rodgers (1957) for a biostratigraphic discontinuity (a discontinuity based and evaluated solely on paleontological evidence). There is some disagreement concerning the definition of the Marshall Paraconformity and uncertainties have been discussed in previous papers (e.g. Carter and Landis, 1982, 1972; Findlay, 1980; Fulthorpe et al., 1996; Lever, 2007; Lewis, 1992). However, I still refer to this surface as the Marshall Paraconformity to conform with historical usage.

Though broadly of middle Oligocene age, the paraconformity in the Canterbury Basin is developed at the base of a sequence of terrigenoclastic greensands (Concord Greensand) and calcarenite (Weka Pass Limestone) that are difficult to date precisely (Carter and Landis, 1972). Strontium isotopes suggest a minimum hiatus extending from 32.4–29 Ma (Fulthorpe et al., 1996). The greensands and limestones are often highly bioturbated. With the breakup of Australia and Antarctica, strong bottom currents originated that reworked the greensands on top of the Marshall Paraconformity (Lewis and Belliss, 1984). This resulted in extensively cross-bedded Weka Pass Limestone and Concord Greensand facies and in the mixing of benthic and planktic bioclastic detritus (Carter and Landis, 1982).

2.1.3 Oceanography

The South Island of New Zealand lies between two major water masses, the warm and saline Subtropical Waters (STW) to the north and the cold Subantarctic Waters (SAW) to the south. The Subtropical Front (STF) (where STW and SAW meet) is deflected south around New Zealand's South Island. This allows warmer STW from the Tasman Sea to be channelled around the South Island, ending up on the eastern side of New Zealand's South Island, off Otago and Canterbury (Figure 2.4).

The northwestward flowing Southland Current (SC), which is thought to consist mainly of SAW, runs parallel to the STF (which in this region is also referred to as the Southland Front (SF)) (Sutton, 2003). The shelf-parallel current has mean flow rates of around 28 cm/s and bursts to 80 cm/s are known (Carter and Carter, 1985; Chiswell, 1996; Heath, 1972). The core of the present-day Southland Current lies above the 200-300 m isobaths (Carter et al., 2004b). Seaward of the STF, SAW move northward and circulate clockwise above the Bounty Trough. The present-day bathymetrical locking of the SC and associated STF on the Canterbury Slope and the Chatham Rise seems to have remained relatively stable in its position during the last glacial-interglacial periods, although a seaward migration during early glacial periods was observed (Carter et al., 2004b). The SC is presumed to affect the margin to a depth of ~800 m, with the strongest thermal gradients occurring in ~500 m (Chiswell, 1996; Sutton, 2003). The presence of large sediment drifts in the Otakou Group suggests that deeper currents parallel to the northward-flowing Southland Current existed and probably strengthened during glacial periods (Carter et al., 2004a).

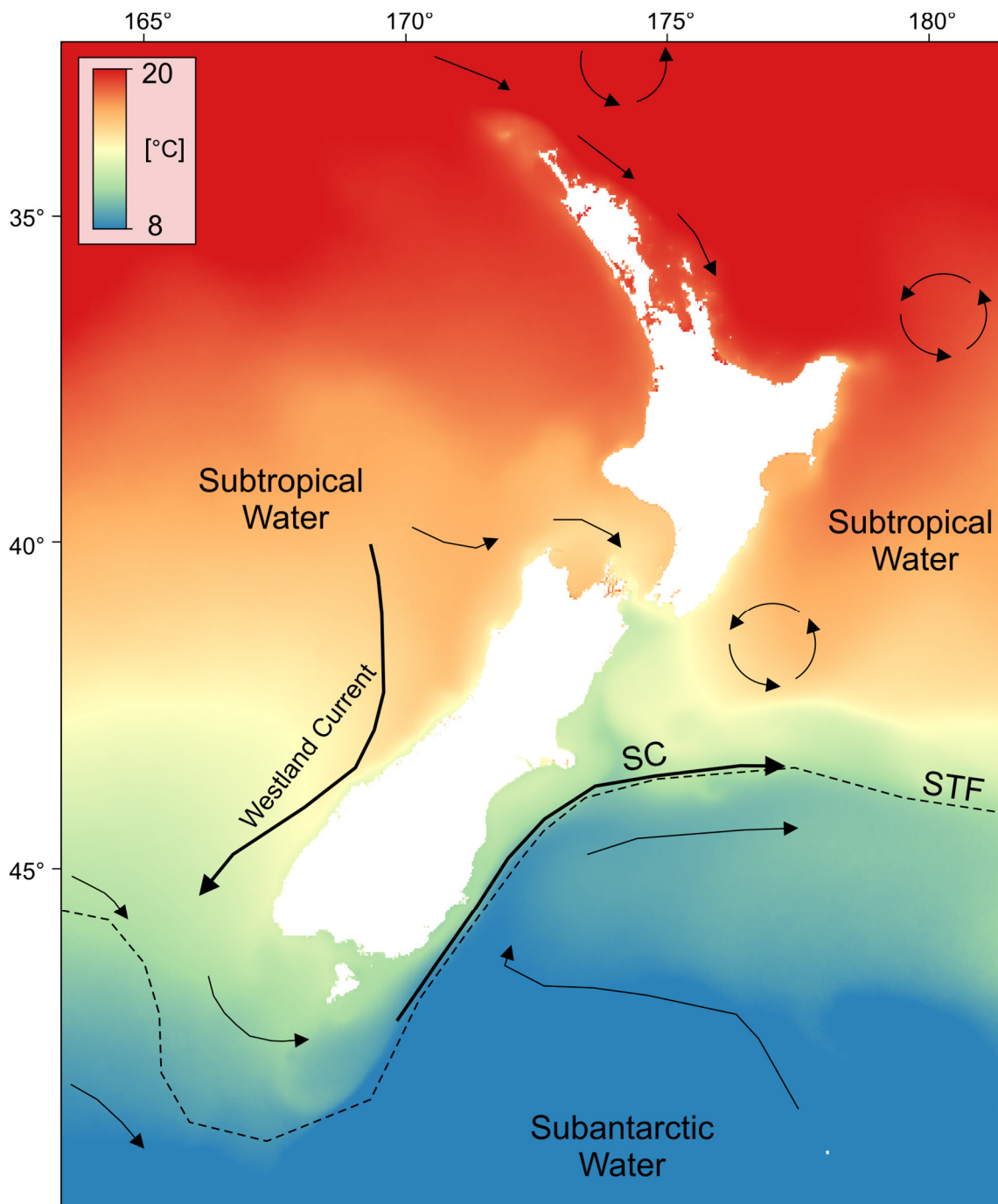


Figure 2.4: Satellite sea-surface temperature data around New Zealand averaged between 1993 and 2012, with the main oceanographic fronts and surface currents according to Carter et al. (2004b). Strong temperature gradients are apparent over the Southland Current (SC) and the Subtropical Front (STF) (sea-surface temperature data from NIWA (2015)).

2.1.4 Volcanic activity

Although the Canterbury Margin is considered to be a magma poor or magma starved rifted margin, distributed volcanoes of various shapes and size are apparent (Barrier, 2019; Bischoff et al., 2019a). The two most prominent volcanic centres in the region are the shield volcanoes of Banks and Otago peninsulas in the north and south of the Canterbury Basin (Figure 3.1). These two Miocene volcanic centres are about 12- 5.8 Ma and 16-11 Ma old, respectively (Adams, 1981; Coombs et al., 2008, 1986; Hoernle et al., 2006; Scott et al., 2020; Sewell, 1988). The much younger basalts of Timaru are of Pliocene to Pleistocene age and offshore sills were reported to be emplaced between Oligocene to early Pliocene (Bischoff et al., 2019b; Mathews and Curtis, 1966; Reeves et al., 2018). Intraplate intermittent volcanic activity in the region ranges from Cretaceous to Pleistocene (Adams, 1981; Barley, 1987).

2.1.5 Fluid flow in the Canterbury Basin

Overpressured fluids migrating through sedimentary strata and seeping out at the seafloor, significantly impacting seabed ecological systems, morphology, and shelf stability, are a common phenomenon in New Zealand's sedimentary basins. Onshore and offshore oil and gas seeps have been reported from most frontier and developed basins off New Zealand's North and South islands (Barnes et al., 2010; McLernon, 1978; Uruski, 2010). Between the Chatham Rise and the Great South Basin, east of New Zealand's South Island, a variety of fluid migration structures have been described. In the Canterbury and Great South basins, seismic data indicate focused and distributed thermogenic gas migration through fine-grained, low permeability strata (Bertoni et al., 2018). Honeycomb structures and giant pockmarks in this region suggest focused fluid migration induced by density inversion and polygonal faulting (Klaucke et al., 2018; Morley et al., 2017; Waghorn et al., 2017). Dolomite chimneys on the Canterbury Slope indicate groundwater and biogenic gas migration through shallow sediments (Orpin, 1997). A large offshore freshwater aquifer system in the basin was studied by Micallef et al. (2020). Fluid sources in the Canterbury Basin, therefore, include biogenic and thermogenic gases

as well as compaction-driven groundwater from polygonal fault systems and freshwater.

The Canterbury Basin and adjacent Great South Basin off the southeast coast of New Zealand are both targets of ongoing petroleum exploration (NZOG, 2018). Six offshore exploration wells, almost exclusively on the shelf, have been drilled in the Canterbury Basin. At least three shows of gas/condensates in non-commercial quantities were discovered (Daly and Hattersley, 2007; Shell BP Todd, 1984; Wilson, 1985) and Sutherland and Browne (2003) highlight its future potential due to the comparable development of nearby hydrocarbon producing basins (e.g. Taranaki).

Pockmarks are abundant on the slope of the Canterbury Basin where they range in diameter from 20 to 700 m (Hillman et al., 2018). The pockmarks occur in patches that are constrained to the crests between submarine canyons and gullies, similar to pockmarks reported in other regions (e.g. Galparsoro et al., (2020), Michel et al. (2017)). Their positions on the seafloor at depths between 500 and 1100 m roughly coincide with shallow areas of the expected gas hydrate stability zone (GHSZ) in this region. This approximate concurrence also led to an interpretation that gas hydrate dissociation and resulting venting during glacial-stage sea-level lowstands were responsible for the pockmark formation (Davy et al., 2010). Multibeam and parasound water column investigations in 2012 and 2013 revealed no evidence of active seepage on the seafloor (Bialas et al., 2013; Schneider von Deimling and Hoffmann, 2012). Water and seafloor samples collected in and around the pockmarks show no geochemical evidence of enhanced methane concentrations on the Otago Margin (Hillman et al., 2015). Since no indications for shallow hydrocarbons were present, Hillman et al. (2015) concluded that ocean current interaction with the Otago submarine canyon complex was likely to be the dominant formation process for pockmarks on the Canterbury Basin slope (Figure 2.5). No active fluid seepage has been reported within the Canterbury Basin.

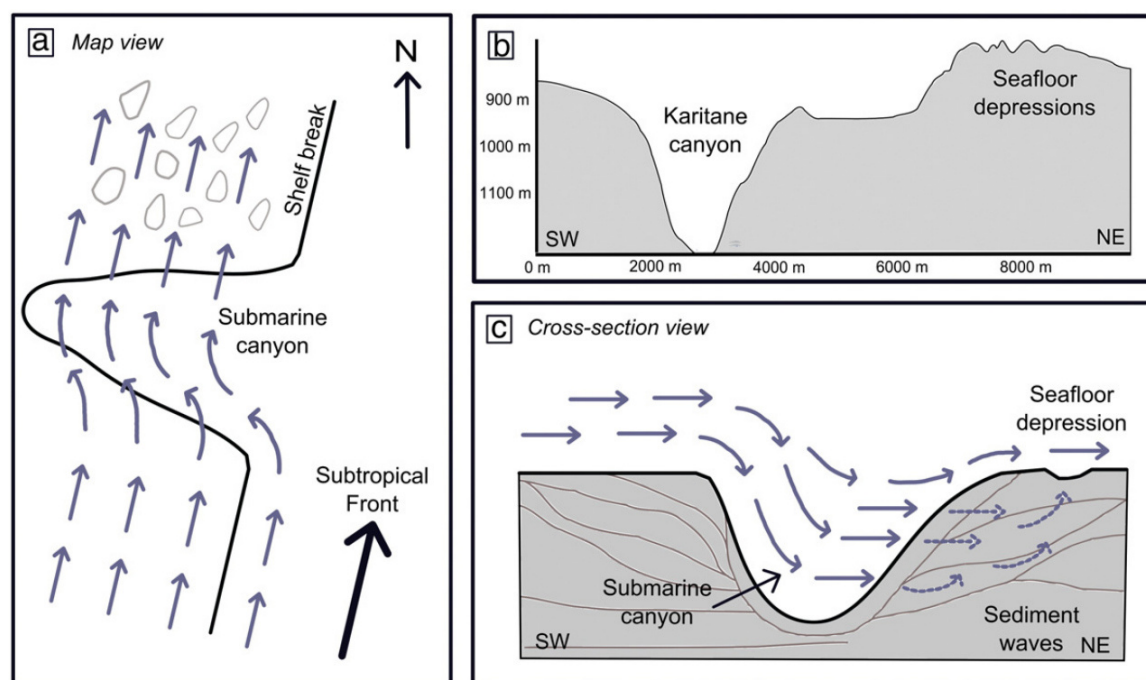


Figure 2.5: Formation mechanism for the Canterbury Slope pockmarks as proposed by Hillman et al. (2015)

2.1.6 Data used

In the Canterbury Basin, I used a variety of geophysical and geological data. I had access to two industrial 3D seismic datasets (Waka 3D and Endurance 3D) located on the Canterbury Slope. I extracted CDP traces along several in- and crosslines from one of the 3D surveys to inspect the amplitude and the velocity structure of the basin. I analysed over 12,000 km of 2D seismic reflection data that were acquired between 1966 and 2014 by various petroleum companies. Different academic seismic datasets from the basin were also made available for this study. I collected high-resolution boomer seismic data as well as multibeam bathymetry and backscatter data on the shelf and had access to different multibeam bathymetry and backscatter data from various other scientific cruises in the region. I used a large sedimentological dataset with nearly 300 sediment samples to groundtruth and verify the acoustic measurements. Additionally, well logs and reports from available petroleum wells (Cutter-1, Clipper-1, Endeavor-1, Galleon-1) and the IODP expedition 317 were used to stratigraphically validate seismic data.

2.2 Eckernförde Bay

2.2.1 Evolution of the Baltic Sea

The Baltic Sea is a relatively shallow intracontinental sea covering an area of $\sim 418,500 \text{ km}^2$. Its average depth is $\sim 50 \text{ m}$ and it is connected to the North Sea via the narrow Danish straits, the Kattegat and Skagerrak. Since the catchment area of the Baltic Sea is approximately four times its own area the surface salinity is comparatively low. This results in a constant halocline with denser highly saline bottom waters, which episodically inflow from the North Sea through the Danish straits, and low saline surface waters discharging back into the North Sea (Mälkki and Perttilä, 2012). The surface water salinity therefore gradually decreases from the Danish Straits ($S=10-25$) to the Bothnian Bay ($S=2-6$) (Uścinowicz, 2014).

The present-day Baltic Sea resulted from a series of Quaternary glaciations, which spread down from Scandinavia and episodically covered the area of the present Baltic Sea. There is evidence that seas, similar to the present Baltic Sea, existed during the interglacial periods (e.g. Holsteinian Sea or Eemian Sea, which existed about 420-360 and 130-115 ka ago, respectively (Head et al., 2005; Winterhalter et al., 1981)). The last glacial period, the Weichselian Glaciation, lasted from 115 to 11.5 ka and is associated with the glaciation of the northern parts of Europe (Figure 2.6). Following the Weichselian Glaciation, the present-day Baltic Sea evolved from a series of lake and sea stages (e.g. Baltic Ice Lake (12.6–10.3 ka), Yoldia Sea (10.3–9.5 ka), Ancylus Lake (9.5–8 ka), Littorina Sea (8–4 ka) (Björck, 1995)). Post-glacial rebound of up to 1.2 cm/yr affects the northern Baltic Sea in particular, while the southwest around Eckernförde is only minimally affected by isostatic uplift and slightly subsides ($<1 \text{ mm/yr}$) (Ekman, 1996; Johansson et al., 2002; Uścinowicz, 2014).

2.2 Eckernförde Bay

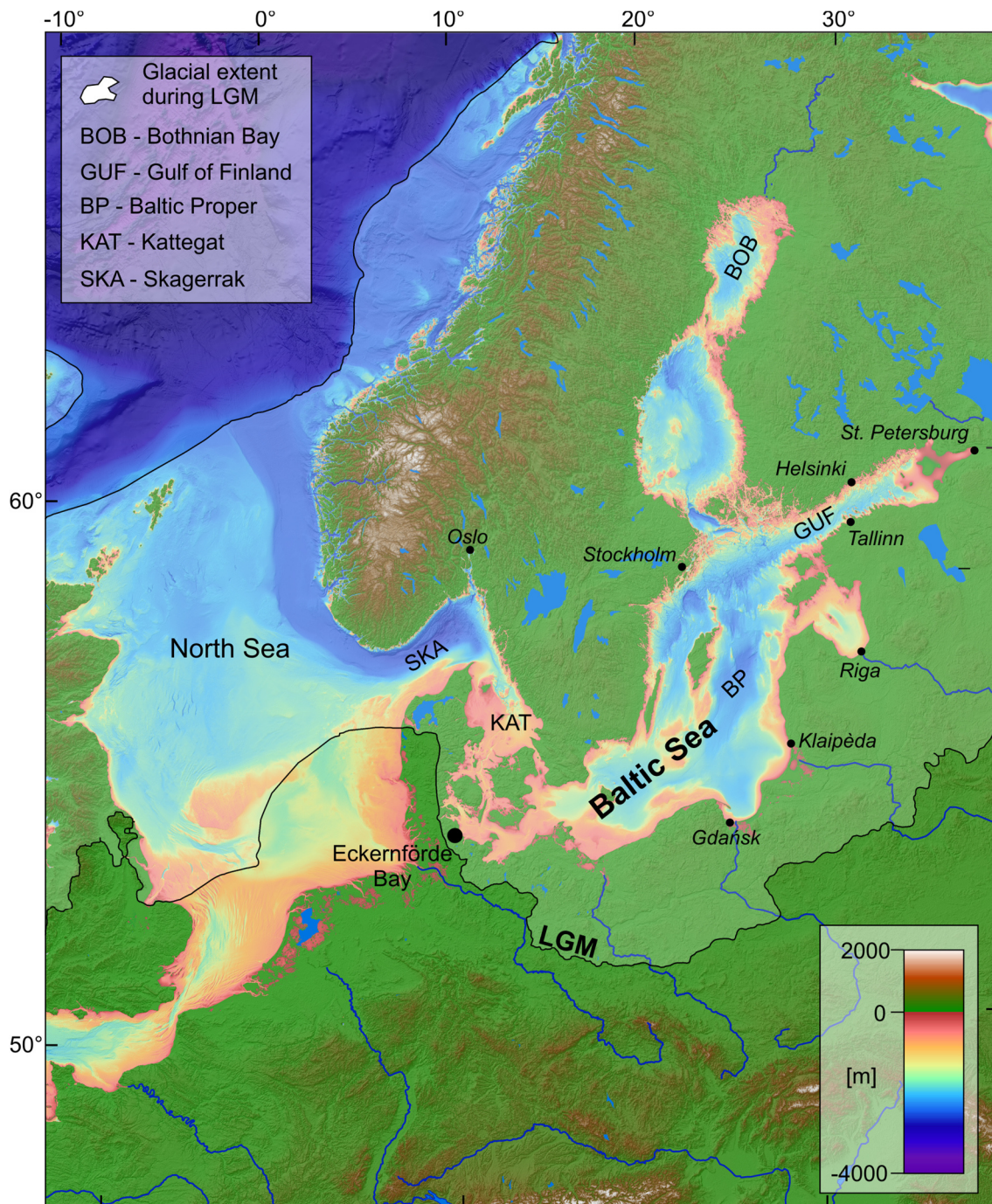


Figure 2.6: Overview of the Baltic Sea area with the glacial extent during the last glacial maximum (DEM was supplied by GEBCO compilation group (2019), Glacial extent after Ehlers et al. (2011)).

2.2.2 Sedimentary setting of Eckernförde Bay

The 17 km long and 3 km wide Eckernförde Bay is located in the western Baltic Sea and was mainly shaped during the end of the Weichselian Glaciation and glacial retreat about 13,000 yr BP. The mouth of Eckernförde Bay is divided into a deeper northern entrance and a shallower southern channel by a morainal sill called Mittelgrund (Figure 2.7). Sediment grainsize distribution in Eckernförde Bay gradually decreases with increasing water depth (Seibold et al., 1971; Werner et al., 1987). The sediments are mainly derived from the retreating till cliffs surrounding the bay with a minor amount contributed by the abrasion of Mittelgrund (Healy and Wefer, 1980; Healy and Werner, 1987).

Mean sedimentation rates in the central basin of 4.2 and 3.9 mm/yr were reported by Balzer et al. (1987) and Nittrouer et al. (1998), respectively; however, Milkert and Werner (1997) and Balzer et al. (1987) show that strong temporal fluctuations occur with sedimentation rates of up to 10 mm/yr. In the inner part of Eckernförde Bay, high organic carbon accumulation rates originate mainly from marine plankton and macroalgal sources (Balzer, 1984; Koezler, 1967). The high organic matter content (between 4 and 5%) of surface sediments, together with seasonally hypoxic bottom water, leads to strong anoxic conditions, a rapid decrease of sulfate and the onset of methanogenesis in the sediment within a few decimetres below the seafloor (Maltby et al., 2018; Steinle et al., 2017; Treude et al., 2005; Whiticar, 2002). Sediments below 20-22 m water depths consist mainly of Holocene mud deposited after the Littorina transgression (< 8000 yr BP (Rößler, 2006)) with gaseous (i.e., methane) sediments of microbial origin below ~0.5-3 m (Martens et al., 1999; Schüler, 1952; Wever et al., 2006, 1998; Whiticar and Werner, 1981). This interstitial gas results in the characteristic acoustic turbidity zone (first described as the “Becken-Effect” by Hinz et al. (1971)) commonly found in many shallow seas and lakes.

Although the bay is only minimally affected by tides, strong surface currents and sea-level changes can occur due to wind forcing, storm surges and the effect of seiches (Dietrich, 1951; Khandriche et al., 1987; Orsi et al., 1996). Bottom currents of up to 55 cm/s, 4 m above the seafloor, have been reported to follow storm surges (Geyer, 1964). The water column in Eckernförde Bay is generally well stratified

with pycnoclines forming due to strong variations of salinity and temperature, caused by the inflow of salty North Sea waters underneath the fresher and warmer surface water (Bange et al., 2011). This stratification becomes less pronounced over winter when cold surface waters and storms mix the entire water column (Smetacek, 1985; Smetacek et al., 1987).

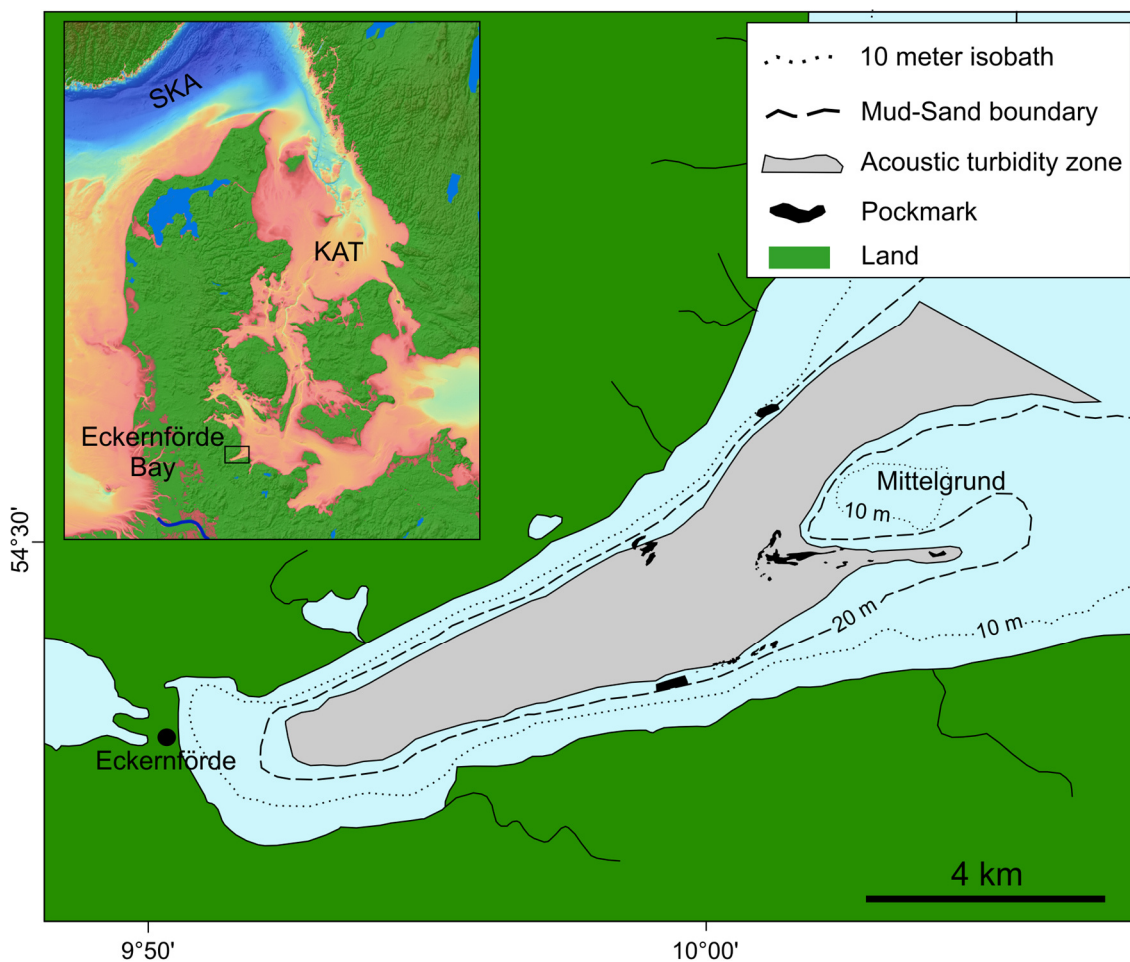


Figure 2.7: Overview of Eckernförde Bay showing the extent of the acoustic turbidity zone and the distribution of pockmarks (modified from (Whiticar, 2002))

2.2.3 Hydrogeology of the Eckernförde region

Two main aquifers in the region of Eckernförde supply potable water through four water producing utilities. Three of these utilities produce from the main ~80 m deep and 100-160 m thick Miocene lignite sand aquifer. One utility produces from a second much shallower sand aquifer which is separated from the Miocene lignite sands in most places by a glacial till unit and a thin unit of mica clay. This much shallower Pleistocene sand unit has thicknesses of 10 to 80 m and is

overlain by 10-50 m thick glacial tills which thin out within the Baltic Sea (Marczinek and Piotrowski, 2002).

2.2.4 Fluid flow in Eckernförde Bay

The two aquifers are known to supply groundwater into Eckernförde Bay where artesian springs feed freshwater into the Baltic Sea. Bussmann and Suess (1998) and Wever et al. (1998) attributed the origin of this groundwater to the major Miocene lignite sand aquifer which reaches a thickness of 100-130 m on the southern side of the bay, in ~100 m depth, and is hydraulically connected to the shallower sand aquifer (Marczinek and Piotrowski, 2002). The shallower Pleistocene sand aquifer occurs between two till units and reaches thicknesses of 10-15 m in the bay (Jensen et al., 2002). Jensen et al. (2002) and Whiticar (2002) concluded, that SGD into Eckernförde Bay is related to marginal areas where the late-glacial seal is thinned, and the Holocene mud coverage is weak enough to be penetrated by artesian groundwater.

In Eckernförde Bay, sulfate reduction is the dominant process for organic carbon degradation in the upper ~30 cm below the seafloor before the sulfate is depleted (Maltby et al., 2018). Below the sulfate-methane transition zone, methanogenesis leads to methane oversaturation and gas formation in the organic-rich mud, resulting in widespread acoustic turbidity zones. The depth of acoustic turbidity changes over time. This variability is mainly the result of temperature and pressure changes affecting the methane solubility (Wever and Fiedler, 1995). On a seasonal scale, atmospheric temperatures control the depth of free gas occurrences within the sediment. Due to the slow heat transfer through the water column, the atmospheric temperature cycle is delayed within the sediment (Figure 2.8). The seasonal variation in depth of the acoustic turbidity is overprinted by smaller-scale variations in e.g. pressure, salinity, or gas concentration in the sediment (Wever et al., 2006).

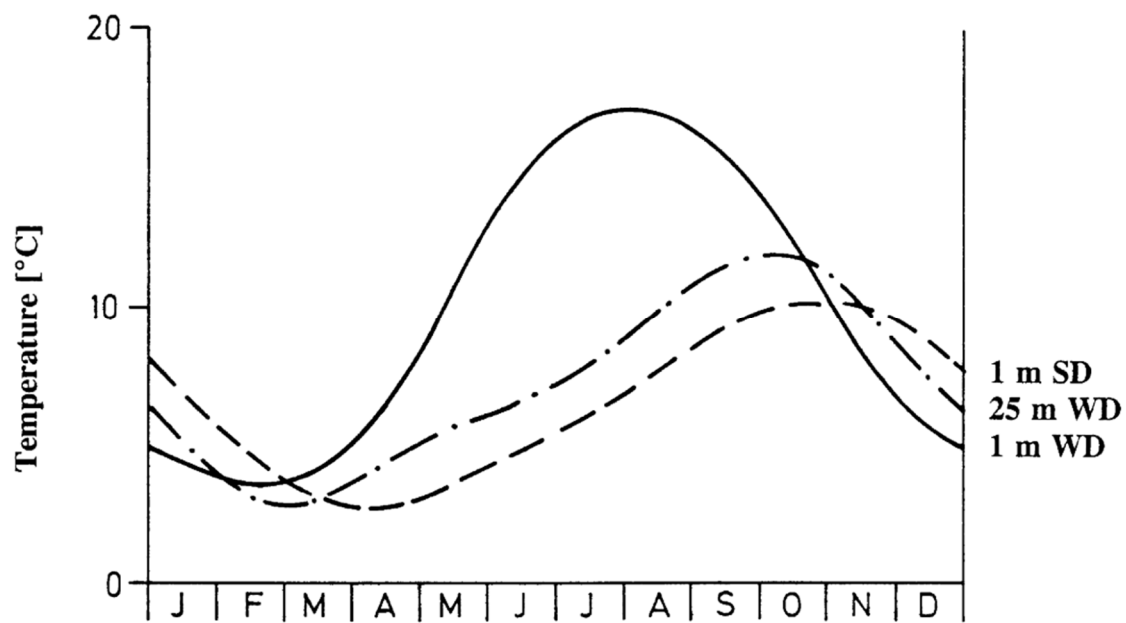


Figure 2.8: Seasonal temperature cycle in 1 m water depth (WD), 25 m water depth and 1 m sediment depth in Eckernförde Bay (adopted from (Wever and Fiedler, 1995))

Several pockmarks form along the coastlines as well as in the central part of Eckernförde around Mittelgrund. Due to the proximity of the pockmarks to the Schwedeneck oilfield they were previously thought to form as a result of leakage from the reservoir. Whiticar and Werner (1981) later showed that the isotopic composition of hydrocarbons extracted from recent sediments is different from those of the deeper Schwedeneck field. It is now widely accepted that pockmarks form as a result of microbial gas and submarine groundwater seepage (Bussmann and Suess, 1998; Jensen et al., 2002; Kaleris et al., 2002; Müller et al., 2011; Patiris et al., 2018; Schlüter et al., 2004; Whiticar, 2002).

2.2.5 Data used

In Eckernförde Bay I acquired multibeam bathymetry and backscatter data during three research cruises. I additionally collected a total of 19 sediment cores in the bay, 13 of which I positioned in the pockmark area and six located close to shore in the northwest of the bay. The geochemical analysis of extracted porewaters helps me to differentiate areas of groundwater and gas seepage and verify subbottom profiler data, which were collected during different cruises and made available for this study. The subbottom profiler data were used to map the extent and depth of the shallow gas in the bay. Seismic reflection data in the region were not considered due to the strong attenuation from the shallow gas and corresponding acoustic turbidity in the region.

Chapter 3

Fluid migration on the Canterbury Shelf and Slope

3.1 Introduction

On the passive continental margin east of New Zealand's South Island, numerous northeast oriented, crescent-shaped pockmarks are present on the Canterbury Basin slope at depths between 500 and 1000 mbsl. Hillman et al. (2015) suggested that all pockmarks on the slope formed at a similar time and constrained their timing of formation to the last ~18 ka. Their elongated forms correlate to the predominant northeastward flowing Southland Current, which seems to modify the pockmarks after their formation. Since no indications for shallow hydrocarbons are present on the Canterbury Slope, Hillman et al. (2015) concluded that ocean current interaction with the Otago submarine canyon complex was likely to be the dominant formation process for pockmarks on the Canterbury Basin slope (Figure 2.5). This interpretation was mainly based on the observation that pockmarks form predominantly on the northeastward facing side of the individual canyons.

An extended bathymetric dataset on the Canterbury Slope shows that pockmarks do not only occur around the canyon system, but are much more widely distributed along the Canterbury Slope (Figure 3.1). New bathymetry data also reveal that pockmark occurrence is not limited to the slope, but that much smaller, previously unidentified pockmarks also occur on the shelf. This widespread pockmark formation on the shallow otherwise relatively flat Canterbury Shelf

3.1 Introduction

indicates additional past or recent fluid seepage in the area. Pockmarks have previously been reported to be modified by bottom currents (Gafeira et al., 2012; Gontz et al., 2002; Michel et al., 2017) and can therefore offer insight into present or paleo current systems on continental slopes.

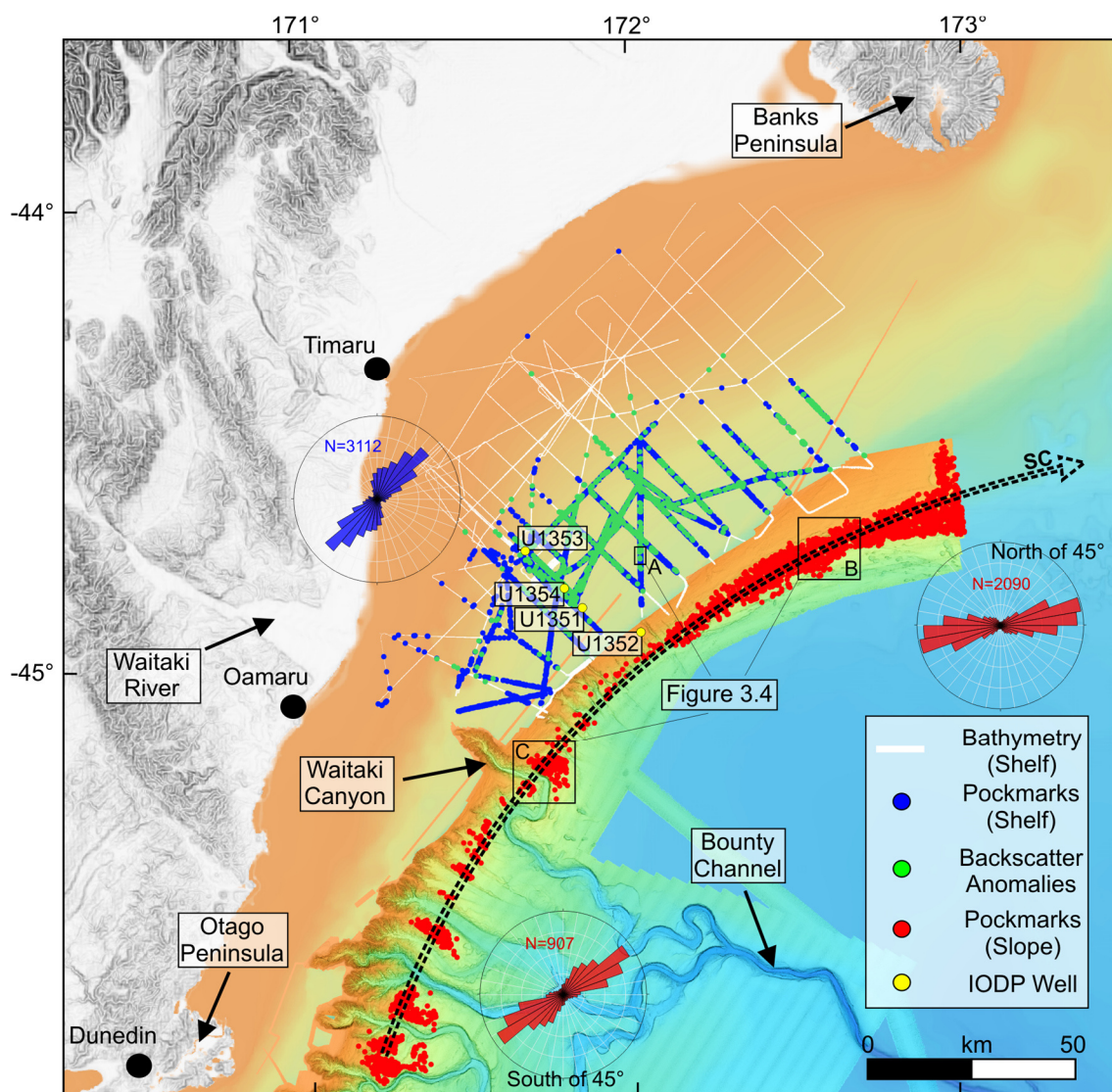


Figure 3.1: Overview of the Canterbury Basin pockmarks and available bathymetry data. Orientation of the long axis of the slope pockmarks north of 45°S and south of 45°S are displayed in the red stereonet plots. The orientation of all shelfal pockmarks with length over width ratios >1.3 are shown in the blue stereonet plot. Approximate location of the Southland Current (SC) is indicated by the blank arrow.

Submarine groundwater is abundant in continental shelves worldwide (Post et al., 2013) and has been attributed previously to the formation of pockmarks on continental shelves (Christodoulou et al., 2003; Goff, 2019; Nardelli et al., 2017). Two main mechanisms contribute to the emplacement of large offshore fresh groundwater reserves: 1) offshore aquifer systems (e.g. Gustafson et al. (2019), Johnston (1983)) and 2) meteorically emplaced groundwater during the Last Glacial Maximum (LGM), including glacial processes that were driving water into the exposed continental shelves (e.g. Cohen et al. (2010), Person et al. (2003, 2007)). Both processes contribute to the present-day fluid flow processes in the Canterbury Basin (Micallef et al., 2020).

I use high-resolution bathymetry and backscatter data, as well as boomer seismic data, complemented by generator injector (GI) gun seismic data and seafloor samples to investigate subsurface geological processes behind pockmark formation and modification. I analyse the pockmark occurrence in relation to the grainsize distribution on the Canterbury Shelf. By characterising the pockmarks shape, their distribution and their interaction with local bottom currents I aim to determine their relative timing of formation. Another goal of this study is to identify possible fluid sources on the shelf and slope. Since the two pockmark regimes appear in two distinct depth intervals, which are separated by a region without any pockmark occurrence, they must be treated individually, and different formation mechanisms need to be considered for each region.

3.2 Methods

This study is based on a range of different datasets that have been used to identify fluid sources within the Canterbury Shelf and Slope. The data used are displayed in Figure 3.1 Figure 3.2 and Figure 3.3.

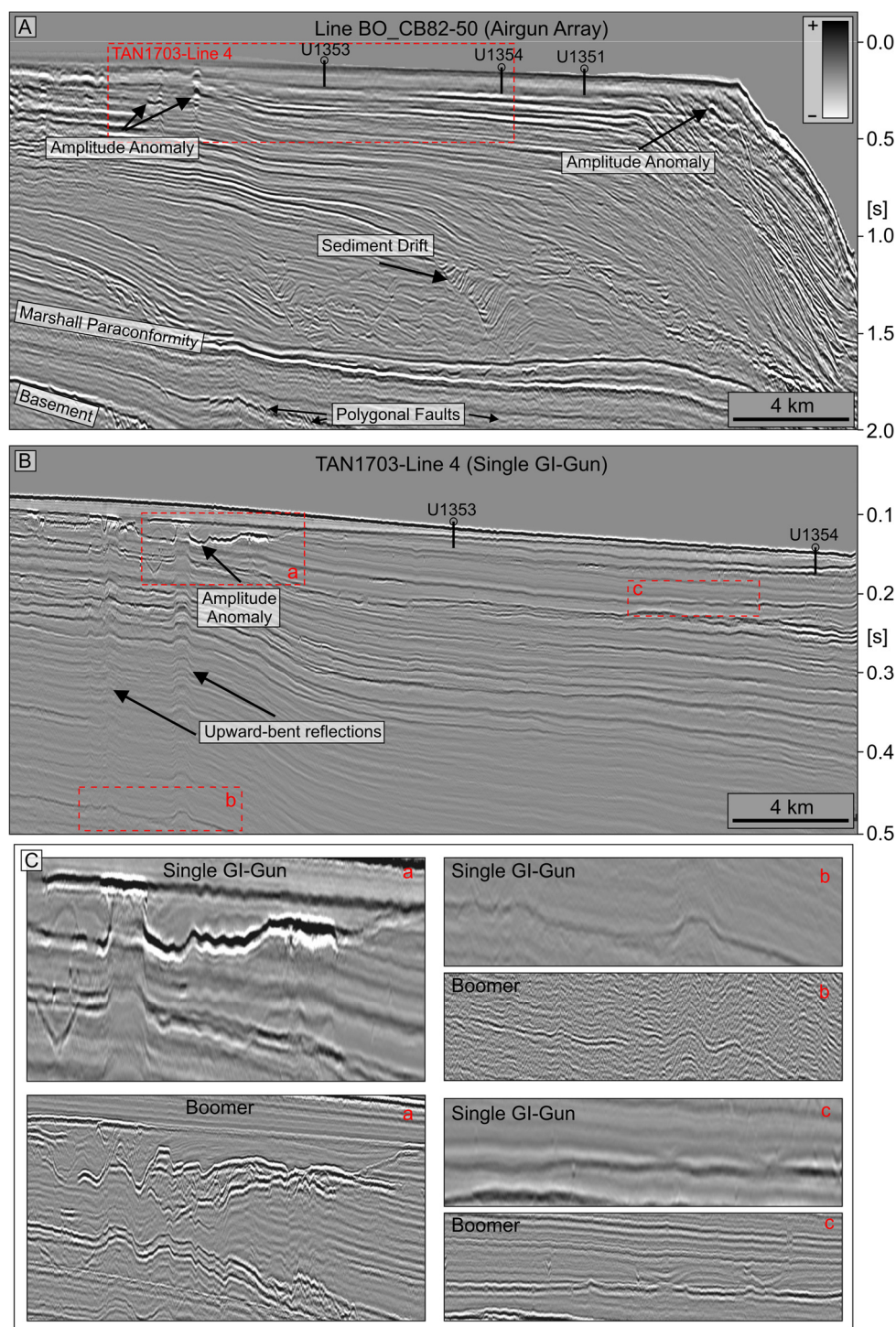


Figure 3.2: Overview of the Canterbury Shelf seismic data showing the different data resolutions used in this study in the vicinity of the IODP sites. Figure 3.3 shows the locations of these profiles. A) Overview industrial seismic line across the shelf showing shallow amplitude anomalies, sediment drift bodies, the regional Marshall Paraconformity and an underlying polygonal fault system. B) Single generator-injector (GI) gun seismic data (TAN1703) showing upward-bent reflections beneath a high-amplitude anomaly. C) Comparison of GI-gun to Boomer seismic data (extracted panels are labelled in B). The higher resolution Boomer data reveal much more detail and the complex sedimentary structure above the upward-bent reflections.

3.2.1 Seismic data

Boomer Seismic (Polaris II)

During two research cruises in 2018 and 2019, I acquired high-resolution boomer seismic data using the University of Otago's research vessel Polaris II (Figure 3.2). I used a Ferranti Ocean Research Equipment (ORE) Geopulse sub-bottom profiling system in combination with a 100 m long Geometrics MicroEel 24-channel streamer. The record length on the shelf was set to 0.5 s, while on the slope I recorded for 2 s. The shot interval was modified according to seafloor depth, ranging between 1.5 s and 3 s. I processed the data using GLOBE Claritas seismic processing software, incorporating stacking velocities from velocity picks made from seismic data collected during the TAN1703 cruise (Mountjoy et al., 2017).

Single generator injector (GI) gun (TAN1703)

2D high-resolution airgun seismic data were acquired during R/V Tangaroa cruise TAN1703 in April 2017 (Mountjoy et al., 2017) (Figure 3.2 and Figure 3.3). A single mini GI gun (13/35 cubic inch) towed at 1.5 m depth was used at pressures between 1800 and 2000 psi in combination with a 300 m GeoEel Digital solid-state streamer (Geometrics) consisting of 24 channels and a group interval of 12.5 m. The shot interval was set to 3 s and the record length to 1.5 s with a sample rate of 0.125 ms. Three birds were used to keep the streamer at a constant depth of 2.5 m. The data were processed by NIWA using GLOBE Claritas seismic data processing software.

Two GI-guns (EW0001)

In January 2000, the R/V Maurice Ewing (Fulthorpe et al., 2000b) collected a series of seismic lines prior to IODP expedition 317 (Figure 3.9 and Figure 3.10). They maintained a line spacing of ~2 km for most of the survey with a total of ~2120 km of seismic data acquired. During this survey, two GI guns (45/45 cubic inch) were fired simultaneously at 2000 psi every 5 s. Reflections were recorded for 3 s with a 1.5 km streamer which was towed between 2.5 and 3.5 m beneath the water surface and consisted of 120 channels with a group spacing of 12.5 m (Fulthorpe et al., 2000b).

Regional seismic reflection data (NZP&M)

I have also used ~10,000 km of 2D seismic reflection data provided by New Zealand Petroleum and Minerals (NZP&M, for details see <https://data.nzpam.govt.nz>) in the Canterbury Basin. These data were acquired during a number of cruises between 1966 and 2014 by various petroleum companies. Due to their focus on the deeper petroleum systems in the Canterbury Basin, the data quality in the shallow parts of the shelf is often poor. In particular, the data acquired prior to 2000 have very low resolution in the upper second of two-way travel time.

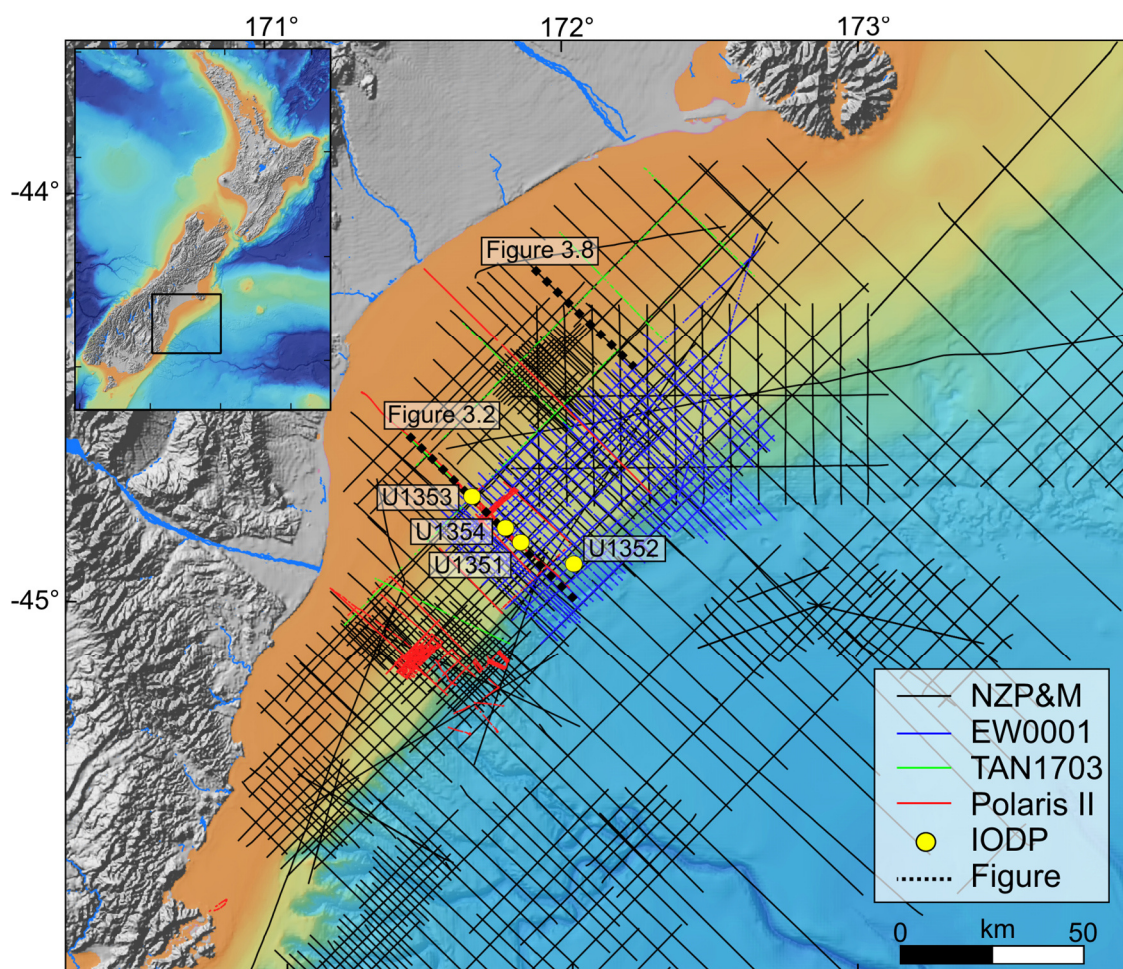


Figure 3.3: Overview of the seismic data availability with the different datasets at various resolutions indicated by different colours. The four IODP Expedition 317 sites are indicated in yellow.

3.2.2 Multibeam data

I have incorporated three separate multibeam bathymetry datasets. On the shelf, multibeam data were acquired during R/V Polaris II cruises 19PL410 and 18PL377 and R/V Tangaroa cruise TAN1703, whereas bathymetry data on the slope were acquired during cruise TAN1608 and provided by the National Institute of Water & Atmospheric Research (NIWA) (Figure 3.1).

On the slope, during cruise TAN1608, a hull-mounted 30 kHz Kongsberg EM302 multibeam system was used. The dataset extends from the shelf edge down to >1000 m water depth and covers the slope and canyon systems of the Canterbury Margin. The dataset was processed using CARIS HIPS&SIPS bathymetry processing software, resulting in a final grid resolution of 20 m (Mitchell et al., 2016).

On the shelf, a high-frequency 200-300 kHz Kongsberg EM2040 system was used during cruise TAN1703. For the highest possible resolution, the EM2040 was operated at 200 kHz over the deeper parts of the shelf (> ~100 m) and at 300 kHz in shallower areas. A 90-450 kHz R2Sonic 2026 system was used during the RV Polaris II cruises, where I acquired multispectral data of 100, 200 and 300 kHz data across the shelf. These high-resolution datasets extend from close to shore (30 m water depth) over the shelf edge to ~300 m. I used QPS Qimera as well as Fledermaus software for data processing and visualisation with final cell sizes of 2.5 m. I acquired sound velocity profiles at regular intervals and assigned them to the data during postprocessing with respect to their time of acquisition. On the shelf, I extracted and analysed the snipped backscatter data of the multibeam using QPS Fledermaus software packages. Attenuation coefficients were derived according to Ainslie & McColm (1998): 50 dB/km and 70 dB/km for 200 and 300 kHz, respectively. During all cruises on the shelf, I assessed multibeam water column data for the identification of acoustic flares.

I characterised the shape, location and depth of seafloor depressions using a semi-automatic tool for ESRI ArcMap developed by Gafeira et al. (2012). Depressions of up to 25 m depth were detected. A minimum and maximum area of 5000 m² and 50 000 m² was applied on the slope, whereas on the shelf, depression areas between 50 m² and 2000 m² were included in the analysis. I automatically picked over 2847 seafloor depressions on the shelf and over 4454 on the slope. I

visually inspected the automated picks and manually removed wrongly identified features. The seafloor depressions were additionally picked by hand and I estimated that the semi-automated method only correctly identified ~30% of all pockmarks that can be visually identified on the shelf. On the slope, on the other hand, nearly 90% of all pockmarks were correctly identified. The statistical analysis of the manual and automatically picked pockmarks is given in Table 3.1.

3.2.3 Sediment grab

I incorporated grain size distribution data from 287 sediment samples from the Canterbury Shelf, data that were analysed and combined by Bostock et al. (2019). They characterised the samples in % Mud, % Sand and % Gravel and used the ordinary Kriging method to interpolate between the data-points on a 1×1 km grid. The samples used in the study were collected during various cruises over a number of years. Many of them were originally acquired and published by Herzer (1981). All of these samples will further constrain the surface sediment distribution and is used to ground truth the backscatter pattern over the shelf.

3.3 Results

3.3.1 Bathymetry

The newly acquired bathymetry data reveal numerous pockmarks on the Canterbury Shelf (Figure 3.1 and Figure 3.4). The discovery of these features was entirely serendipitous and unexpected since previous mapping of the shelf (during R/V Maurice Ewing cruise EW0001, 2000) did not reveal any pockmarks in the same location. This is likely to be the result of the low-frequency (14-16 kHz Atlas Hydrosweep DS) deep-sea multibeam system operated during the EW0001 cruise on the shallow shelf, which does not provide sufficient resolution to identify the metre-scale pockmarks. These newly discovered shelf pockmarks show various sizes, ranging from ~7 to ~80 m with a vertical relief averaging ~1 m.

Previously reported pockmarks in the region have been limited to the margin slope in water depths of 500-1000 m (Figure 3.4). Those “slope pockmarks”

show highly elongated and crescent-shaped forms facing in the northeastern direction. They range in size from 50 to 700 m with a seafloor relief of 10 to 20 m. The long axis is aligned perpendicular to the slope, following the Southland Current which flows northeastward. All slope pockmarks show steeper slopes on their southwestern sides, whereas the northeastern sides appear to be washed out with much more gentle slopes.

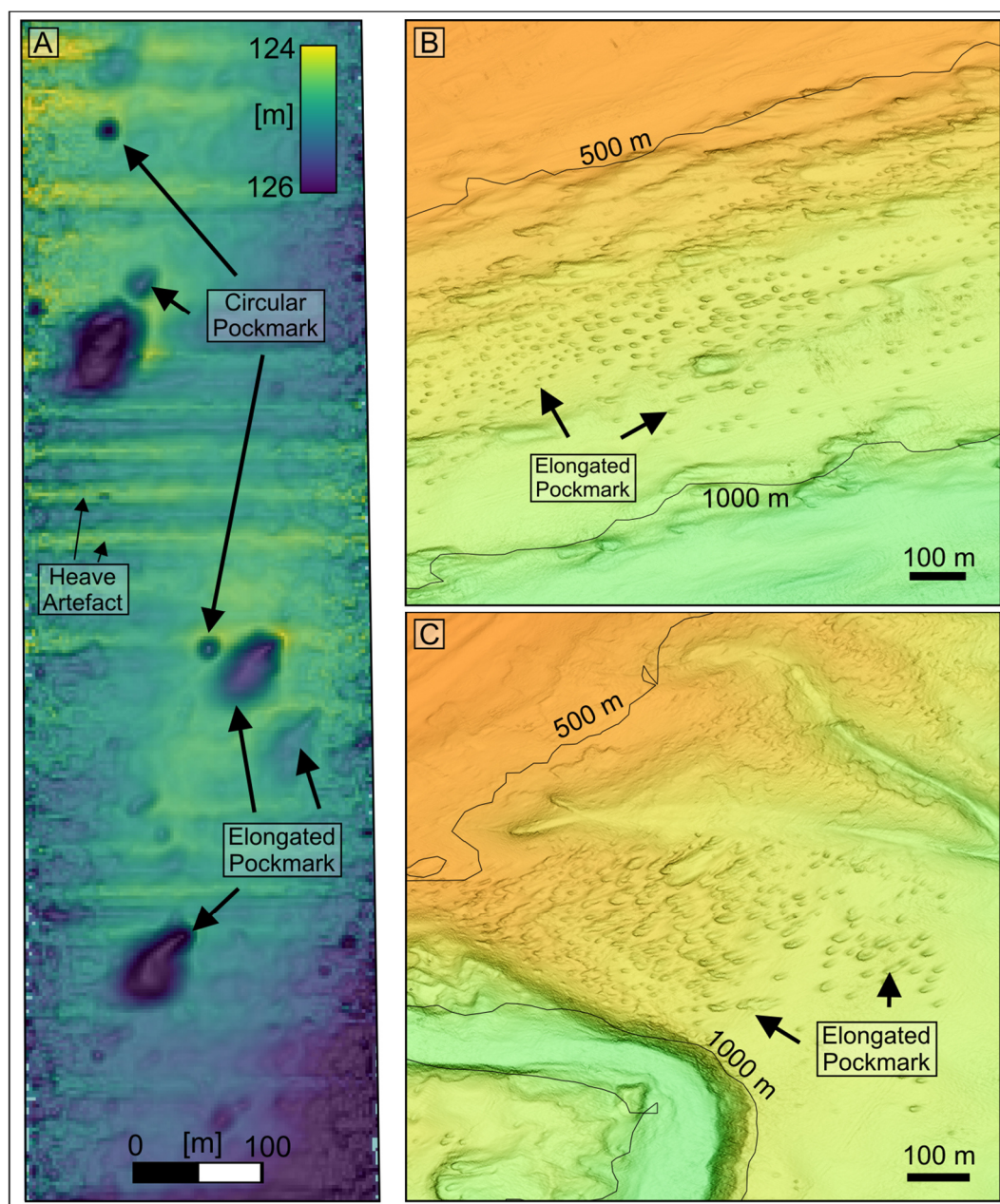


Figure 3.4: Pockmarks on the shelf and slope. A) Circular and elongated pockmarks on the shelf. B) Elongated pockmarks on the northern slope. C) Elongated pockmarks on the northern side of the Waitaki Canyon. Locations in Figure 3.1.

3.3 Results

The pockmarks on the shelf mainly occur on the outer shelf, before the shelf edge, in water depths of 80-140 m (Figure 3.5). To the northeast and southwest, the multibeam data coverage limits my knowledge of the extent of the pockmarks on the shelf. The shape of the pockmarks varies from perfectly circular to highly elongated and crescent-shaped forms. Circular and elongated pockmarks are evenly distributed over the shelf with slightly stronger elongations towards the shelf edge. No preferred location for elongated or circular pockmarks is evident, with elongated and circular pockmarks occurring in close proximity to one another. I calculated the length over width ratio for each pockmark as an indication of their elongation. The automatically picked pockmarks on the shelf show a much higher ratio than the manually picked pockmarks (Table 3.1). This could be either an effect of the manual picking process, which tends to not perfectly represent the pockmark shape, or the automatic picking process, which tends to create angular shapes with higher length over width ratios. Although the pockmarks are not perfectly represented by either the manual or the automatic picking, the overall trend is obvious throughout both picking methods.

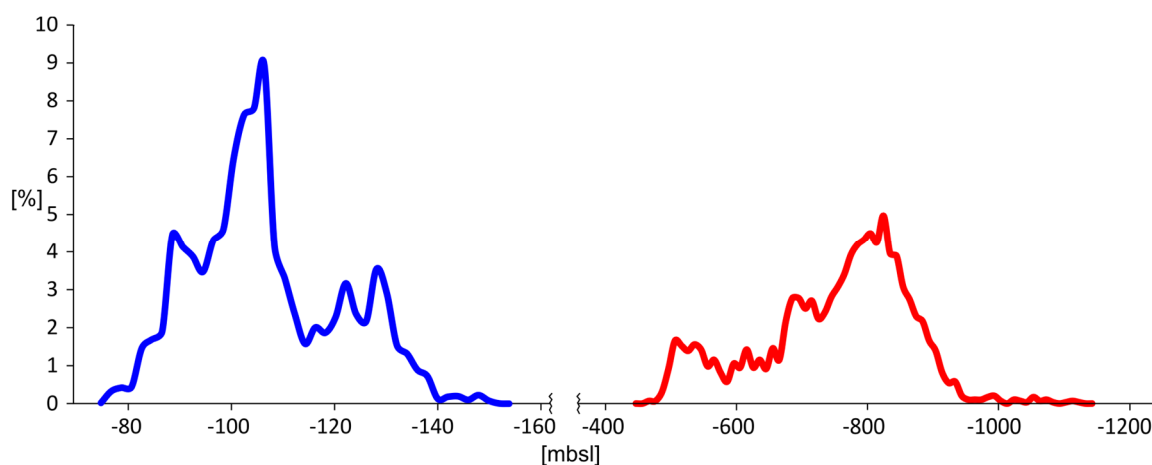


Figure 3.5: Pockmark distribution on the shelf (blue) and on the slope (red). The vertical axis is % of pockmarks per bin, which was calculated for bin sizes of 2 m and 10 m for the shelf and the slope, respectively.

The crescent-shaped elongated pockmarks on the shelf show a preferred orientation of their long axes in the SW-NE ($\sim 75^\circ$) direction, similar to the previously reported pockmarks on the slope (Hillman et al., 2015). The steeper slope of the elongated pockmarks on the shelf is mostly on the northeastern side, in

contrast to the pockmarks on the slope that show steeper gradients on the southwestern side. Many of the elongated pockmarks on the shelf appear to be washed out with an apparent fan on the southwestern side. Although the crescent form of the shelf and slope pockmarks is somewhat similar, their orientations are opposite (Figure 3.4 and Figure 3.12).

Table 3.1: Statistics of the identified pockmarks on the slope as well as on the shelf of the Canterbury Basin.

	Automatic-Slope	Manual-Shelf	Automatic-Shelf
Number identified	4452	11676	2847
Min water depth [m]	-430	-23	-71
Max water depth [m]	-1136	-183	-181
Average water depth [m]	-761	-107	-108
Average Size [m²]	14469	538	302
Average Long/short axis	2.17	1.3	1.8
Average Orientation [°]	76	81	72

3.3.2 Backscatter

The overall seafloor backscatter on the Canterbury Shelf is highly variable. Although the multibeam system was not calibrated for backscatter strength, and different frequencies were used on the shallow shelf compared to the outer shelf, the overall backscatter strength correlates well with the sediment samples from the shelf (Figure 3.6). The strongest backscatter (~ -10 dB) is found in the north of the basin close to shore. Similarly, strong backscatter of ~ -10 to -15 dB is also visible in the southeast over the shelf edge, on the slope, in water depths > 180 m. The lowest backscatter (~ -30 to -40 dB) is observed in the central and southwestern parts of the basin. Even in close proximity to shore (as close as 5 km in the west) backscatter strengths of not more than -30 dB are observed. The northeastern part of the basin, south of Banks Peninsula, is characterised by variable alternating high and very high backscatter (~ -15 to -25 dB).

The broad-scale backscatter strength correlates well with the grain size analysis of the sediment samples distributed over the shelf (Bostock et al., 2019a). In the north of the basin, close to shore, the high backscatter correlates with large amounts of gravel while the central and western shelf is characterised by low

3.3 Results

backscatter correlating to sands and mud. Where pockmarks occur on the shelf, the broad-scale backscatter ranges between -35 dB in the west and -15 dB in the east.

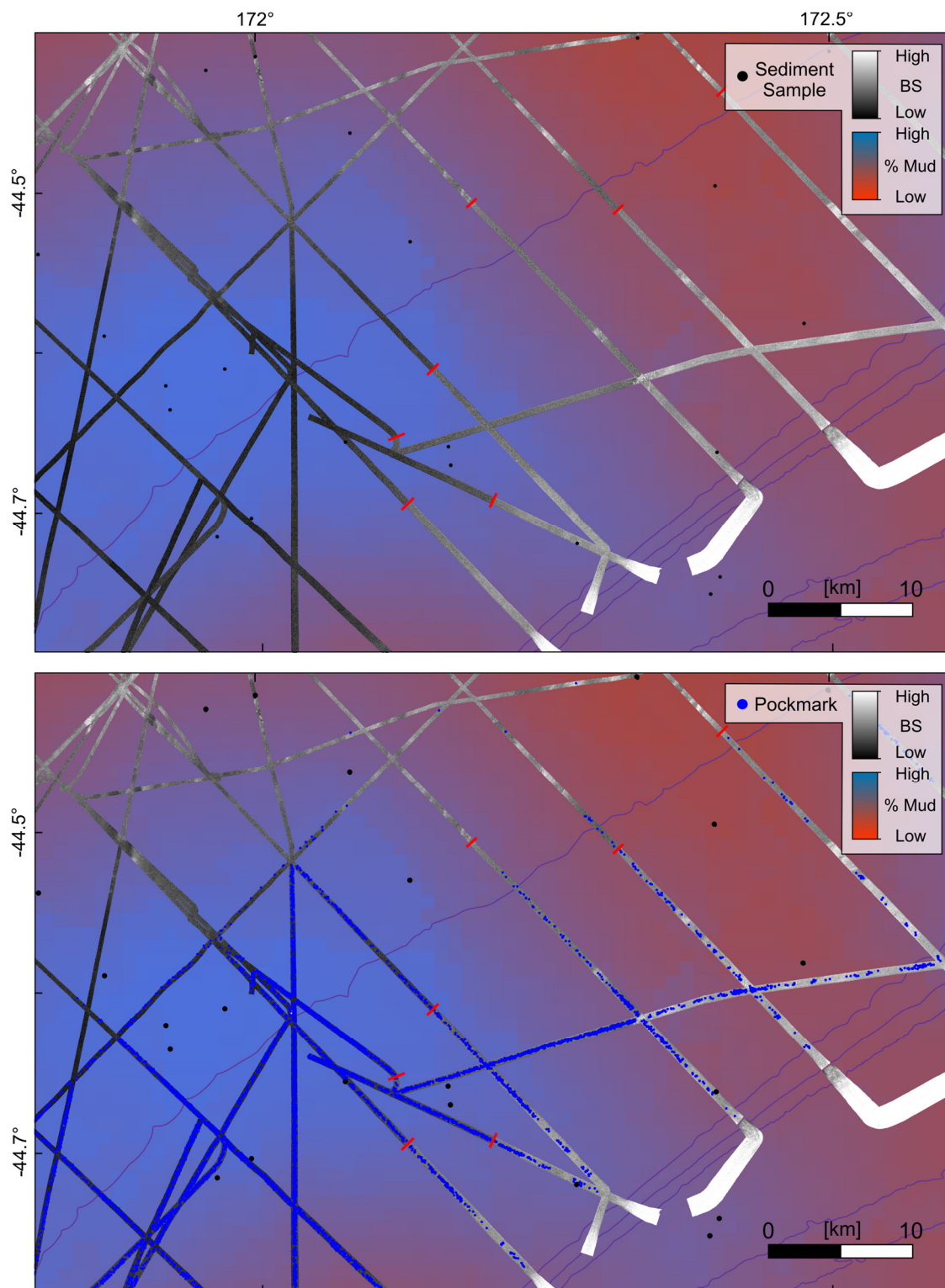


Figure 3.6: Multibeam backscatter data on top of the regional lithology map from Bostock et al. (2019). Black dots show sediment samples and the red lines indicate where the frequency changed from 300 kHz on the shallow shelf in the northwest to 200 kHz in the southeast.

Grab samples indicate a sandy seafloor composition in the east with minor amounts of gravel and/or mud, while the western pockmark region is dominated by a muddy lithology with small amounts of sand. The pockmark density on the shelf appears to be mainly driven by the depth range where they occur (80-140 m) but also corresponds with the backscatter strength of the hosting sediments. While pockmark densities of up to 90 pockmarks/km² are observed in the muddy, low backscattering areas, densities decrease down to fewer than 10 pockmarks/km² in the same depth range in the sandy and gravelly eastern parts of the shelf.

The pockmarks themselves show variable backscatter strength. While most of the pockmarks have no distinct backscatter difference compared to their surroundings, some show highly elevated backscatter strength (~15 dB difference compared to their surrounding). These distinct high backscatter pockmarks make up only ~5% of the pockmarks on the shelf. The elevated backscatter anomalies are predominantly associated with circular pockmarks, whereas most elongated and crescent-shaped pockmarks tend to have similar backscatter strength to their surrounding (Figure 3.7). This is highlighted by a low average length over width ratio of ~1.2 for all the pockmarks with elevated backscatter signals.

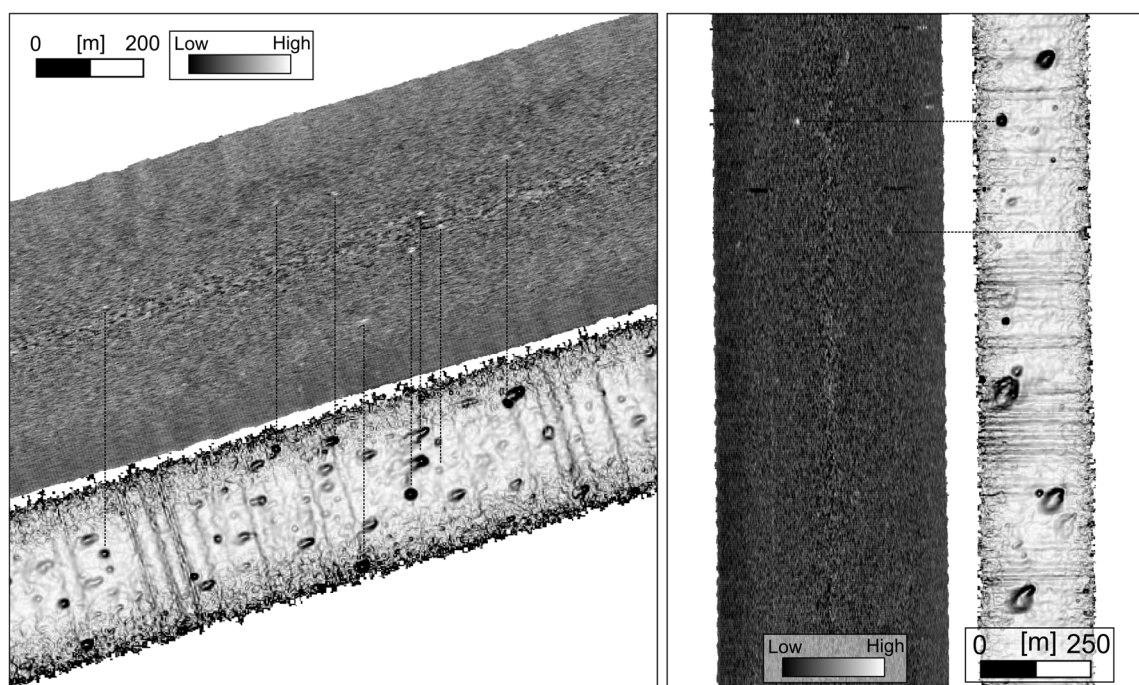


Figure 3.7: Bathymetric slope and multibeam backscatter data of different pockmark areas on the shelf. Strong backscatter is mainly associated with circular pockmarks.

3.3.3 Seismic data

The abundant seismic datasets on the Canterbury Shelf have previously been used to investigate margin evolution (Lu et al., 2005), sediment drifts (Fulthorpe et al., 2010; Lu et al., 2003), volcanics (Barrier, 2019) and potential hydrocarbon reservoirs. I use the seismic data to investigate near-surface fluid migration which could result in pockmark formation on the seafloor. Potential deep fluid sources such as volcanic intrusions and thermogenic hydrocarbons were also considered. Although abundant volcanic edifices and intrusions were mapped out in the Canterbury Basin by Barrier (2019) and Bischoff et al. (2019), it appears that many of these mapped intrusions are migration artefacts and other amplitude anomalies in the seismic data. Some volcanic intrusions in the north of the basin are apparent in the seismic data though (Figure 3.8). These intrusions are interpreted to be of Miocene age and appear about 0.9 s TWT beneath the seafloor. No structural conduits like faults or pipes connect any of the identified volcanics to the present-day seafloor. This also applies for deeper thermogenic hydrocarbon sources. I did not identify structural pathways such as chimneys or pipes in the seismic data on the shelf.

Upward bent reflections in the high-resolution Boomer data, as well as in the GI-gun seismic data, were among the only potential structural indications for upward migrating fluids (Figure 3.2). These two vertical anomalies with strongly upward bent reflections (~ 0.01 s) extend from a layer with very strong reflectivity down to the end of the record (0.5 s). The upper termination of the upward bent reflections is a complex surface with very strong amplitudes. Between the seafloor and this highly reflective surface, a unit of continuous and parallel horizons shows thicknesses of up to 0.02 s in the northwest and thins out further seaward on the shelf. At the same location where upward bent reflections occur in the high-resolution Boomer and GI-gun seismic data, anomalously high amplitudes exist in the low-frequency, commercially acquired seismic line (Figure 3.2A). These strong amplitude anomalies extend down to about 0.6 s, where they gradually decrease until no enhanced amplitudes are observed and reflections become undisrupted again.

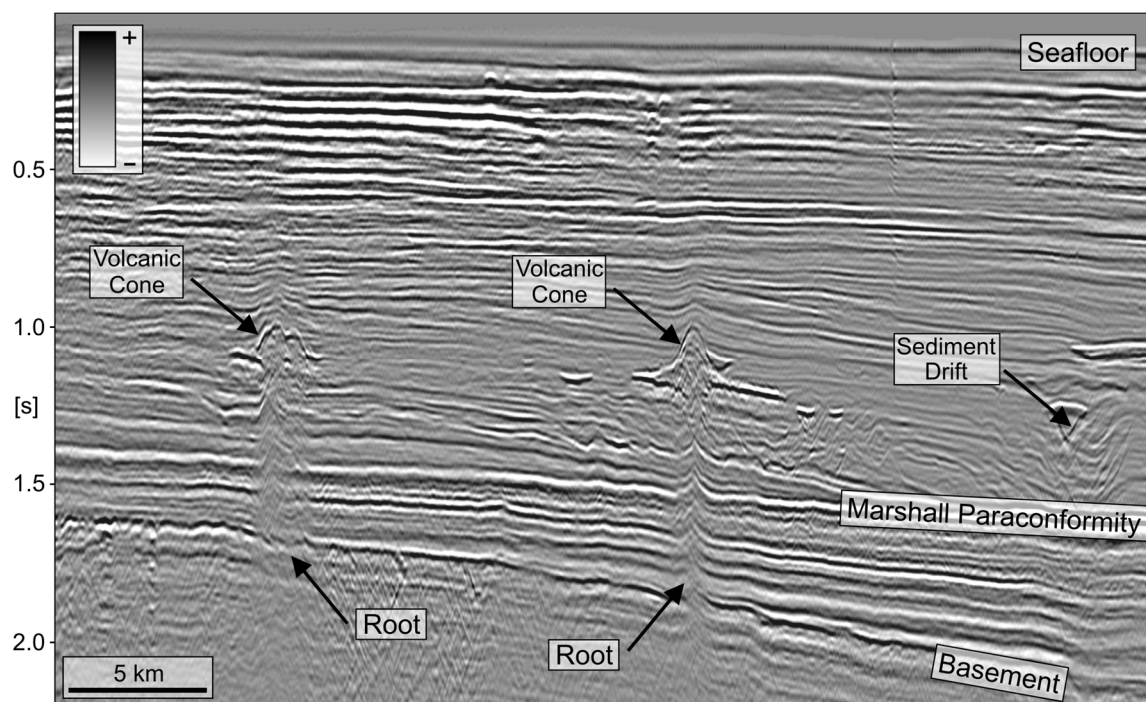


Figure 3.8: Seismic section imaging Miocene volcanic cones in the Canterbury Basin. Location in Figure 3.3.

Large sediment drift bodies (Figure 3.2) form above the Marshall Paraconformity in the Otakou Group and build up the modern-day shelf, as previously reported by Lu et al. (2003). High-amplitude reversed polarity reflections (compared to the seafloor reflection) are abundant on the outer shelf and upper slope (Figure 3.9 and Figure 3.10). Over the shelf, these amplitude anomalies increase in abundance and size from shore to slope (Figure 3.9). While there is nearly no disturbance of the shallow reflections beneath the seafloor in the northwest, strong, negative polarity reflections are abundant close to and beneath the shelf edge. These amplitude anomalies occur exclusively beneath seafloor depths shallower than ~ 400 m, and gradually decrease in strength and frequency towards the shore.

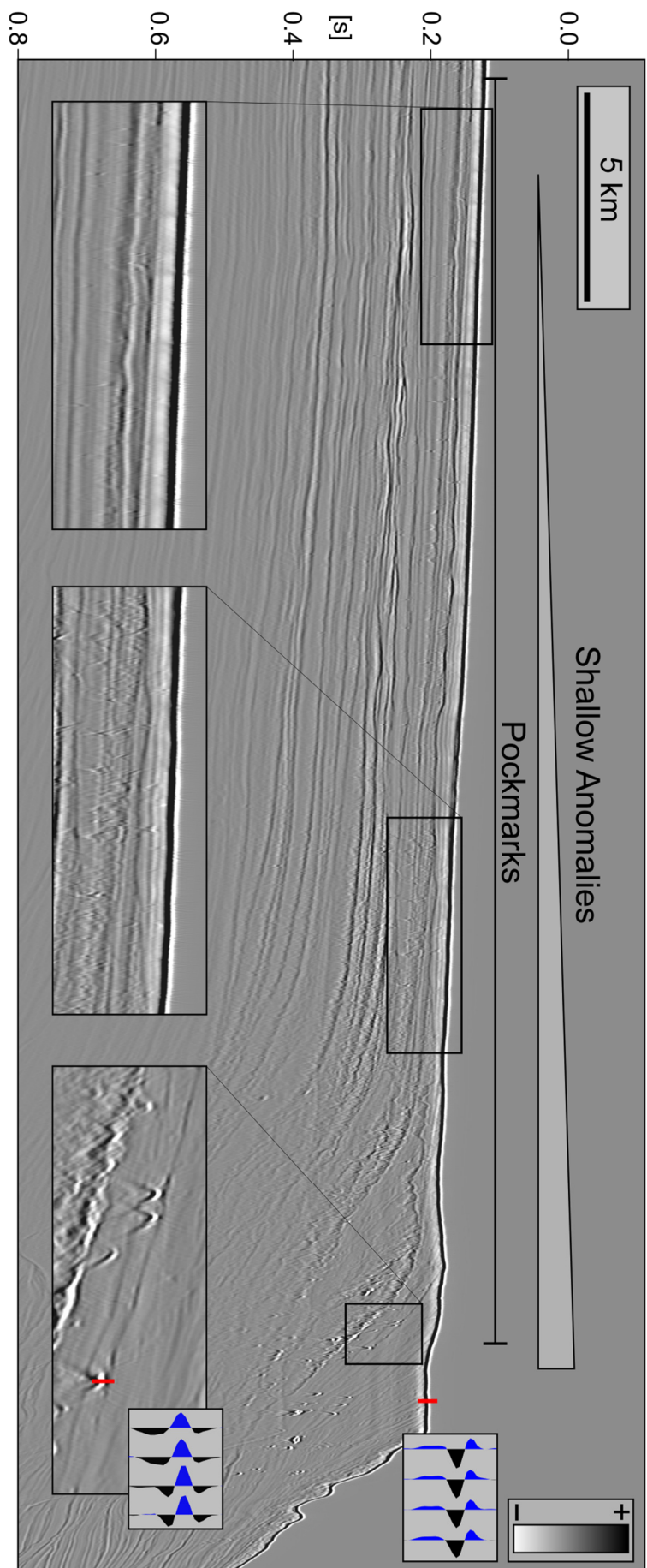


Figure 3.9: Seismic cross-section of the Canterbury Shelf indicating increased shallow amplitude anomalies from shore towards the shelf edge. Location in Figure 3.11.

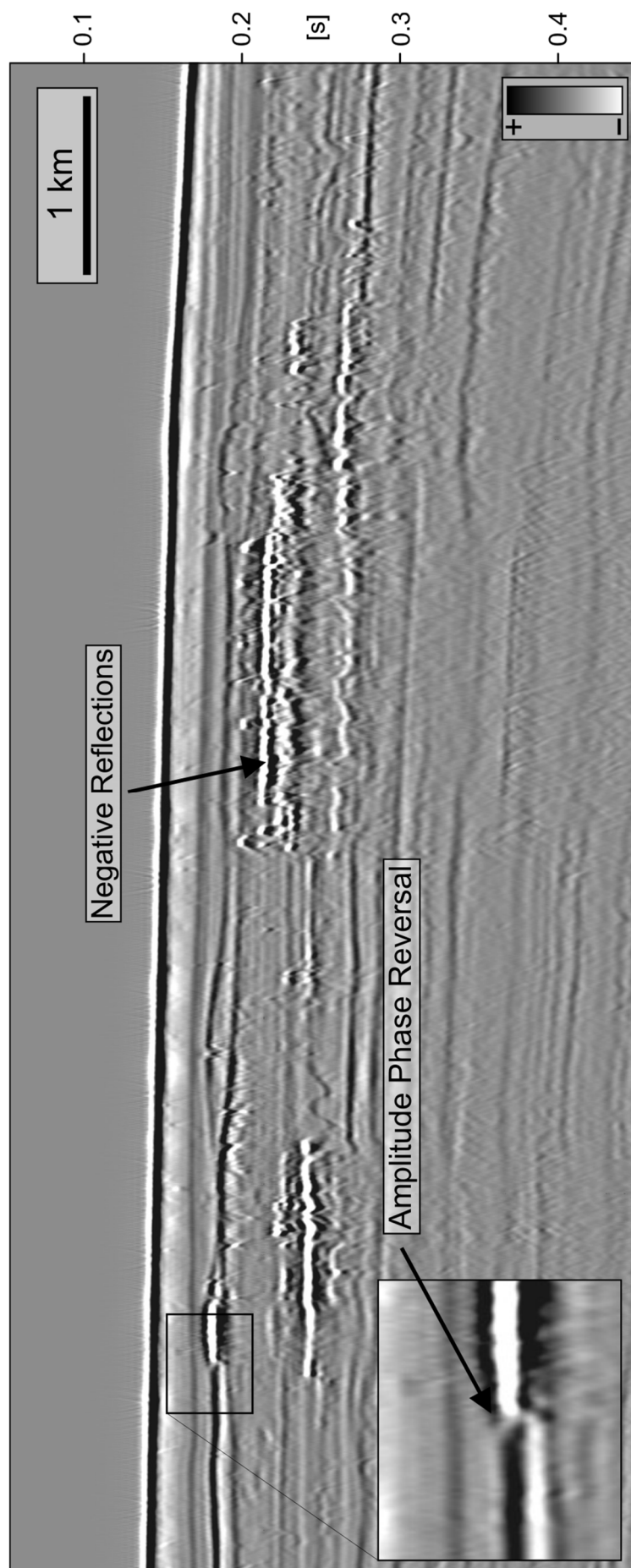


Figure 3.10: Seismic line on the Canterbury Shelf showing extensive negative reflection anomalies and amplitude phase reversals. Location is shown in Figure 3.11.

3.3.4 Water column imaging

Despite intensive multibeam water column imaging (WCI) investigations during R/V Polaris II cruises 19PL410 and 18PL377 and R/V Tangaroa cruise TAN1703, no distinct indications for escaping fluids have been observed, neither on the shelf, nor above the slope pockmarks.

3.4 Discussion

3.4.1 Formation of Canterbury Shelf pockmarks

Formation mechanisms for the abundant pockmarks on the Chatham Rise and the Canterbury Slope are still debated, with gas hydrates (Davy et al., 2010), bottom current and canyon interaction (Hillman et al., 2015), polygonal faults and paleo pockmarks (Waghorn et al., 2017) and mineral dewatering mechanisms (Klaucke et al., 2018) having all been discussed previously. The most recent study by (Stott et al., 2019) suggests CO₂ venting as a possible cause.

Based on the results of this study I evaluate three different pockmark formation mechanisms and their likelihood of occurring on the Canterbury Shelf and slope. These include:

- Groundwater expulsion
- Sediment compaction
- Gas venting

3.4.1.1 Groundwater expulsion

Submarine groundwater discharge (SGD) has been reported from numerous places globally and has previously been suggested to form seafloor depressions (see Chapter 5, Bussmann & Suess, 1998; Christodoulou et al., 2003; Goff, 2019; Hübscher & Borowski, 2006). Various mechanisms have been introduced to result in SGD, including artesian seepage of meteoric groundwater through karstic (Evans and Lizarralde, 2003; Moore and Shaw, 1998; Reusch et al., 2015) and dispersive systems (Hübscher and Borowski, 2006; Whiticar and Werner, 1981), overburden and sediment compaction processes (Chenrai and Huuse, 2017; Dugan and

Flemings, 2000), salinity driven convection cells (Goff, 2019; Siegel et al., 2014), glacial processes (Person et al., 2007), tidal pumping (Santos et al., 2009) and many others. In many of these studies groundwater is not considered to be emplaced solely by meteorically driven aquifers or subaerial exposure during sea-level low stands, but also includes recirculated seawater and brackish porewater and therefore does not have to be low in salinity. The term SGD has been used in many different studies and has led to serious misunderstandings (e.g. Taniguchi et al. (2002) defines “*the term SGD to represent all direct discharge of subsurface fluids across the land–ocean interface*”, technically including oil and gas seepage). I adopt the definition from Kim & Swarzenski (2010) that SGD can consist of fresh groundwater, recirculated seawater and a combination thereof.

Onshore, in the Canterbury Plains, New Zealand’s largest aquifer system is well documented and supplies potable water for the city of Christchurch and for agricultural purposes (Stewart et al., 2002). The aquifers extend down to depths of at least 500 m and consist of fluvio-glacial gravel deposits (Brown et al., 1995; Taylor and Fox, 1996). Cliffs along the Canterbury shoreline have been eroded by numerous U-shaped gullies with theatre heads and steep walls. These gullies are the result of groundwater seepage from the cliffs, eroding the finer-grained material and creating alveoli that result in slope failure (Marchis et al., 2018). It therefore seems likely that meteorically driven deeper aquifers could pass the present-day shoreline. Post et al. (2013) suggested that, in general, near-coast aquifers may result in SGD as far as 100 km offshore.

At IODP Site U1353 (Figure 3.3), which is located about 40 km offshore in a water depth of 84 m, reduced chlorinity of down to 400 mmol/L (compared to 550 mmol/L in the upper metres) occurred at 50 mbsf (Fulthorpe et al., 2010). No reduced salinities were observed in the IODP holes further offshore on the shelf in water depths of 110 and 125 m. Since the global sea-level was about 122 m below present-day sea-level during the last glacial maximum (about 20,000 years ago) and little post-glacial or tectonic adjustment have been observed in this region since then, well Sites U1353 and U1354 (Figure 3.3) were probably subaerially exposed. This could have allowed the development of freshwater lenses that may be preserved within the present-day shelf. Because this low salinity anomaly only

occurs at well Site U1353 and not in the two seaward sites on the shelf (U1354/U1351), Fulthorpe et al. (2010) suggested that the low salinities probably resulted from modern intrusions of meteoric water from land, rather than from historic remains of freshwater emplaced prior to shelf submergence. Gas hydrate dissociation is another mechanism that can lead to significant salinity reduction (porewater freshening) (Hesse and Harrison, 1981), but this is not feasible on the shelf because water depths are too shallow for gas hydrates to be stable.

Extensive controlled-source electromagnetic (CSEM) data on the Canterbury Shelf provide evidence that the aquifer system in the shelf is active and connected to terrestrial aquifer systems (Weymer et al., 2019). This offshore groundwater system is described in detail by Micallef et al. (2020), who suggest that the offshore groundwater system is predominantly confined at the top by a fine-grained low-permeability unit deposited during interglacials. The 3D characterisation of the offshore groundwater system suggests that it extends as far as 60 km offshore, perpendicular to the coastline and out onto the shelf into water depths of up to 100 m (Micallef et al., 2020). Modelling results indicate that flow rates into the shelf are not sufficient to emplace the estimated 213 km³ in the present-day shelf. Micallef et al. (2020) therefore suggested that much of the low salinity groundwater in the shelf was emplaced during sea-level low stands, with present-day residence times in the outer shelf of >300,000 yr.

The high-resolution multibeam data show that pockmarks on the shelf are confined to water depths of 70-180 m, which is beyond the suggested freshwater occurrence in the shelf. Micallef et al. (2020) also calculated the groundwater flux within the shelf and indicated that in the pockmark area the groundwater flux would not exceed $\sim 0.001 \text{ m yr}^{-1}$, which is insufficient for pockmark formation even in muddy sediments. Reduced salinities in the bottom waters down to $S < 31$ could suggest active discharge in water depths of up to $\sim 70 \text{ m}$ (Micallef et al., 2020). No reduced salinities were measured in deeper areas of the shelf though. Low salinities in bottom waters therefore occur in regions where no seafloor anomalies are observed. The spatial distribution of pockmarks does not correlate with the present-day freshwater system.

Similar to the aquifer system extending into the Canterbury Shelf, Gustafson et al. (2019) report on confined aquifers extending 90 km into the US Atlantic margin and spanning at least 350 km of the coastline. Pockmarks on this shelf were later reported by Goff (2019) and interpreted to form as a result of SGD, either induced by the confined freshwater aquifer or salinity driven convection cells as introduced by Siegel et al. (2014). These 10s of kilometres wide and 100s of metres deep convection cells could occur on periodically glaciated margins where freshwater emplacement takes place during glaciation. Since the Canterbury Shelf was not covered by ice during the Quaternary (Barrell, 2011), I rule out these suggested convection cells as possible formation mechanisms.

3.4.1.2 Sediment compaction

Overpressured fluids at depth can originate due to rapid sedimentation and disequilibrium compaction (Osborne and Swarbrick, 1997), which in turn can result in SGD. Hillman et al. (2015) investigated a potential connection between an Eocene polygonal fault system and the slope pockmarks. Since polygonal faults are thought to originate due to porewater expulsion from fine-grained material, they are able to create pockmarks (Berndt et al., 2003; Ho et al., 2016; Klauke et al., 2018; Maia et al., 2016). However, a kilometre-thick sedimentary unit without any structural indications for fluid migration pathways between the slope pockmarks and the Eocene polygonal faulted tier make such a connection unlikely.

Compaction and overload driven groundwater flow, as introduced by Dugan & Flemings (2000) or Chenrai & Huuse (2017), would likely channel fluids towards the seafloor. Their modelling results suggest porewaters to be expelled in the lower region of the slope where the escaping porewaters would create pockmarks (e.g. Chenrai & Huuse, 2017). This process therefore could contribute to the formation of the slope pockmarks but is unlikely to supply fluids for the formation of the shelf pockmarks.

3.4.1.3 Gas venting

Gas venting is probably the most common pockmark formation mechanism described in the literature. On the Canterbury Shelf, reversed polarity reflections compared to the seafloor are frequently observed in the seismic data (Figure 3.9

and Figure 3.10). Such reflections are commonly associated with free gas accumulations (Judd and Hovland, 1992). These amplitude anomalies on the Canterbury Shelf increase in frequency with distance from shore and are most prominent around the shelf edge. The distribution of free gas apparent in seismic data is shown in Figure 3.11. Despite extensive water column imaging efforts in this region, no indications for active gas venting have been observed (R/V Polaris II cruises 19PL410 and 18PL377 and R/V Tangaroa cruise TAN1703). Increased methane concentrations of over 20,000 ppmv (~8 mmol/L) in the two IODP well Sites located farthest from shore (U1351 and 1352; Figure 3.3) occur below the sulfate methane transition zone (SMTZ) at a depth of about 16 mbsf (Fulthorpe et al., 2010). The two Sites situated closer to shore (1353 and 1354; Figure 3.3) are characterised by the absence, or low levels, of methane in the upper 150 m. This correlates with my seismic observations (Figure 3.9 and Figure 3.11), which suggest potential free gas occurrence further out on the shelf but not in the region of the IODP well sites. Although it seems likely that the seismic amplitude anomalies are caused by methane gas accumulations, a recent study by Stott et al. (2019) suggested that carbonates from the Hikurangi Plateau, which was subducted beneath the Chatham Rise during the late Cretaceous, dissociated into buoyant CO₂, which migrates up towards the seafloor. CO₂ derived from mantle melt or decarbonation reactions of crustal rocks has previously been reported to cause seafloor pockmarks elsewhere, but only in volcanically active regions (Passaro et al., 2016). In the deep water well Caravel-1 on the Canterbury Slope, dawsonite minerals (NaAl(CO₃)(OH)₂) indicate that large quantities of CO₂ were present during the Eocene (Blanke, 2015). CO₂ hydrates could have formed beneath the seafloor on the slope, where they store, accumulate and episodically release CO₂ during glacial maxima when the hydrate dissociates due to depressurisation (Stott et al., 2019). This seems to be a potential mechanism for pockmarks on the margin slope, or the Chatham Rise, in water depths where CO₂ hydrates are theoretically stable but is unlikely in shallow areas on the shelf. Although I cannot rule out the possibility of CO₂ induced pockmark formation on the shelf, I suggest it is more likely that microbial gas formed below the SMTZ and that expulsion of this gas led to pockmark formation.

3.4.2 Modification and distribution of Canterbury Shelf pockmarks

3.4.2.1 Sedimentary environment

The sediment grab samples used in this study are well distributed over the Canterbury Shelf. Although no detailed grain size analysis exists of the sediment grab samples, the overall grain size distribution of the shelf is apparent (Bostock et al., 2019a). Although the sediment grab samples do not show a distinct change in seafloor material between shelf and slope, a noticeable change in backscatter occurs (Figure 3.6). While the shelf shows moderate backscatter responses, the slope is characterised by very strong backscatter signals. I assume the strong backscatter on the slope results mainly from diagenetic processes such as compaction and consolidation, creating a harder surface compared to similar sediment compositions on the shelf. Reduced coarse sediment supply to the slope, combined with stronger eroding bottom currents (i.e. Southland Current), could result in the exposure of more compacted sediments with a similar grain size distribution to the shelfal sediments. Present-day erosion rates on the upper slope are suggested to be relatively high due to high current velocities of up to ~13 cm/s (Hillman et al., 2018; Lu et al., 2003).

Pockmarks on the shelf occur predominantly in the mud patch in the southwest of the shelf but are also widespread in coarser-grained areas of mainly sandy sediments and stronger backscattering strength. Some grab samples even indicate sandy to gravelly seafloor materials in regions where pockmarks occur. Although the bathymetric coverage on the shelf is limited, it is notable that the pockmark density declines in regions with coarser-grained seafloor material (Figure 3.6). The sediment grab samples (Figure 3.11) show that the pockmarks are not confined to a specific lithology on the shelf. Goff (2019) investigated pockmarks on the New Jersey shelf and noted that they are confined to the so called “New England mud patch”, a fine-grained lithology deposited on the shelf. He suggested that fluid escape occurs in wider regions of the shelf, but pockmarks only form in the mud patch. However, it seems that in the Canterbury Basin fluid venting is confined to the outer shelf, and pockmarks occur in different lithologies where fluids are venting.

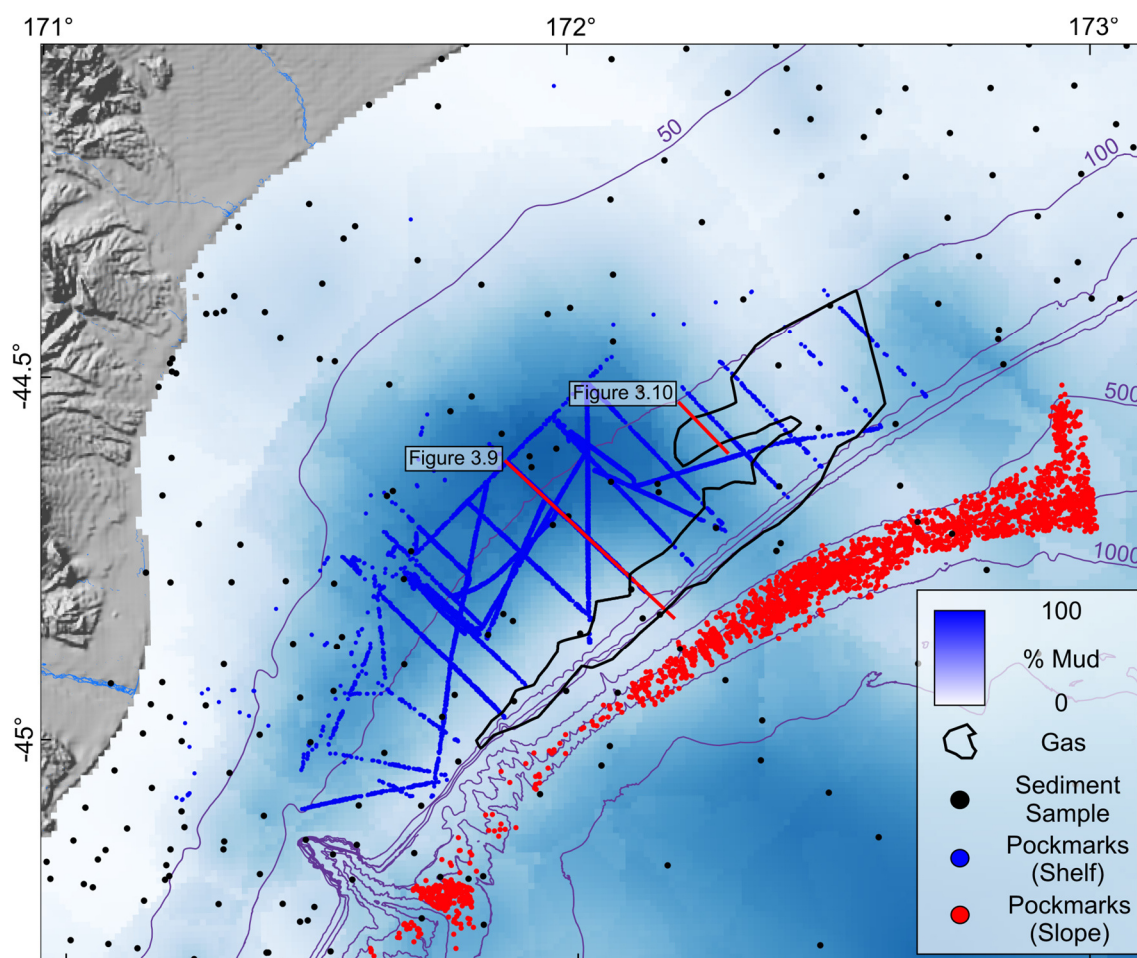


Figure 3.11: Distribution of mud on the shelf with overlain pockmark occurrences. Distribution of shallow gas is outlined in black.

3.4.2.2 Bottom currents

Pockmarks in the Canterbury Basin show a pronounced alignment perpendicular to the shoreline, on the shelf as well as on the slope. The shore parallel Sub-tropical Front (STF) or Southland Front (SF) separates Subantarctic Waters from Subtropical Waters (Sutton, 2003). The two water masses converge on the upper continental slope (~ 400 mbsl). The associated northward flowing Southland Current is well established in the region (Chiswell, 1996; Fulthorpe et al., 2010; Lu et al., 2003; Sutton, 2003). The narrower continental shelf between Dunedin and Oamaru (Figure 3.1) constricts the Southland Front, resulting in increased geostrophic current speed in the South, before opening up again around the Waitaki Canyon (Chiswell, 1996).

Andresen et al. (2008) showed how originally circular pockmarks can be modified by contour parallel bottom currents in the North Sea. The parallel

alignment of the northeastward facing crescent-shaped form of the slope pockmarks with the northeastward flowing Southland Current has previously been noted by Hillman et al. (2015). The Southland Current is known to have formed large scale sediment drifts on the Canterbury margin over the last 15 Ma (Figure 3.2 and Figure 3.8) (Fulthorpe et al., 2010). I find that many pockmarks on the shelf show a similar alignment parallel to shore, but in the opposite direction to the slope pockmarks. The geometry of seafloor depressions can be affected by various mechanisms, including tidal flow, storm waves, gravity sliding, bottom currents or the seafloor topography (Andresen et al., 2008; Schattner et al., 2016). In this case, the pockmarks are too deep to be affected by storms and waves and the only plausible mechanism for their alignment seems to be the subsequent modification by bottom currents.

The southwest-facing crescent-shaped form of the pockmarks suggests a current flowing in the southwest direction across the shelf (Figure 3.12). To my knowledge, there have been no reports of any southwestward flowing currents on the shelf (i.e. opposing the Southland Current) on the Canterbury Slope. However, anomalous surface water temperature differences have been measured around the Waitaki Canyon by Fenaughty & Bagley (1981) and Beentjes & Stevenson (2001). The Waitaki Canyon is the most significant bathymetric feature in the Canterbury Basin and Beentjes et al. (2002) interpreted the sea-surface temperature differences to result from disturbances in the Southland Current as it flows over the Waitaki Canyon. They also report a temperature increase of $+0.6^{\circ}\text{C}$ in the southern compared to the northern Canterbury Basin in water depths of 100-200 m. They interpret this temperature difference to result from inshore eddy currents from the Southland Current induced by the Waitaki Canyon. Although these potential southwestward flowing bottom currents could not be confirmed during the recent research cruises of this study, they could have important implications for longshore sediment drift and distribution. The elliptical nature of the pockmarks also suggests that bottom currents might be more important in the evolution of the form of these pockmarks than the initial formation mechanism of gas seepage.

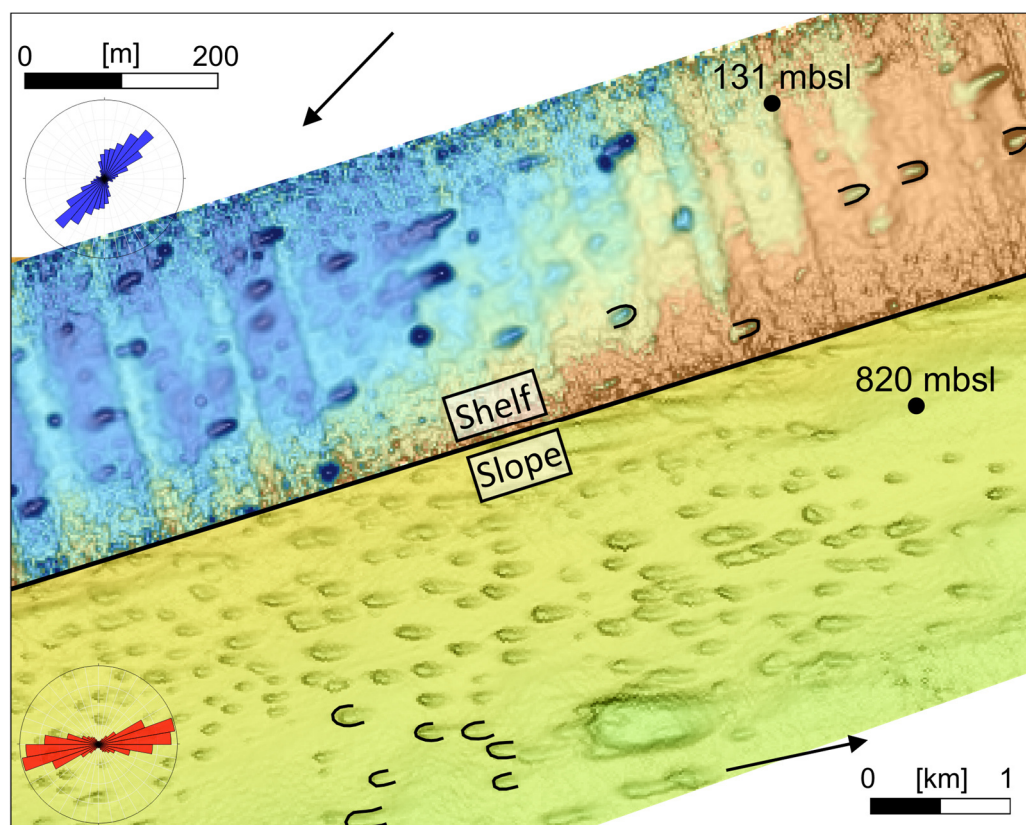


Figure 3.12: Comparison of pockmarks on the shelf and slope, showing the opposite facing crescent-shaped form.

3.4.3 Activity and age of Canterbury Shelf pockmarks

Holocene sediments cover the present-day Canterbury Shelf, with a thickness of 9.9 m at the innermost IODP shelf Site U1352, decreasing towards the slope (Fulthorpe et al., 2010). This constrains the timing of the formation of the shelfal pockmarks to the last ~10 ka. I did not observe any active gas seepage out of the pockmarks during several research cruises, suggesting either a quiescent phase of gas venting or an inactive pockmark system.

Enhanced backscatter from the bottom of pockmarks is a common phenomenon and is often attributed to authigenic carbonate precipitation due to the microbially driven oxidation of methane (Boetius et al., 2000; Hovland et al., 1987; Ritger et al., 1987). The oxidation occurs either in oxic environments through aerobic methane-oxidising bacteria or in anoxic environments where methane is utilized by sulfate-reducing bacteria (Reeburgh, 1983; Rudd and Taylor, 1980). Both processes result in methane oxidation and carbonate cementation of the shallow sediments and can act as a self-sealing mechanisms for hydrocarbon seeps

(Hovland, 2002; Hovland et al., 1985). The cemented sediments at the bottom of the pockmark are generally associated with high-amplitude reflections in seismic data and enhanced backscatter signals in multibeam data (Böttner et al., 2019; Dandapath et al., 2010; Hovland et al., 1987). The suspension of fine-grained material due to fluid escape, leaving only the coarser-grained material behind, similarly can result in a strongly reflective area with a rough surface resulting in a strong backscatter response. This strong scattering area at the bottom of pockmarks can be enhanced by increased biological activity around seep sites that leave behind skeleton remains, dead and living shells and other biological remains (Hovland et al., 2002; Hovland and Thomsen, 1989; Reusch et al., 2015). Hovland et al. (2002) have described these pockmarks with high reflectivity and strong scattering objects in their centre as “eyed” pockmarks.

In the Canterbury Basin, pockmarks with a strong backscatter response occur in close proximity to pockmarks that don't show a distinct elevated backscatter signal. The backscatter behaviour also seems to correlate with those pockmarks that are more circular (i.e. low length over width ratios). Since the pockmark density is quite high, I assume that all shelfal pockmarks were formed by the same mechanism. If this was the case, the low backscatter in the more elongated pockmarks could indicate that the time of pockmark formation varies over the shelf. This would be supported by the differences in elongation of the pockmarks. Circular and current modified pockmarks can occur very close to each other, at distances <10 m. I assume that the circular pockmarks with a strong backscatter signal formed more recently than the elongated, current modified pockmarks without elevated backscatter intensity. It could also be possible that southwestward flowing currents that modify the pockmarks only occur episodically. In this case, the younger pockmarks would not have been subjected to modification by the bottom currents. The reduced backscatter of the elongated pockmarks, compared to the younger, circular pockmarks, could indicate recent sedimentation and infill of the pockmarks that covers up the strong backscattering objects at their centre (e.g. coarser material, carbonates or biological remains). This would be in accordance with the possibility that the bottom currents are not actively modifying and scouring the pockmarks, therefore enabling sediments to settle and deposit on the shelf.

3.5 Conclusions

Pockmarks are abundant on the eastern side of New Zealand's South Island. In the Canterbury Basin, two distinct pockmark areas are confined to water depths of 80-140 m and 500 to 1000 m. Although shallow gas is abundant on the outer shelf, the gas seems to be confined to sediments below a seafloor depth range of 100 to 400 m. No free gas is apparent below the pockmarks on the slope. On the shelf, free gas occurs below the present-day pockmarks located furthest offshore, while no free gas is apparent beneath the shallowest pockmarks (water depths <100 m). Counterintuitively, much of the free gas seems to occur beneath the shelf edge, where no pockmarks occur. To explain this observation, I assume that sub-seafloor gas in regions where pockmarks are present on the seafloor has already migrated to the surface and contributed to pockmark formation.

Overload and sediment compaction dewatering mechanisms, as suggested by Chenrai & Huuse (2017) or Dugan & Flemings (2000), are likely to contribute to fluid expulsion on the slope. Modelling approaches from Micallef et al. (2020) suggest that freshwater from offshore aquifers or historically emplaced meteorically derived water is unlikely to be strong enough to form pockmarks.

Although all pockmarks examined on the Canterbury Slope have similar appearances and degrees of modification and are therefore interpreted to have formed at the same time, I suggest that shelfal pockmarks form episodically. The oldest shelfal pockmarks have probably been partially infilled by recent sedimentation and experienced modification from past southwestward-flowing bottom currents. More recently formed pockmarks on the shelf show strong backscatter signals in their centre and no modification from bottom currents. The bottom currents seem to be episodic disturbances in the southland current, most likely induced by bathymetrical features such as the Waitaki Canyon (Beentjes et al., 2002).

Chapter 4

Seismic evidence for repeated vertical fluid flow through polygonally faulted strata in the Canterbury Basin, New Zealand

4.1 Introduction

Fluid transport through focused flow systems is a widespread phenomenon in sedimentary basins. Fluid migration and accumulation processes play important roles in hydrocarbon exploration, hazard assessment, and environmental conservation (Anka et al., 2012). On the seafloor, pockmarks can be indicative of underlying fluid migration pathways such as faults, pipes or chimney structures (Berndt et al., 2003; Hovland et al., 2005; Løseth et al., 2011). Pockmarks can form due to episodic dewatering and sediment compaction in sedimentary basins, often in combination with a non-tectonic class of faults, known as polygonal faults. These faults only form in very fine to fine-grained tiers of sedimentary strata where they alter the bulk permeability of the otherwise low matrix permeability and expel as much as 60 percent water by volume, which is why they are considered a major fluid source (Berndt et al., 2003; Cartwright et al., 2007; Cartwright and Lonergan, 1996; Verschuren, 1992). Pipe structures in the overburden of polygonal fault systems show that polygonal fault systems can act as a long term source for fluid flow (Berndt et al., 2003) as well as pathways for upward fluid migration from deeper strata (Gay et al., 2004). Ho et al., (2016) suggest the lower parts of polygonal faults may behave as fluid conduits while the upper parts of the fault

planes appear to be sealed. The polygonal planform may be modified by the underlying morphology as well as by anisotropic stress fields (Ho et al., 2018a).

Sedimentary volcanoes (often classified as mud volcanoes, but also sometimes consisting of coarser-grained, non-cohesive material) are a specific category of natural gas/oil seepage and in general confirm the existence of overpressured hydrocarbon reservoirs in the region (Mazzini and Etiope, 2017; van Loon, 2010). They are an important pathway for degassing deeply buried sediments and represent a significant source of methane in the atmosphere (Dimitrov, 2002). However, in most cases, methane escaping from the seafloor is dissolved and consumed as it rises through the water column (McGinnis et al., 2006) where it has implications for marine biogeochemistry (Leifer and Judd, 2002).

The Canterbury Basin off the southeast coast of New Zealand is the target of on-going commercial petroleum exploration (NZOG, 2018). Six offshore exploration wells (Figure 4.1) have been drilled with at least three shows of gas condensates in uncommercial quantities (Daly and Hattersley, 2007; Shell BP Todd, 1984; Wilson, 1985). However, fundamental questions persist regarding sub-surface fluid flow in the basin.

In this chapter, I focus on three-dimensional (3D) seismic expressions of fluid migration pathways through sedimentary sequences that include several extensive tiers of polygonal faults. Seismic data analysis, particularly in 3D, is ideally suited to this research because seismic reflectivity and coherency are highly sensitive to both structural deformation and fluid flow processes (Marfurt et al., 1998; Simm and Bacon, 2014). In particular, I examine formation mechanisms of cylindrical faults around a fluid conduit. The aims of this chapter are: (1) to investigate the nature, and provide a seismic characterisation, of recent and buried fluid migration pathways, (2) to constrain the timing of fluid migration in the Canterbury Basin and (3) to present a conceptual integrated model for the formation of the fluid migration pathways.

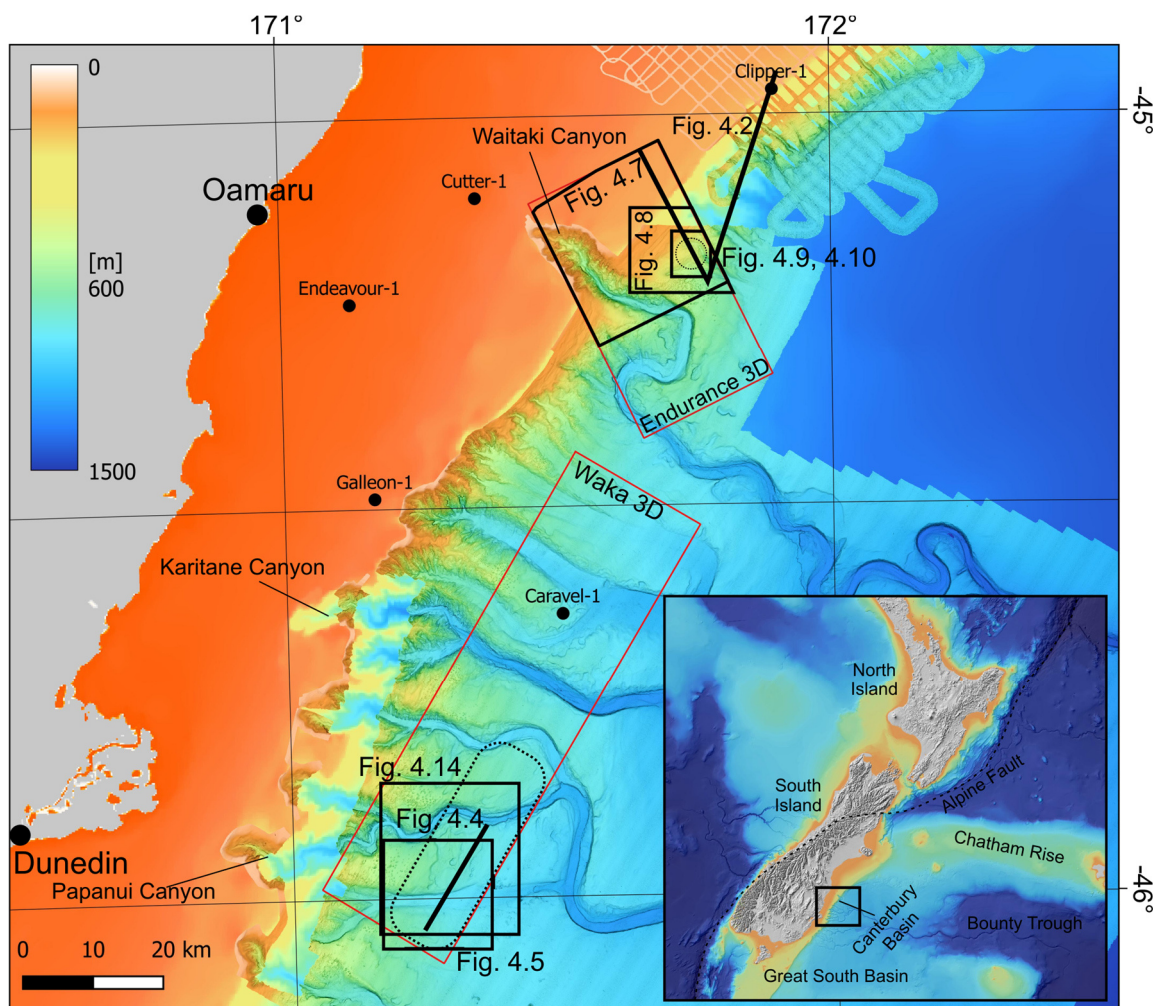


Figure 4.1: Bathymetric overview map of the Otago margin working area (Data source: Mitchell et al. (2016), NIWA et al. (2012)). The inset map in the lower right shows the location (black box) of the main map. The footprints of two 3D seismic surveys (Waka 3D and Endurance 3D) on the Otago submarine canyon complex are outlined in red (Data source: Anadarko and Origin Energy (2009), NZOG and Beach Energy, (2013)). Buried pockmarks are observed within the region outlined with a dotted black line within the Waka 3D box.

4.2 Data

Recent exploration efforts by the petroleum industry in this region have involved the collection of two extensive 3D seismic datasets covering the Otago Canyon system (Figure 4.1). The 3D datasets cover total areas of 1151 and 680 km² at full fold. One dataset (Waka 3D) is publicly available while the second proprietary seismic dataset (Endurance 3D) was made available for this study. An inline and crossline spacing of 25 x 12.5 m in both datasets allows me to accurately map faults and horizons. Additionally, several CDP-sorted pre-stack 2D lines extracted from the Endurance 3D volume were made available for this study and are used for high-density velocity analysis and investigations of the amplitude variations with angle (AVA).

The seismic data are complemented by high-resolution multichannel seismic boomer data in shallow regions. Due to differences in seismic resolution and location, the two 3D seismic datasets show distinct differences in amplitude characteristics and the stratigraphic successions that they image are somewhat different. The three main stratigraphic units in the Canterbury Basin (Onekakara, Kekenodon and Otakou groups) are readily distinguished in the Endurance 3D seismic dataset which partly covers the shelf and the prograding clinoforms. In contrast, the Waka 3D volume, which is more basinward and further south, does not image the prograding clinoforms but instead covers the channel-levee system on the slope of the margin and the Eocene to basement strata.

The stratigraphic analysis is based on nearby petroleum wells. An overview of the Canterbury Basin with the three main stratigraphic groups, the extent of the polygonal fault systems and the different stratigraphic ages is shown in Figure 4.2.

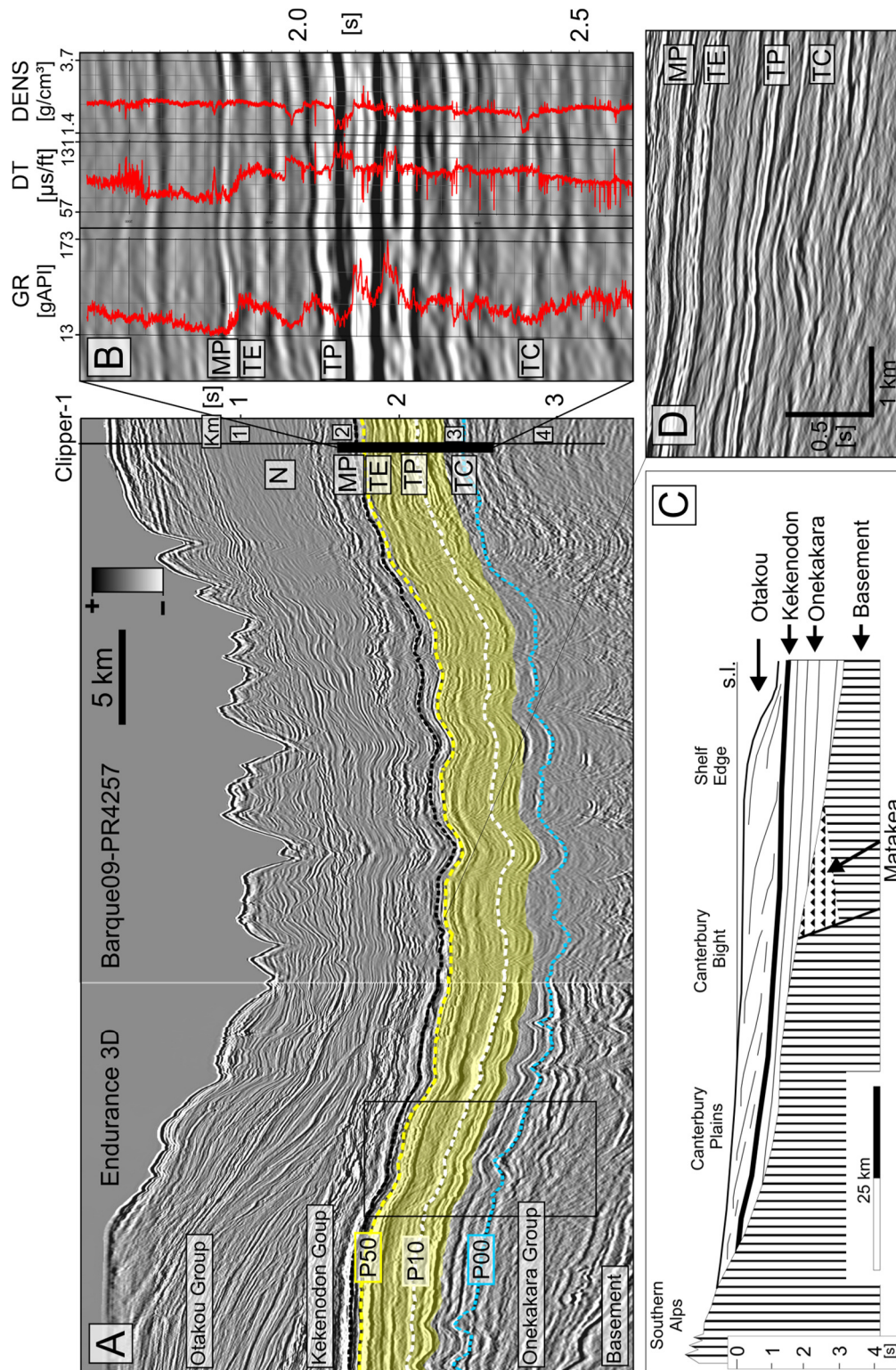


Figure 4.2: A) Composite seismic tie line to the Clipper-1 well. Approximate extent of the polygenically faulted tiers are shown in yellow. Neogene (N), Marshall Paraconformity (MP/black), top Eocene (TE/P50/yellow), top Paleocene (TP/P10/white) and top Cretaceous (TC/P00/turquoise) are shown as dashed lines. Horizon names after Strogon and King (2014). B) Gamma Ray (GR), Sonic (DT) and Density (DENS) logs are shown in the area of interest. C) Schematic cross-section through the Canterbury Basin after Fulthorpe and Carter (1989). D) Undisturbed view of the horizons specified.

4.2.1 Waka 3D seismic data

In 2009, Petroleum Geo-Services (PGS) acquired the Waka 3D seismic data volume (licence block: PEP38262) using the *M/V Nordic Explorer* with six parallel 5.1 km-long hydrophone streamers and a streamer separation of 100 m. Two Doderer G gun 3090 cu. in. arrays at 2000 psi were operated in flip-flop mode. A line spacing of 25 m was achieved. The traces, with a record length of 6 s and a sampling interval of 2 ms, were processed to zero phase, binned using a 12.5 x 25 m grid, and had a pre-stack Kirchhoff time migration applied. In all seismic data shown the phase was rotated by 180° to conform with the Society of Exploration Geophysicists convention where a positive reflection coefficient is represented by a positive amplitude.

4.2.2 Endurance 3D seismic data

The Endurance 3D seismic survey (licence block: PEP52717) was acquired by the licence operator, New Zealand Oil and Gas, contracting the vessel *M/V Polarcus Alima* in 2013. The data were acquired with twelve 8.1 km-long streamers with a separation of 100 m. Two Bolt LLX-LLXT 3480 cu. in. arrays were operated in flip-flop mode at 2000 psi. The data were recorded with an 8 s record length and a sample interval of 2 ms and processed on board by ION Geophysical. Amplitudes were preserved during a pre-stack Kirchhoff depth migration. The final bin size is 12.5 x 25 m. For this study, the post-stack dataset is available along with seven pre-stack lines for AVA and velocity analysis.

4.2.3 Boomer 2D seismic data

As part of the funded work for this thesis, I led a University of Otago group that acquired high-resolution boomer seismic data in targeted areas within block PEP52717 using the University of Otago's *R/V Polaris II*. We operated a Ferranti Ocean Research Equipment (ORE) Geopulse sub-bottom profiler source together with a 75 m-long Geometrics MicroEel 24-channel streamer acquisition system. I used GLOBE Claritas® seismic processing software to apply a frequency filter between 100 and 1000 Hz as well as an FK-filter and a Kirchhoff time migration.

4.3 Methods

A subset of about 200 km of pre-stack CDP sorted 2D seismic data were extracted from the pre-stack time-migrated Endurance 3D volume for additional analyses. I carried out a high-density velocity analyses on these lines to refine the shallow velocity model and used the HampsonRussell software to evaluate AVA anomalies.

The original 3D seismic dataset was processed by ION (Lewis et al., 2014). They used a despiking routine followed by ION's "SWDnoise" noise attenuation process which decomposes the data into frequency bands and identifies and attenuates anomalous amplitudes. Guided waves were modelled in Tau-P space and subtracted from the shot gathers. Using the far field signature, an operator was derived to convert to zero phase. The wavelet distortion with time was corrected for using an inverse Q phase filter. Multiples were removed using a surface-related multiple elimination (SRME) method. A shot Tau-P mute was applied for additional noise attenuation. A parabolic radon demultiple routine was used to remove the last persistent effects of multiple reflections before application of a 3D Kirchhoff pre-stack depth migration and the conversion back to the time domain.

4.3.1 Velocity analysis

Velocity analyses based on semblance calculations are a standard procedure undertaken during long-offset seismic processing to determine accurate normal moveout (NMO) corrections and to better constrain migration. This procedure usually involves interactively picking optimal stacking velocities in CDP gathers spaced at regular intervals along a profile and interpolating laterally between the picked locations. For the highest spatial resolution, the semblance of every CDP can be picked. I adopted an automated high-density semblance-based velocity analysis scheme – details described by Crutchley et al. (2016) – implemented in the GLOBE Claritas seismic processing software to explore acoustic velocity behaviour in the vicinity of shallow bright spots. I automatically picked the semblance along a 2D seismic line extracted from the 3D dataset in 20 ms windows. The automatic semblance picks determine the maximum semblance function for each CDP. Spurious picks are an inevitable consequence of the automatic picking routine due

to random or coherent seismic noise. However, the statistical approach succeeds because of the high-density of velocity picks, that will mainly contain picks from real reflections representing the underlying geology. To obtain 2D velocity models from the picks, it is essential to filter out interval velocity values that are geologically implausible and then smooth the model laterally and in time.

4.3.2 AVA analysis

The 8 km-long streamer provides more than sufficient offsets to study amplitude variation with angle (AVA) in these data. The Zoeppritz equations describe the general isotropic and elastic behaviour of a P-wave incident on an impedance boundary (Zoeppritz, 1919). They define the P-wave reflection coefficients at various angles as well as the partitioning of P- and S-wave and transmitted components. In practice, these equations are often unpractical and too complex to estimate how amplitudes change with changing rock properties. Therefore, several authors derived simplified approximations. One of the most popular approximations was derived by Aki & Richards (1980) which has been reworked for different purposes (e.g. Wiggins et al. (1983)):

$$R(\theta) = \mathbf{A} + \mathbf{B}\sin^2\theta + \mathbf{C}\sin^2\theta\tan^2\theta$$

$$\text{where } \mathbf{A} = \frac{1}{2} \left(\frac{\Delta V_p}{V_p} + \frac{\Delta \rho}{\rho} \right), \quad \mathbf{B} = \frac{\Delta V_p}{2V_p} - 4 \left(\frac{V_s}{V_p} \right)^2 \left(\frac{\Delta V_s}{V_s} \right) - 2 \left(\frac{\Delta V_s}{V_p} \right)^2 \left(\frac{\Delta \rho}{\rho} \right)$$

$$\text{and } \mathbf{C} = \frac{1}{2} \frac{\Delta V_p}{V_p}$$

$$\text{with } V_p = \frac{V_{p1} + V_{p2}}{2}, V_s = \frac{V_{s1} + V_{s2}}{2}, \rho = \frac{\rho_1 + \rho_2}{2}$$

$$\Delta V_p = V_{p2} - V_{p1}, \quad \Delta V_s = V_{s2} - V_{s1}, \quad \text{and } \Delta \rho = \rho_2 - \rho_1$$

This equation (often referred to as the Aki and Richards approximation) is the basis for most AVA analysis today. The first term of the equation (A) represents the zero offset/angle reflection coefficient also known as ‘‘Intercept’’. The second term (B) describes the angle dependent effect on the reflection coefficient (often called ‘‘Gradient’’) while (C) determines the curvature of the reflectivity response close to the critical angle.

According to Shuey (1985), the third term can be dropped for angles of less than 30°-40°, leaving a simple linear regression two-term equation known as Shuey's equation:

$$R(\theta) = A + B\sin^2\theta$$

This simplified version is generally not used to predict seismic amplitudes at various angles but is rather a tool to easily derive regression coefficients A and B for a range of AVA attributes. Rutherford & Williams (1989) and later Castagna & Swan (1997) classified AVA responses of gas-charged sand with an overlying shale layer into four categories or classes (Figure 4.3).

Class 1: Gas-charged sands have a higher relative impedance than the overlying shale, resulting in a strong positive intercept amplitude that decreases with angle, with a potential phase reversal.

Class 2: Gas-charged sands have a similar impedance to the overlying shale resulting in a small intercept amplitude and negative gradient.

Class 3: Gas-charged sands have a lower relative impedance than the overlying shale resulting in a strong negative intercept amplitude and negative gradient.

Class 4: Gas-charged sands have a lower relative impedance than the overlying shale resulting in a strong negative intercept amplitude and positive gradient.

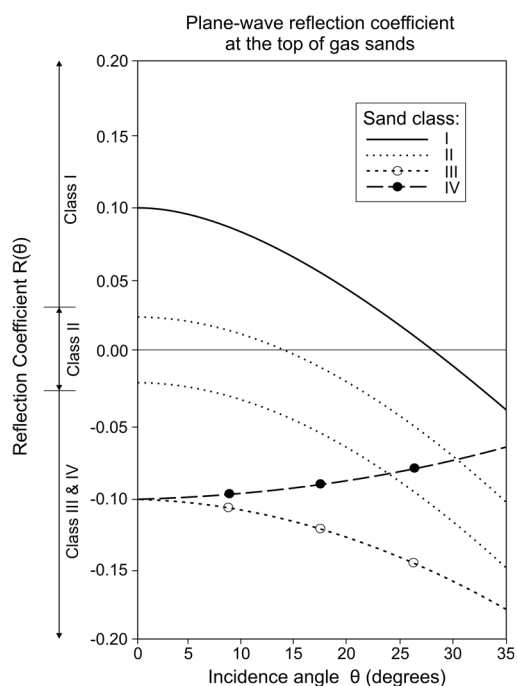


Figure 4.3: Possible AVA responses of a gas-charged sand with overlying shale, as proposed by Castagna & Swan (1997).

Gas-charged sands, due to their low impedance and abnormally low Poisson's ratios, embedded into sediments with a higher impedance and 'normal' Poisson's ratio should generally result in a negative reflection coefficient with an increase of reflected P-wave energy with increasing angle of incidence (Class 3 AVA anomalies) (Castagna and Backus, 1993).

I used several AVA techniques including AVA gradient analysis, AVA classification by cross-plotting and AVA attribute analysis. In Figure 4.10 I show an AVA attribute that displays the product of Intercept (A) and Gradient (B) and therefore positively highlights Class 3 AVA anomalies as well as positive intercept amplitudes with a positive gradient i.e.:

$$(-A) * (-B) = +AB = (+A) * (+B)$$

4.3.3 Interpretation

I loaded the data into the IHS Markit Kingdom software for visualisation and interpretation. This software also provides algorithms for seismic attribute analysis. The semblance-based coherency attribute highlights lateral changes between adjacent traces and hence was used to detect and map structural discontinuities. In general, 3D seismic coherency calculations are efficient for delineating fault systems (Marfurt et al., 1998). The attribute uses a 3D semblance based coherency algorithm to detect lateral variations in stratigraphy, lithology or porosity. The semblance is a measure of coherent power between a certain number of traces versus the total power of all traces. The semblance at a certain time or depth is calculated by:

$$Semb(z) = \frac{\sum_{\tau=-\frac{N}{2}}^{\frac{N}{2}} \{ \sum_{m=1}^M f_m(z + \tau) \}^2 - \sum_{\tau=-\frac{N}{2}}^{\frac{N}{2}} \sum_{m=1}^M f_m^2(z + \tau)}{\sum_{\tau=-\frac{N}{2}}^{\frac{N}{2}} \sum_{m=1}^M f_m^2(z + \tau)}$$

where $f_m(z)$ is the m 'th trace of the gather

N is the length of the computational window in time and depth

and z specifies either time or depth

Lateral similarity variations depend on the number of trace inputs which are specified depending on the signal-to-noise ratio, the bed curvature and the resolution of the seismic data. Poor signal-to-noise ratios and low-quality data require more traces, whereas higher curvature and higher resolution datasets require fewer traces. The time window over which the similarity attribute is calculated depends on the data resolution but also on the aim of the study. Detection of small stratigraphic features and discontinuities requires a small time window corresponding to the highest frequency apparent in the data. On the contrary, near-vertical features such as faults can be better enhanced using longer time windows.

Changes in seismic reflection patterns can be visualised by the energy envelope, which is useful for revealing pronounced acoustic impedance contrasts associated with gas accumulation, changes in depositional environments or sequence boundaries.

I picked key horizons in the datasets and stratigraphically validated them using Galleon-1, Cutter-1, Endeavour-1 and Clipper-1 exploration wells (Figure 4.1). Horizons without calibration were named “intra” (e.g. intra-Eocene) to reflect the age estimation. Horizons were picked after Strogon and King (2014)(Figure 4.2) but are mainly labelled using the international chronostratigraphic chart. I picked reflections based on their seismic character (e.g., reflectivity, continuity, dip and stratigraphic framework) and used seismic attributes to identify discontinuities and lithological changes.

4.4 Results

4.4.1 Polygonal faults

Three individual polygonally faulted tiers in Paleocene to Oligocene strata are identifiable in the Canterbury Basin seismic data. The uppermost Eocene polygonal faulted tier, “tier-1” extends up to the Marshall Paraconformity with a total thickness of ~400 ms TWT. In the lower Eocene strata, “tier-2” has a thickness of ~100 ms TWT and partly intersects with an upper Paleocene to lowermost Eocene polygonal faulted “tier-3” (Figure 4.4). These three faulted tiers are separated by layers of mostly continuously bedded strata that contain only rare faults. The faults of tier-1 show the typical decrease in throw towards the upper and lower boundaries of the tier (Figure 4.5). Observed dips range between 20° and 40° measured orthogonal to strike direction and the spacing between faults ranges from 200 to 300 m. The maximum throw is up to 30 m whereas the minimum observable throw is determined by the vertical resolution of the seismic data (~10 m in the Waka 3D and ~20 m in the Endurance 3D seismic datasets). Most faults have a gently listric behaviour, as described elsewhere (Cartwright, 2011, 1994a).

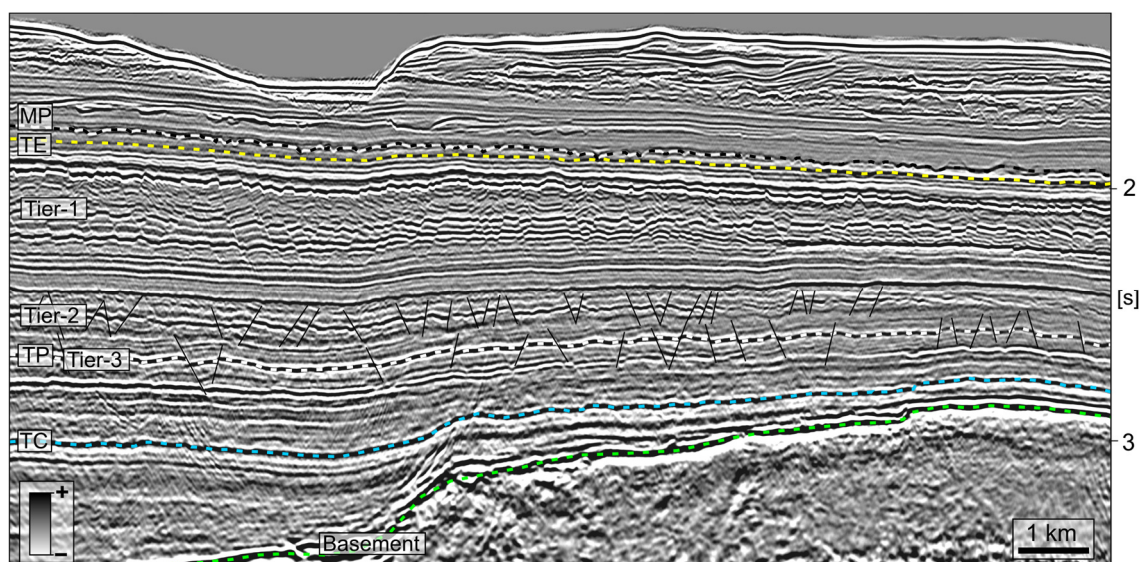


Figure 4.4: Overview of the three tiers of polygonal faults within Eocene and Paleocene strata. Key seismic reflectors are annotated and labelled according to the same colour scheme and nomenclature as in Figure 4.2. The broken green line marks the Basement.

The upper extent of polygonal faults is generally coincident with the Marshall Paraconformity although some faults are observed to cross the unconformity terminating in a layer of turbidite channel-levee deposits. The data show no evidence of faults continuing up to the seafloor or any direct connection of faults to present-day seafloor pockmarks. On the surface of the Marshall Paraconformity, depressions are observed which often seem to nucleate on the uppermost extent of polygonal fault planes (Figure 4.5). The depressions are between 100 and 300 m in diameter and exhibit the same northeast-facing oval to crescent-shape as modern-day seafloor pockmarks (Hillman et al., 2018). The dip of the maximum similarity seismic attribute highlights strong dips along the Marshall Paraconformity (Figure 4.5B). The dips in most pockmarks are steeper along their southwestern sides. Seismic reflectivity is higher within the pockmarks compared to surrounding strata. The pockmarks mainly occur in the southern part of the basin.

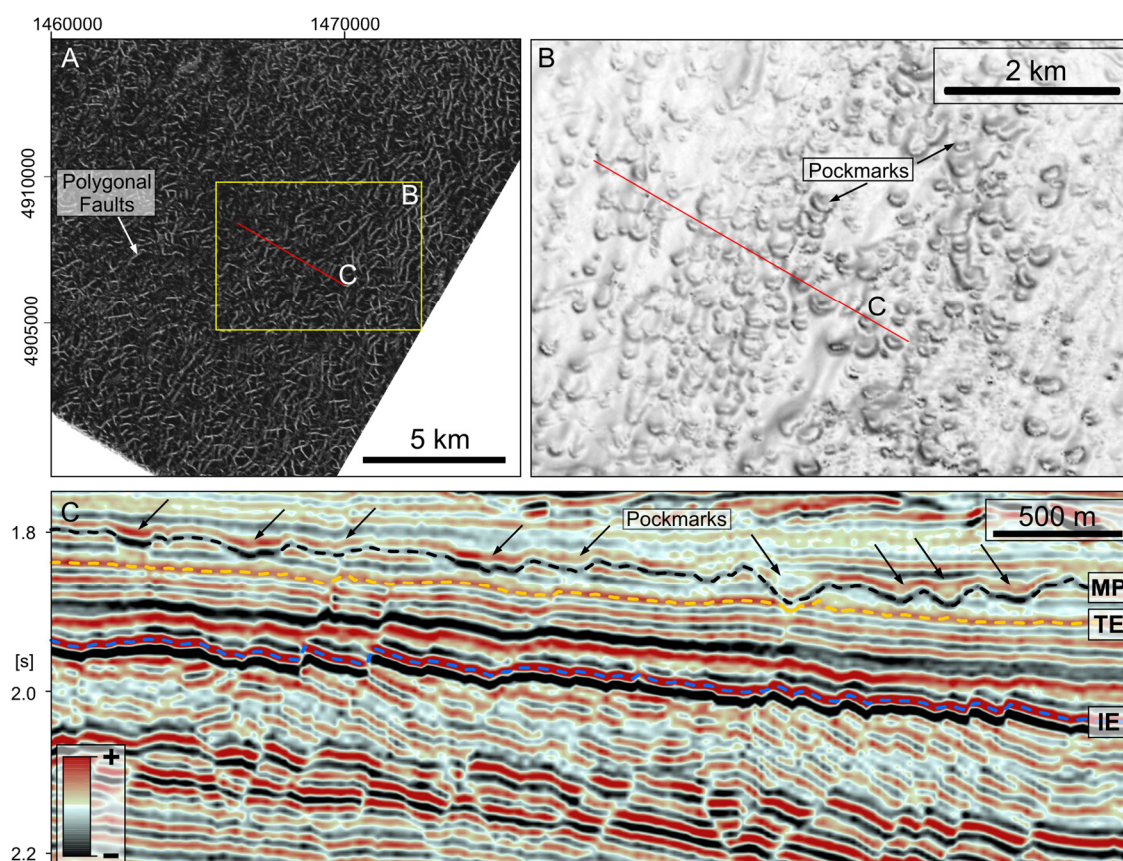


Figure 4.5: A) Horizon slice of the similarity seismic attribute extracted along the broken blue horizon in C. Light colours indicate low similarity values and are therefore indicative of discontinuities. B) Horizon slice of the “dip of maximum similarity” seismic attribute along the black horizon (MP: Marshall Paraconformity) marked in C. Darker colours indicate steeper dips along the horizon. C) Seismic section through a polygonal fault system and buried pockmark field (see Figure 4.1 for line location).

4.4.2 Surface of the Marshall Paraconformity

While numerous buried seafloor depressions are apparent on the surface of the Marshall Paraconformity in the Waka3D seismic dataset (Figure 4.5), the same surface shows widespread buried channel systems in the Endurance 3D as well as in the Waka3D data (Figure 4.6). The channels run roughly parallel to the present-day coastline in the Waka 3D and bend basinward in the Endurance 3D. Basinward and further north, additional possible channels and canyons were interpreted from 2D seismic lines by Barrier (2019) and the Canterbury paleogeography was interpreted. In Figure 4.6, the location of the buried channels and their expression on the surface of the Marshall Paraconformity are shown with a seismic cross-section from the Endurance 3D dataset. Dashed red lines in Figure 4.6A are interpolated

where no data are available. The channels are clearly visible in a 2D seismic line between the two 3D seismic datasets (Figure 4.6).

In the north of the canyon, a circular, crater-like morphology is apparent (Figure 4.8C). It is composed of a central mound with a height of ~ 100 m and a rim surrounding the mound with a radius of ~ 2 km. This crater-like structure is further described in Section 4.4.4.

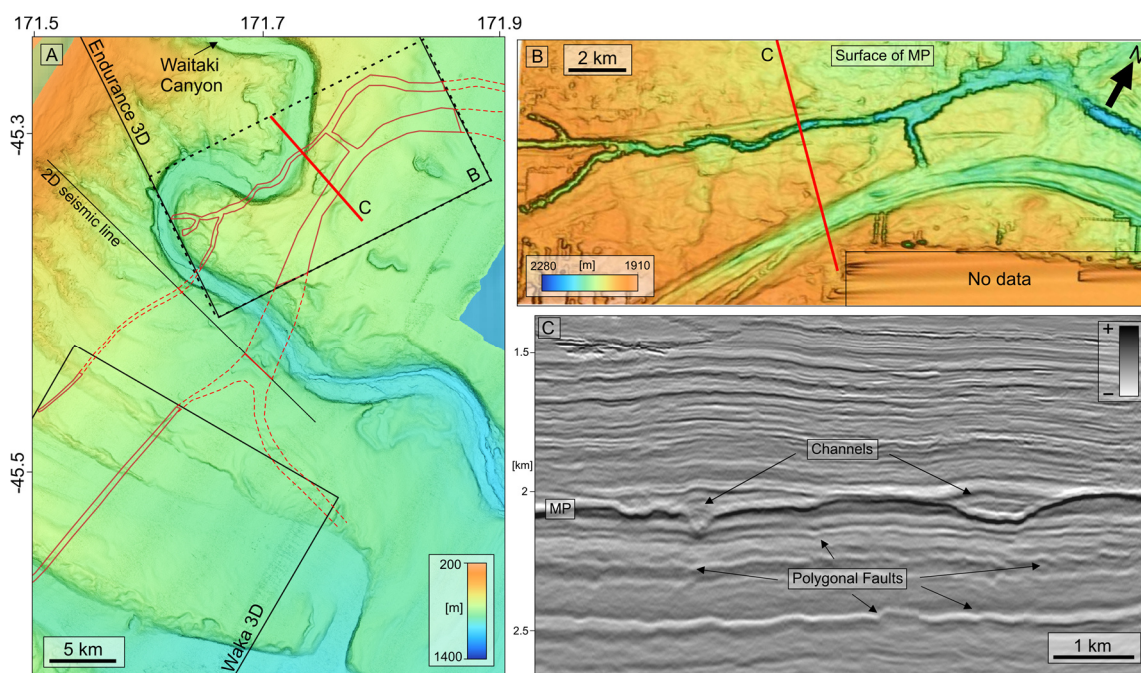


Figure 4.6: Comparison of A) present-day submarine canyon system – exemplified by the Waitaki Canyon and channel, with the locations of buried channels on the Marshall Paraconformity outlined in red. B) buried channel system apparent on the surface of the Marshall Paraconformity (MP). C) Seismic cross-section through the buried channels, above the Eocene polygonal fault.

4.4.3 Mounded structures associated with radial faults

The polygonal fault systems observed in the seismic data are variably affected by a range of sub-circular mounded structures originating from Cretaceous strata (Figure 4.7). The descriptive term “mounded structure” is used here prior to evaluating the formation mechanisms of the features in the discussion. The mounds at the Top Cretaceous reflector show diameters between 1 and 3.5 km and heights ranging from 90 to 350 m. The topographic aspect ratios (height divided by width) are close to 0.1 at the Top Cretaceous horizon and drop down to a mean of 0.056 on the Intra Paleocene horizon.

The internal structure of the mounds appears chaotic and Cretaceous sediment layers beneath the mounds are disrupted or deflected upwards (Figure 4.7). The mounds mainly affect Cretaceous and Lower Paleocene strata while Upper Paleocene and Eocene sediments seem widely unaffected and mainly onlap onto the flanks of the mounds (Figure 4.7A). In two cases though, amplitude anomalies above Mound 7 and Mound 9 are recognised and extend up to the Oligocene Marshall Paraconformity or even the present-day seafloor (Figure 4.8 and Figure 4.10).

In the Paleocene polygonal faulted tier-3, in the proximity of the mounded structures, faults predominantly developed in a radial sense, with fault segments radiating outward from the centre of the mounds over a radius of up to 3 km (highlighted by arrows in Figure 4.7C and D). These radial faults are confined to tier-3 and often appear in parallel pairs with a separation of 100-200 m at the intra-Paleocene level, narrowing towards the base of the tier. This phenomenon of parallel polygonal faults has previously been described and interpreted by Cartwright (2011) as an indication for the high maturity of the polygonal fault system.

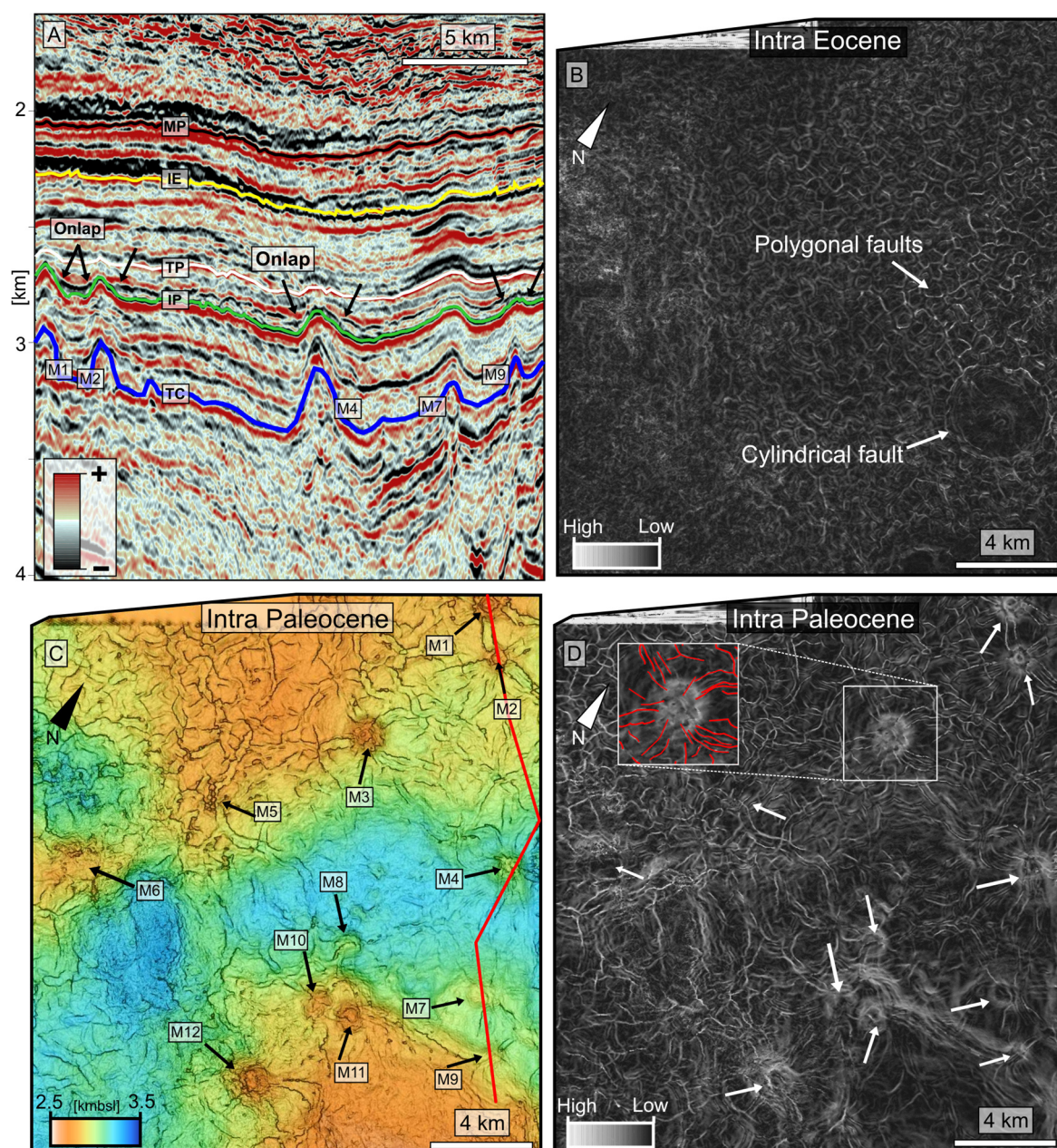


Figure 4.7: A) Seismic cross-section through mounded structures originating from Cretaceous strata. Upper Paleocene strata onlap onto the mounds. B) The dip of maximum similarity attribute extracted along the Intra Eocene horizon highlights polygonal as well as cylindrical faults. C) The surface of the Intra Paleocene horizon highlighting mounded structures with associated radial faults. The red line is the arbitrary seismic line shown in (A). D) The dip of maximum similarity attribute extracted along the Intra Paleocene horizon highlights polygonal and radial faults striking away from the mounds. Note: Each map (B, C and D) covers an identical areal extent and is plotted at the same scale.

4.4.4 Seismic character of cylindrical faults

Although the upper Eocene tier-1 polygonal faults are widely unaffected by the mounded structures and extend over a large area of the Canterbury Basin, including both 3D seismic datasets, there is a distinct cylindrical region without polygonal faults within this tier, located above the Cretaceous Mound M7 (Figure 4.7B and Figure 4.8). This cylindrical area has a radius of ~ 2 km and is bounded by discontinuities as indicated by low similarity values in Figure 4.7B. In seismic cross-sections, the cylindrical structure shows amplitude anomalies with enhanced and slightly different reflectivity behaviour in the interior of the cylinder (Figure 4.8). Disturbed and disrupted reflections characterise the highly faulted tier-1 surrounding the cylinder. Within the cylinder, reflections abruptly become smoother and more continuous. At the base of the polygonally faulted tier-1, the cylinder becomes slightly narrower and is characterised by low frequencies and high amplitudes starting with a broad negative polarity reflection (Figure 4.8A and B). These strong, low-frequency reflections appear to be confined to the lower Eocene strata below the uppermost tier-1 of polygonal faults. The strata surrounding the cylindrical Lower Eocene anomalies are mainly characterised by weak to very weak seismic amplitudes.

Although the cylindrical column of anomalies is bounded by faults in the polygonal faulted tier-1, the low-frequency amplitude anomalies below do not show any structural boundaries. The cylindrical anomalies are centred on the vertical axis of the Cretaceous mounded structure, denoted here as Mound M7. Reflections above Mound M7 are convex, but continuous, and are not disrupted by overlapping (Figure 4.8A and B) as is observed with the other mounded structures (Figure 4.7A).

A vertical stack of upward-bent reflections marks the centre of the cylindrical faults in the polygonal fault system (Figure 4.8B). These form a connection from Mound M7 to an irregular, ~ 100 m high and 500 m wide, elevated region that can be mapped on the Marshall Paraconformity (Figure 4.8C). This elevated mound is surrounded by a crater-rim like morphological expression ~ 4 km in diameter (Figure 4.8C). The semblance based high-density velocity analysis I conducted does not reveal a distinct velocity variation within or around the cylindrical anomaly. Also, no indications of cylindrical faults, other discontinuities

or pulled-up reflections are observed in the strata above the Marshall Paraconformity in this region.

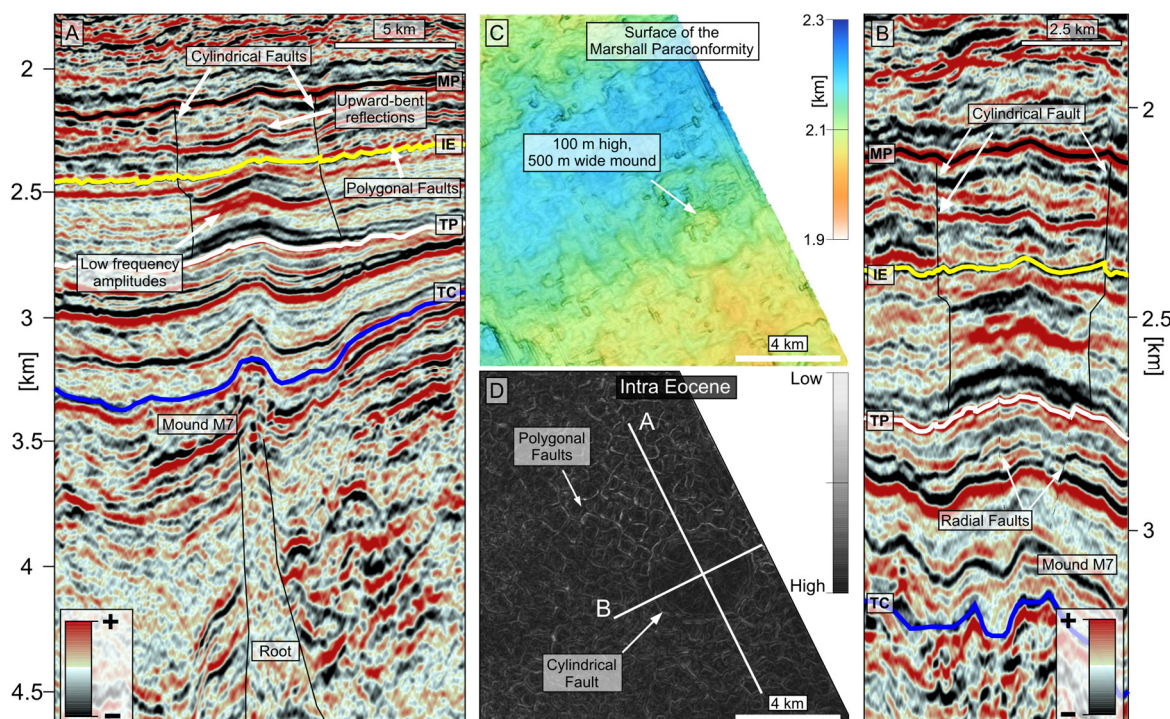


Figure 4.8: Map view and seismic cross-sections of the cylindrical feature. A/B) Seismic inline and crossline through the cylindrical faults. Low-frequency amplitude anomalies appear in lower Eocene strata below the polygonally faulted tier-1. Cylindrical faults form in the upper Eocene polygonally faulted tier-1. C) Depth map of the Marshall Paraconformity (MP-black horizon in A and B). D) The similarity attribute extracted along the Intra Eocene (IE-yellow) horizon shown in (A) and (B). Light colours indicate low similarity values and are therefore indicative of discontinuities.

In Figure 4.9B, sediment thicknesses between two Eocene horizons (red and yellow, Figure 4.9D) show drastically decreased sediment volumes within the cylindrical anomaly compared to the surrounding strata. In contrast, younger stratigraphic units within the cylinder (between the red and turquoise horizons in Figure 4.9D) appear to be thicker than the corresponding horizons outside (Figure 4.9A).

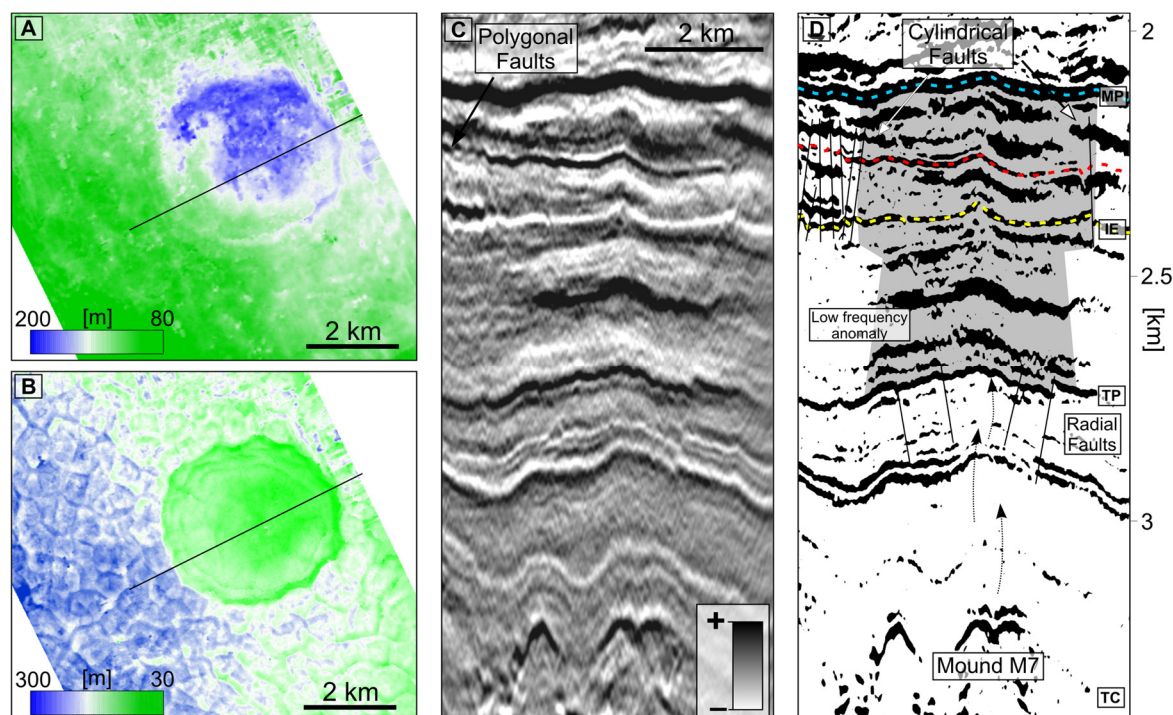


Figure 4.9: A) Layer thickness between turquoise and red horizons in D. B) Layer thickness between red and yellow horizons in D. C) Seismic crossline through the cylindrical anomaly, with interpretation in D. D) Black and white image of the energy envelope. Grey shaded area shows a cylindrical feature with cylindrical faults in the upper Eocene tier-1 of polygonal faults and low-frequency amplitude anomalies below. Radial faults spread out below the cylindrical feature, and above Mound M7. MP-Marshall Paraconformity (blue), IE-Intra Eocene (green), TP-Top Paleocene, TC-Top Cretaceous.

4.4.5 Shallow bright spots / chimneys

In the crest of a gully to the northeast of the Waitaki Canyon, shallow bright spots exhibit a strong phase reversal and are underlain by a curtain of acoustic suppression (Figure 4.10). Detailed high-frequency boomer seismic surveying, which targeted the bright spots, also reveals a zone of reduced amplitudes beneath shallow high-amplitude reflections (Figure 4.10D). The boomer seismic data reveal that the bright spots are located only a few tens of metres below the present-day seafloor. The summation of energy in the upper 100 m of the seafloor shows the distribution of shallow bright spots in blue colours in Figure 4.10C.

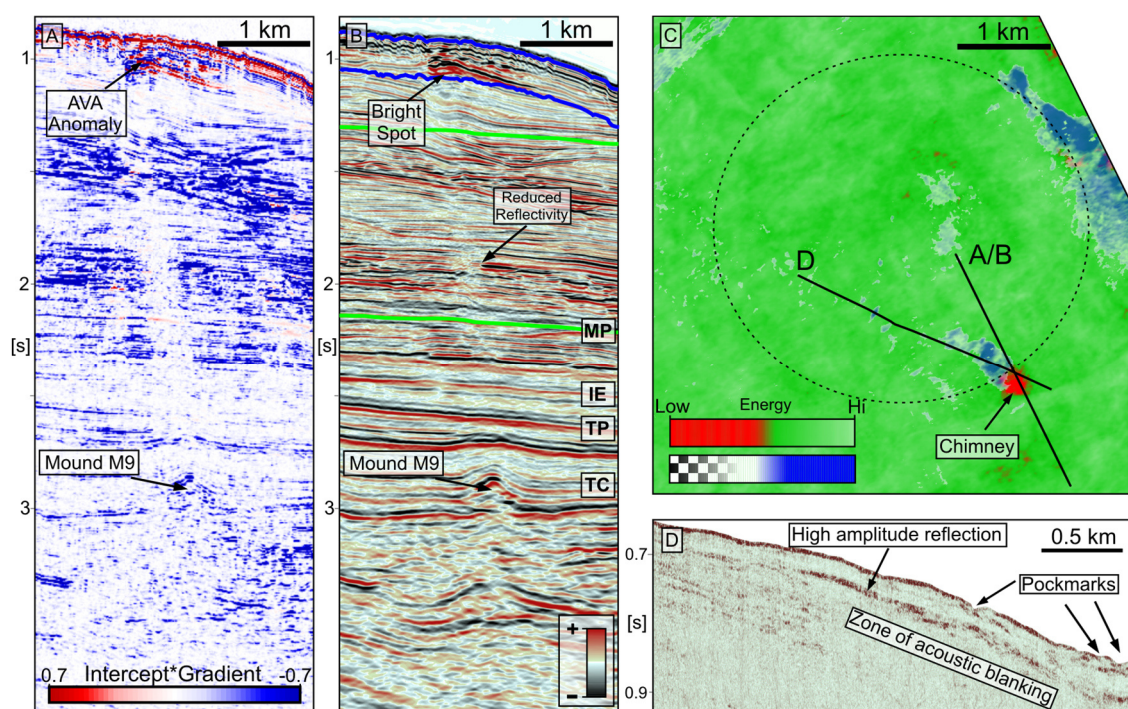


Figure 4.10: A) AVA-Product (Intercept \times Gradient) of the seismic section in B. Shallow bright spots show a distinct AVA anomaly with a subvertical zone of low AVA-Products connecting the bright spot to Mound M9. B) Seismic section showing the bright spot and slightly reduced reflectivity below. C) Map view around bright spots. Blue colours indicate high bulk energy in the uppermost 100 m beneath the seafloor (between blue horizons in B). Red/Green colours represent high/low bulk energy summations (respectively) between the green horizons. The dashed line indicates the location of cylindrical faults deeper beneath Mound M9. D) High-resolution boomer seismic data across the bright spot shown in (A) and (B). A high-amplitude reflection and an acoustically transparent zone below are visible.

The 3D industry seismic data reveal a near vertical zone of slightly reduced seismic amplitudes that connects one of the mounded structures (Mound M9) to the shallow bright spots (Figure 4.10A and B). Red colours in Figure 4.10C indicate low reflection energy values extracted in a 1 km thick window above the Marshall Paraconformity, while green colours represent higher values. The circular red region in Figure 4.10C, therefore, represents a sub-vertical, cylindrical low energy zone that connects Mound M9 to the shallow bright spots. This sub-vertical low energy cylinder is well imaged in the AVA section where it is characterised by an AVA product close to zero (Figure 4.10A). This very steeply basinward-dipping reduced amplitude zone is the result of small AVA intercept values rather than small AVA gradients. While an acoustic curtain and pulled down reflections are visible in the seismic amplitude data up to 400 ms below the bright spots, the corridor of low

AVA product extends downward roughly 3 s and terminates at the Cretaceous stratigraphic level at Mound M9. AVA analysis of the shallow bright spots beneath the seafloor reveals Class 3 AVA behaviour (increasing negative amplitudes with angle) resulting in a positive anomaly in the AVA attribute.

4.4.6 Velocity structure

I investigated seismic velocities along several 2D seismic profiles using a semblance based high-density velocity analysis. Velocities at the seafloor were set to 1500 m/s and gradually increase to about 3500 to 4000 m/s in the limestones around the Marshall Paraconformity (Figure 4.11). Below the Marshall Paraconformity, a low-velocity zone (LVZ) marks the Onekakara Group where polygonal faults are apparent. Within this group velocities gradually increase again and reach values of ~5000 m/s within the basement.

In the shallow areas velocities around the bright spots do not seem to be particularly different from their surroundings. No distinct low-velocity zone is apparent although the velocity increase with depth seems to be reduced in the vicinity of the bright spots (Figure 4.12).

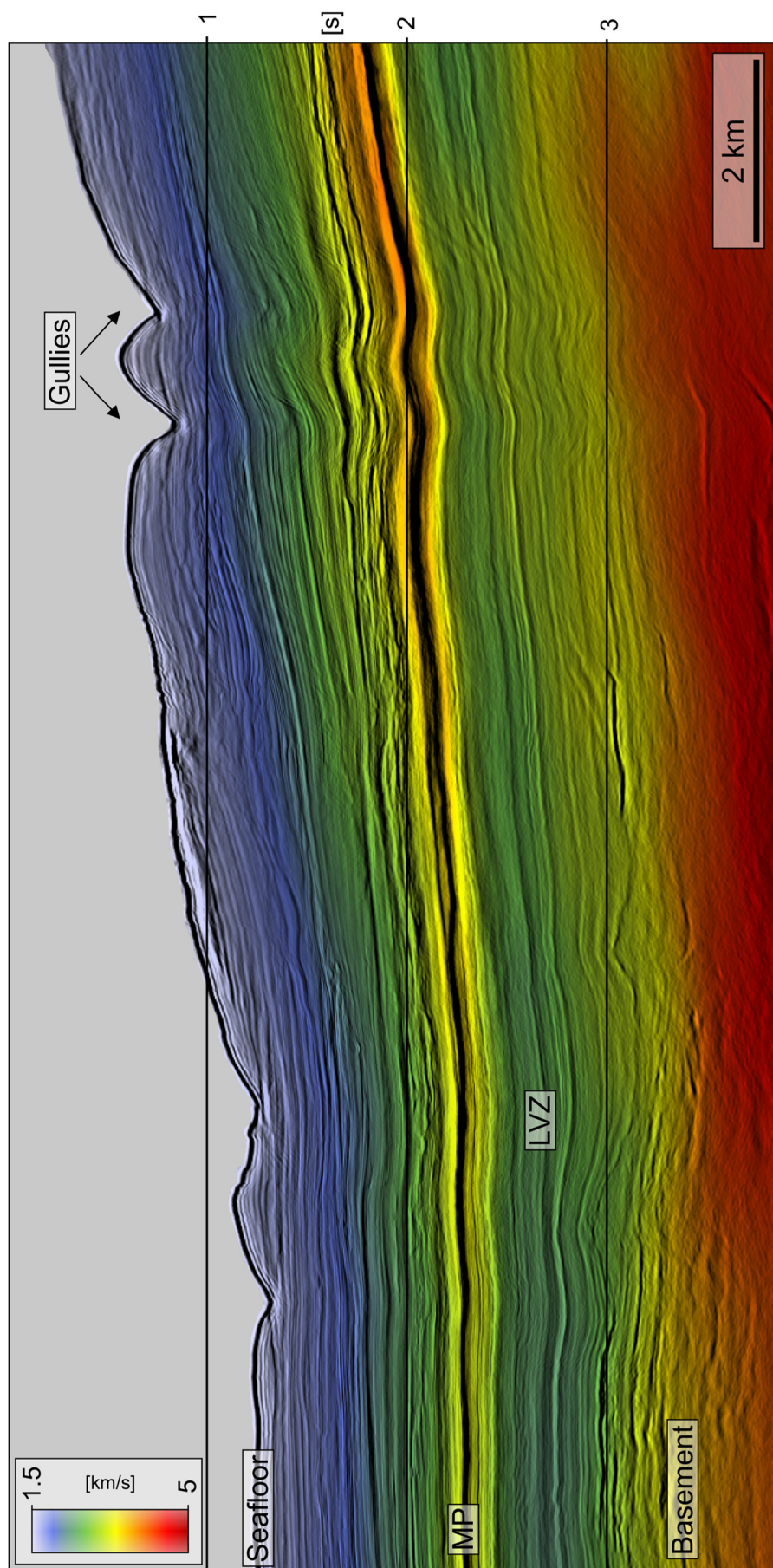


Figure 4.11: Seismic velocity structure of the Canterbury Basin, showing high velocities around the Marshall Paraconformity (MP) and a low velocity zone (LVZ) in the polygonally faulted intervals.

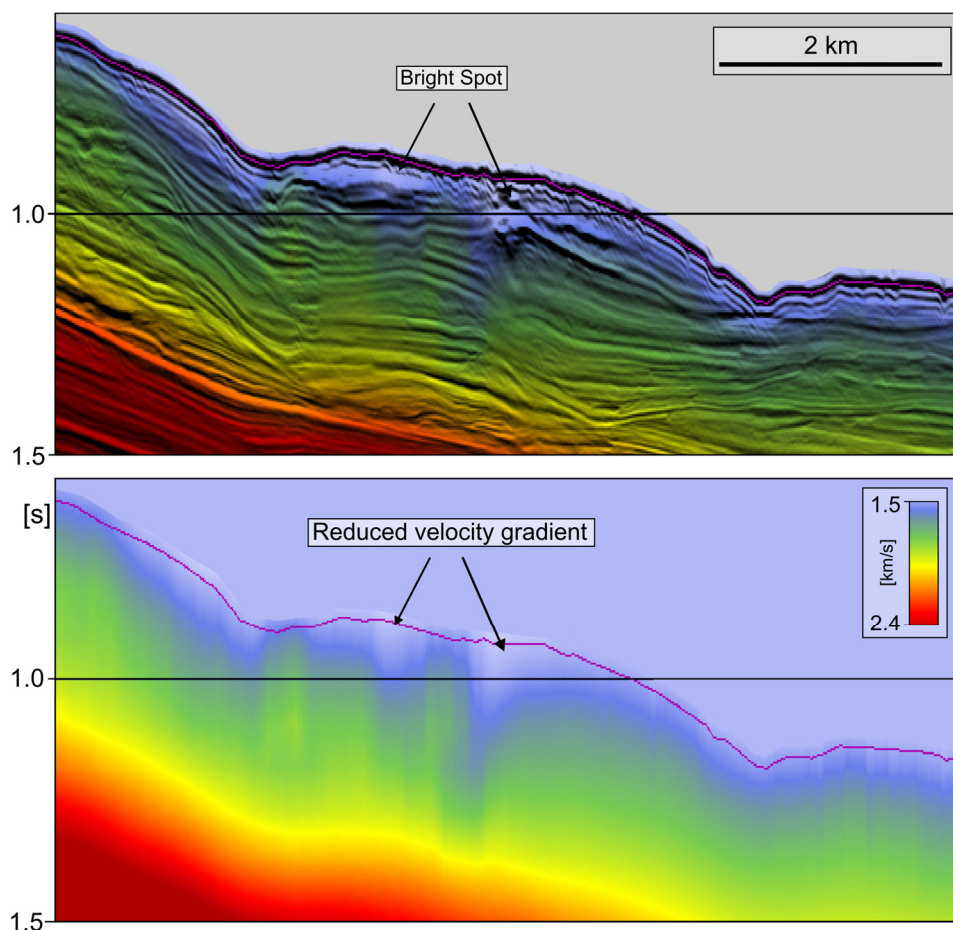


Figure 4.12: Seismic velocities around the shallow bright spots do not reveal a distinct low-velocity zone, but rather show a reduction in the shallow velocity gradient compared to surrounding sediments.

4.4.7 Angle stacks

Although I generally inspected the full angle stacks for data interpretation, I also generated different angle stacks by transforming offset gathers into angle gathers using the seismic velocities. This helps to quickly identify anomalous AVA behaviour and to examine if the far offset reflections reveal different structures compared to near offset reflections. In Figure 4.13, the reduced reflectivity is shown beneath the shallow bright spots. The low amplitudes are apparent in the near as well as the far-angle stacks. The overall lower frequency observed in the far angle stack is mainly the result of trace stretching during NMO-correction.

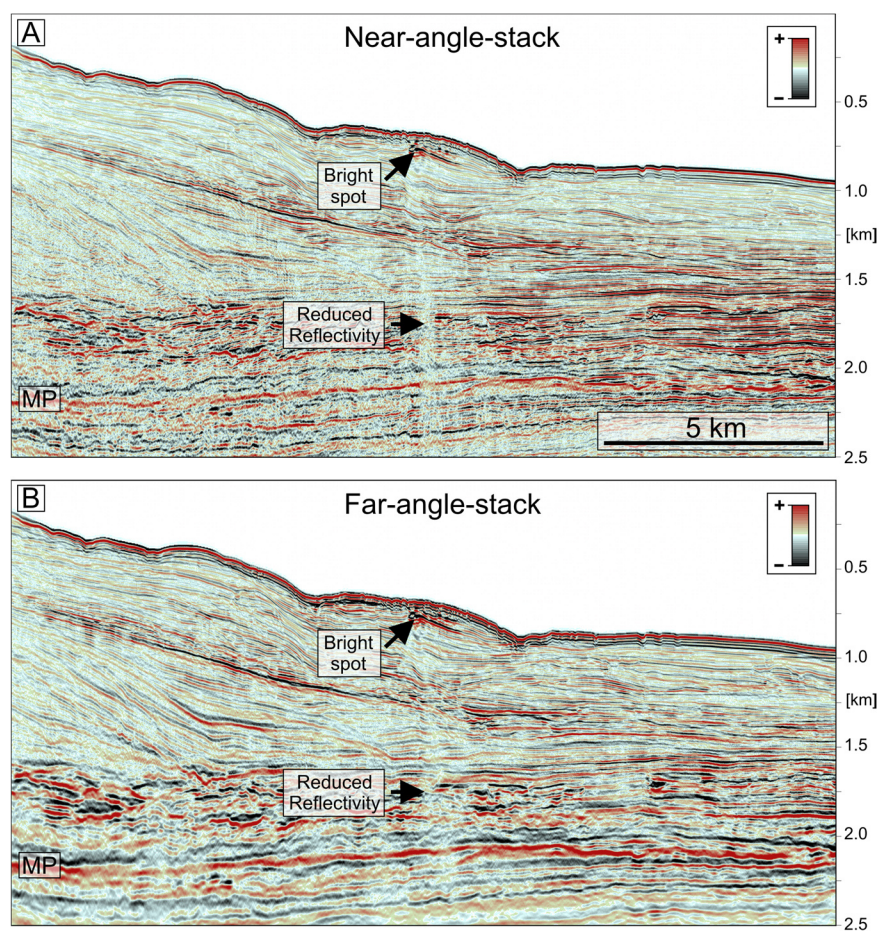


Figure 4.13: The near angle stack (5° - 14°) and far angle stack (32° - 41°) across the shallow bright spots both show the sub-vertical zone of reduced reflectivity. Marshall Paraconformity (MP).

4.5 Discussion

4.5.1 Formation mechanisms of the cylindrical anomaly

Upward-bent or pulled-up reflections are common phenomena in seismic data. They are often attributed to increased velocities in areas of enhanced gas hydrate concentrations or authigenic carbonate cement within fluid conduits (Hustoft et al., 2010). Pulled-up reflections in this sense are an artefact of seismic imaging that is caused by erroneous seismic velocities (in the conduits) used for processing the data. By contrast, fluids ascending vertically due to overpressured sequences can also hydraulically fracture the overburden and cause up-warped reflections through physical disruption of the strata (Karstens and Berndt, 2015; Løseth et al., 2011).

The up-warped reflections I observe in the centre of the cylindrical amplitude anomaly above the mounded structure M7 show no indications of enhanced velocities in the semblance-based velocity analysis. As such, I can be confident that they represent real upward bending of sedimentary layers rather than being an artefact of seismic imaging. Due to the similar seismic expression to structures observed by Berndt (2005), Berndt et al. (2003), Gay et al. (2012), Karstens and Berndt (2015) or Løseth et al. (2011), I interpret that the up-bending represents a structural conduit for upward migrating fluids. The location of the crater-like circular expression on the surface of the Marshall Paraconformity above the fluid conduit (Figure 4.8) suggests an intrinsic link between the conduit and the circular feature.

Sediment volcanoes exhibit a wide variety of morphologies on land, at the seabed and in buried surfaces (Mazzini and Etiope, 2017; van Loon, 2010). They are the surface expression of a three-phase discharge (sediments, liquids, and gas) related to gravitational instability and hydrocarbon producing systems (Etiope and Martinelli, 2009). Onshore analogues of crater-like mud volcano morphologies sourced from hydrocarbon-bearing basins have previously been described by Mazzini and Etiope (2017) and Stoppa (2006). The crater-like morphology on the Marshall Paraconformity clearly indicates extruded and discharged sediments onto the unconformity with the feeding system indicated by the upward-bent reflections.

I therefore interpret the intrinsic link between the conduit and the crater-like impression to indicate some type of sediment volcanism. The decreased and increased thicknesses of two stratigraphic intervals within the cylinder compared to its surrounding (Figure 4.9A and B) suggest remobilisation and removal of sediment from the deeper sequence and intrusion of the sediment into the shallower sequence.

The source of the deposited sediments above Mound M7 is difficult to assess and could be from either the Cretaceous stratigraphic level beneath Mound M7 or partly from younger stratigraphic levels (Figure 4.9A and B). The fluids and overpressure necessary to transport the solid phase in sedimentary volcanoes in general similarly can be sourced from different stratigraphic levels (Planke et al., 2003).

4.5.2 Cylindrical and radial faults

Curved and listric faults are not uncommon in polygonal fault systems. Cartwright (2011) suggested a lithological effect on fault curvature and noted that biosiliceous tiers tend most often to create listric faults. Circular patterns (in planview) within polygonally faulted tiers have been reported above and around morphological depressions such as pockmarks (Ho et al., 2018b, 2013; Morgan et al., 2015). Concentric extensional faults are described in the literature in various geological settings, e.g., around collapsing salt diapirs (Stewart, 2006), in glaciers (Malthe-Sorensen et al., 1999), volcanic and mining-related settings (Branney, 1995) and in polygonal fault systems developing due to a local anisotropic stress field above buried pockmarks (Ho et al., 2013; Morgan et al., 2015). Concentric reverse fault patterns have only rarely been described since they pose a “space problem”; they have been described in the literature around rapid and forceful intrusions (Galland et al., 2009; Quatrehomme and İşcan, 1998).

Concentric normal fault patterns associated with fluid flow have previously been reported around mud volcanoes in Azerbaijan (Davies and Stewart, 2005; Planke et al., 2003). While Planke et al. (2003) describe a circular subsidence fault pattern with a radial distance of about 100 m dipping towards the centre, Davies and Stewart (2005) report on concentric faults similar to the ones observed here in

the polygonal fault system dipping away from the central feeder system over distances of several kilometres. They attribute their existence to shear stress at the base of the mud volcano due to lateral compaction of the edifice muds. I don't observe a large mud volcanic edifice and the cylindrical faults are confined to the polygonal fault system. This suggests a compactional origin due to differential compaction and dewatering mechanisms within tier-1 rather than shear stress-related mechanisms.

Gay et al. (2012) imaged a cone-shaped amplitude anomaly around a fluid conduit in seismic data and inferred, through sandbox models, that it represents a zone of sediment deformation by upward migrating fluids. This would imply a different stress field within the cylinder that surrounds the pipe, which would affect pore pressure and therefore sediment compaction. I assume the strong low-frequency reflections beneath the Intra Eocene horizon (Figure 4.8) to be fluids expelled by the sediment volcano feeder system which accumulated beneath the low permeability tier-1 containing the polygonal faults. This cylindrical accumulation could be the reason for an axisymmetrical stress field within the cylinder in the upper Eocene tier-1, rather than a conical shaped anomaly like that described by (Gay et al., 2012).

While concentric faults are mainly associated with subsidence, radial faults generally occur in regions of doming (Hansen et al., 2005; Stewart, 2006; Waghorn et al., 2017). Radial faults above hydrothermal vents and sills have previously been described by Hansen and Cartwright (2006), Kjoberg et al. (2017) or Schmiedel et al. (2017). Although sill intrusions exist in the area (Reeves et al., 2018), no indications for a direct connection between the mounds to magmatic intrusions are observed. I therefore assume the radial fault patterns I observe (Figure 4.7) to have resulted from an anisotropic stress field induced by Cretaceous sediment intrusions into Paleocene sediments. Although I don't interpret the mounds themselves to be of volcanic origin, fluids and overpressure required for sediment remobilisation could have originated from volcanic activity at depth. The Paleocene age of the intrusions is mainly indicated by overlapping reflections onto the seismically chaotic mounded structures (Figure 4.7). Hansen et al. (2005) described similar buried mounded structures with radial fault patterns within an overlying polygonal fault

system in the Vøring Basin on the Norwegian continental shelf. Due to the similar seismic expression, the same aspect ratios, and the analogous influence on the surrounding polygonal fault system to what Hansen et al. (2005) described, I assume a similar formation mechanism by intruding sediments and a resulting anisotropic stress field surrounding the mounds.

4.5.3 Lack of polygonal faults within the cylindrical feature

It is intriguing that although the upper Eocene polygonal fault system extends over the entire basin, no polygonal faults have formed within a ~2 km radial distance of the central fluid conduit around Mound M7. Horizontal, continuous and mainly undisturbed reflections within the cylindrical structure suggest that polygonal faults never nucleated within this body (i.e., ruling out a reworking, overprinting or healing of faults in this zone).

Despite two decades of research on polygonal fault nucleation and development the processes leading to shear failure are still widely debated and mechanisms like density inversion (Henriet et al., 1991; Watterson et al., 2000), overpressure collapse (Cartwright, 1994b), volumetric contraction (Cartwright and Lonergan, 1996), syneresis (Cartwright and Dewhurst, 1998; Dewhurst et al., 1999), low coefficient of friction (Goult, 2001b), particle scale contraction (Shin et al., 2008) and diagenetically induced shear failure (Cartwright, 2011) have been proposed. Since all mechanisms include sediment compaction and episodic fluid expulsion of very-fine to fine-grained tiers, a local difference in sediment composition (i.e. grain size) or burial history (compaction) could be invoked to explain the absence of polygonal fault nucleation within this cylinder. I cannot envisage any feasible geological process that would result in a local, cylinder-shaped change in depositional lithology or burial history. Compaction, however, can also be influenced by local pore fluid pressure and sediment composition could have been changed by remobilisation and the intrusion of sediments.

The differential stress field that would be expected within the cylindrical feature (discussed in Section 4.5.2 with respect to the study of (Gay et al., 2012)) could have had important implications for pore fluid pressure and sediment compaction, thereby influencing polygonal fault development. Over-pressured

fluids migrating upwards through the plumbing system of the sediment volcano could have introduced increased pore fluid pressure around the feeder system. This would reduce the effective stress of the sediment and therefore affect compaction, contraction and diagenesis of the material. Since these are the main driving forces for all polygonal fault formation mechanisms described in the literature, it seems possible that a local change in compaction history and effective stress could affect polygonal fault nucleation. In this case, I interpret that the cylindrical pattern surrounding the fluid pipe would mark the radial limits of where a pipe-induced increase in pore pressure was no longer strong enough to prevent polygonal faults from propagating which could explain the perfectly circular planform.

Alternatively, a change in lithology due to intruding coarser-grained material e.g. intruding sandy sediments into the fine-grained sedimentary sequences is known to prevent polygonal faults from nucleating (Cartwright, 2011; Cartwright et al., 2003). Sand intrusions often exhibit conical or saucer-shaped geometries, especially when intruding pervasive polygonal fault systems (Bureau et al., 2013; Chenrai and Huuse, 2020; Hurst et al., 2003; Monnier et al., 2014; Shoulders et al., 2007) and are mainly characterised by high-amplitude anomalies, a highly disrupted top and base and often chaotic internal reflections (Bureau et al., 2013; Hurst et al., 2003; Hurst and Cartwright, 2005). Although I do not observe these characteristics, it is possible that thin (sub-seismic scale) permeable stringers (i.e. sand injectites) could intrude the surrounding of the sediment volcano feeder pipe. Such permeable stringers would enable dewatering of their host strata. In the upper Eocene polygonal faulted tier-1 localized dewatering in this way could prevent polygonal fault nucleation. Figure 4.9 clearly indicates remobilisation and intrusion of sediments into this tier. An increased volume of coarser-grained material intruding tier-1 also could have changed the bulk lithology to a degree that it was no longer prone to polygonal fault formation.

The higher amplitudes and lower frequency of strata within the cylinder below polygonal fault tier-1 (Figure 4.8A and B) indicate a change in physical properties within this zone. I interpret this as being due to the presence of some amount of free gas within the cylinder, which would contribute to both an increase in amplitude and a decrease in frequency. Again, thin gas-charged sand stringers

might cause the low-frequency high-amplitude reflections in the cylinder below tier-1 (Figure 4.8). Since the anomalous high-amplitude reflections cannot be directly correlated to horizons surrounding the cylinder I assume accumulation of some amount of free gas below the polygonal fault tier-1 and horizontal radial migration.

Within tier-1, horizons are offset by polygonal and cylindrical faults but can generally be traced throughout the 3D survey and through the cylinder. This indicates deposition of sediments within the cylinder was contemporaneous to its surrounding and prior to the vertical migration of sediments and fluids.

4.5.4 Recent fluid migration

Although a distinct low-velocity zone around the bright spots is not obvious, the amplitude reversal, the acoustic curtain and the possible connection to deeper strata and the distinct class 3 AVA anomaly suggest that the shallow bright spots represent free gas (Figure 4.10).

The 300-m-wide near-vertical zone of reduced AVA attribute connects the shallow gas to Mound M9 at about 3 s TWT (Figure 4.10A). I do not interpret the blanked-out zone to be an imaging artefact (e.g., the high-reflection coefficient of shallow gas causing a zone of “acoustic turbidity” or a “seismic curtain” beneath) since it is not vertically aligned beneath the shallow gas but is rather offset slightly basinward (Figure 4.10B). Importantly, I note that the blanked-out zone is also visible in far angle stacks (32° - 41°) where the shallow gas can be under-shot to avoid any vertical imaging artefacts (Figure 4.13). I therefore interpret the feature to be a geological conduit (or “chimney”) that focuses fluid flow. Mound M9 appears to be the root of the chimney. Since Mound M9 shows no distinct differences to adjacent mounds at depth, I assume that it must have recently reactivated to create the chimney. The migrated seismic section shows mainly continuous reflections with no indications of sediment modification or deformation in or around the chimney, at the resolution of these data (Figure 4.10B). The presented data therefore suggest that active sediment remobilisation of Cretaceous sediment eased during the Paleocene below Mound M9. Paleocene to Eocene strata in this area mainly consists of fine-grained material with high porosities but low permeabilities

(Blanke, 2015). Since no faults are visible, I assume capillary invasion by gas and small-scale fracturing (sub-seismic scale) to be the most likely process for chimney formation.

4.5.5 Timing of fluid migration

Polygonal faults, in general, form during the early burial history of their host sediments (Berndt et al., 2012; Cartwright and Dewhurst, 1998). Pockmark formation above or within polygonal fault systems due to porewater expulsion and sediment compaction would therefore be expected to be contemporaneous with the faulting (Andresen and Huuse, 2011; Gay et al., 2004; Maia et al., 2016). In some cases, pipes or chimneys form within or above polygonal fault systems, channelling and episodically releasing fluids to form pockmarks (Berndt et al., 2003; Gay and Berndt, 2007; Ho et al., 2018a). In these cases, pockmarks can also form asynchronous to polygonal faults. However, no such pipes are observed above or within the tiers of polygonal faulting in this dataset. Although there seem to be several types of interaction between polygonal fault and pockmark formation, the location and extension of polygonal faults beneath and up to the Marshall Paraconformity suggest nucleation and growth prior to or during the formation of the Marshall Paraconformity.

Hillman et al. (2018) reported on the modification of present-day seafloor depressions by submarine currents on the Canterbury Slope. Due to their analogous expression in shape and size and their spatial proximity (Figure 4.14), I assume that similar currents are responsible for the northward facing elongated shape of the buried pockmarks in this study. This shows the potential of buried pockmarks to study past oceanographic conditions. Higher amplitudes in the seafloor craters are probably due to the removal of fine-grained material by seeping fluids leaving only coarse-grained highly reflective material or due to authigenic carbonate precipitation.

Our results show that Cretaceous sediment intrusions push up the lower Paleocene strata, creating mounded structures. Onlapping strata indicate a mid-Paleocene age of formation for most of the intrusions. Only Mound M7 seems to deflect Eocene and Oligocene sediments, indicating a later stage of formation.

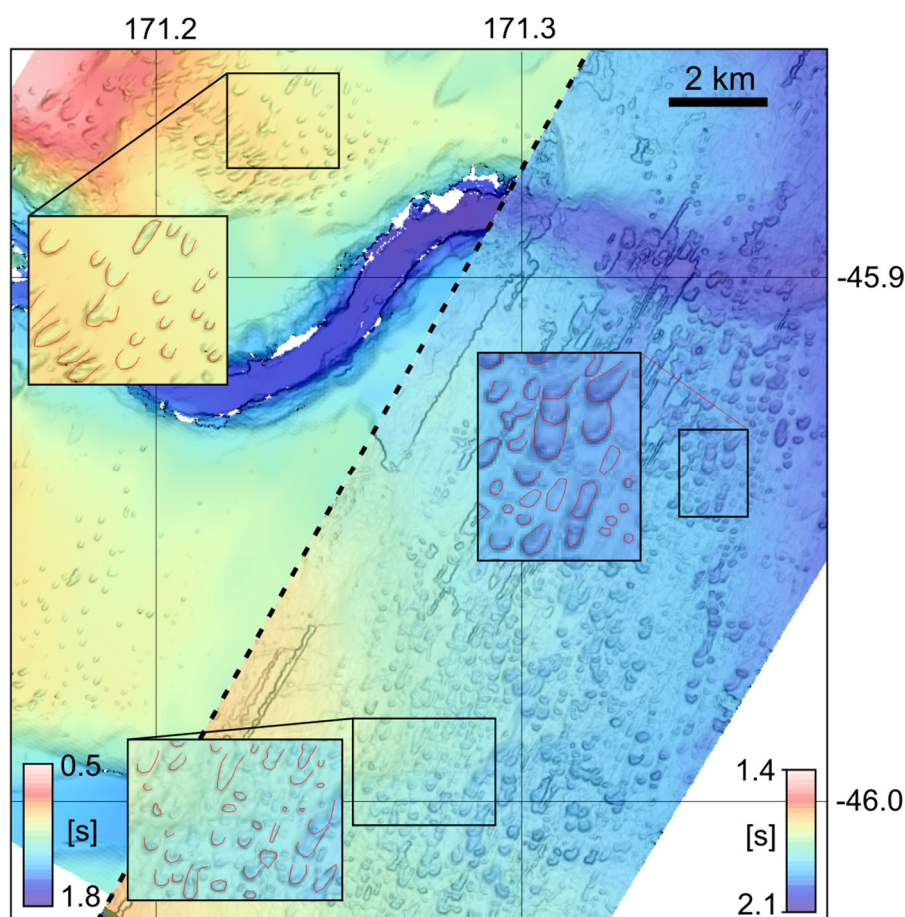


Figure 4.14: Comparison between present-day seafloor pockmarks (left of dotted line) and buried pockmarks on the Marshall Paraconformity (right of dotted line) (Figure 4.5) both, mapped in the Waka 3D dataset at different stratigraphic levels but in close spatial proximity.

The lack of any seismic evidence of fluid flow above the Marshall Paraconformity in the vicinity of anomalous Mound M7 suggests that fluid flow activity associated with Mound M7 has not occurred during the Neogene. In contrast, my results suggest relatively recent activity in the chimney above Mound M9. I assume that the feeder system beneath Mound M7 was sealed off and that the overpressured Cretaceous sequences beneath the level of the mounds switched to Mound M9, resulting in the establishment of a new chimney system (Figure 4.15).

The radial and polygonal faults in the Paleocene tier-3 probably formed during or shortly after the up-doming of Cretaceous sediment-pillows and laccoliths, as also suggested by Hansen et al. (2005). The polygonal and cylindrical faults in the upper Eocene tier-1 suggest that fluid actively migrated and altered the stress field during polygonal fault nucleation. This suggests that the sediment volcano formed prior to or simultaneously with the polygonal faults. Since

polygonal faults, in general, form during the early burial history of their host and the mud volcano edifice forms on the upper boundary of the polygonal faults (Marshall Paraconformity) a simultaneous formation seems likely.

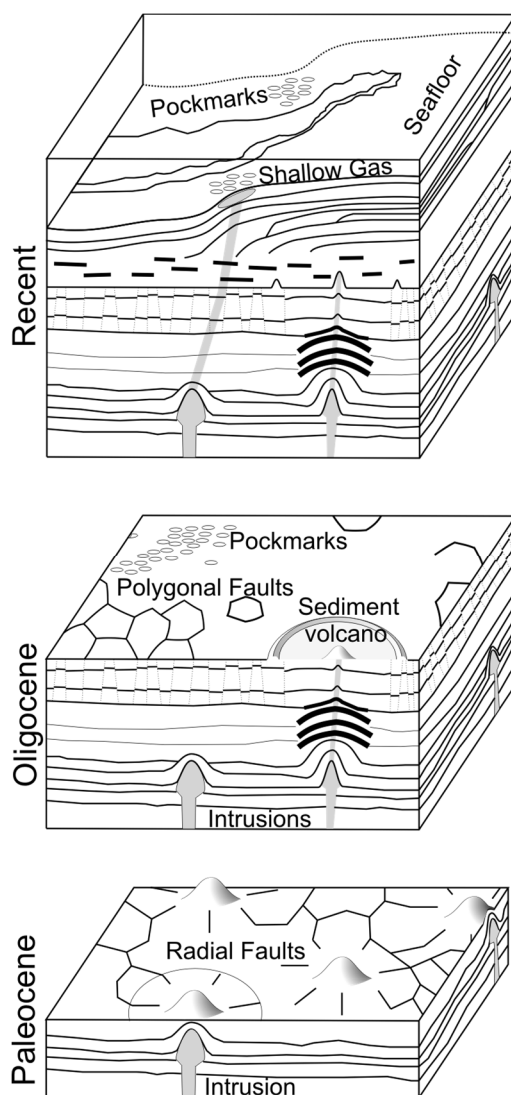


Figure 4.15: Schematic summary of mud and fluid migration in the Canterbury Basin. Paleocene mud intrusions are followed by Oligocene sediment volcanism and polygonal faults. Recent fluid migration from a reactivated sediment intrusion reaches all the way to the present-day seafloor.

4.6 Conclusions

Three fluid migration events imaged in the seismic data point to the existence of recent and past sediment migration and gas emissions in the Canterbury Basin, originating from Cretaceous sediments. Due to the difference in timing, the events show very different structural effects on the overburden sediment.

Shallow gas, manifesting itself in bright spots in the seismic data, represents a recent focused fluid migration event sourced from the same stratigraphic level as the sediment volcano. Due to the more lithified sediments at this stage, overburden sediment appears to be less deformed by the migrating fluids compared to the conduit feeding the sediment volcano.

Cretaceous intrusions into Paleocene strata indicate widespread sediment remobilisation in the Canterbury Basin during the Paleocene. I have imaged the plumbing system of an ancient sediment volcano that expelled material onto the surface of the Marshall Paraconformity. Reduced sediment thicknesses around the feeder system indicate that the Paleocene/Eocene sediment that hosts the plumbing system probably provided additional material that ascended and was intruded back into other (shallower) sedimentary formations. The sediment volcano plumbing system likely formed prior to or simultaneously with the upper Eocene polygonal fault system. Pockmarks on the same buried surface where sediments were extruded indicate additional fluid expulsion from another source, potentially the polygonal fault system. Present-day seafloor depressions as well as buried pockmarks could not be related to any hydrocarbon seepage and should therefore not be used as hydrocarbon proxies in this case.

The lack of polygonal faults within a cylindrical feature around the fluid conduit (over a radial distance of 2 km) is a striking observation which could be explained by a number of processes.

- 1) Increased pore pressure and decreased effective stress around the sediment volcano feeder pipe resulted in a different compaction history compared to the surrounding strata.

4.6 Conclusions

2) Permeable, thin (sub-seismic scale) stringers intruded into the fine-grained material of polygonal fault tier-1. These permeable stringers supported dewatering of tier-1 and therefore changed the compaction history.

3) Remobilised coarser-grained material extruded outward from the feeder pipe and changed the lithology within a cylindrical area sufficiently to prevent polygonal fault nucleation.

Chapter 5

Complex eyed pockmarks and submarine groundwater discharge revealed by acoustic data and sediment cores in Eckernförde Bay, SW Baltic Sea

5.1 Introduction

Escalating water demand in coastal areas and the nature and dynamics of interconnected onshore and offshore aquifers have significantly increased scientific interest in submarine groundwater discharge (SGD) over recent decades. SGD often carries large amounts of nutrients into the sea with diverse implications for the coastal ecosystems and environments (Lecher et al., 2016; Moore, 2010). Cho et al. (2018) estimated that the global nutrient flux into the oceans through SGD even exceeds riverine inputs. Future climate change and, in particular, an expected increased frequency of global droughts (IPCC, 2014; Seager et al., 2007) have provided traction to research into offshore groundwater reserves as a possible source of potable and agricultural water (Berndt and Micallef, 2019). Therefore, cost- and time-effective detection and characterisation of submarine groundwater systems, the dynamics of their discharge, and their temporal and spatial variation, are crucial for a potential exploitation in the future.

Numerous methods have been used to detect and quantify SGD (Burnett et al., 2006) including optical systems (Karpen et al., 2004), geochemical water-column investigations of tracers like the natural radionuclides radium and radon

(Burnett and Dulaiova, 2003; Moore, 1996; Moore et al., 2008; Scholten et al., 2013), dissolved silicon (Oehler et al., 2019), methane and chloride (Dulaiova et al., 2010; Schlüter et al., 2004), remote sensing (Shaban et al., 2005; Tamborski et al., 2015; Wilson and Rocha, 2012) and direct investigations using cores and different types of seepage meters (Bugna et al., 1996; Burnett and Dulaiova, 2003; Cable et al., 1997; Sauter et al., 2001). Only a few geophysical methods, like geoelectric (Stieglitz, 2005; Viso et al., 2010), controlled source electromagnetic (CSEM) (Gustafson et al., 2019; Müller et al., 2011), or autonomous underwater vehicle (AUV) investigations (Sauter et al., 2003) have been used to explore SGD. Other hydroacoustic studies often postulate SGD solely based on geomorphological characteristics, but without any geochemical verification (e.g. Goff, 2019; Hillman et al., 2015; Jakobsson et al., 2020).

Submarine hydrocarbon seeps likewise attract much interest because of the specific micro-environments they create at the seafloor (Berndt, 2005; Judd and Hovland, 2009) and their influence on slope stability (Chapron et al., 2004; Riboulot et al., 2019), representing a risk to infrastructure (Cayocca et al., 2001; Mulder and Chochonat, 1996). Since they often emit methane, a potent greenhouse gas, they can contribute to climate change and exacerbate symptoms of global warming like ocean acidification and oxygen depletion in the oceans (Biastoch et al., 2011; Borges et al., 2016; Leifer et al., 2006; Lohrberg et al., 2020; Solomon et al., 2009).

In Eckernförde Bay, sulfate reduction is the dominant process for organic carbon degradation in the upper ~30 cm below the seafloor before the sulfate is depleted (Maltby et al., 2018). Below the sulfate-methane transition zone (SMTZ) methanogenesis leads to methane oversaturation and gas formation in the organic-rich mud, resulting in widespread acoustic turbidity zones (Figure 5.1). Several pockmarks form along the coastlines as well as in the central part of Eckernförde around Mittelgrund as a result of gas and submarine groundwater seepage (Bussmann and Suess, 1998; Jensen et al., 2002; Kaleris et al., 2002; Müller et al., 2011; Patiris et al., 2018; Schlüter et al., 2004; Whiticar, 2002). In Eckernförde Bay questions remain regarding the fluid contributions to pockmark formation as well as the different pockmark classifications given by different authors (Albert et al., 1998; Whiticar, 2002). Although numerous research cruises and international

research projects (e.g., Coastal Benthic Boundary Layer [CBBL], Submarine Groundwater Fluxes and Transport Processes from Methane-Rich Coastal Sedimentary Environment [Sub-GATE]) have investigated the geological, geomechanical, geochemical and geophysical background of the pockmarks and their host sediments, the internal pockmark geomorphology is still poorly constrained. Sidescan and multibeam data published by Sauter et al. (2003) and Schlüter et al. (2004) show the delineation and depth of the pockmarks but are unable to reveal their internal structure and morphology.

In this chapter, I investigate the geomorphological expressions of SGD and gas escape as well as the subbottom characteristics within the pockmarks in Eckernförde Bay. I conducted hydroacoustic surveys using multi-frequency singlebeam, multibeam and subbottom profiler data in 2014, and 2019 and use data from cruises in 2017 and 2018 and ground truth observations from these data with porewater geochemistry from 13 sediment cores as well as CTD casts and transects of the water column. This high-frequency (up to 400 kHz) study, on the one hand, provides very high-resolution bathymetry enabling me to acquire targeted and accurately positioned sediment cores for porewater-analysis and groundtruthing. On the other hand, the high-frequency has limited but significant seafloor penetration and therefore provides subsurface information. I investigate a new type of pockmark associated with SGD in gaseous mud. Hovland et al. (2002) described complex- unit- and eyed-pockmarks but a combination of them has not been reported previously. I aim to improve the characterisation of pockmarks forming by SGD and gas and to determine possible acoustic indications for groundwater discharge in regions of organic-rich gaseous mud.

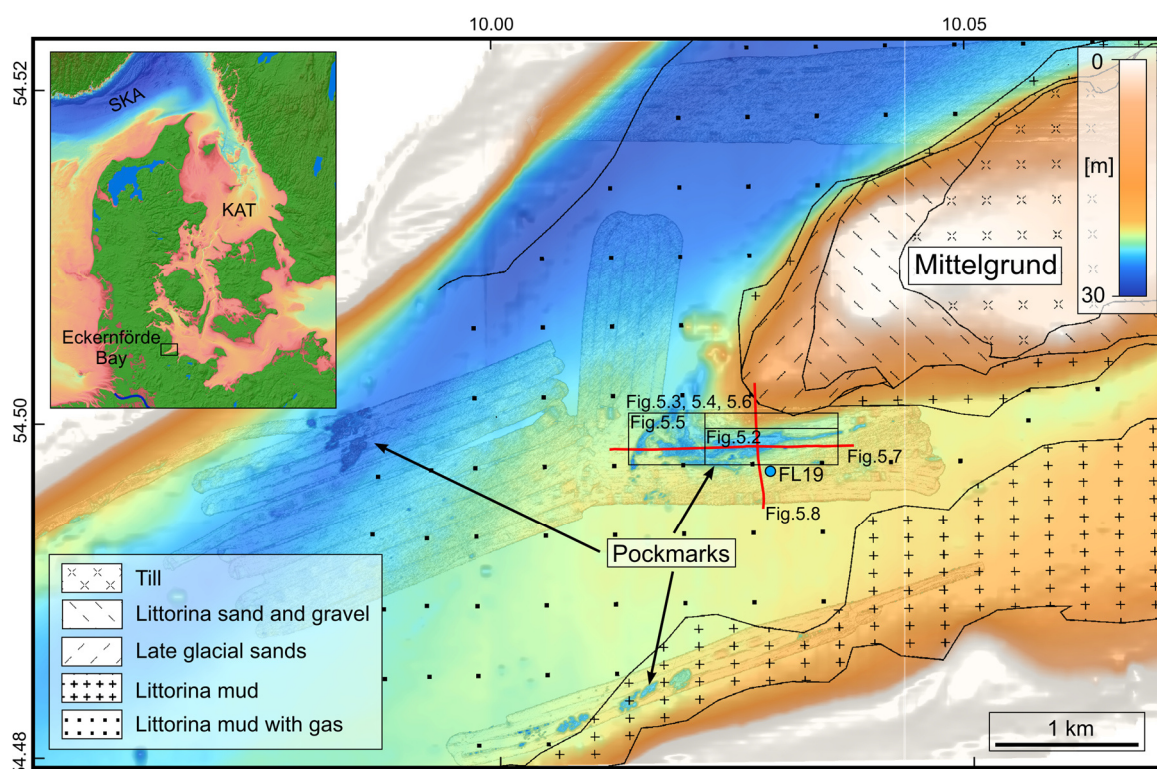


Figure 5.1: Overview bathymetric map of Eckernförde Bay with geological surface sediments overlaid, as described by Jensen et al. (2002). High-resolution bathymetry from cruise AL447 (2014) overlays the regional bathymetry kindly provided by the Federal Marine Hydrographic agency. The sediment background core FL19 is indicated by the blue dot. Littorina sediments were deposited during or after the Littorina transgression (< 8000 yr BP).

5.2 Data

5.2.1 Multibeam echo sounder

The multibeam echo sounder (MBES) data used in this study are a series of repeated surveys of the pockmarks carried out over a 4.5-yr period. The data were acquired on R/V Alkor and R/V Littorina during four surveys in October-November 2014 (cruise AL447), August 2017 (cruise AL501), May 2019 (cruise L1905) and September 2019 (cruise AL527). Three different MBES systems were used during variable weather conditions resulting in grids with different resolutions.

For cruise AL447 in 2014, an EM2040c system was installed on R/V Alkor with a 200-400 kHz transducer combined with a CodaOctopus F180 motion sensor. During cruises AL501 and AL527 in 2017 and 2019, a Norbit Wideband Multibeam System (iWBMS) with integrated motion sensor was operated at 400 kHz. For cruise

L1905 in 2019, I used a 180 kHz Seabeam1000 system. More specific information on the MBES data acquisition can be found in the corresponding cruise reports (Krastel et al., 2017, 2019; Schneider von Deimling et al., 2014, 2019). The data were assessed, calibrated and cleaned using software packages including MBSystems, QPS Qimera/Fledermaus and Hypack/Hysweep. I acquired sound velocity profiles in regular intervals which were assigned to the data during postprocessing with respect to their time of acquisition. Tidal corrections were applied using the tidal gauge in Eckernförde with reference to NHN, DHHN92.

The final processed data have horizontal resolutions of up to 0.5 m and decimetre scale vertical resolutions enabling the imaging of 3 - 15 cm deep trawl marks. The backscatter amplitude data were corrected for the variation with grazing angle. I ensured the highest possible resolution by using the raw backscatter time-series data for each footprint (snippets) where available and compensated for the angle of incidence using reference grids.

5.2.2 Subbottom profiler

Subbottom profiler data were acquired with the R/V Alkor and R/V Elisabeth Mann Borgese in late October 2014 (cruise AL447), the beginning of July 2018 (cruise EMB187) and August 2018 (cruise AL514). I used the parametric Innomar SES-2000 medium system creating secondary peak frequencies between 4 and 15 kHz. For cruises AL447, AL514 and EMB187 4, 4, and 6 kHz were used respectively. The data were converted into SEG-Y format and further processed and interpreted using the IHS Markit Kingdom software packages.

5.2.3 Sediment cores

During the L1905 cruise in May 2019, I used a Frahm-Lot (100 cm core liner, diameter of 10 cm; MBT GmbH – MacArtney Germany) to collect a total of 13 sediment cores with sediment recovery between 20 and 60 cm.

For porewater sampling, the plastic liner was pre-drilled along the side with diameters of 2.5 and 8 mm, respectively, then drill-holes were closed with adhesive stripes, to insert syringes or Rhizons directly after core recovery. After retrieval of

sediment cores on deck, 3 ml of sediment was subsampled by inserting plastic syringes in a 2-4 cm interval into the predrilled holes. The sampled sediment from each syringe was pushed into a 20 ml headspace vial containing 9 ml of saturated NaCl-solution (Sommer et al., 2009). Headspace vials were crimped with a rubber stopper and aluminium cap and stored for gas chromatographic analysis at GEOMAR. Headspace gas (100 μ l) was injected into a Shimadzu gas chromatograph (GC-2014, flame ionization detector, carrier gas: He 5.0; HayeSepTM Q 80/100 column, column length: 2 m; column diameter: 1/8 in.). The detection limit for CH₄ was 0.1 ppmV. Precision was about 4% (2σ).

Porewater was sampled onboard in 1-4 cm intervals by Rhizon extraction (Rhizosphere Research Products; e.g. Seeberg-Elverfeldt et al., 2005) for subsequent sulfate and chloride ion concentration determinations onshore. The ion concentrations were analysed at GEOMAR by using ion chromatography (Metrohm IC761; conductivity detector, eluent: Na₂CO₃/NaHCO₃, column: Metrosep A Supp 5 100/4.0) with a precision of about 2% (2σ) determined with IAPSO seawater standard. The porosity of sediment was determined from about 10-15 g of wet sediment samples, weighted before and after freeze-drying.

Methane solubility calculations have been performed for bottom water conditions (Water depth = 26 m, Temperature = 15°C, and Salinity = 20 (~312 mmol/l chloride)) according to Yamamoto et al. (1976).

To maximise the accuracy of positioning of the vessel and the cores, I used a Stonex S9i GNSS receiver with Real Time Kinematic (RTK) corrections received from the ascos (AXIO-NET GmbH) satellite reference service resulting in centimetre-scale accuracy at the receiver. The positioning of on-board coring equipment and cable deployment resulted in metre-scale accuracy for the core position (indicated by 5-m-diameter circles in Figure 5.2 and Figure 5.5).

5.2.4 EK60

During cruises AL447 (October 2014) and AL514 (August 2018), the fix mounted Kongsberg EK60 fishery echosounder was operated at multiple frequencies at 38, 70, 120, and 200 kHz for gas bubble detection and to identify potential anomalies associated with SGD. The four frequencies were calibrated with

copper spheres in the beginning of the cruise. Pulse length and power were constant throughout the cruise.

5.2.5 CTD

During R/V Littorina Cruise L1905 I acquired three CTD water column profiles with two towed transects using a Sea & Sun CTD. For the transects the CTD was towed ~1 m above the seafloor.

5.3 Results

5.3.1 Bathymetry

The high-resolution bathymetry data south of Mittelgrund show the internal morphology of the targeted pockmarks in a water depth of ~25 m (Figure 5.2, Figure 5.3, Figure 5.4 and Figure 5.5). The pockmarks show a mean elevation difference of ~1.8 m compared to the surrounding area. They are elongated features and align around Mittelgrund, with widths of up to 200 m and lengths of over 1 km. The seafloor morphology within the pockmarks is highly variable. In some areas, I observe a smooth and relatively flat seafloor, while other regions show a highly uneven surface with anomalous mounds and depressions. These depressions within the pockmarks – which I hereafter refer to as “intra-pockmarks” – mainly occur on the side furthest from Mittelgrund. The smoother areas – which I hereafter refer to as “background-pockmark” – mainly occur on the side closest to Mittelgrund, although patches of smoother pockmark seafloor are also observed beyond the intra-pockmarks further from Mittelgrund.

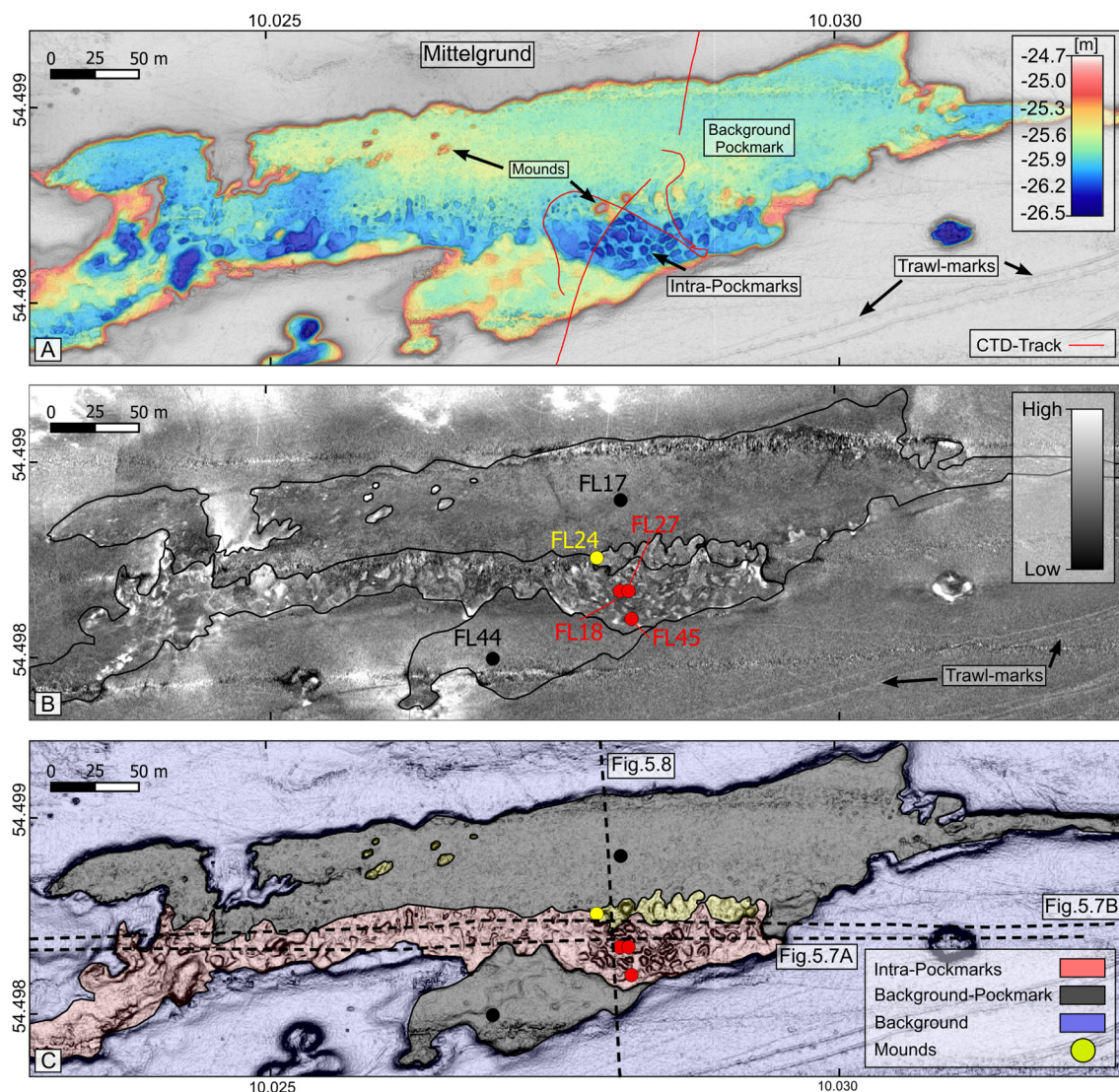


Figure 5.2: Bathymetric overview of the eastern Mittelgrund pockmark (data from cruise AL447 in October 2014). A: Bathymetric map highlighting the large scale eastern Mittelgrund pockmark (coloured region) and its internal intra-pockmark and background-pockmark regime. Example mounds are also labelled, and the red line shows the towed CTD-tracks. B: Corrected (300 kHz) backscatter image showing the high-amplitude responses of the intra-pockmarks. Coloured dots show core locations and the black lines delineate the classification regime shown in (C). C: Slope map overlaid with pockmark classification (semi-transparent colours) as described in the text. Dashed lines show the location of the subbottom profiler data displayed in Figure 5.7 and Figure 5.8 and coloured dots show core locations.

I divide the pockmark area southwest of Mittelgrund into three different regimes based on bathymetric morphology and their acoustic character. In Figure 5.2C I distinguish between (1) background (blue), (2) background-pockmark (black), and (3) intra-pockmark (red). The background regime describes the area outside the pockmarks (i.e., beyond both background-pockmark and intra-pockmark) which is morphologically characterised by a smooth surface with several 3 - 15 cm deep trawl-marks, especially to the southeast and west of the pockmark area. Within the pockmarks, the background-pockmark regime makes up most of the eastern Mittelgrund pockmark area (~70 %; see Figure 5.2) and shows a remarkably even surface. The intra-pockmark regime on the contrary shows a highly uneven surface, with depressions (intra-pockmarks) of various sizes and shapes, from circular to very complex forms. They show diameters between a couple of metres and ~30 m with a vertical relief that ranges from decimetre scales up to 1 m. The intra-pockmark regime shows a high pockmark density with depressions occurring close to each other without much space between them. The different regimes are in some places divided and in other places intersected and interrupted by several circular to elliptical anomalous mounded structures with heights of up to 50 cm. The various data resolutions and data qualities of the multibeam surveys permitted a comparison of the bathymetry over the 4.5-yr time period. My visual inspection and differencing of the grids revealed only slight bathymetric changes over the course of the sampling period. No changes were observed between 2014 and 2017. Systematic artefacts due to different track lines and temporal changes in yaw, pitch and roll could be observed. The lower resolution of the L1905 (May 2019) dataset also revealed no changes to previous datasets, while the comparison of the 2017 and late 2019 data shows sediment deposition within the intra-pockmarks in the east and slightly deeper intra-pockmark areas in the west (Figure 5.3 and Figure 5.4). The background-pockmark regime does not show any distinct elevation changes over time while the intra-pockmarks seem to infill (Figure 5.3 D and E). The overall morphology of the pockmarks and the different regimes seems steady over time.

5.3 Results

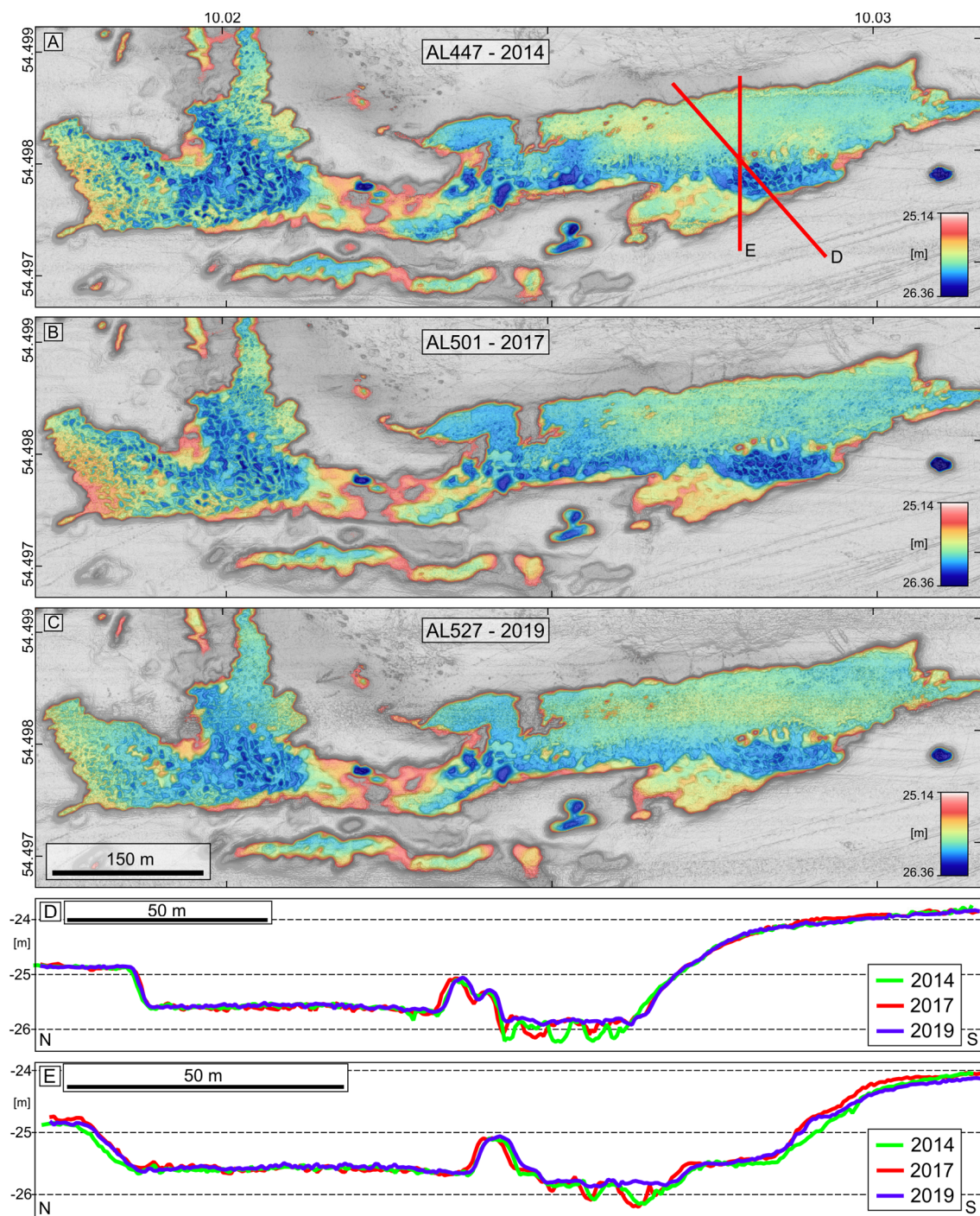


Figure 5.3: Bathymetry of A) 2014, B) 2017, and C) 2019. Profiles through the pockmarks (D, E) show no changes in the background-pockmark over time but indicate sediment deposition in the intra-pockmark regime.

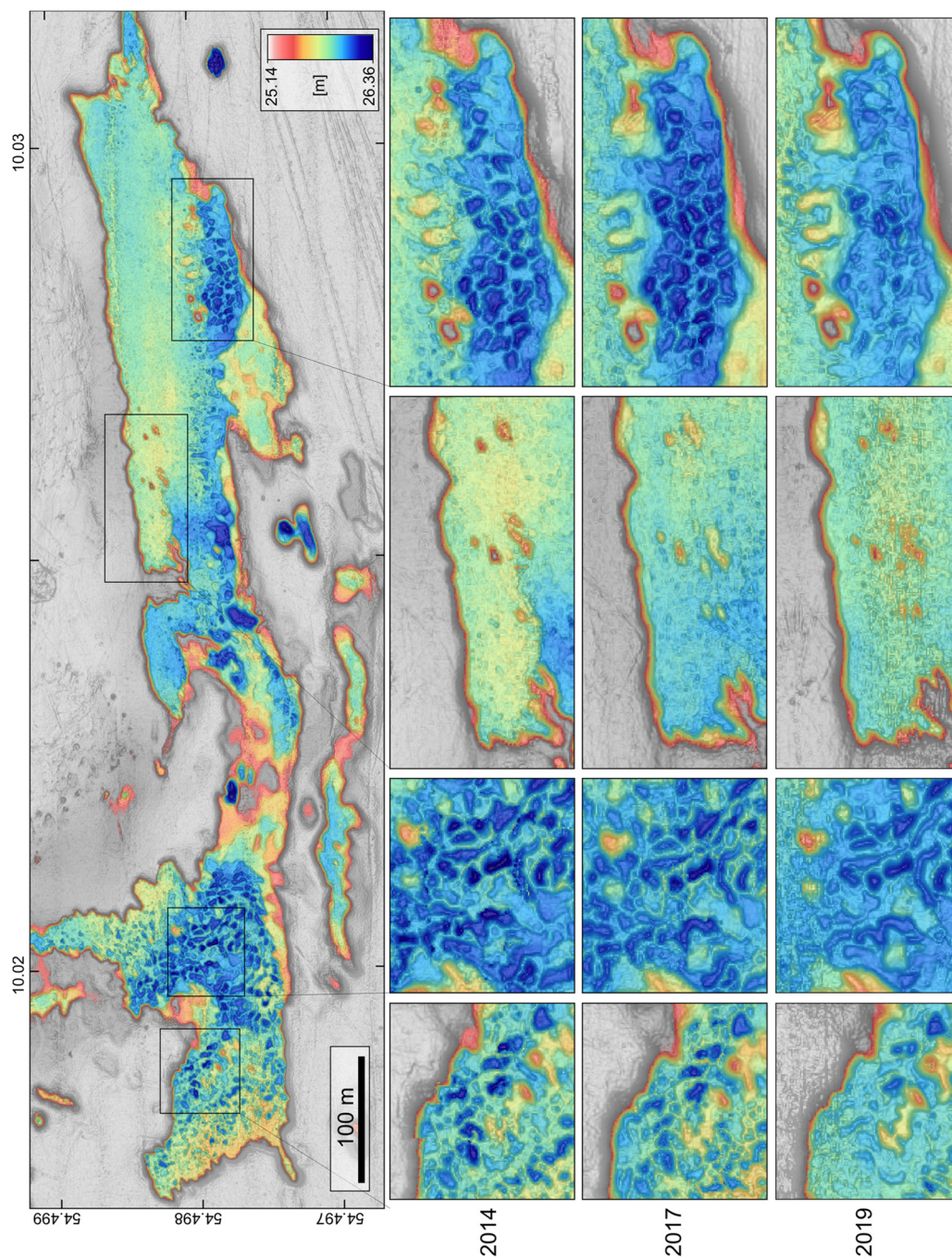


Figure 5.4: Bathymetrical changes over time. In most areas no changes were observed between 2014 and 2017. Between 2017 and 2019 a slight infill of the intra-pockmarks can be observed.

5.3.2 Backscatter

By thorough inspection of the geolocated multibeam snippet backscattering strength, I found a good correlation to the morphological data (Figure 5.2 and Figure 5.5). Outside the pockmarks, in the background regime, I generally find low backscattering strength (averaging -36 dB) with slightly enhanced amplitudes (\sim -30 dB) within the trawl marks in the southeast and west (Figure 5.2B). North and northeast of the pockmarks are areas of very strong backscatter that correspond to the Mittelgrund late-glacial sands.

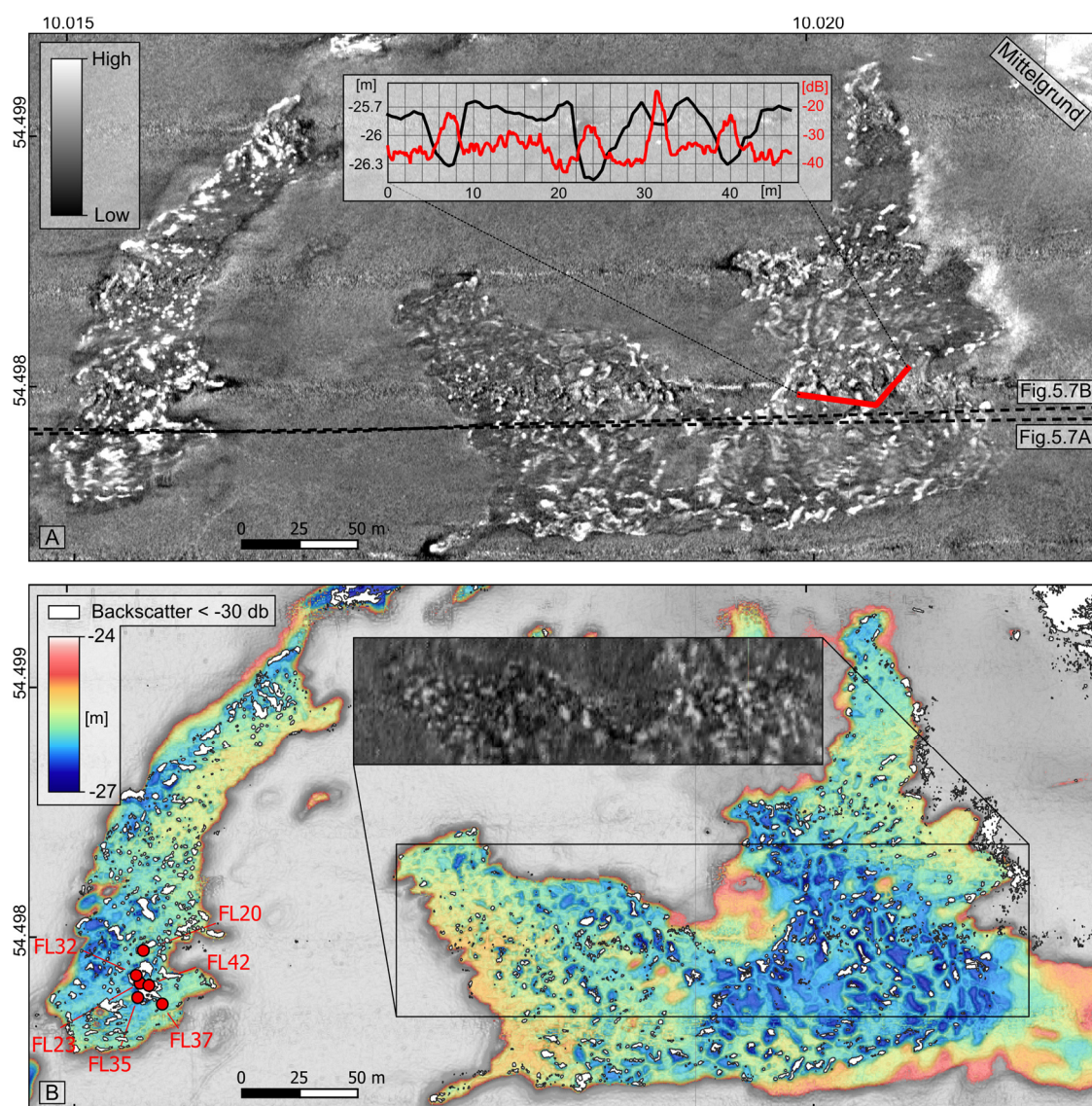


Figure 5.5: A) 300 kHz backscatter image of the western Mittelgrund pockmark showing the patchy strong backscatter strength of the intra-pockmarks (cruise AL447, October 2014). Inset graph shows the clear inverse correlation between relative backscatter strength (dB) and seafloor elevation (m). B) Bathymetry of the pockmark with strong backscatter values ($<$ -30 dB) overlain in white. Inset shows the 180 kHz backscatter image of cruise L1905, May 2019.

Within the pockmarks, the background-pockmark area does not show any elevated backscatter signals (< -30 dB) and is characterised by a rather consistent and homogeneous response (Figure 5.2B). The intra-pockmark areas on the other hand, exhibit highly variable acoustic responses that vary from very strong (< -20 dB) to very low (> -40 dB) signal strength (Figure 5.2B). This relationship can also clearly be seen in backscatter data from the western Mittelgrund pockmark (Figure 5.5A). The strong backscatter values appear in patches and correlate with the bathymetric lows of the individual intra-pockmarks (Figure 5.5A). Nearly all individual intra-pockmarks show increased backscatter strength, with the strongest responses (< -30 dB) shown in white in Figure 5.5B. Backscatter values similar in strength to those of the late-glacial sands of Mittelgrund (~ -20 dB) are observed in several of the intra-pockmarks.

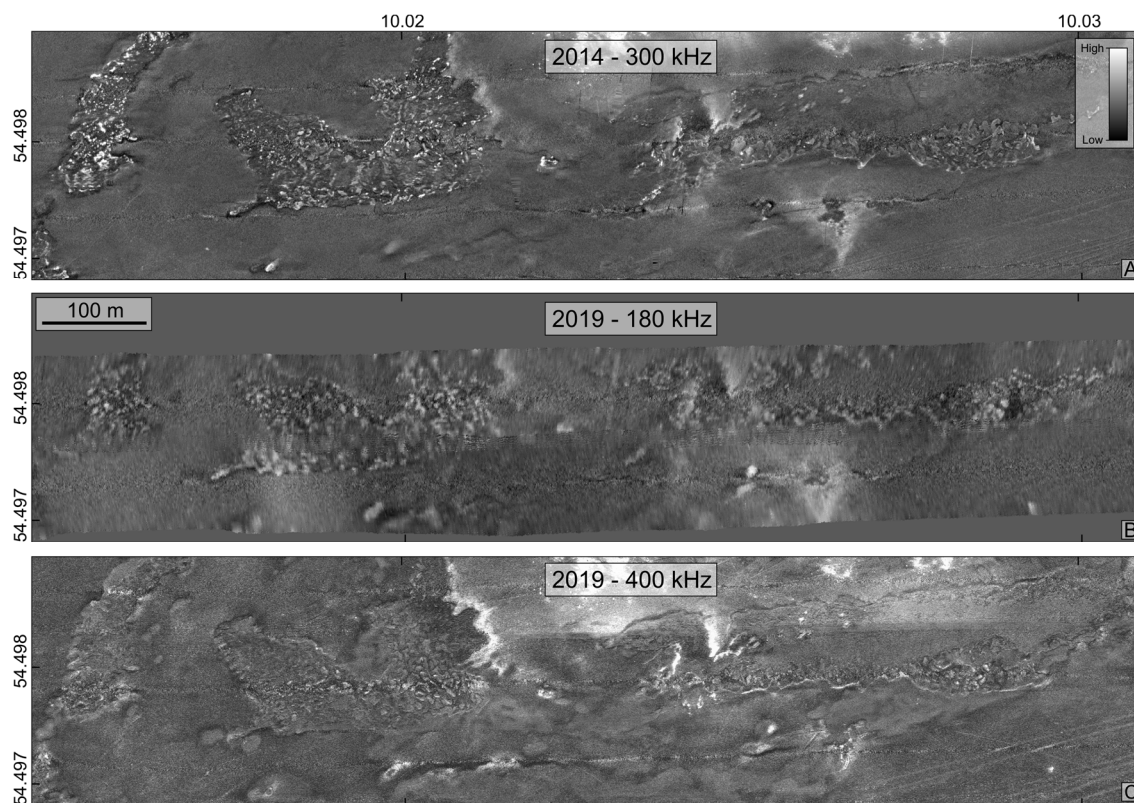


Figure 5.6: Backscatter changes over time. A) October 2014 (AL447), B) May 2019 (L1905), and C) September 2019 (AL527)

Although the data quality from the surveys varies due to different equipment and weather conditions, the patchy backscatter pattern of the intra-pockmarks remains obvious across all datasets (Figure 5.6). Since different frequencies were used and the backscattering strength was not calibrated, only relative backscatter changes can be interpreted.

5.3.3 Subbottom profiling

The subbottom profiler data show the characteristic shallow gas front of Eckernförde Bay with the acoustic turbidity zone below (Figure 5.7) as observed by Hinz et al. (1971). The depth beneath the seafloor of the free gas front varies significantly over time. During the early July 2018 measurement campaign, the average depth of free gas in the background regime was ~ 70 cm while in October 2014 gas occurrences at a depth of ~ 40 cm were observed, in accordance with reports by Wever et al. (1998). In July 2018 (Figure 5.7A), the acoustic manifestations of shallow gas accumulations in the background regime appear as condensed regions of high reflectivity with sharply delineated tops. In October 2014 (Figure 5.7B), by contrast, where the gas accumulations occur closer to the seafloor, they have a less condensed and more distributed acoustic manifestation. In the intra-pockmark regime, I observe similar changes over time, although they do not seem to be as pronounced as the temporal changes observed outside of the pockmarks (in the background regime). High-amplitude reflections occur in the uppermost 50 cm throughout the datasets in the intra-pockmark regime.

Outside of the pockmarks, in the background area, the free gas manifestation shows strong horizontally continuous amplitudes with occasional regions where the gas front is absent or occurs at greater depths (Figure 5.7), previously described by Albert et al. (1998) as acoustic windows. Within the pockmarks, free gas appears closer to the seafloor but the gas front is less continuous and the reflected acoustic energy is more distributed over a wider depth interval (Figure 5.7 and Figure 5.8). Several patches, indicating free gas, occur close to the seafloor.

I extracted the reflected acoustic energy within a 50 cm window below the seafloor by computing the envelope of each trace and subsequently summing the envelope within that window (Figure 5.7 and Figure 5.8). The sum of energy shows

strongly elevated energy levels at shallow sub-seafloor depths within the intra-pockmark regime compared to the background-pockmark and background regimes.

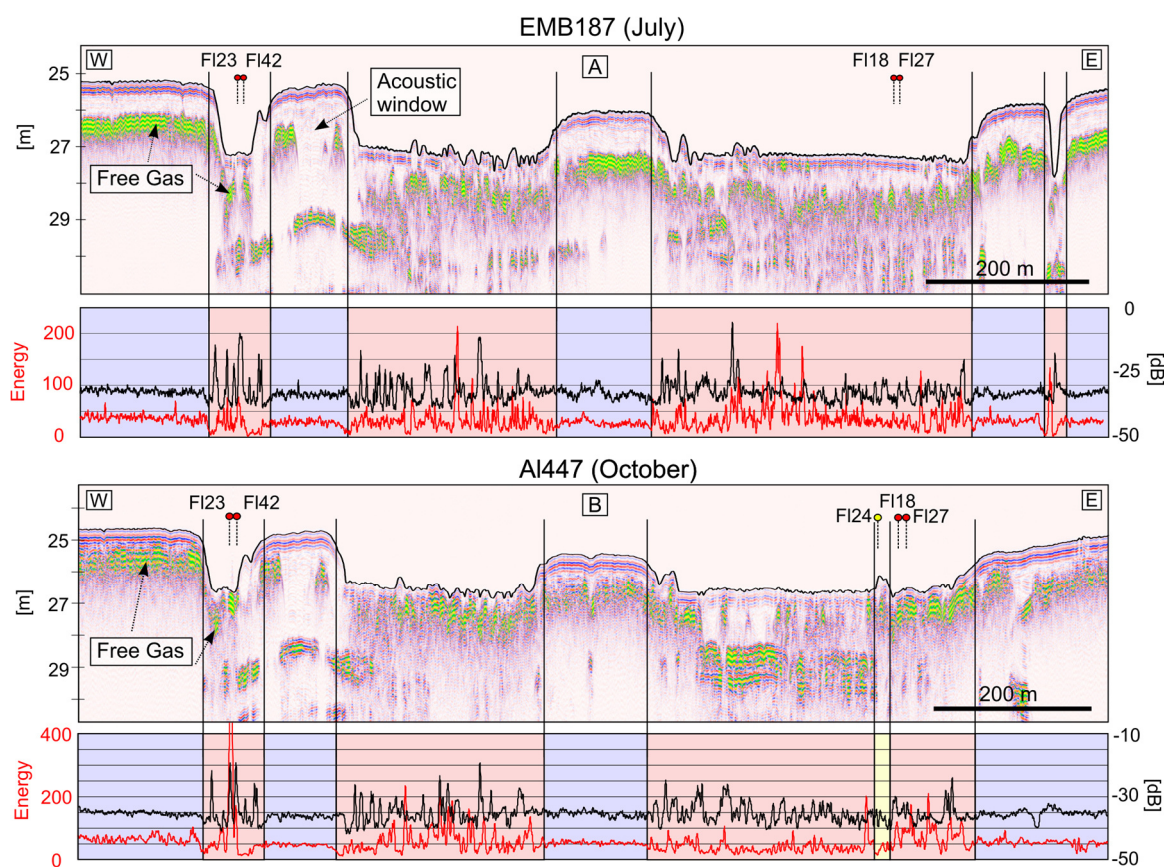


Figure 5.7: Innomar subbottom profiler data across the Mittelgrund pockmarks, with the energy extracted from the upper 50 cm beneath the seafloor in red and the along-track multibeam backscatter in black (in the accompanying plots). A: Profile acquired during July 2018, B: Profile acquired during October 2014 (locations in Figure 5.1, Figure 5.2 and Figure 5.5). Sediment core locations along the profile are marked by labelled dots. Semi-transparent colours in the dots and behind the energy plots are representative of different seafloor classifications as defined in Figure 5.2C.

The background-pockmark area, delineated in grey in Figure 5.8, shows a very weak seafloor reflection and no internal reflections above a layered high-amplitude southward dipping unit. This unit extends from the surface of Mittelgrund in the north beneath the pockmarks and is commonly referred to as the late-glacial sands (Jensen et al., 2002). High energies in the 50 cm below the seafloor are observed in the north of the profile shown in Figure 5.8 around Mittelgrund, where the late-glacial sands subcrop at the seafloor and create a rough and hummocky morphology.

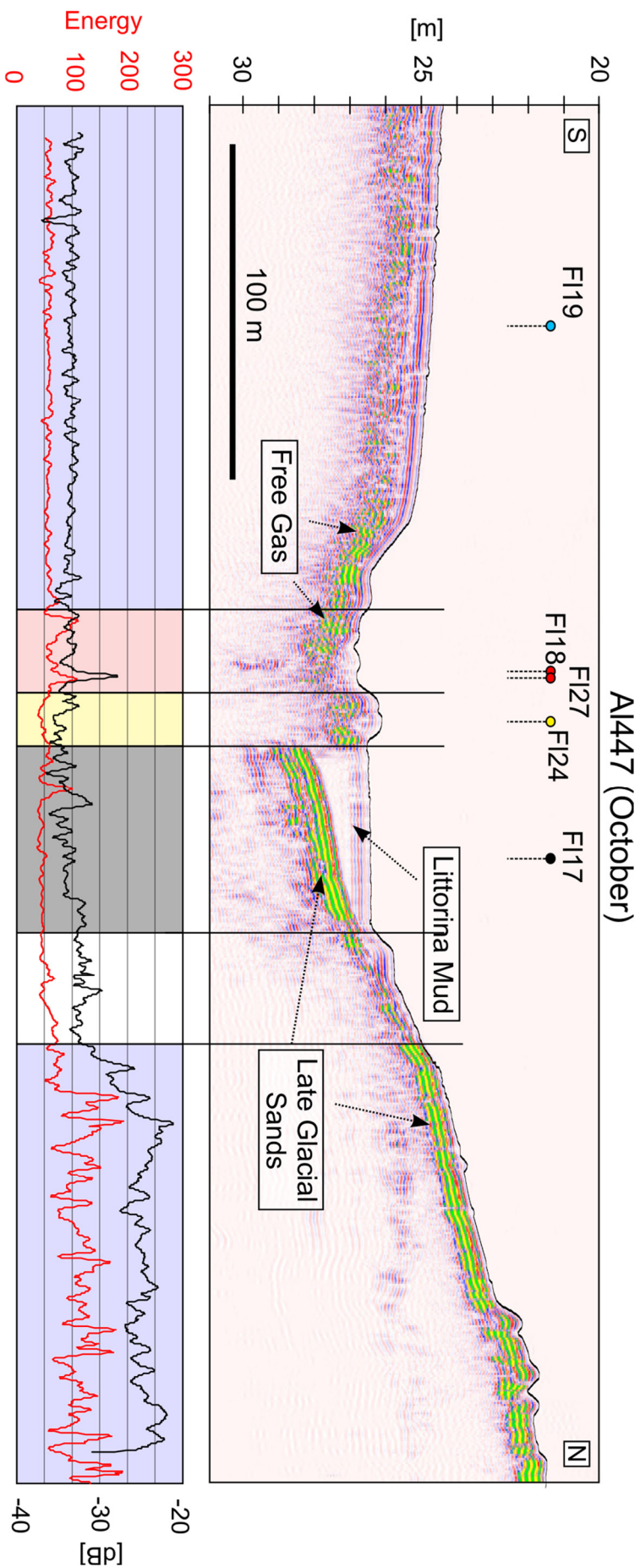


Figure 5.8: Top: north-south profile through the pockmarks covering Mittelgrund in the north and the inner bay in the south. Location of the profile is given in Figure 5.1 and Figure 5.2. Bottom: the energy extracted from the upper 50 cm beneath the seafloor is displayed in red and the along-track multibeam backscatter in black. Sediment core locations along the profile are marked by labelled dots. Semi-transparent colours in the dots and behind the energy plots are representative of different seafloor classifications as defined in Figure 5.2C.

This late-glacial sand unit is only visible in the northern part of the pockmark area (in the background-pockmark regime). Distal from Mittelgrund, in the intra-pockmark regime, free gas occurs close to the seafloor, limiting the acoustic penetration. The transparent unit above the late-glacial sands in the background-pockmark region shows no signs of free gas and low to moderate reflection energy in the subbottom profiler as well as in the backscatter data.

5.3.4 Sediment cores

I obtained sediment cores, 20-60 cm in length, from all three acoustically distinguishable regimes (Figure 5.2, Figure 5.5 and Figure 5.9). All sediment cores consisted of a dark-grey to black muddy lithology with a variable centimetre-scale brown fluffy layer on top. The water content of the mud throughout the cores was extremely high, with porosities averaging 93% in the upper centimetres as previously reported by Silva and Brandes (1998). More than 50% of the attempts to recover a sediment core on deck failed due to discharge of the soft, unconsolidated, weak and water-saturated mud, resulting in loss of the core before sampling could take place.

Porewater geochemistry profiles, i.e. methane-, chloride-, and sulfate-concentration versus depth from these cores are shown in Figure 5.9. No distinct differences in porosity or other sediment properties were observed in the cores. The background core (FL19, Figure 5.1, Figure 5.8 and Figure 5.9) shows no enhanced methane concentrations in the uppermost 30 cm and an increase of methane to ~ 2 mM below 50 cm. Sulfate in the core decreases between sediment surface and 30 cm depth (SMTZ) from about 16 mM down to below ~ 2 mM, while the chloride concentration in the porewater is more or less constant with depth at about 290-320 mM.

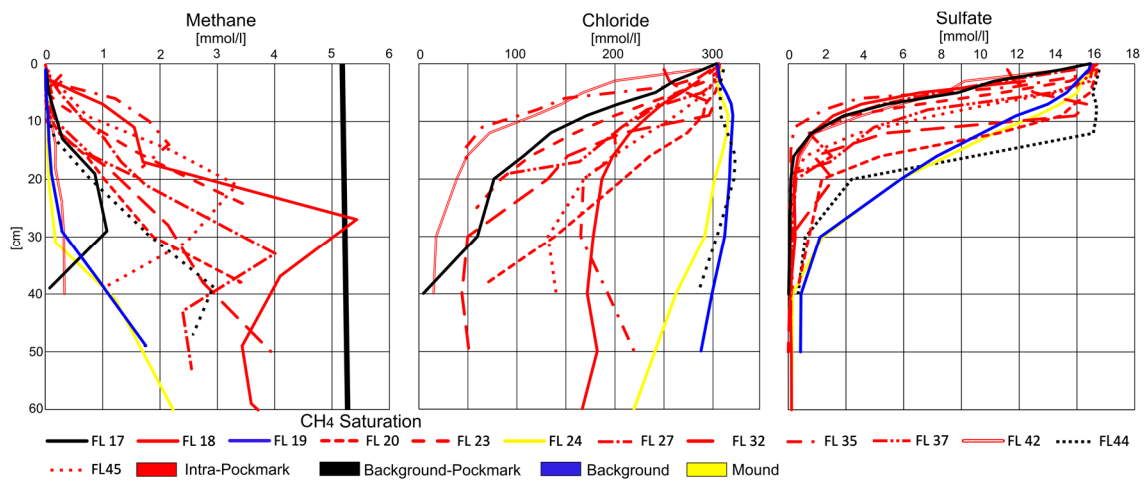


Figure 5.9: Porewater methane, chloride and sulfate concentrations in all sediment cores collected, colour-coded by regime.

The cores collected in the background-pockmark area show a higher SMTZ located at about 10 cm below the sediment surface; however, maximum methane concentrations below this depth are about 1 mM, which is well below the methane solubility at this depth (i.e. 5.18-5.27 mM; Figure 5.9). No free gas voids were observed in the background and background-pockmark sediment after core recovery on deck. Core FL17 in the background-pockmark regime shows one of the strongest gradients in sulfate decrease, while core FL44 displays one of the lowest. Chlorinity profiles vary in the background-pockmark area. While the northernmost core FL17 shows a strong decrease with depth to ~5 mM of chloride, the southernmost core FL44 shows chloride variability similar to the background core FL19.

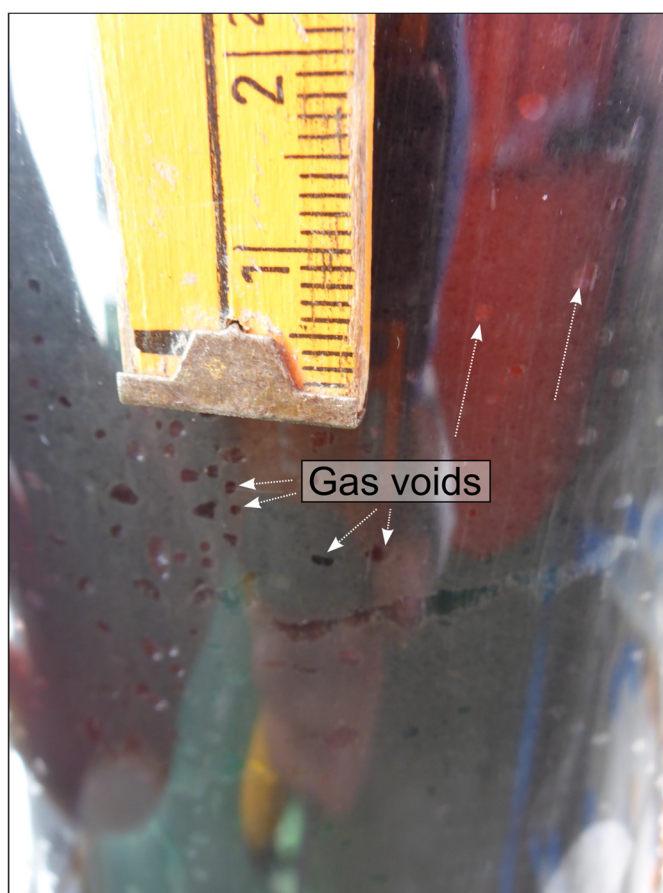


Figure 5.10: Voids in the sediment cores containing free gas immediately after core recovery (core FL18).

With core FL24 I targeted one of the mound structures where only minor porewater freshening with depth is observed. The sulfate and methane concentration profiles of FL24 are comparable to background core FL19 (Figure 5.9).

In the intra-pockmark regime, all cores show a strong groundwater influence from below. Porewater chloride concentrations of less than 100 mM (~30 % of the bottom water concentration) were measured at about 10 cm (Figure 5.9). These low chloride values are accompanied by high methane concentrations of up to 2 mM at 10 cm and strong methane concentration gradients with depth. The SMTZ occurs between ~5 and 15 cm in the intra-pockmark regime and methane concentrations of up to 5.42 mM were measured in core FL18 at about 30 cm (Figure 5.9). As bubble formation even under in situ pressure conditions is anticipated based on the measured methane concentration, the scattered methane concentration measured below 30 cm is probably related to strong degassing effects on deck. Indeed, several cores from this region showed evidence of free gas bubbles beneath ~10 cm, when they came to the surface (Figure 5.10). This includes core FL42, which for an unknown reason, does not show enhanced dissolved CH₄ porewater concentrations higher than 0.3 mM. I attribute this lack of methane to degassing during core acquisition and unfortunately too long storage time on deck until sampling (Abegg and Anderson, 1997; Wever et al., 1998).

5.3.5 CTD

I conducted three CTD casts with two towed transects in different regions of Eckernförde Bay. The location of the towed CTD transect is shown in Figure 5.1A. All of the casts and transects show low saline surface water of $S \sim 14$ (~218 mmol/l chloride) with an increasing salinity to ~ 20 (~312 mmol/l chloride) in the bottom water, as characteristic for the Baltic Sea (Bange et al., 2011; Lennartz et al., 2014). Although I managed to tow the CTD as close as ~1 m above the seafloor, none of the CTD casts or transects showed any groundwater influence on the water-column, neither within nor outside of the pockmarks.

5.4 Discussion

5.4.1 Characterisation of Eckernförde Bay pockmarks

Albert et al. (1998) have noted that pockmarks closer to the coast of Eckernförde Bay appear to be a different type altogether to those around Mittelgrund. This was based on the observation of low methane and low chloride concentrations, as measured by Whiticar and Werner (1981) and later by Whiticar (2002) in the Mittelgrund pockmarks, compared to high methane concentrations in pockmarks closer to the coast.

The high-frequency multibeam approach enabled me to collect targeted sediment cores with a metre-scale accuracy. These new data suggest a classification of the pockmarks into different regimes rather than separating the coastal and Mittelgrund pockmarks into different types based on different eroding agents from below. Depending on core location, even within the same pockmark, methane and chloride concentrations can vary significantly (Figure 5.9). While the background regime shows no influence of groundwater, a comparatively deep SMTZ and only a moderate positive methane gradient below the SMTZ, the cores from within the pockmarks are variable. In the northern background-pockmark regime low methane concentrations correlate with a thin organic-rich *Littorina* mud cover above the late-glacial sands (Figure 5.8). The subbottom profiler data show no signs of free gas or internal reflections in this area. I observe a moderate methane concentration gradient below the SMTZ with maximum methane concentrations well below the solubility of methane in porewater (core FL17, Figure 5.9). The even seafloor of the background-pockmark area therefore corresponds to high groundwater influence with low methane concentrations. The background-pockmark sulfate profile of core 44 shows anomalously high concentrations of sulfate compared to the other cores, down to 12 cm. The high sulfate is accompanied by moderate methane concentrations and high chloride concentrations indicating limited groundwater influence. The sigmoidal shape of the sulfate concentration profile below 12 cm indicates a non-steady state of anaerobic microbial methane oxidation (AOM) related to sulfate reduction during the respective season (Schulz, 2006). Although the porosity of this core is not anomalous compared to other cores,

a high permeability and effective exchange of porewater with bottom water at the top of the core could be the cause. The background-pockmark regime therefore varies in sulfate and chloride according to the location of the core, the thickness of the *Littorina* mud cover, and the influence of ascending groundwater.

In the intra-pockmark regime, the mud reaches thicknesses of more than 1 m above the late-glacial sands and the SMTZ is shifted to shallower depths compared to the background-pockmark. Free gas occurs very close to the seafloor as seen in the subbottom profiler data as well as in the sediment cores, and the elevated methane concentrations are reaching oversaturation at depth (e.g., FL27, Figure 5.9). Although Jensen et al. (2002) reported that the late-glacial sands extend over the entire Eckernförde basin, I cannot resolve this southward dipping unit outside the background-pockmark area due to the acoustic turbidity where free gas is present. All the cores in this morphologically rough intra-pockmark region show a strong groundwater influence with high methane concentrations and a shallow SMTZ.

5.4.2 Formation and modification processes of the intra-pockmarks

The formation of the Eckernförde pockmarks has been debated for decades. Bottom currents (Werner, 1978), military activities (Edgerton et al., 1966), gas seepage (Fabian and Roese, 1962) and groundwater seepage (Khandriche and Werner, 1995; Whiticar and Werner, 1981) have all been proposed as formation mechanisms since their discovery by Edgerton et al. (1966). It is now widely accepted that episodic artesian groundwater springs, in combination with bottom currents, erode the pockmarks (Bussmann and Suess, 1998; Jensen et al., 2002; Kaleris et al., 2002; Müller et al., 2011; Patiris et al., 2018; Schlüter et al., 2004; Whiticar, 2002). The newly observed (this study) eyed intra-pockmarks in Eckernförde Bay seem to host both high methane and low chloride concentrations. Albert et al. (1998) proposed that the Eckernförde pockmarks act as morphological sinks for organic material and therefore could enhance methanogenesis close to the sediment-water interface. Khandriche and Werner (1995) suggested that the erosion of the pockmarks, once initiated, leads to a positive feedback mechanism

since deeper sediment layers with a higher gas content are exposed to water currents. Since the depth of the gas front varies within the sediments by tens of centimetres (magnitudes higher than accumulation or erosion rates) due to seasonal variations and short-term weather conditions, I assume that the high gas content close to the seafloor within the pockmarks is the result of groundwater seepage rather than erosion. The high gas content combined with the low chlorinity very close to the seafloor induces sediment instabilities and a reduction in shear strength (Sills and Wheeler, 1992) which consequently make sediments more easily erodible. In areas where only minor gas concentrations were measured in the pockmarks (background-pockmark area) I find an even and flat seafloor morphology, whereas in areas with strong methane gradients (intra-pockmark area) I observe a scoured surface which likely indicates lower shear strength and additional erosion. Since I did not observe any indications for seafloor scouring by bottom currents (e.g. elongation, preferred orientation or azimuthal variations in the slope of the intra-pockmarks) I propose that the abnormally shallow gas (which forms due to SGD, see section 5.4.3.) and the episodic release of groundwater are the main drivers of intra-pockmark formation. I suggest that the free gas changes the geotechnical properties, i.e. reduces the shear strength (Sills and Wheeler, 1992), meaning that even weak groundwater discharge phases erode the very fine sediments. The background-pockmark, on the other hand, shows no indications for elevated methane concentrations and I therefore presume that its morphology is the sole result of groundwater discharge during strong discharge phases.

5.4.3 Enhanced backscatter signals of intra-pockmarks

High backscatter at the bottom of pockmarks, as I observed in Eckernförde Bays intra-pockmarks, is a common phenomenon (Dandapath et al., 2010; Hovland et al., 2002; Judd and Hovland, 2009; Loncke et al., 2004). Seeping fluids frequently result in authigenic carbonate precipitation due to the microbially driven anaerobic oxidation of methane once methane enters the SMTZ (e.g. Boetius et al., 2000; Ritger et al., 1987). These carbonates are often associated with high-amplitude, positive-polarity reflections and a high backscatter signal in pockmarks (Böttner et al., 2019; Dandapath et al., 2010; Ho et al., 2012; Judd and Hovland, 2009). Similarly, the

suspension of fine-grained material due to fluid escape, leaving the coarser-grained material behind as well as enhancing biological activity due to seeping fluids (skeleton remains, dead and living shells, etc.) can create a strong impedance contrast and a rougher surface area and therefore result in strong backscatter values in pockmarks (Hovland, 1989; Hovland et al., 2002; Reusch et al., 2015). These pockmarks containing highly reflective objects at their centres have commonly been described as ‘eyed’ pockmarks (Hovland et al., 2002).

In Eckernförde Bay, the carbonate concentration in the sediment is extremely low (<2%) due to undersaturation in bottom waters (Lewy, 1975; Wefer et al., 1987), ruling out carbonate precipitation as a plausible cause of high backscatter. Also, the pockmark area, which was well sampled over recent decades, shows a surface sedimentary composition that consists of homogeneous Holocene mud without a significant amount of coarser-grained material (section 5.3.4, Jensen et al., 2002; Martens et al., 1999; Schlüter et al., 2004; Whiticar, 2002). Similar to carbonate, gas-bearing sediments induce a strong impedance contrast to the surrounding water-saturated sediments which creates a strong (albeit negative polarity) reflection. Beneath the intra-pockmarks, the closely spaced subbottom profiler data show that the shallow gas front occurs closer to the seafloor and becomes patchier compared to the surrounding regions. This is highlighted by the sum of acoustic energy extracted within a 50 cm window beneath the seafloor (Figure 5.7). The upper 50 cm includes the strong reflections associated with the shallow gas in the intra-pockmark regime (see CH₄ saturation in Figure 5.9) while excluding the reflections associated with deeper gas in the background. Additionally, the sediment cores collected within the intra-pockmarks show elevated methane concentrations compared to the background-pockmark and background cores. In several sediment cores recovered on deck, I visually detected free gas bubbles ~10 cm beneath the sediment-water interface (Figure 5.10). Moreover, measured methane concentrations of the intra-pockmark regime are comparable to the solubility limit of methane at in situ pressure, temperature and salinity conditions (Figure 5.9). This, together with the good correlation of multibeam backscatter strength and subbottom profiler reflectivity shown in Figure 5.7 and Figure 5.8, suggests that the elevated backscatter results from free shallow gas within the sediment at depth of ~10-20 cm.

Tang et al. (1994) reported that backscatter from a 40 kHz benthic acoustic measurement system results from gas voids about 1 m beneath the seafloor in Eckernförde Bay. In a geologically very similar environment to Eckernförde Bay, Schneider von Deimling et al. (2013) showed how a 12 kHz multibeam system can be used to map shallow gas in up to 12 m sediments depth, while a 95 kHz system detected the sediment-water interface. My results indicate that, in the soft muddy sediments of Eckernförde Bay (with low attenuation coefficients of $\sim 0.1\text{--}0.2 \text{ dB m}^{-1} \text{ kHz}^{-1}$ (Jackson and Richardson, 2007)), even the 400 kHz systems penetrate the upper few decimetres of the seafloor, and volume scattering provides information on subsurface sediment properties (in this case, partially gas saturated sediment). A large-scale seafloor backscatter classification approach in Eckernförde Bay by Alevizos et al. (2018) classified parts of the Mittelgrund pockmarks to consist of sand with small amounts of gravel due to the elevated backscatter signals in the pockmarks. The intra-pockmarks indeed exhibit exceptionally high backscatter values with signal strengths comparable to the backscatter of the late-glacial sands of Mittelgrund. However, no substantial amount of sand or gravel has been reported from sediment cores or grabs in this region and the automated seafloor classification likely incorrectly identified the free gas as sand.

The depth of the shallow gas front in Eckernförde Bay changes over time on a short term (effective pressure dependent) and seasonal (water temperature dependent) basis (Treude et al., 2005; Wever et al., 2006, 1998). On a seasonal basis, the bottom-waters have highest temperatures around October-November with lowest bottom-water temperatures during March-April (Lennartz et al., 2014). While a decrease in water temperature increases the solubility of methane, a temperature increase reduces the solubility and therefore increases the amount of free gas bubbles. The free gas front is therefore expected to be deepest during March-April and shallowest between October and November (Wever et al., 1998). I observe this phenomenon in the subbottom data where the EMB187 line (acquired on 7th July 2018) shows a free gas front around 70 cm below the seafloor in the background area compared to ~ 40 cm below the seafloor in the AL447 data (acquired on 22nd October 2014).

Although the different multibeam systems used for acquisition were not calibrated for the target strength (i.e., pockmark backscatter cannot be directly compared) the backscatter distribution pattern of the intra-pockmarks seems to be unaffected by seasonal variations and show the same strong patchy backscatter character throughout all three datasets (22nd October, 8th September, and 16th May). This suggests that free shallow gas constantly resides in the uppermost decimetres within the intra-pockmark regime and affects multibeam backscatter systems with 180, 300, and 400 kHz. This is supported by strong amplitudes close to the seafloor-water interface in all subbottom profiler data (Figure 5.7). I suggest that this phenomenon results mainly from the ascending groundwater, which is thought to intensify the upward migration of dissolved as well as free methane gas (Khandriche and Werner, 1995), thereby increasing gas concentrations closer to the seafloor. Moreover, as sulfate is rapidly depleted in porewater by ascending groundwater (Figure 5.9), the SMTZ is uplifted and thus the depths where methanogenesis would lead to oversaturation. Therefore, gas bubble formation is uplifted in areas of SGD.

5.4.4 Acoustic indicators for groundwater

One aim of this study was to find hydroacoustic indications for SGD in the water column or the seafloor. Khandriche and Werner (1995), as well as Bussmann & Suess (1998) reported decreased salinities in the water column down to $S=2.9$ (~45 mmol/l chloride) near the bottom of a pockmark, indicating a strong groundwater outflow during their surveying. However, repeated dedicated water column analysis of multibeam water column imaging data and Simrad EK60 singlebeam data over several years revealed no indications of groundwater influence on the water-column above the pockmark sites. I could observe several small gas seeps and single gas bubbles in the acoustic water column data though (Figure 5.11). Horizontal, locally continuous pycnoclines observed in the EK60 data do not seem to be affected by fluid seepage above the pockmarks (Figure 5.11). This agrees with findings from Bussmann and Suess (1998) who reported that the water column stability was not affected by less dense groundwater at the base of the pockmarks. The lack of observed acoustic reflections from discharging

groundwater may indicate a quiescence phase during the sampling periods. My sediment porewater chloride profiles (collected May 2019) and also published chloride records from Albert et al., (1998), Bussmann et al. (1999), Müller et al. (2011) or Schlüter et al. (2004) indicate that mixing of low saline groundwater with seawater already occurs in the upper sediments preventing the low saline groundwater from seeping out. In Eckernförde Bay the discharge rate is highly variable since groundwater discharges episodically (Bussmann and Suess, 1998; Schlüter et al., 2004). Unfortunately, no long-term seepage meters were available during the surveys. Even during a strong groundwater outflow event, like observed by Khandriche and Werner (1995) or (Bussmann and Suess, 1998), strong mixing between fresh and saltwater could occur, resulting in a gradual transition of acoustic impedances between the two water bodies which prevents the development of a reflection at their interface. I therefore used a different attempt to find acoustic indications for SGD by analysing the seafloor morphology and backscatter characteristics.

In general, the sediment cores I collected in Eckernförde Bay show a strong relation between methane concentrations and groundwater. Only in core FL17, low chloride porewaters occur close to the sediment surface but no enhanced methane concentrations were observed, nor do I find acoustic indications for free gas in the background-pockmark area. I attribute this to the relatively thin organic-rich sediment cover above the late-glacial sands of Mittelgrund which are dipping south beneath the pockmark (Figure 5.8). The thickness of organic-rich Littorina mud covering the sands increases with distance from Mittelgrund, and once the Littorina mud reaches thicknesses of more than ~ 1 m, free gas occurs in the sediments.

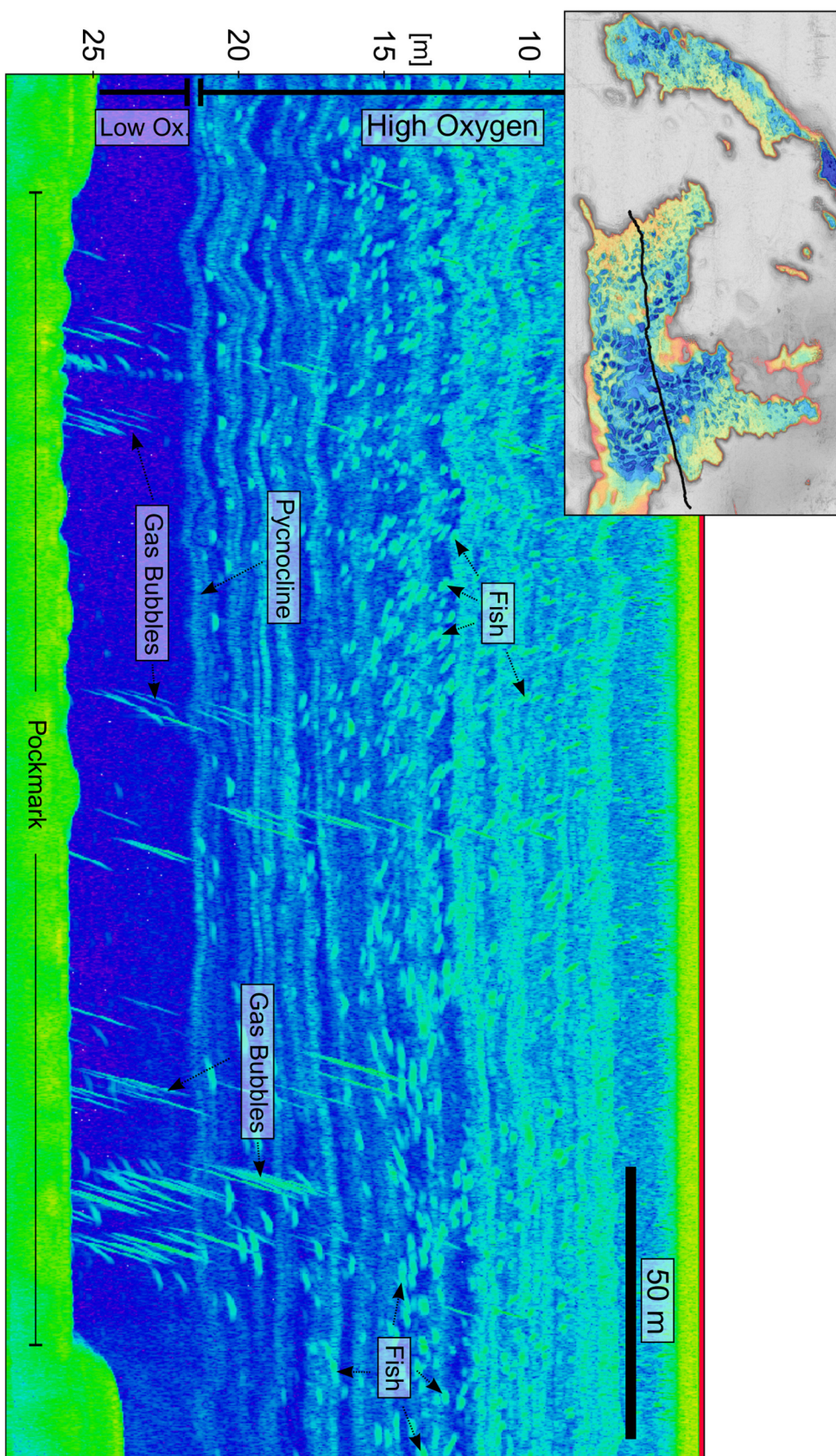


Figure 5.11: EK60 single beam operated at 70 kHz across the western Mittelgrund pockmark. Pycnoclines, fish and gas bubbles are highlighted.

With this one exception, all porewater profiles show increased methane concentrations where chloride concentrations are low. In previous studies, Bugna et al. (1996) and Dulaiova et al. (2010) used elevated methane concentrations in groundwater as a tracer for SGD. Ascending groundwater is not only often already enriched in dissolved methane but also suppresses sulfate mixing into the sediment and therefore increases the amount of metabolizable organic carbon reaching the methanogenic zone, allowing gas to form closer to the seafloor (Albert et al., 1998; Dulaiova et al., 2010). Albert et al. (1998) modelled the influence of different groundwater fluxes on methane concentrations in Eckernförde Bay and showed how an increased groundwater flux can lead to enhanced methane concentrations close to the seafloor when assuming a higher input of metabolizable organic material into morphological sinks like pockmarks. As discussed earlier I acoustically detected and highly accurately located the free gas phase in the muddy sediments of Eckernförde Bay. The free gas phase and therefore the high backscatter in the pockmarks directly correlate with low chloride concentrations. I therefore assume that in areas with sufficient organic material and methanogenesis, acoustic investigations can provide indications for groundwater seepage. Since Fleischer et al. (2001) showed how globally abundant gaseous muds are in coastal waters and shallow adjacent seas, this approach will have significant implications for future efforts to detect and characterise SGD.

5.5 Conclusions

Using high-resolution acoustic data in combination with 13 precisely located sediment cores I reveal the nature of different pockmark classifications made by previous authors in Eckernförde Bay. I propose a classification of the pockmarks into different regimes according to their morphological and backscatter characteristics rather than differentiating them into different types based exclusively on the porewater geochemistry. I discovered a new form of eyed intra-pockmarks with enhanced backscatter signals at their bases which is neither caused by authigenic carbonates nor by a change in seafloor material, but rather by shallow gas occurring close to the seafloor. This implies that even when using high-frequencies, significant signal penetration and volume scattering needs to be considered and seabed classification methods must take this into account. I assume that submarine groundwater discharge 1) enhances upward migration of dissolved and free methane gas bubbles to the seafloor, and 2) enhances methanogenesis close to the seafloor due to decreased sulfate concentrations in groundwater. This leads to an extremely shallow, consistent and more stable gas front within the intra-pockmarks, less affected by temperature changes than the surrounding area. I suggest that this consistent shallow gas alters the geotechnical properties of the unconsolidated sediments making them more easily erodible by the discharging groundwater than the surrounding sediments. The intra-pockmarks are therefore a manifestation of groundwater flow that mobilises free gas, which in turn promotes sediment weaknesses and subsequent erosion. Recognizing this process is important for understanding how pockmarks can be caused by SGD and why they occur where they do. Ultimately, this will help in identifying and characterising offshore groundwater systems which may become important sources of fresh water in the future.

I showed that high-frequency multibeam data can be used to detect shallow gas within the sediment in regions of SGD. The seafloor morphology combined with backscatter data can, therefore, be used to obtain indications for potential groundwater seepage in organic-rich, gaseous, and muddy sediments. Since shallow gas in muddy sediments is a common global phenomenon, my study highlights the importance of investigating how SGD and shallow gas interact close to the seafloor.

I showcase that even at 400 kHz frequency, backscattering strength is significantly increased by subsurface volume scattering from shallow gas. My study also highlights the potential for shallow gas to confuse bathymetric depth and backscatter interpretations, in addition to studies dealing with lower frequencies (e.g., Gaida et al., 2019; Schneider von Deimling et al., 2013). In particular, I show that high-resolution hydroacoustic surveys followed by targeted coring can be used to identify specific locations of SGD and provide new insight into how SGD influences seafloor geochemistry and morphology. The knowledge on the occurrence of SGD in deeper basins and oceans is limited (Post et al., 2013) because of the lack of suitable detection techniques. The methodology I presented describes a possible way to survey SGD associated with methane release and can be used elsewhere around the world to improve the identification and characterisation of SGD.

Chapter 6

Conclusions

Through the different studies presented in this thesis, I have examined fluid migration processes at multiple scales in two geologically different areas. This multi-scale approach enabled me to identify a range of processes that result in fluid migration and seafloor seepage and helps to constrain the timing of fluid expulsion over geological time scales. It also provided insight into the different fluids involved in pockmark formation processes and their interactions with one another. I constrained pockmark modification and formation processes in the Canterbury Basin as well as in Eckernförde Bay, characterising them using seismic and hydroacoustic data. In the following, I will summarize the main findings and provide integrated conclusions of the different studies.

6.1 Main findings

Timing of focused and basin-wide fluid migration and their role in the formation of buried and present-day seafloor pockmarks in the Canterbury Basin.

I was able to constrain the timing of focused fluid migration as well as the basin-wide fluid expulsion by polygonal faults to three individual phases.

1. During the Paleocene, Cretaceous sediments intruded the overlying strata resulting in up-doming of the Paleocene host rock. The sediment intrusions likely formed due to overpressured sediments at depth. The mounded structures affect the overlying Paleocene polygonal fault system due to an

anisotropic stress field above the intrusions. This anisotropic stress field results in radial faults (with a length of up to 3 km) spreading away from the mound like intrusions.

2. During the Oligocene, basin-wide fluid expulsion occurred in the form of dewatering of the Eocene strata and related polygonal fault formation. Above the Eocene polygonal faults, pockmarks have formed on the Oligocene Marshall Paraconformity. Several channels on this surface reveal the paleo-slope direction and a crater-like structure indicates sediment deposition on this surface. These sediments are likely been sourced from Cretaceous strata, similar to the Paleocene intrusions, and extruded on the Marshall Paraconformity through a sediment volcano that was active during the Oligocene.
3. More recently, fluid expulsion from the present-day seafloor is indicated by numerous pockmarks on the Canterbury Shelf and Slope. Although shallow gas accumulations on the Canterbury Slope – associated with a recent gas migration event from Cretaceous strata – are evident in the seismic data, the spatially widespread pockmark occurrence and the local gas manifestation on the slope make a correlation unlikely. Since I could not find any indication of active gas seepage in several extensive datasets on the shelf and slope, different formation mechanisms had to be evaluated for the present-day seafloor pockmarks. While the slope pockmarks likely formed during a monogenetic fluid expulsion event, the shelf pockmarks seem to have formed episodically over time.

Fluids involved in pockmark formation in the Canterbury Basin

Above the Eocene polygonal fault system, widespread buried pockmarks form on the Oligocene Marshall Paraconformity surface. These are likely related to the dewatering of the Eocene fine-grained sediments and the channelling of the fluids along the polygonal faults. No indications for past or present gas accumulations in the Eocene tier could be identified.

The present-day seafloor depressions observed on the Canterbury Shelf probably formed due to gas seepage. In several regions on the shelf, gas is still

apparent in the seismic data. Although the regions of free gas occurrence and the regions where pockmarks occur only partly overlap, it seems possible that gas has escaped from these seafloor depressions in the past. This is supported by the spatial concurrence of free gas and low pockmark densities on the seafloor.

On the slope, on the other hand, I could only identify one localised area with free shallow gas that is probably related to thermogenic gas migration from depth. On the rest of the well-explored slope, there are no indications of free gas in the shallow subsurface. As Hillman et al. (2015) already stated, a gas-induced pockmark formation mechanism seems unlikely. Similarly, a canyon related formation mechanism (as introduced by Hillman et al. (2015)) could be ruled out because of the widespread pockmark distribution on the slope. It seems possible that CO₂ hydrates as proposed by Stott et al. (2019) or sediment compaction related processes, as proposed elsewhere by Chenrai & Huuse (2017) or Dugan & Flemings (2000), have contributed to their formation.

Effects of focused fluid migration on polygonal faults

The Eocene polygonal fault system is apparent throughout the Canterbury Basin, but the formation of these faults is clearly suppressed in the surroundings of a fluid conduit that was feeding an ancient sediment volcano on the surface of the Marshall Paraconformity. It appears that dewatering of the fine-grained sediments is focused at the centre of a cylindrical region, 2 km in radius, probably contributing to the discharge of fluids and sediments onto the ancient surface that is now represented by the Marshall Paraconformity.

I assume this phenomenon occurred either because of a differential stress field induced by buoyant upward-migrating fluids that accumulate at depth, or because of permeable stringers intruding into the surroundings of the feeding pipe and therefore facilitating the dewatering of near-by sediments. This would make additional dewatering pathways like faults redundant, which is why they do not occur in this region.

Relationship between sediment grain size distribution and pockmark occurrence on the Canterbury Shelf

Sediment grainsizes on the Canterbury Shelf range from muds to gravelly sands, which are variable distributed over the shelf (Bostock et al., 2019a). Pockmarks are restricted to deeper parts of the shelf (80-140 m) but occur in all different sediment regimes on the shelf. The low-resolution grain size distribution from Bostock et al. (2019a) corresponds well to the regional backscatter data, which gives insight into more detailed sediment distribution patterns. Although only limited data are available on the shelf, it is apparent that the pockmark density correlates to the regional backscatter strength and therefore the different grain sizes. While I observed over 90 pockmarks/km² in the muddy areas of the shelf, fewer than 10 pockmarks/km² occur in the sands. This suggests that fluid expulsion was not restricted to certain areas but occurred over large regions of the shelf.

Acoustic indicators for submarine groundwater discharge (SGD)

I found acoustic indications for SGD in the form of complex eyed pockmarks in Eckernförde Bay. No indications for freshwater discharge in the water column above pockmarks were apparent in the hydroacoustic data. This seems to result from the mixing of groundwater and seawater within the upper few centimetres of the sediments.

Although I observed no direct seismic manifestation of groundwater expulsion into the water column, I was still able to provide new insights into morphological characteristics of SGD as well as acoustic manifestations of SGD at the seafloor. In organic-rich, gaseous muddy sediments the free gas phase occurs closer to the seafloor in areas of SGD, compared to regions without SGD. The depth of the free gas, which can be mapped using hydroacoustic data, can therefore provide indications for potential SGD locations.

Effects of shallow gas on high-frequency multibeam backscatter data

I show that even with a 400 kHz multibeam system, subsurface volume scatter must be considered in seabed classification approaches. To date, these high-frequencies were thought to only detect the water-sediment interface without penetrating the subsurface. In the weakly attenuating muds of Eckernförde Bay,

significant signal penetration into the subsurface occurs in areas of SGD. This is revealed by the exceptionally high backscatter within the intra-pockmarks which is associated with free gas that lies tens of centimetres beneath the seafloor.

Influence of SGD on pockmark formation and shallow gas distribution in the muddy sediments of Eckernförde Bay

SGD clearly influences the distribution and the depth of free gas occurrences in Eckernförde Bay. In regions of SGD, the upward migration of dissolved as well as free methane gas towards the seafloor is enhanced. Additionally, the SMTZ is uplifted due to suppressed sulfate diffusion into the sediment and therefore rapid sulfate depletion with depth. As a result, free gas occurs closer to the seafloor in regions of SGD compared to regions without SGD. This shallow gas creates the eyed pockmarks observed in Eckernförde Bay. In regions of sufficient organic matter accumulation and resulting free gas occurrence, intra-pockmarks and an uneven surface with a strong relief are seen, whereas, in areas, where groundwater forms the pockmark without additional gas seepage, the pockmark seafloor is smooth and flat. I therefore assume that gas enhances erosion and pockmark formation, but groundwater seems to be the main driver of pockmark formation in Eckernförde Bay.

Contribution of different fluids in the formation of pockmarks

I managed to acoustically differentiate three distinct areas in Eckernförde Bay that correlate to different fluid expulsion regimes, which I refer to as the “background regime”, the “pockmark-background regime” and the “intra-pockmark regime”. The background regime is characterised by a comparatively deep gas occurrence and is not affected by groundwater seepage. In the pockmark-background regime, no gas occurs because of limited organic mud covering the late-glacial sands, but groundwater seepage affects the seafloor morphology. The intra-pockmark regime is affected by gas as well as groundwater seepage, which leads to the strongest topographic depressions and high backscatter signals.

6.2 Final concluding remarks

Pockmark formation mechanisms in many regions are still poorly constrained (Judd and Hovland, 2009). This includes the present-day and the buried pockmarks on the Canterbury Shelf and Slope. I present a new form of eyed pockmarks associated with SGD in Eckernförde Bay. Their formation mechanism includes enhanced gas concentration due to groundwater seepage, leading to oversaturation of methane close to the seafloor. The interstitial gas reduces the shear strength of the shallow sediments making them prone to erosion by bottom currents or seepage events. New Zealand's largest onshore aquifer system and reduced salinities observed in IODP well Site U1353 suggested a possible connection of pockmarks on the Canterbury Shelf to offshore groundwater systems. Modelling results from Micallef et al. (2020) indicated that groundwater flow rates on the shelf would not be sufficient to induce pockmark formation on the shelf. However slow, seeping groundwater on the shelf would still reduce the diffusion of sulfate into the sediment and therefore elevate the sulfate-methane-transition zone, leading to enhanced methane concentrations closer to the seafloor. Although I do not observe present-day indications for methane beneath all of the pockmarks on the shelf, it may still be a formation process that was active in the past. The increased recognition of SGD in many regions worldwide will reveal how widespread this phenomenon is.

6.3 Recommendations for future work

Several aspects of the different studies presented in this thesis remain open for discussion and require further investigation. This section briefly discusses potential future research directions and suggestions for projects that might aid in furthering our understanding of the processes behind pockmark formation and sub-seafloor fluid flow.

6.3.1 Pockmark formation processes

On the Canterbury Shelf, bottom currents and the sediment distribution are still poorly constrained. The limited multibeam data on the shelf, although sufficient

to give some insight into shelfal processes and the pockmark distribution and their alignment, cannot reveal changes in secondary modification processes of the pockmarks (e.g. elongation, alignment) over the shelf, as expected if the alignment was caused by eddy currents. A designated multibeam backscatter survey on the shelf with a constant frequency, pulse width, and power combined with seafloor samples would help to better constrain the sediment distribution pattern on the shelf. I observed several distinct seafloor backscatter changes in the shallower regions of the Canterbury Basin (Figure 6.1), which would be a good target for analysing multibeam frequency penetration as well as sedimentation processes on the Canterbury Shelf. Sediment cores and targeted seafloor samples on the shelf, within and outside of both the elongated and the circular pockmarks would help to better understand their formation history. Geochemical analysis of the cores could test the hypothesis of a shallower SMTZ beneath pockmarks compared to their surroundings. Investigations into the high-backscatter pockmarks on the shelf could help to constrain their formation fluid; i.e. if it was methane, then carbonate precipitation could be the reason for the high backscatter.

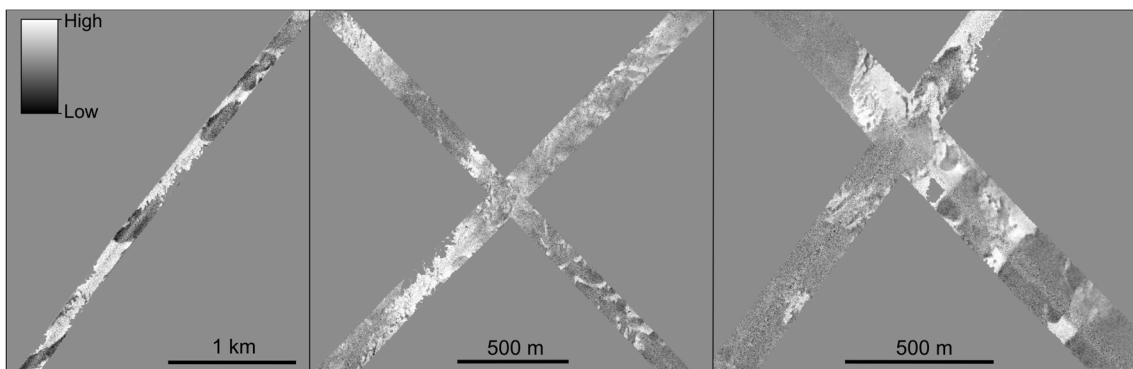


Figure 6.1: Backscatter patterns on the Canterbury Shelf, indicating pronounced changes of seafloor material.

The relationships between pockmarks, polygonal fault systems and the dewatering pathways of buried fine-grained sediments remain unclear. Further mapping of seismic horizons above polygonal fault systems to identify potential seeping structures such as pockmarks could further constrain the dewatering mechanisms of fine-grained sediments.

6.3.2 Submarine groundwater discharge

A key consideration that remains unexplored is the potential change in water column reflectivity around SGD. The acoustic detection of groundwater seepage would enormously increase the effectiveness of locating groundwater seep sites. So far, point measurements of geochemical water analysis are primarily used to locate and characterise SGD. It seems likely that I did not observe any changes in the water column reflectivity above the pockmarks in Eckernförde Bay because of low discharge rates and the mixing of fresh groundwater and saline bottom water already within the seafloor sediments prior to discharge into the overlying sea. This is supported by the sediment cores that show high salinities at the top of the core decreasing with depth.

I am interested in designing a study above localised SGD sites in karstic regions, where discharge rates exceed $1 \text{ m}^3/\text{s}$. The water column reflectivity in these regions could be supplemented by continuous resistivity measurements using geoelectric methods combined with CTD casts.

6.3.3 Temporal variations of Eckernförde Bay pockmarks

The pockmarks of Eckernförde Bay have been the subject of numerous projects. Detailed multibeam studies conducted in 2014 and 2017 reveal no distinct changes in the seafloor morphology of these pockmarks. Previous studies (e.g. Khandriche & Werner (1995)) suggest that sediment ripples form above pockmarks in Eckernförde Bay. Bottom currents in the region reach more than 55 cm/s . It is intriguing that although two hurricane-force storm events (Orkan Axel, January 2017; and Orkan Niklas, March 2015) and an associated storm surge with a reoccurrence interval of 15-20 years have occurred in the western Baltic Sea during this time period (Perlet and Holfort, 2017), with no apparent changes in seafloor morphology observed. Further analysis of deposition and erosion rates within the pockmarks as well as bottom current analysis could help to understand variations in pockmark morphology. The morphological depressions of the intra-pockmarks seem to be preferred areas of sediment deposition and would make a good target to determine sediment transport processes in Eckernförde Bay.

References

- Abegg, F., Anderson, A.L., 1997. The acoustic turbid layer in muddy sediments of Eckernfoerde Bay, Western Baltic: Methane concentration, saturation and bubble characteristics. *Marine Geology* 137, 137–147. doi:10.1016/S0025-3227(96)00084-9
- Adams, C.J., 1981. Migration of late Cenozoic volcanism in the South Island of New Zealand and the Campbell Plateau. *Nature* 294, 153–155.
- Adkins, J.F., McIntyre, K., Schrag, D.P., 2002. The Salinity, Temperature, and $\delta^{18}\text{O}$ of Glacial Deep Ocean. *Science* 298, 1769–1773.
- Ainslie, M.A., McColm, J.G., 1998. A simplified formula for viscous and chemical absorption in sea water. *The Journal of the Acoustical Society of America* 103, 1671–1672.
- Aki, K., Richards, P.G., 1980. *Quantitative Seismology: Theory and Methods*. Freeman.
- Albert, D.B., Martens, C.S., Alperin, M.J., 1998. Biogeochemical processes controlling methane in gassy coastal sediments—Part 2: groundwater flow control of acoustic turbidity in Eckernförde Bay Sediments. *Continental Shelf Research* 18, 1771–1793.
- Alevizos, E., Snellen, M., Simons, D.G., Siemes, K., Greinert, J., 2018. Multi-angle backscatter classification and sub-bottom profiling for improved seafloor characterization. *Marine Geophysical Research* 39, 289–306. doi:10.1007/s11001-017-9325-4
- Anadarko and Origin Energy, 2009. Waka 3D - provided by New Zealand

- Petroleum and Minerals (NZPM).
- Andresen, K.J., 2012. Fluid flow features in hydrocarbon plumbing systems: What do they tell us about the basin evolution? *Marine Geology* 332, 89–108.
- Andresen, K.J., Huuse, M., 2011. “Bulls-eye” pockmarks and polygonal faulting in the Lower Congo Basin: Relative timing and implications for fluid expulsion during shallow burial. *Marine Geology* 279, 111–127.
doi:10.1016/j.margeo.2010.10.016
- Andresen, K.J., Huuse, M., Clausen, O.R., 2008. Morphology and distribution of Oligocene and Miocene pockmarks in the Danish North Sea -implications for bottom current activity and fluid migration. *Basin Research* 20, 445–466.
doi:10.1111/j.1365-2117.2008.00362.x
- Anka, Z., Berndt, C., Gay, A., 2012. Hydrocarbon leakage through focused fluid flow systems in continental margins. *Marine Geology* 334, 1–3.
doi:10.1016/j.margeo.2012.10.012
- Baciu, C.L., Caracausi, A., Italiano, F., Etiope, G., 2007. Mud volcanoes and methane seeps in Romania: main features and gas flux. *Annals of geophysics* 50, 501–512.
- Balzer, W., 1984. Organic matter degradation and biogenic element cycling in a nearshore sediment (Kiel Bight). *Limnology and Oceanography* 29, 1231–1246.
- Balzer, W., Erlenkeuser, H., Hartmann, M., Müller, P.J., Pollehne, F., 1987. Diagenesis and exchange processes at the benthic boundary, in: *Seawater-Sediment Interactions in Coastal Waters*. Springer, pp. 111–161.
- Bange, H.W., Hansen, H.P., Malien, F., Laß, K., Dale, A.W., Karstensen, J., Petereit, C., Friedrichs, G., 2011. Boknis Eck time series station (SW Baltic Sea): measurements from 1957 to 2010. *LOICZ inprint* 2011, 16–22.
- Barley, M.E., 1987. Origin and evolution of Mid-Cretaceous, garnet-bearing, intermediate and silicic volcanics from Canterbury, New Zealand. *Journal of Volcanology and Geothermal Research* 32, 247–267.
- Barnes, P.M., Lamarche, G., Bialas, J., Henrys, S., Pecher, I., Netzeband, G.L., Greinert,

- J., Mountjoy, J.J., Pedley, K., Crutchley, G.J., 2010. Tectonic and geological framework for gas hydrates and cold seeps on the Hikurangi subduction margin, New Zealand. *Marine Geology* 272, 26–48.
- Barrell, D.J.A., 2011. Quaternary Glaciers of New Zealand, in: *Developments in Quaternary Science*. Elsevier Inc., pp. 1047–1064. doi:10.1016/B978-0-444-53447-7.00075-1
- Barrier, A., 2019. Tectonics, sedimentation and magmatism of the Canterbury Basin, New Zealand. University of Canterbury, Christchurch, New Zealand, Dissertation for the degree of Doctor of Philosophy in Geology.
- Beentjes, M.P., Bull, B., Hurst, R.J., Bagley, N.W., 2002. Demersal fish assemblages along the continental shelf and upper slope of the east coast of the South Island, New Zealand. *New Zealand Journal of Marine and Freshwater Research* 36, 197–223. doi:10.1080/00288330.2002.9517080
- Beentjes, M.P., Stevenson, M.L., 2001. Review of the east coast South Island summer trawl survey time series, 1996-97 to 1999-2000 - Final Research Report for Ministry of Fisheries Research Project MOF1999/040 Objective 1. NIWA.
- Berndt, C., 2005. Focused fluid flow in passive continental margins. *Philosophical Transactions of the Royal Society A: Mathematical, Physical and Engineering Sciences* 363, 2855–2871. doi:10.1098/rsta.2005.1666
- Berndt, C., Bünz, S., Mienert, J., 2003. Polygonal fault systems on the mid-Norwegian margin: a long-term source for fluid flow. *Subsurface Sediment Mobilisation*, Geological Society, London, Special Publications 216, 283–290. doi:10.1144/GSL.SP.2003.216.01.18
- Berndt, C., Jacobs, C., Evans, A., Gay, A., Elliott, G., Long, D., Hitchen, K., 2012. Kilometre-scale polygonal seabed depressions in the Hatton Basin, NE Atlantic Ocean: Constraints on the origin of polygonal faulting. *Marine Geology* 332–334, 126–133. doi:10.1016/j.margeo.2012.09.013
- Berndt, C., Micallef, A., 2019. Could offshore groundwater rescue coastal cities? *Nature* 574, 36.

- Bertoni, C., Cartwright, J.A., Foschi, M., Martin, J., 2018. Spectrum of gas migration phenomena across multilayered sealing sequences. *AAPG Bulletin* 102, 1011–1034. doi:10.1306/0810171622617210
- Bialas, J., Klauke, I., Mögeltönder, J., 2013. RV SONNE Fahrtbericht/Cruise Report S0226-CHRIMP CHatham Rise Methane Pockmarks, 07.01.-06.02. 2013/Auckland–Lyttelton, 07.02.–01.03. 2013/Lyttelton-Wellington.
- Biaostoch, A., Treude, T., Rüpke, L.H., Riebesell, U., Roth, C., Burwicz, E.B., Park, W., Latif, M., Böning, C.W., Madec, G., Wallmann, K., 2011. Rising Arctic Ocean temperatures cause gas hydrate destabilization and ocean acidification. *Geophysical Research Letters* 38. doi:10.1029/2011GL047222
- Bischoff, A., Nicol, A., Barrier, A., Wang, H., 2019a. Paleogeography and volcanic morphology reconstruction of a buried monogenetic volcanic field (part 2). *Bulletin of Volcanology* 81. doi:10.1007/s00445-019-1317-6
- Bischoff, A., Rossetti, M., Nicol, A., Kennedy, B., 2019b. Seismic reflection and petrographic interpretation of a buried monogenetic volcanic field (part 1). *Bulletin of Volcanology* 81, 1–19. doi:10.1007/s00445-019-1316-7
- Björck, S., 1995. A review of the history of the Baltic Sea, 13.0-8.0 ka BP. *Quaternary International* 27, 19–40. doi:10.1016/1040-6182(94)00057-C
- Blanke, S.J., 2015. Caravel-1: Lessons Learned in the Deepwater Canterbury Basin, in: International Conference and Exhibition, Melbourne, Australia 13-16 September 2015. Society of Exploration Geophysicists and American Association of Petroleum Geologists, p. 519.
- Boetius, A., Ravenschlag, K., Schubert, C.J., Rickert, D., Widdel, F., Gieseke, A., Amann, R., Jørgensen, B.B., Witte, U., Pfannkuche, O., 2000. A marine microbial consortium apparently mediating anaerobic oxidation of methane. *Nature* 407, 623–626. doi:10.1038/35036572
- Bohrmann, G., Heeschen, K., Jung, C., Weinrebe, W., Baranov, B., Cailleau, B., Heath, R., Hühnerbach, V., Hort, M., Masson, D., Trummer, I., 2002. Widespread fluid expulsion along the seafloor of the Costa Rica convergent margin. *Terra Nova* 14, 69–79. doi:10.1046/j.1365-3121.2002.00400.x

- Bohrmann, G., Ivanov, M., Foucher, J.P., Spiess, V., Bialas, J., Greinert, J., Weinrebe, W., Abegg, F., Aloisi, G., Artemov, Y., Blinova, V., Drews, M., Heidersdorf, F., Krabbenhörf, A., Klauke, I., Krastel, S., Leder, T., Polikarpov, I., Saburova, M., Schmale, O., Seifert, R., Volkonskaya, A., Zillmer, M., 2003. Mud volcanoes and gas hydrates in the Black Sea: New data from Dvurechenskii and Odessa mud volcanoes. *Geo-Marine Letters* 23, 239–249. doi:10.1007/s00367-003-0157-7
- Borges, A. V., Champenois, W., Gypens, N., Delille, B., Harlay, J., 2016. Massive marine methane emissions from near-shore shallow coastal areas. *Scientific Reports* 6, 27908. doi:10.1038/srep27908
- Bostock, H., Jenkins, C., Mackay, K., Carter, L., Nodder, S.D., Orpin, A.R., Pallentin, A., Wysoczanski, R., 2019a. Distribution of surficial sediments in the ocean around New Zealand/Aotearoa. Part B: continental shelf. *New Zealand Journal of Geology and Geophysics* 62, 24–45. doi:10.1080/00288306.2018.1523199
- Bostock, H., Jenkins, C., Mackay, K., Carter, L., Nodder, S.D., Orpin, A.R., Pallentin, A., Wysoczanski, R., 2019b. Distribution of surficial sediments in the ocean around New Zealand/Aotearoa. Part A: continental slope and deep ocean. *New Zealand Journal of Geology and Geophysics* 62, 1–23. doi:10.1080/00288306.2018.1523198
- Böttner, C., Berndt, C., Reinardy, B., Geersen, J., Karstens, J., Bull, J.M., Callow, B.J., Lichtschlag, A., Schmidt, M., Elger, J., Schramm, B., Haeckel, M., 2019. Pockmarks in the Witch Ground Basin, Central North Sea. *Geochemistry, Geophysics, Geosystems* 20, 1698–1719. doi:10.1029/2018GC008068
- Branney, M.J., 1995. Downsag and extension at calderas: new perspectives on collapse geometries from ice-melt, mining, and volcanic subsidence. *Bulletin of Volcanology* 57, 303–318. doi:10.1007/BF00301290
- Brothers, L.L., Kelley, J.T., Belknap, D.F., Barnhardt, W.A., Andrews, B.D., Maynard, M.L., 2011a. More than a century of bathymetric observations and present-day shallow sediment characterization in Belfast Bay, Maine, USA: implications for pockmark field longevity. *Geo-Marine Letters* 31, 237–248. doi:10.1007/s00367-011-0228-0
- Brothers, L.L., Kelley, J.T., Belknap, D.F., Barnhardt, W.A., Koons, P.O., 2011b.

- Pockmarks: self-scouring seep features, in: Proc 7th Int Conf Gas Hydrates. pp. 17–21.
- Brown, K., 1990. The nature and hydrogeologic significance of mud diapirs and diatremes for accretionary systems. *Journal of Geophysical Research: Solid Earth* 95, 8969–8982.
- Brown, L.J., Beetham, R.D., Paterson, B.R., Weeber, J.H., 1995. Geology of Christchurch, New Zealand. *Environmental and Engineering Geoscience* 1, 427–488.
- Browne, G.H., Field, B.D., 1988. A review of Cretaceous-Cenozoic sedimentation and tectonics, east coast, South Island, New Zealand. *Sequences, Stratigraphy, Sedimentology: Surface and Subsurface Memoir* 15, 37–48.
- Browne, G.H., Naish, T.R., 2003. Facies development and sequence architecture of a late Quaternary fluvial-marine transition, Canterbury Plains and shelf, New Zealand: implications for forced regressive deposits. *Sedimentary Geology* 158, 57–86. doi:10.1016/S0037-0738(02)00258-0
- Bugna, G.C., Chanton, J.P., Cable, J.E., Burnett, W.C., Cable, P.H., 1996. The importance of groundwater discharge to the methane budgets of nearshore and continental shelf waters of the northeastern Gulf of Mexico. *Geochimica et Cosmochimica Acta* 60, 4735–4746. doi:10.1016/S0016-7037(96)00290-6
- Bureau, D., Mourgues, R., Cartwright, J.A., Foschi, M., Abdelmalak, M.M., 2013. Characterisation of interactions between a pre-existing polygonal fault system and sandstone intrusions and the determination of paleo-stresses in the Faroe-Shetland basin. *Journal of Structural Geology* 46, 186–199. doi:10.1016/j.jsg.2012.09.003
- Burnett, W.C., Aggarwal, P.K., Aureli, A., Bokuniewicz, H.J., Cable, J.E., Charette, M.A., Kontar, E., Krupa, S., Kulkarni, K.M., Loveless, A., Moore, W.S., Oberdorfer, J.A., Oliveira, J., Ozyurt, N., Povinec, P., Privitera, A.M.G., Rajar, R., Ramessur, R.T., Scholten, J., Stieglitz, T., Taniguchi, M., Turner, J. V, 2006. Quantifying submarine groundwater discharge in the coastal zone via multiple methods. *Science of the Total Environment* 367, 498–543. doi:10.1016/j.scitotenv.2006.05.009

- Burnett, W.C., Dulaiova, H., 2003. Estimating the dynamics of groundwater input into the coastal zone via continuous radon-222 measurements. *Journal of Environmental Radioactivity* 69, 21–35. doi:10.1016/S0265-931X(03)00084-5
- Bussmann, I., Damm, E., Schlüter, M., Wessels, M., 2013. Fate of methane bubbles released by pockmarks in Lake Constance. *Biogeochemistry* 112, 613–623. doi:10.1007/s10533-012-9752-x
- Bussmann, I., Dando, P., Niven, S., Suess, E., 1999. Groundwater seepage in the marine environment: role for mass flux and bacterial activity. *Marine Ecology Progress Series* 178, 169–177. doi:10.3354/meps178169
- Bussmann, I., Suess, E., 1998. Groundwater seepage in Eckernförde Bay (Western Baltic Sea): Effect on methane and salinity distribution of the water column. *Continental Shelf Research* 18, 1795–1806. doi:10.1016/S0278-4343(98)00058-2
- Cable, J.E., Burnett, W.C., Chanton, J.P., 1997. Magnitude and variations of groundwater seepage along a Florida marine shoreline. *Biogeochemistry* 38, 189–205.
- Carter, L., Carter, R.M., 1985. Current modification of a mass failure deposit on the continental shelf, north Canterbury, New Zealand. *Marine geology* 62, 193–211.
- Carter, L., Carter, R.M., Nelson, C.S., Fulthorpe, C.S., Neil, H.L., 1990. Evolution of Pliocene to Recent abyssal sediment waves on Bounty Channel levees, New Zealand. *Marine Geology* 95, 97–109. doi:10.1016/0025-3227(90)90043-J
- Carter, R.M., 1988. Post-breakup stratigraphy of the kaikoura synthem (cretaceous-cenozoic), continental margin, southeastern New Zealand. *New Zealand Journal of Geology and Geophysics* 31, 405–429. doi:10.1080/00288306.1988.10422141
- Carter, R.M., 1985. The Mid-Oligocene Marshall Paraconformity, New Zealand: Coincidence with Global Eustatic Sea-Level Fall or Rise? *The Journal of Geology* 93, 359–371.

- Carter, R.M., Fulthorpe, C.S., Lu, H., 2004a. Canterbury drifts at Ocean Drilling Program site 1119, New Zealand: Climatic modulation of southwest Pacific intermediate water flows since 3.9 Ma. *Geology* 32, 1005–1008. doi:10.1130/G20783.1
- Carter, R.M., Gammon, P.R., Millwood, L., 2004b. Glacial-interglacial (MIS 1-10) migrations of the Subtropical Front across ODP Site 1119, Canterbury Bight, Southwest Pacific Ocean. *Marine Geology* 205, 29–58. doi:10.1016/S0025-3227(04)00017-9
- Carter, R.M., Landis, C.A., 1982. Oligocene unconformities in the South Island. *Journal of the Royal Society of New Zealand* 12, 42–46. doi:10.1080/03036758.1982.10427165
- Carter, R.M., Landis, C.A., 1972. Correlative Oligocene unconformities in southern Australasia. *Nature* 237, 12–13.
- Carter, R.M., Norris, R.J., 1976. Cainozoic history of southern New Zealand: An accord between geological observations and plate-tectonic predictions. *Earth and Planetary Science Letters* 31, 85–94. doi:10.1016/0012-821X(76)90099-6
- Cartwright, J.A., 2011. Diagenetically induced shear failure of fine-grained sediments and the development of polygonal fault systems. *Marine and Petroleum Geology* 28, 1593–1610. doi:10.1016/j.marpetgeo.2011.06.004
- Cartwright, J.A., 1994a. Episodic basin-wide fluid expulsion from geopressured shale sequences in the North sea basin. *Geology* 22(5), 447–450.
- Cartwright, J.A., 1994b. Episodic basin-wide hydrofracturing of overpressured Early Cenozoic mudrock sequences in the North Sea Basin. *Marine and Petroleum Geology* 11, 587–607. doi:10.1016/0264-8172(94)90070-1
- Cartwright, J.A., Dewhurst, D.N., 1998. Layer-bound compaction faults in fine-grained sediments. *Geological Society of America Bulletin* 110, 1242–1257.
- Cartwright, J.A., Huuse, M., Aplin, A., 2007. Seal bypass systems. *AAPG Bulletin* 91, 1141–1166. doi:10.1306/04090705181
- Cartwright, J.A., James, D., Bolton, A., 2003. The genesis of polygonal fault systems:

- a review. Geological Society, London, Special Publications 216, 223–243.
- Cartwright, J.A., Lonergan, L., 1996. Volumetric contraction during the compaction of mudrocks: A mechanism for the development of regional-scale polygonal fault systems. *Basin Research* 8, 183–193. doi:10.1046/j.1365-2117.1996.01536.x
- Cartwright, J.A., Santamarina, C., 2015. Seismic characteristics of fluid escape pipes in sedimentary basins: Implications for pipe genesis. *Marine and Petroleum Geology* 65, 126–140. doi:10.1016/j.marpetgeo.2015.03.023
- Castagna, J.P., Backus, M.M., 1993. Offset-dependent reflectivity—Theory and practice of AVO analysis. Society of Exploration Geophysicists.
- Castagna, J.P., Swan, H.W., 1997. Principles of AVO crossplotting. *The Leading Edge* 16, 337. doi:10.1190/1.1437626
- Cathles, L.M., Su, Z., Chen, D., 2010. The physics of gas chimney and pockmark formation, with implications for assessment of seafloor hazards and gas sequestration. *Marine and Petroleum Geology* 27, 82–91. doi:10.1016/j.marpetgeo.2009.09.010
- Cayocca, F., Sultan, N., Cochonat, P., Bourillet, J.F., 2001. Evaluation of the risk of marine slope instability: A pseudo-3d approach for application to large areas. *Marine Georesources and Geotechnology* 19, 107–133. doi:10.1080/10641190109353807
- Cevatoglu, M., Bull, J.M., Vardy, M.E., Gernon, T.M., Wright, I.C., Long, D., 2015. Gas migration pathways, controlling mechanisms and changes in sediment acoustic properties observed in a controlled sub-seabed CO₂ release experiment. *International Journal of Greenhouse Gas Control* 38, 26–43. doi:10.1016/j.ijggc.2015.03.005
- Chapron, E., Van Rensbergen, P., De Batist, M., Beck, C., Henriot, J.P., 2004. Fluid-escape features as a precursor of a large sublacustrine sediment slide in Lake Le Bourget, NW Alps, France. *Terra Nova* 16, 305–311. doi:10.1111/j.1365-3121.2004.00566.x
- Chenrai, P., Huuse, M., 2020. Sand injection and polygonal faulting in the Great

- South Basin, New Zealand. Geological Society, London, Special Publications SP493-2018-107. doi:10.1144/SP493-2018-107
- Chenrai, P., Huuse, M., 2017. Pockmark formation by porewater expulsion during rapid progradation in the offshore Taranaki Basin, New Zealand. *Marine and Petroleum Geology* 82, 399–413. doi:10.1016/j.marpetgeo.2017.02.017
- Chiswell, S.M., 1996. Variability in the Southland current, New Zealand. *New Zealand Journal of Marine and Freshwater Research* 30, 1–17. doi:10.1080/00288330.1996.9516693
- Cho, H., Kim, G., Kwon, E.Y., Moosdorf, N., Garcia-Orellana, J., Santos, I.R., 2018. Radium tracing nutrient inputs through submarine groundwater discharge in the global ocean. *Scientific Reports* 8, 2439. doi:10.1038/s41598-018-20806-2
- Christodoulou, D., Papatheodorou, G., Ferentinos, G., Masson, M., 2003. Active seepage in two contrasting pockmark fields in the Patras and Corinth gulfs, Greece. *Geo-Marine Letters* 23, 194–199. doi:10.1007/s00367-003-0151-0
- Clausen, J.A., Gabrielsen, R.H., Reksnes, P.A., Nysöther, E., 1999. Development of intraformational (Oligocene-Miocene) faults in the northern North Sea: Influence of remote stresses and doming of Fennoscandia. *Journal of Structural Geology* 21, 1457–1475. doi:10.1016/S0191-8141(99)00083-8
- Clayton, C., Hay, S., 1994. Gas migration mechanisms from accumulation to surface. *Bulletin of the Geological Society of Denmark* 41, 12–23.
- Cohen, D., Person, M., Wang, P., Gable, C.W., Hutchinson, D., Marksamer, A., Dugan, B., Kooi, H., Groen, K., Lizarralde, D., Evans, R.L., Day-Lewis, F.D., Lane, J.W., 2010. Origin and Extent of Fresh Paleowaters on the Atlantic Continental Shelf, USA. *Ground Water* 48, 143–158. doi:10.1111/j.1745-6584.2009.00627.x
- Coombs, D.S., Adams, C.J., Roser, B.P., Reay, A., Coombs, D.S., Adams, C.J., Roser, B.P., Coombs, D.S., Adams, C.J., 2008. Geochronology and geochemistry of the Dunedin Volcanic Group, eastern Otago, New Zealand. *New Zealand Journal of Geology and Geophysics* 51, 195–218. doi:10.1080/00288300809509860

- Coombs, D.S., Cas, R.A., Kawachi, Y., Landis, C.A., McDonough, W.F., Reay, A., 1986. Cenozoic volcanism in north, east and central Otago. *Royal Society of New Zealand Bulletin* 23, 278–312.
- Crutchley, G.J., Maslen, G., Pecher, I.A., Mountjoy, J.J., 2016. High-resolution seismic velocity analysis as a tool for exploring gas hydrate systems : An example from New Zealand ' s southern Hikurangi margin. *Interpretation* 4, 1–12.
- Daly, C., Hattersley, G., 2007. Cutter-1 well completion report-Basic Data-Tap Oil Limited In: *New Zealand Open-file Petroleum Report 3385*. Crown Minerals, Wellington.
- Dandapath, S., Chakraborty, B., Karisiddaiah, S.M., Menezes, A., Ranade, G., Fernandes, W., Naik, D.K., Prudhvi Raju, K.N., 2010. Morphology of pockmarks along the western continental margin of India: Employing multibeam bathymetry and backscatter data. *Marine and Petroleum Geology* 27, 2107–2117. doi:10.1016/j.marpetgeo.2010.09.005
- Davies, R.J., Stewart, S.A., 2005. Emplacement of giant mud volcanoes in the South Caspian Basin: 3D seismic reflection imaging of their root zones. *Journal of the Geological Society, London* 162, 1–4.
- Davy, B., Pecher, I.A., Wood, R., Carter, L., Gohl, K., 2010. Gas escape features off New Zealand: Evidence of massive release of methane from hydrates. *Geophysical Research Letters* 37, 1–5. doi:10.1029/2010GL045184
- Dewhurst, D.N., Cartwright, J.A., Lonergan, L., 1999. The development of polygonal fault systems by syneresis of colloidal sediments. *Marine and Petroleum Geology* 16, 793–810. doi:10.1016/S0264-8172(99)00035-5
- Dietrich, G., 1951. Oberflächenströmungen im Kattegat, im Sund und in der Beltsee. *Deutsche Hydrografische Zeitschrift* 4, 129–150.
- Dimitrov, L.I., 2002. Mud volcanoes — the most important pathway for degassing deeply buried sediments. *Earth-Science Reviews* 59, 49–76.
- Dimitrov, L.I., Woodside, J., 2003. Deep sea pockmark environments in the eastern Mediterranean. *Marine Geology* 195, 263–276. doi:10.1016/S0025-3227(02)00692-8

- Dugan, B., Flemings, P.B., 2000. Overpressure and Fluid Flow in the New Jersey Continental Slope: Implications for Slope Failure and Cold Seeps. *Science* 289, 288–291. doi:10.1126/science.289.5477.288
- Dulaiova, H., Camilli, R., Henderson, P.B., Charette, M.A., 2010. Coupled radon, methane and nitrate sensors for large-scale assessment of groundwater discharge and non-point source pollution to coastal waters. *Journal of Environmental Radioactivity* 101, 553–563. doi:10.1016/j.jenvrad.2009.12.004
- Dunbar, C.O., Rodgers, J., 1957. *Principles of stratigraphy*. John Wiley and Sons.
- Dupuis, M., Imbert, P., Odonne, F., Vendeville, B., 2019. Mud volcanism by repeated roof collapse: 3D architecture and evolution of a mud volcano cluster offshore Nigeria. *Marine and Petroleum Geology* 110, 368–387. doi:10.1016/j.marpetgeo.2019.07.033
- Ecker, C., Dvorkin, J., Nur, A., 1998. Sediments with gas hydrates: Internal structure from seismic AVO. *Geophysics* 63, 1659–1669.
- Edgerton, H.E., Seibold, E., Vollbrecht, K., Werner, F., 1966. Morphologische Untersuchungen am Mittelgrund (Eckernförde Bucht, westliche Ostsee). *Meyniana* 16, 37–50.
- Ehlers, J., Ehlers, J., Gibbard, P.L., Hughes, P.D., 2011. Quaternary glaciations-extent and chronology: a closer look. Elsevier.
- Ekman, M., 1996. A consistent map of the postglacial uplift of Fennoscandia. *Terra Nova* 8, 158–165.
- Elger, J., Berndt, C., Rüpke, L., Krastel, S., Gross, F., Geissler, W., 2018. Submarine slope failures due to pipe structure formation. *Nature Communications* 9, 1–6. doi:10.1038/s41467-018-03176-1
- Etiopie, G., Baciu, C.L., Schoell, M., 2011. Extreme methane deuterium, nitrogen and helium enrichment in natural gas from the Homorod seep (Romania). *Chemical Geology* 280, 89–96. doi:10.1016/j.chemgeo.2010.10.019
- Etiopie, G., Martinelli, G., 2009. “Pieve Santo Stefano” is not a mud volcano: Comment on “Structural controls on a carbon dioxide-driven mud volcano

- field in the Northern Apennines” (by Bonini, 2009). *Journal of Structural Geology* 31, 1270–1271. doi:10.1016/j.jsg.2009.06.009
- Evans, R.L., Lizarralde, D., 2003. Geophysical evidence for karst formation associated with offshore groundwater transport: An example from North Carolina. *Geochemistry, Geophysics, Geosystems* 4, 1–9. doi:10.1029/2003GC000510
- Fabian, H.S., Roese, K.L., 1962. Das Erdölfeld Schwedeneck. *Erdöl-Zeitschrift* 78, 283–294.
- Fenaughty, J.M., Bagley, N.W., 1981. WJ Scott New Zealand trawl survey: South Island East Coast. Fisheries Technical Report-New Zealand Ministry of Agriculture and Fisheries, Fisheries Management Division (New Zealand).
- Ferguson, G., Gleeson, T., 2012. Vulnerability of coastal aquifers to groundwater use and climate change. *Nature Climate Change* 2, 342–345. doi:10.1038/nclimate1413
- Field, B.D., Browne, G.H., Davy, B.W., Herzer, R.H., Hoskins, R.H., Raine, J.I., Wilson, G.J., Sewell, R.J., Smale, D., Watters, W.A., 1989. Cretaceous and Cenozoic sedimentary basins and geological evolution of the Canterbury region, South Island, New Zealand. *New Zealand Geological Survey basin studies* 2. 94 p.
- Fildani, A., Normark, W.R., Kostic, S., Parker, G., 2006. Channel formation by flow stripping: Large-scale scour features along the Monterey East Channel and their relation to sediment waves. *Sedimentology* 53, 1265–1287.
- Findlay, R.H., 1980. The marshall paraconformity. *New Zealand Journal of Geology and Geophysics* 23, 125–133. doi:10.1080/00288306.1980.10424198
- Fleischer, P., Orsi, T.H., Richardson, M.D., Anderson, A.L., 2001. Distribution of free gas in marine sediments: A global overview. *Geo-Marine Letters* 21, 103–122. doi:10.1007/s003670100072
- Fraser, D.R.A., Gorman, A.R., Pecher, I.A., Crutchley, G.J., Henrys, S.A., 2016. Gas hydrate accumulations related to focused fluid flow in the Pegasus Basin, southern Hikurangi Margin, New Zealand. *Marine and Petroleum Geology* 77, 399–408. doi:10.1016/j.marpetgeo.2016.06.025

- Fulthorpe, C.S., Austin, J.A., Saustrup, S., Dolan, J., Lu, H., Cathro, D., Burger, R., Browne, G.H., Herr, S., Diebold, J., Stennett, J., Gutierrez, C., Arko, B., Hegel, K., Hanley, J., Maiwiriwiri, R., 2000a. R/V Maurice Ewing Cruise EW0001 High-Resolution Multichannel Seismic Survey, Offshore Canterbury Basin, New Zealand.
- Fulthorpe, C.S., Carter, R.M., 1989. Test of seismic sequence methodology on a Southern Hemisphere passive margin: The Canterbury Basin, New Zealand. *Marine and Petroleum Geology* 6, 348–359. doi:10.1016/0264-8172(89)90031-7
- Fulthorpe, C.S., Carter, R.M., Miller, K.G., Wilson, J., 1996. Marshall Paraconformity: A mid-Oligocene record of inception of the Antarctic Circumpolar Current and coeval glacio-eustatic lowstand? *Marine and Petroleum Geology* 13, 61–77. doi:10.1016/0264-8172(95)00033-X
- Fulthorpe, C.S., Frohlich, C., Mann, P., 2000b. Processed multichannel seismic data in the Canterbury Basin, New Zealand, acquired during R/V Maurice Ewing expedition EW0001 (2000). Interdisciplinary Earth Data Alliance (IEDA). doi:doi:10.1594/IEDA/500007
- Fulthorpe, C.S., Hoyanagi, K., Blum, P., Guèrin, G., Slagle, A.L., Blair, S.A., Browne, G.H., Carter, R.M., Ciobanu, M.C., Claypool, G.E., Crundwell, M.P., Dinarès-Turel, J., Ding, X., George, S.C., Hepp, D.A., Jaeger, J., Kawagata, S., Kemp, D.B., Kim, Y.G., Kominz, M.A., Lever, H., Lipp, J.S., Marsaglia, K.M., McHugh, C.M., Murakoshi, N., Ohi, T., Pea, L., Richaud, M., Suto, I., Tanabe, S., Tinto, K.J., Uramoto, G., Yoshimura, T., 2010. Integrated Ocean Drilling Program Expedition 317 Preliminary Report, Canterbury Basin Sea Level: Global and local controls on continental margin stratigraphy. *Integrated Ocean Drilling Program: Preliminary Reports* 1–133. doi:10.2204/iodp.pr.317.2010
- Gafeira, J., Long, D., Diaz-Doce, D., 2012. Semi-automated characterisation of seabed pockmarks in the central North Sea. *Near Surface Geophysics* 10, 301–312.
- Gaida, T.C., Mohammadloo, T.H., Snellen, M., Simons, D.G., 2019. Mapping the Seabed and Shallow Subsurface with Multi-Frequency Multibeam

- Echosounders. *Remote Sensing* 12, 52. doi:10.3390/rs12010052
- Galland, O., Planke, S., Neumann, E.R., Malthe-Sørensen, A., 2009. Experimental modelling of shallow magma emplacement: Application to saucer-shaped intrusions. *Earth and Planetary Science Letters* 277, 373–383. doi:10.1016/j.epsl.2008.11.003
- Galparsoro, I., Muxika, I., Garmendia, J.M., Rodríguez, J.G., 2020. Continental shelf, canyons and pockmark fields in the southeastern Bay of Biscay, in: *Seafloor Geomorphology as Benthic Habitat*. Elsevier, pp. 769–781. doi:10.1016/B978-0-12-814960-7.00046-4
- García-García, A., Orange, D.L., Maher, N.M., Heffernan, A.S., Fortier, G.S., Malone, A., 2004. Geophysical evidence for gas geohazards off Iskenderun Bay, SE Turkey. *Marine and Petroleum Geology* 21, 1255–1264. doi:10.1016/j.marpetgeo.2004.08.002
- Gay, A., Berndt, C., 2007. Cessation / reactivation of polygonal faulting and effects on fluid flow in the Vøring Basin , Norwegian Margin. *Journal of the Geological Society* 164, 129–141.
- Gay, A., Lopez, M., Cochonat, P., Sermondadaz, G., 2004. Polygonal faults-furrows system related to early stages of compaction-Upper Miocene to present sediments of the Lower Congo Basin. *Basin Research* 16, 101–116. doi:10.1111/j.1365-2117.2003.00224.x
- Gay, A., Mourgues, R., Berndt, C., Bureau, D., Planke, S., Laurent, D., Gautier, S., Lauer, C., Loggia, D., 2012. Anatomy of a fluid pipe in the Norway Basin: Initiation, propagation and 3D shape. *Marine Geology* 332–334, 75–88. doi:10.1016/j.margeo.2012.08.010
- GEBCO, 2019. *Compilation Group 2019 Grid* (doi:10.5285/836f016a-33be-6ddc-e053-6c86abc0788e).
- Geyer, D., 1964. Eigenschwingungen und Erneuerung des Wasser in der Eckernförder Bucht unter besonderer Berücksichtigung der Sturmflut vom 5.-6. Dezember 1961. *Kieler Meeresforschung* 21, 33–54.
- Goff, J.A., 2019. *Modern and Fossil Pockmarks in the New England Mud Patch*:

- Implications for Submarine Groundwater Discharge on the Middle Shelf. *Geophysical Research Letters* 46, 12213–12220. doi:10.1029/2019GL084881
- Gontz, A.M., Belknap, D.F., Kelley, J.T., 2002. Seafloor Features and Characteristics of the Black Ledges Area, Penobscot Bay, Maine, USA. *Journal of Coastal Research* 36, 333–339. doi:10.2112/1551-5036-36.sp1.333
- Goult, N.R., 2008. Geomechanics of polygonal fault systems: a review. *Petroleum Geoscience* 14, 389–397. doi:10.1144/1354-079308-781
- Goult, N.R., 2001a. Polygonal fault networks in fine-grained sediments - An alternative to the syneresis mechanism. *First Break* 19, 69–73. doi:10.1046/j.1365-2397.2001.00137.x
- Goult, N.R., 2001b. Mechanics of layer-bound polygonal faulting in fine-grained sediments. *Journal of the Geological Society* 159, 239–246.
- Gustafson, C., Key, K., Evans, R.L., 2019. Aquifer systems extending far offshore on the U.S. Atlantic margin. *Scientific Reports* 9. doi:10.1038/s41598-019-44611-7
- Hammer, Ø., Webb, K.E., Depreiter, D., 2009. Numerical simulation of upwelling currents in pockmarks, and data from the Inner Oslofjord, Norway. *Geo-Marine Letters* 29, 269–275. doi:10.1007/s00367-009-0140-z
- Hansen, D.M., Cartwright, J.A., 2006. The three-dimensional geometry and growth of forced folds above saucer-shaped igneous sills. *Journal of Structural Geology* 28, 1520–1535. doi:10.1016/j.jsg.2006.04.004
- Hansen, J.P. V, Cartwright, J.A., Huuse, M., Clausen, O.R., 2005. 3D seismic expression of fluid migration and mud remobilization on the Gjallar Ridge, offshore mid-Norway. *Basin Research* 17, 123–139. doi:10.1111/j.1365-2117.2005.00257.x
- Hardage, B.A., Carr, D.L., Lancaster, D.E., Simmons Jr, J.L., Elphick, R.Y., Pendleton, V.M., Johns, R.A., 1996. 3-D seismic evidence of the effects of carbonate karst collapse on overlying clastic stratigraphy and reservoir compartmentalization. *Geophysics* 61, 1336–1350.
- Head, M.J., Seidenkrantz, M.S., Janczyk-Kopikowa, Z., Marks, L., Gibbard, P.L., 2005.

- Last Interglacial (Eemian) hydrographic conditions in the southeastern Baltic Sea, NE Europe, based on dinoflagellate cysts. *Quaternary International* 130, 3–30. doi:10.1016/j.quaint.2004.04.027
- Healy, T.R., Wefer, G., 1980. The efficacy of submarine abrasion vs. cliff retreat as a supplier of marine sediment in the Kieler Bucht, Western Baltic. *Meyniana* 32, 89–96.
- Healy, T.R., Werner, F., 1987. Sediment budget for a semi-enclosed sea in a near-homogeneous lithology; example of Kieler Bucht, western Baltic. *Senckenbergiana maritima* 19, 195–222.
- Heath, R.A., 1972. The southland current. *New Zealand Journal of Marine and Freshwater Research* 6, 497–533. doi:10.1080/00288330.1972.9515444
- Heiniö, P., Davies, R.J., 2009. Trails of depressions and sediment waves along submarine channels on the continental margin of Espirito Santo Basin, Brazil. *Bulletin of the Geological Society of America* 121, 698–711. doi:10.1130/B26190.1
- Henriet, J.P., De Batist, M., Verschuren, M., 1991. Early fracturing of Palaeogene clays, southernmost North Sea: relevance to mechanisms of primary hydrocarbon migration. Generation, accumulation and production of Europe's hydrocarbons 1, 217–227.
- Herzer, R.H., 1981. Late Quaternary stratigraphy and sedimentation of the Canterbury continental shelf, New Zealand. *New Zealand Oceanographic Institute Memoir* 89 ISSN 2538-.
- Hesse, R., Harrison, W.E., 1981. Gas hydrates (clathrates) causing pore-water freshening and oxygen isotope fractionation in deep-water sedimentary sections of terrigenous continental margins. *Earth and Planetary Science Letters* 55, 453–462. doi:10.1016/0012-821X(81)90172-2
- Hill, J.C., Gayes, P.T., Driscoll, N.W., Johnstone, E.A., Sedberry, G.R., 2008. Iceberg scours along the southern U.S. Atlantic margin. *Geology* 36, 447. doi:10.1130/G24651A.1
- Hillman, J.I.T., Gorman, A.R., Pecher, I.A., 2015. Geostatistical analysis of seafloor

- depressions on the southeast margin of New Zealand's South Island - Investigating the impact of dynamic near seafloor processes on geomorphology. *Marine Geology* 360, 70–83.
doi:10.1016/j.margeo.2014.11.016
- Hillman, J.I.T., Klauke, I., Pecher, I.A., Gorman, A.R., Schneider von Deimling, J., Bialas, J., 2018. The influence of submarine currents associated with the Subtropical Front upon seafloor depression morphologies on the eastern passive margin of south island, New Zealand. *New Zealand Journal of Geology and Geophysics* 0, 1–14. doi:10.1080/00288306.2018.1434801
- Hinz, K., Kögler, F.C., Richter, I., Seibold, E., 1971. Reflexionsseismische Untersuchungen mit einer pneumatischen Schallquelle und einem Sedimentecholot in der westlichen Ostsee. *Meyniana* 21, 17–24.
- Ho, S., Carruthers, D.T., Imbert, P., 2016. Insights into the permeability of polygonal faults from their intersection geometries with Linear Chimneys: a case study from the Lower Congo Basin. *Carnets de géologie* 16, 17–26.
- Ho, S., Carruthers, D.T., Imbert, P., Cartwright, J.A., 2013. Spatial Variations in Geometries of Polygonal Faults Due to Stress Perturbations & Interplay with Fluid Venting Features. 75th EAGE Conference & Exhibition London.
doi:10.3997/2214-4609.20131054
- Ho, S., Cartwright, J.A., Imbert, P., 2012. Vertical evolution of fluid venting structures in relation to gas flux, in the Neogene-Quaternary of the Lower Congo Basin, Offshore Angola. *Marine Geology* 332–334, 40–55.
doi:10.1016/j.margeo.2012.08.011
- Ho, S., Hovland, M., Blouet, J., Wetzels, A., Imbert, P., Carruthers, D.T., 2018a. Formation of linear planform chimneys controlled by preferential hydrocarbon leakage and anisotropic stresses in faulted fine-grained sediments, offshore Angola. *Solid Earth* 9, 1437–1468.
doi:https://doi.org/10.5194/se-9-1437-2018
- Ho, S., Imbert, P., Hovland, M., Wetzels, A., Philippe, J., Daniel, B., 2018b. Downslope-shifting pockmarks: interplay between hydrocarbon leakage, sedimentations, currents and slope's topography. *International Journal of Earth Sciences*

- 107, 2907–2929. doi:10.1007/s00531-018-1635-5
- Hoernle, K., White, J.D.L., Van Den Bogaard, P., Hauff, F., Coombs, D.S., Werner, R., Timm, C., Garbe-schönberg, D., Reay, A., Cooper, A.F., 2006. Cenozoic intraplate volcanism on New Zealand: Upwelling induced by lithospheric removal. *Earth and Planetary Science Letters* 248, 335–352. doi:10.1016/j.epsl.2006.06.001
- Hoffmann, J.J.L., 2016. Comparative analysis of different 3D seismic datasets for imaging breakup volcanic complexes. Christian-Albrechts-University zu Kiel.
- Hoffmann, J.J.L., 2013. Appearance and possible evolution of submarine large scale scour features on southern Chatham Rise (New Zealand). Christian-Albrechts-University zu Kiel.
- Hoffmann, J.J.L., Gorman, A.R., Crutchley, G.J., 2019. Seismic evidence for repeated vertical fluid flow through polygonally faulted strata in the Canterbury Basin, New Zealand. *Marine and Petroleum Geology* 109, 317–329. doi:10.1016/j.marpetgeo.2019.06.025
- Hoffmann, J.J.L., Schneider von Deimling, J., Schröder, J.F., Schmidt, M., Held, P., Crutchley, G.J., Scholten, J., Gorman, A.R., 2020. Complex Eyed Pockmarks and Submarine Groundwater Discharge Revealed by Acoustic Data and Sediment Cores in Eckernförde Bay, SW Baltic Sea. *Geochemistry, Geophysics, Geosystems* 21. doi:10.1029/2019GC008825
- Hovland, M., 2002. On the self-sealing nature of marine seeps. *Continental Shelf Research* 22, 2387–2394. doi:10.1016/S0278-4343(02)00063-8
- Hovland, M., 1989. The formation of pockmarks and their potential influence on offshore construction. *Quarterly Journal of Engineering Geology* 22, 131–138.
- Hovland, M., 1982. Pockmarks and the Recent geology of the central section of the Norwegian Trench. *Marine Geology*. doi:10.1016/0025-3227(82)90073-1
- Hovland, M., Gardner, J. V., Judd, A.G., 2002. The significance of pockmarks to understanding fluid flow processes and geohazards. *Geofluids* 2, 127–136.
- Hovland, M., Heggland, R., De Vries, M.H., Tjelta, T.I., 2010. Unit-pockmarks and their potential significance for predicting fluid flow. *Marine and Petroleum*

- Geology 27, 1190–1199. doi:10.1016/j.marpetgeo.2010.02.005
- Hovland, M., Judd, A.G., 1988. Seabed pockmarks and seepages: Impact on geology, biology and the marine environment. London. Graham and Trotman, 293.
- Hovland, M., Sommerville, J.H., 1985. Characteristics of two natural gas seepages in the North Sea. *Marine and Petroleum Geology* 2, 319–326.
- Hovland, M., Svensen, H., Forsberg, C.F., Johansen, H., Fichler, C., Fosså, J.H., Jonsson, R., Rueslåtten, H., 2005. Complex pockmarks with carbonate-ridges off mid-Norway: Products of sediment degassing. *Marine Geology* 218, 191–206. doi:10.1016/j.margeo.2005.04.005
- Hovland, M., Talbot, M., Olaussen, S., Aasberg, L., 1985. Recently formed methane-derived carbonates from the North Sea floor. Thomas B.M. (eds) *Petroleum Geochemistry in Exploration of the Norwegian Shelf*. Springer, Dordrecht, Netherlands, pp. 263–266.
- Hovland, M., Talbot, M.R., Qvale, H., Olaussen, S., Aasberg, L., 1987. Methane-related carbonate cements in pockmarks of the North Sea. *Journal of Sedimentary Petrology*, 57, 881–892. doi:10.1306/212f8c92-2b24-11d7-8648000102c1865d
- Hovland, M., Thomsen, E., 1989. Hydrocarbon-based communities in the North Sea? *Sarsia* 74, 29–42.
- Hübscher, C., Borowski, C., 2006. Seismic evidence for fluid escape from Mesozoic cuesta type topography in the Skagerrak. *Marine and Petroleum Geology* 23, 17–28. doi:10.1016/j.marpetgeo.2005.07.004
- Hurst, A., Cartwright, J.A., 2005. Sand injectites: an emerging global play in deep-water clastic environments, in: *Petroleum Geology: North-West Europe and Global Perspectives— Proceedings of the 6th Petroleum Geology Conference*. pp. 133–144. doi:10.1144/0060133
- Hurst, A., Cartwright, J.A., Huuse, M., Jonk, R., Schwab, A., Duranti, D., Cronin, B., 2003. Significance of large-scale sand injectites as long-term fluid conduits: Evidence from seismic data. *Geofluids* 3, 263–274. doi:10.1046/j.1468-8123.2003.00066.x

- Hustoft, S., Bünz, S., Mienert, J., 2010. Three-dimensional seismic analysis of the morphology and spatial distribution of chimneys beneath the Nyegga pockmark field, offshore mid-Norway. *Basin Research* 22, 465–480. doi:10.1111/j.1365-2117.2010.00486.x
- Hustoft, S., Mienert, J., Bünz, S., Nouzé, H., 2007. High-resolution 3D-seismic data indicate focussed fluid migration pathways above polygonal fault systems of the mid-Norwegian margin. *Marine Geology* 245, 89–106. doi:10.1016/j.margeo.2007.07.004
- Imbert, P., Ho, S., 2012. Seismic-scale funnel-shaped collapse features from the Paleocene-Eocene of the North West Shelf of Australia Seismic-scale funnel-shaped collapse features from the Paleocene – Eocene of the North West Shelf of Australia. *Marine Geology* 332–334, 198–221. doi:10.1016/j.margeo.2012.10.010
- IPCC, 2014. *Climate Change 2014: Synthesis Report. Contribution of Working Groups I, II and III to the Fifth Assessment Report of the Intergovernmental Panel on Climate Change* [Core Writing Team, R.K. Pachauri and L.A. Meyer (eds.)]. IPCC, Geneva, Switzerland 151.
- Jackson, D., Richardson, M., 2007. *High-frequency seafloor acoustics*. Springer Science & Business Media.
- Jakobsson, M., O'Regan, M., Mörth, C.M., Stranne, C., Weidner, E., Hansson, J., Gyllencreutz, R., Humborg, C., Elfving, T., Norkko, A., Norkko, J., Nilsson, B., Sjöström, A., 2020. Potential links between Baltic Sea submarine terraces and groundwater seeping. *Earth Surface Dynamics* 8, 1–15. doi:10.5194/esurf-8-1-2020
- Jennings, J.N., 1971. *Karst*. Canberra, ACT: Australian National University Press.
- Jensen, J.B., Kuijpers, A., Bennike, O., Laier, T., Werner, F., 2002. New geological aspects for freshwater seepage and formation in Eckernförde Bay, western Baltic. *Continental Shelf Research* 22, 2159–2173. doi:10.1016/S0278-4343(02)00076-6
- Johansson, J.M., Davies, J.L., Scherneck, H.G., Milne, G.A., Vermeer, M., Mitrovica, J.X., Bennett, R.A., Jonsson, B., Elgered, G., Elosegui, P., Koivula, H., Poutanen, M.,

- Ronnang, B.O., Sharpio, I.I., 2002. Continuous GPS measurements of postglacial adjustment in Fennoscandia 1. Geodetic results. *Journal of Geophysical Research* 107, 2157. doi:10.1029/2001JB000400
- Johnston, R.H., 1983. The saltwater-freshwater interface in the Tertiary limestone aquifer, southeast Atlantic outer-continental shelf of the U.S.A. *Journal of Hydrology* 61, 239–249. doi:10.1016/0022-1694(83)90251-2
- Judd, A.G., Hovland, M., 2009. Seabed fluid flow: the impact on geology, biology and the marine environment. Cambridge University Press.
- Judd, A.G., Hovland, M., 1992. The evidence of shallow gas in marine sediments. *Continental Shelf Research* 12, 1081–1095. doi:10.1016/0278-4343(92)90070-Z
- Kaleris, V., Lagas, G., Marczynek, S., Piotrowski, J.A., 2002. Modelling submarine groundwater discharge: an example from the western Baltic Sea. *Journal of Hydrology* 265, 76–99. doi:10.1016/S0022-1694(02)00093-8
- Kamp, P.J.J., 1987. Age and origin of the New Zealand Orocline in relation to Alpine Fault movement. *Journal of the Geological Society, London* 144, 641–652.
- Kamp, P.J.J., Tippett, J.M., 1993. Dynamics of Pacific plate crust in the South Island (New Zealand) zone of oblique continent-continent convergence. *Journal of Geophysical Research: Solid Earth* 98, 16105–16118.
- Karpen, V., Thomsen, L., Suess, E., 2004. A new 'schlieren' technique application for fluid flow visualization at cold seep sites. *Marine Geology* 204, 145–159. doi:10.1016/S0025-3227(03)00370-0
- Karstens, J., Berndt, C., 2015. Seismic chimneys in the Southern Viking Graben – Implications for palaeo fluid migration and overpressure evolution. *Earth and Planetary Science Letters* 412, 88–100. doi:10.1016/j.epsl.2014.12.017
- Kastner, M., Solomon, E.A., Harris, R.N., Torres, M., 2014. Fluid origins, thermal regimes, and fluid and solute fluxes in the forearc of subduction zones, in: *Developments in Marine Geology*. Elsevier, pp. 671–733.
- Kelley, J.T., Dickson, S.M., Belknap, D.F., Barnhardt, W.A., Henderson, M., 1994. Giant sea-bed pockmarks: Evidence for gas escape from Belfast Bay, Maine.

- Geology 22, 59. doi:10.1130/0091-7613(1994)022<0059:GSBPEF>2.3.CO;2
- Khandriche, A., Werner, F., 1995. Freshwater induced pockmarks in Bay of Eckernförde, western Baltic. Proceedings of the Third Marine Geological Conference "The Baltic" 2, 155–164.
- Khandriche, A., Werner, F., Erlenkeuser, H., 1987. Auswirkungen der Oststürme vom Winter 1978/79 auf die Sedimentation im Schlickbereich der Eckernförder Bucht (Westliche Ostsee). *Meyniana* 38, 125–151.
- Kim, G., Swarzenski, P.W., 2010. Submarine groundwater discharge (SGD) and associated nutrient fluxes to the coastal ocean, in: Carbon and Nutrient Fluxes in Continental Margins. Springer, pp. 529–538.
- King, J.J., Cartwright, J.A., 2020. Ultra-slow throw rates of polygonal fault systems. *Geology* 48, 473–477. doi:10.1130/g47221.1
- King, L.H., MacLean, B., 1970. Pockmarks on the Scotian shelf. *Geological Society of America Bulletin* 81, 3141–3148.
- King, P.R., 2000. Tectonic reconstructions of New Zealand : 40 Ma to the Present Tectonic reconstructions of New Zealand : 40 Ma to the Present. *New Zealand Journal of Geology and Geophysics* 43, 611–638. doi:10.1080/00288306.2000.9514913
- Kjoberg, S., Schmiedel, T., Planke, S., Svensen, H.H., Millett, J.M., Jerram, D.A., Galland, O., Lecomte, I., Schofield, N., Haug, Ø.T., Helsem, A., 2017. 3D structure and formation of hydrothermal vent complexes at the Paleocene-Eocene transition, the Møre Basin, mid-Norwegian margin. *Interpretation* 5, SK65–SK81. doi:10.1190/INT-2016-0159.1
- Klaucke, I., Sarkar, S., Bialas, J., Berndt, C., Dannowski, A., Dumke, I., Hillman, J.I.T., Koch, S., Nodder, S., Papenberg, C., Schneider von Deimling, J., 2018. Giant depressions on the Chatham Rise off shore New Zealand – Morphology, structure and possible relation to fluid expulsion and bottom currents. *Marine Geology* 399, 158–169. doi:10.1016/j.margeo.2018.02.011
- Koegler, F.C., 1967. Geotechnical properties of recent marine sediments from the Arabian Sea and the Baltic Sea. *Marine Geotechnique*. University of Chicago

- Press, Urbana, IL 170–176.
- Konikow, L.F., 2011. Contribution of global groundwater depletion since 1900 to sea-level rise. *Geophysical Research Letters* 38, 1–5.
doi:10.1029/2011GL048604
- Kopf, A.J., 2002. Significance of mud volcanism. *Reviews of Geophysics* 40.
doi:10.1029/2000RG000093
- Krämer, K., Holler, P., Herbst, G., Bratek, A., Ahmerkamp, S., Neumann, A., Bartholomä, A., Van Beusekom, J.E.E., Holtappels, M., Winter, C., 2017. Abrupt emergence of a large pockmark field in the German Bight, southeastern North Sea. *Scientific Reports* 7, 1–8. doi:10.1038/s41598-017-05536-1
- Krastel, S., Berndt, C., Schneider von Deimling, J., Kowalczyk, L., Horstmann, R., Filbrandt, C., Haehnle, L., Koech, D., Growe, K., Hagen, A., Bergmann, L., Klein, L., Hagemann, K., Schulze, I., 2017. Cruise Report R/V Alkor, Cruise No: AL501 - University of Kiel.
- Krastel, S., Berndt, C., Schneider von Deimling, J., Lenz, K.F., Held, P., Kühn, M., Nilsson, P.O., Hans, A.C., Michaela, T., Liebsch, J., Prigan, T., May, T., Klein, J., Rathjens, K., 2019. R/V ALKOR Cruise Report AL527 - University of Kiel.
- Kvenvolden, K.A., Cooper, C.K., 2003. Natural seepage of crude oil into the marine environment. *Geo-Marine Letters* 23, 140–146. doi:10.1007/s00367-003-0135-0
- Langmuir, C., Humphris, S., Fornari, D., Van Dover, C., Von Damm, K., Tivey, M.K., Colodner, D., Charlou, J.L., Desonie, D., Wilson, C., Fouquet, Y., Klinkhammer, G., Bougault, H., 1997. Hydrothermal vents near a mantle hot spot: The Lucky Strike vent field at 37°N on the Mid-Atlantic Ridge. *Earth and Planetary Science Letters* 148, 69–91. doi:10.1016/s0012-821x(97)00027-7
- Lapointe, B.E., O'Connell, J.D., Garrett, G.S., 1990. Nutrient couplings between on-site sewage disposal systems, groundwaters, and nearshore surface waters of the Florida Keys. *Biogeochemistry* 10, 289–307.
- Laurent, D., Gay, A., Baudon, C., Berndt, C., Soliva, R., Planke, S., Mourgues, R., Lacaze, S., Pauget, F., Mangue, M., Lopez, M., 2012. High-resolution

- architecture of a polygonal fault interval inferred from geomodel applied to 3D seismic data from the Gjallar Ridge, Vøring Basin, Offshore Norway. *Marine Geology* 332–334, 134–151. doi:10.1016/j.margeo.2012.07.016
- Lecher, A.L., Chien, C., Paytan, A., 2016. Submarine groundwater discharge as a source of nutrients to the North Pacific and Arctic coastal ocean. *Marine Chemistry* 186, 167–177. doi:10.1016/j.marchem.2016.09.008
- Lee, M.W., Collett, T.S., 2001. Elastic properties of gas hydrate – bearing sediments. *Geophysics* 66, 763–771.
- Lee, M.W., Hutchinson, D.R., Collett, T.S., Dillon, W.P., 1996. Seismic velocities for hydrate-bearing sediments using weighted equation. *Journal of Geophysical Research: Solid Earth* 101, 20347–20358. doi:10.1029/96jb01886
- Leifer, I., Judd, A.G., 2002. Oceanic methane layers : the hydrocarbon seep bubble deposition hypothesis. *Terra Nova* 14, 417–424.
- Leifer, I., Luyendyk, B.P., Boles, J., Clark, J.F., 2006. Natural marine seepage blowout: Contribution to atmospheric methane. *Global Biogeochemical Cycles* 20. doi:10.1029/2005GB002668
- Lennartz, S.T., Lehmann, A., Herrford, J., Malien, F., Hansen, H.P., Biester, H., Bange, H.W., 2014. Long-term trends at the Boknis Eck time series station (Baltic Sea), 1957–2013: does climate change counteract the decline in eutrophication? *Biogeosciences* 11, 6323–6339. doi:10.5194/bg-11-6323-2014
- Lever, H., 2007. Review of unconformities in the late Eocene to early Miocene successions of the South Island, New Zealand: ages, correlations, and causes. *New Zealand Journal of Geology and Geophysics* 50, 245–261.
- Lewis, D.W., 1992. Anatomy of an unconformity on mid-oligocene amuri limestone, canterbury, New Zealand. *New Zealand Journal of Geology and Geophysics* 35, 463–475. doi:10.1080/00288306.1992.9514541
- Lewis, D.W., Belliss, S.E., 1984. Mid Tertiary Unconformities in the Waitaki Subdivision, North Otago. *Journal of the Royal Society of New Zealand* 14, 251–276. doi:10.1080/03036758.1984.10426303

- Lewis, E., Filomeno, G., Lai, J., Wilkinson, S., 2014. Processing Report on the broadband pre-processing and 3D pre-stack depth migration of seismic data from the Endurance 3D survey, PEP52717, Canterbury Basin.
- Lewy, Z., 1975. Early diagenesis of calcareous skeletons in the Baltic Sea, Western Germany. *Meyniana* 27, 29–33.
- Li, J., Mitra, S., Qi, J., 2020. Seismic analysis of polygonal fault systems in the Great South Basin, New Zealand. *Marine and Petroleum Geology* 111, 638–649. doi:10.1016/j.marpetgeo.2019.08.052
- Link, W.K., 1952. Significance of oil and gas seeps in world oil exploration. *AAPG bulletin* 36, 1505–1540.
- Lohrberg, A., Schmale, O., Ostrovsky, I., Niemann, H., Held, P., Schneider von Deimling, J., 2020. Discovery and quantification of a widespread methane ebullition event in a coastal inlet (Baltic Sea) using a novel sonar strategy. *Scientific Reports* 10, 1–13. doi:10.1038/s41598-020-60283-0
- Loncke, L., Mascle, J., Fanil Scientific Parties, 2004. Mud volcanoes, gas chimneys, pockmarks and mounds in the Nile deep-sea fan (Eastern Mediterranean): geophysical evidences. *Marine and Petroleum Geology* 21, 669–689. doi:10.1016/j.marpetgeo.2004.02.004
- López-Rodríguez, C., De Lange, G.J., Comas, M., Martínez-Ruiz, F., Nieto, F., Sapart, C.J., Mogollón, J.M., 2019. Recent, deep-sourced methane/mud discharge at the most active mud volcano in the western Mediterranean. *Marine Geology* 408, 1–17. doi:10.1016/j.margeo.2018.11.013
- Løseth, H., Wensaas, L., Arntsen, B., Hanken, N.M., Basire, C., Graue, K., 2011. 1000 M Long Gas Blow-Out Pipes. *Marine and Petroleum Geology* 28, 1040–1060. doi:10.1016/j.marpetgeo.2010.10.001
- Lu, H., Fulthorpe, C.S., Mann, P., 2003. Three-dimensional architecture of shelf-building sediment drifts in the offshore Canterbury Basin, New Zealand. *Marine Geology* 193, 19–47. doi:10.1016/S0025-3227(02)00612-6
- Lu, H., Fulthorpe, C.S., Mann, P., Kominz, M.A., 2005. Miocene-recent tectonic and climatic controls on sediment supply and sequence stratigraphy: Canterbury

- basin, New Zealand. *Basin Research* 17, 311–328. doi:10.1111/j.1365-2117.2005.00266.x
- Maia, A.R., Cartwright, J.A., Andersen, E., 2016. Shallow plumbing systems inferred from spatial analysis of pockmark arrays. *Marine and Petroleum Geology* 77, 865–881. doi:10.1016/j.marpetgeo.2016.07.029
- Mälkki, P., Perttilä, M., 2012. Baltic Sea Water Exchange and Oxygen Balance, in: *Lecture Notes in Earth Sciences*. Wiley Online Library, pp. 151–161. doi:10.1007/978-3-642-25550-2_10
- Maltby, J., Steinle, L., Löscher, C.R., Bange, H.W., Fischer, M.A., Schmidt, M., Treude, T., 2018. Microbial methanogenesis in the sulfate-reducing zone of sediments in the Eckernförde Bay, SW Baltic Sea. *Biogeosciences* 15, 137–157. doi:10.5194/bg-15-137-2018
- Malthe-Sørensen, A., Walmann, T., Jamtveit, B., Feder, J., Jossang, T., 1999. Simulation and characterization of fracture patterns in glaciers. *Journal of Geophysical Research: Solid Earth* 104.
- Manley, P.L., Manley, T.O., Watzin, M.C., Gutierrez, J., 2004. Lakebed pockmarks in Burlington Bay, Lake Champlain: I. Hydrodynamics and implications of origin, in: *Lake Champlain: Partnerships and Research in the New Millennium*. Springer, Boston, MA, pp. 299–329.
- Marchis, R., Spatola, D., Fenton, C., Micallef, A., 2018. Rapid gully erosion along uncemented gravel cliffs (Canterbury Plain, New Zealand): Insights from repeat UAV surveys, in: *EGU General Assembly Conference Abstracts*. p. 11921.
- Marczinek, S., Piotrowski, J.A., 2002. Grundwasserströmung und-beschaffenheit im Einzugsgebiet der Eckernförder Bucht, Schleswig-Holstein. *Grundwasser* 7, 101–110.
- Marfurt, K.J., Kirlin, R.L., Farmer, S.L., Bahorich, M.S., 1998. 3-D seismic attributes using a semblance-based coherency algorithm. *Geophysics* 63, 1150. doi:10.1190/1.1444415
- Marsaglia, K.M., Nolasco, J.M., 2016. Composition of Pliocene to Quaternary mixed

- terrigenous and calcareous sandy beds in contourite drift deposits at ODP Site 1119 off New Zealand: Insights into sandy drift development and drift petroleum reservoir characterization. *Marine and Petroleum Geology* 72, 98–109. doi:10.1016/j.marpetgeo.2016.01.006
- Martens, C.S., Albert, D.B., Alperin, M.J., 1999. Stable isotope tracing of anaerobic methane oxidation in the gassy sediments of Eckernförde Bay, German Baltic Sea. *American Journal of Science* 299, 589–610.
- Mathews, W.H., Curtis, G.H., 1966. Date of the Pliocene-Pleistocene Boundary in New Zealand. *Nature* 979–980.
- Mazzini, A., 2009. Mud volcanism : Processes and implications. *Marine and Petroleum Geology* 26, 1677–1680. doi:10.1016/j.marpetgeo.2009.05.003
- Mazzini, A., Etiope, G., 2017. Mud volcanism: An updated review. *Earth-Science Reviews* 168, 81–112. doi:10.1016/j.earscirev.2017.03.001
- Mazzini, A., Svensen, H., Planke, S., Forsberg, C.F., Tjelta, T.I., 2016. Pockmarks and methanogenic carbonates above the giant Troll gas field in the Norwegian North Sea. *Marine Geology* 373, 26–38. doi:10.1016/j.margeo.2015.12.012
- McGinnis, D.F., Greinert, J., Artemov, Y., Beaubien, S.E., Wüest, A., 2006. Fate of rising methane bubbles in stratified waters: How much methane reaches the atmosphere? *Journal of Geophysical Research: Oceans* 111, 1–15. doi:10.1029/2005JC003183
- McLernon, C.R., 1978. Indications of petroleum in New Zealand. New Zealand Geological Survey Open-file Petroleum Report 839.
- Medialdea, T., Somoza, L., Pinheiro, L.M., Fernández-Puga, M.C., Vázquez, J.T., León, R., Ivanov, M.K., Magalhaes, V., Díaz-del-Río, V., Vegas, R., 2009. Tectonics and mud volcano development in the Gulf of Cádiz. *Marine Geology* 261, 48–63. doi:10.1016/j.margeo.2008.10.007
- Micallef, A., Person, M., Haroon, A., Weymer, B.A., Jegen, M., Schwalenberg, K., Faghih, Z., Duan, S., Cohen, D., Mountjoy, J.J., Woelz, S., Gable, C.W., Avers, T., Kumar Tiwari, A., 2020. 3D characterisation and quantification of an offshore freshened groundwater system in the Canterbury Bight. *Nature*

- Communications 11, 1372. doi:10.1038/s41467-020-14770-7
- Michel, G., Dupré, S., Baltzer, A., Ehrhold, A., Imbert, P., Pitel, M., Loubrieu, B., Scalabrin, C., Lazure, P., Marié, L., Geldof, J.B., Deville, É., 2017. Pockmarks on the South Aquitaine Margin continental slope: The seabed expression of past fluid circulation and former bottom currents. *Comptes Rendus - Geoscience* 349, 391–401. doi:10.1016/j.crte.2017.10.003
- Milkert, D., Werner, F., 1997. Formation and distribution of storm layers in western Baltic Sea muds. *Oceanographic Literature Review* 4, 326.
- Milne, A.D., 1975. Resolution-1 Well completion report, Petroleum Report Series PR648, Operator: Shell BP Todd.
- Mitchell, J.S., Mackay, K.A., Neil, H.L., Mackay, E.J., Pallentin, A., Notman, P., 2012. Undersea New Zealand, 1: 5,000,000. NIWA chart, miscellaneous series 92.
- Mitchell, J.S., Pallentin, A., Kane, T., 2016. TAN1608 Voyage report, Otago Multibeam 2: Great South Basin and Southern Canterbury Shelf - National Institute of Water & Atmospheric Research Ltd.
- Monnier, D., Imbert, P., Gay, A., Mourgues, R., Lopez, M., 2014. Pliocene sand injectites from a submarine lobe fringe during hydrocarbon migration and salt diapirism: a seismic example from the Lower Congo Basin. *Geofluids* 14, 1–19. doi:10.1111/gfl.12057
- Moore, W.S., 2010. The Effect of Submarine Groundwater Discharge on the Ocean. *Annual Review of Marine Science* 2, 59–88. doi:10.1146/annurev-marine-120308-081019
- Moore, W.S., 1996. Large groundwater inputs to coastal waters revealed by ²²⁶Ra enrichments. *Nature* 380, 612–614.
- Moore, W.S., Sarmiento, J.L., Key, R.M., 2008. Submarine groundwater discharge revealed by ²²⁸Ra distribution in the upper Atlantic Ocean. *Nature Geoscience* 1, 309–311. doi:10.1038/ngeo183
- Moore, W.S., Shaw, T.J., 1998. Chemical signals from submarine fluid advection onto the continental shelf. *Journal of Geophysical Research: Oceans* 103, 21543–21552. doi:10.1029/98JC02232

- Moosdorf, N., Oehler, T., 2017. Societal use of fresh submarine groundwater discharge: An overlooked water resource. *Earth-Science Reviews* 171, 338–348. doi:10.1016/j.earscirev.2017.06.006
- Morgan, D.A., Cartwright, J.A., Imbert, P., 2015. Perturbation of polygonal fault propagation by buried pockmarks and the implications for the development of polygonal fault systems. *Marine and Petroleum Geology* 65, 157–171. doi:10.1016/j.marpetgeo.2015.03.024
- Morley, C.K., Maczak, A., Rungprom, T., Ghosh, J., Cartwright, J.A., Bertoni, C., Panpichityota, N., 2017. New style of honeycomb structures revealed on 3D seismic data indicate widespread diagenesis offshore Great South Basin, New Zealand. *Marine and Petroleum Geology* 86, 140–154. doi:10.1016/j.marpetgeo.2017.05.035
- Motyka, R.J., Poreda, R.J., Jeffrey, A.W.A., 1989. Geochemistry, isotopic composition, and origin of fluids emanating from mud volcanoes in the Copper River basin, Alaska. *Geochimica et Cosmochimica Acta* 53, 29–41. doi:10.1016/0016-7037(89)90270-6
- Mountjoy, J.J., Micallef, A., Jegen, M., Woelz, S., Otero, D.C., Eton, N., Gerring, P., Hart, A., Luebben, N., Mueller, C., Quinn, W., Schwalenberg, K., Spatola, D., Weymer, B., 2017. Voyage Report, RV Tangaroa Voyage TAN1703.
- Mueller, R.J., 2015. Evidence for the biotic origin of seabed pockmarks on the Australian continental shelf. *Marine and Petroleum Geology* 64, 276–293. doi:10.1016/j.marpetgeo.2014.12.016
- Mulder, T., Chochonat, P., 1996. Classification of offshore mass movements. *Journal of Sedimentary Research* 66, 43–57.
- Müller, H., von Dobeneck, T., Nehmiz, W., Hamer, K., 2011. Near-surface electromagnetic, rock magnetic, and geochemical fingerprinting of submarine freshwater seepage at Eckernförde Bay (SW Baltic Sea). *Geo-Marine Letters* 31, 123–140. doi:10.1007/s00367-010-0220-0
- Nardelli, B., Budillon, F., Watteaux, R., Ciccone, F., Conforti, A., De Falco, G., Di Martino, G., Innangi, S., Tonielli, R., Iudicone, D., 2017. Pockmark morphology and turbulent buoyant plumes at a submarine spring. *Continental Shelf*

- Research 148, 19–36. doi:10.1016/j.csr.2017.09.008
- Nelson, C.S., Healy, T.R., 1984. Pockmark-like structures on the poverty bay sea bed — possible evidence for submarine mud volcanism. *New Zealand Journal of Geology and Geophysics* 27, 225–230.
doi:10.1080/00288306.1984.10422530
- Nelson, H., Thor, D.R., Sandstrom, M.W., Kvenvolden, K.A., 1979. Modern biogenic gas-generated craters (sea-floor “pockmarks”) on the Bering Shelf, Alaska. *Bulletin of the Geological Society of America* 90, 1144–1152.
doi:10.1130/0016-7606(1979)90<1144:MBGCSP>2.0.CO;2
- Nermoen, A., Galland, O., Jettestuen, E., Fristad, K., Podladchikov, Y.Y., Svensen, H., Malthe-Sørensen, A., 2010. Experimental and analytic modeling of piercement structures. *Journal of Geophysical Research: Solid Earth* 115.
- Nikolovska, A., Sahling, H., Bohrmann, G., 2008. Hydroacoustic methodology for detection, localization, and quantification of gas bubbles rising from the seafloor at gas seeps from the eastern Black Sea. *Geochemistry, Geophysics, Geosystems* 9, 1–13. doi:10.1029/2008GC002118
- Nittrouer, C.A., Lopez, G.R., Donelson, W.L., Bentley, S.J., D’Andrea, A.F., Friedrichs, C.T., Craig, N.I., Sommerfield, C.K., 1998. Oceanographic processes and the preservation of sedimentary structure in Eckernförde Bay, Baltic Sea. *Continental Shelf Research* 18, 1689–1714. doi:10.1016/S0278-4343(98)00054-5
- NIWA, 2015. Average sea–surface temperature, 1993–2012, <https://data.mfe.govt.nz/x/pqivkX>.
- NIWA, Mitchell, J.S., Neil, H., 2012. TAN1209 Voyage Report, OS20/20 Canterbury - Great South Basin, Prepared for Land Information New Zealand - National Institute of Water & Atmospheric Research Ltd.
- NZOG, 2018. New Zealand Oil & Gas Ltd: Activities Report 1–4.
- NZOG and Beach Energy, 2013. Endurance 3D - Final Acquisition Report - Client: New Zealand Oil and Gas.
- Odonne, F., Imbert, P., Dupuis, M., Aliyev, A.A., Abbasov, O.R., Baloglanov, E.E.,

- Vendeville, B.C., Gabalda, G., Remy, D., Bichaud, V., Juste, R., Pain, M., Blouin, A., Dofal, A., Gertauda, M., 2020. Mud volcano growth by radial expansion: Examples from onshore Azerbaijan. *Marine and Petroleum Geology* 112, 104051. doi:10.1016/j.marpetgeo.2019.104051
- Oehler, T., Tamborski, J.J., Rahman, S., Moosdorf, N., Ahrens, J., Mori, C., Neuholz, R., Schnetger, B., Beck, M., 2019. DSI as a Tracer for Submarine Groundwater Discharge. *Frontiers in Marine Science* 6, 563. doi:10.3389/fmars.2019.00563
- Ormö, J., Lindström, M., 2000. When a cosmic impact strikes the sea bed. *Geological Magazine* 137, 67–80.
- Orpin, A.R., 1997. Dolomite chimneys as possible evidence of coastal fluid expulsion, uppermost Otago continental slope, southern New Zealand. *Marine Geology* 138, 51–67. doi:10.1016/S0025-3227(96)00101-6
- Orsi, T.H., Werner, F., Milkert, D., Anderson, A.L., Bryant, W.R., 1996. Environmental overview of Eckernförde Bay, northern Germany. *Geo-Marine Letters* 16, 140–147. doi:10.1007/BF01204501
- Osborne, M.J., Swarbrick, R.E., 1997. Mechanisms for generating overpressure in sedimentary basins: a reevaluation. *AAPG bulletin* 81, 1023–1041.
- Passaro, S., Tamburrino, S., Vallefucio, M., Tassi, F., Vaselli, O., Giannini, L., Chiodini, G., Caliro, S., Sacchi, M., Rizzo, A.L., Ventura, G., 2016. Seafloor doming driven by degassing processes unveils sprouting volcanism in coastal areas. *Scientific Reports* 6, 22448. doi:10.1038/srep22448
- Patiris, D.L., Tsabaris, C., Schmidt, M., Karageorgis, A.P., Prospathopoulos, A.M., Alexakis, S., Linke, P., 2018. Mobile underwater in situ gamma-ray spectroscopy to localize groundwater emanation from pockmarks in the Eckernförde bay, Germany. *Applied Radiation and Isotopes* 140, 305–313. doi:10.1016/j.apradiso.2018.07.037
- Paull, C.K., Iii, W.U., Holbrook, W.S., Hill, T.M., Keaten, R., Winters, W.J., Lorenson, T.D., 2008. Origin of pockmarks and chimney structures on the flanks of the Storegga Slide , offshore Norway 43–51. doi:10.1007/s00367-007-0088-9
- Pellikka, H., Leijala, U., Johansson, M.M., Leinonen, K., Kahma, K.K., 2018. Future

- probabilities of coastal floods in Finland. *Continental Shelf Research* 157, 32–42. doi:10.1016/j.csr.2018.02.006
- Perlet, I., Holfort, J., 2017. Sturmflut vom 04./05.01.2017. Hamburg.
- Person, M., Dugan, B., Swenson, J.B., Urbano, L., Stott, C., Taylor, J., Willett, M., 2003. Pleistocene hydrogeology of the Atlantic continental shelf, New England. *Geological Society of America Bulletin* 115, 1324–1343.
- Person, M., McIntosh, J., Bense, V., Remenda, V.H., 2007. Pleistocene hydrology of North America: The role of ice sheets in reorganizing groundwater flow systems. *Reviews of Geophysics* 45, 1–28. doi:10.1029/2006RG000206
- Pettinga, J.R., 2003. Mud volcano eruption within the emergent accretionary Hikurangi margin, southern Hawke's Bay, New Zealand. *New Zealand Journal of Geology and Geophysics* 46, 107–121. doi:10.1080/00288306.2003.9514999
- Piekarski, J.-K., 2020. Middle Cenozoic unconformities in the Waihao Valley, South Canterbury Basin. University of Otago.
- Pilcher, R., Argent, J., 2007. Mega-pockmarks and linear pockmark trains on the West African continental margin. *Marine Geology* 244, 15–32. doi:10.1016/j.margeo.2007.05.002
- Planke, S., Millett, J.M., Maharjan, D., Jerram, D.A., Abdelmalak, M.M., Groth, A., Hoffmann, J.J.L., Berndt, C., Myklebust, R., 2017. Igneous seismic geomorphology of buried lava fields and coastal escarpments on the Vøring volcanic rifted margin. *Interpretation* 5. doi:10.1190/INT-2016-0164.1
- Planke, S., Svensen, H., Hovland, M., Banks, D.A., Jamtveit, B., 2003. Mud and fluid migration in active mud volcanoes in Azerbaijan. *Geo-Marine Letters* 23, 258–268. doi:10.1007/s00367-003-0152-z
- Plaza-Faverola, A., Bünz, S., Mienert, J., 2010. Fluid distributions inferred from P-wave velocity and reflection seismic amplitude anomalies beneath the Nyegga pockmark field of the mid-Norwegian margin. *Marine and Petroleum Geology* 27, 46–60. doi:10.1016/j.marpetgeo.2009.07.007
- Post, V.E.A., Groen, J., Kooi, H., Person, M., Ge, S., Edmunds, W.M., 2013. Offshore

- fresh groundwater reserves as a global phenomenon. *Nature* 504, 71–78.
doi:10.1038/nature12858
- Prien, R., Scholten, J., Schröder, J.F., Held, P., Liebtrau, V., Bannasch, R., Kniese, L., Glushko, I., Voronin, V., Sokolovskyi, R., Latacz, M., Pallentin, M., 2018. R/V Elisabeth Mann Borgese EMB187 cruise report - Leibniz-Institut für Ostseeforschung. Warnemuende.
- Quatrehomme, G., İşcan, M.Y., 1998. Analysis of beveling in gunshot entrance wounds. *Forensic Science International* 93, 45–60. doi:10.1016/S0379-0738(98)00030-9
- Reeburgh, W.S., 1983. Rates of Biogeochemical. *Ann. Rev. Earth Planet. Sci.* 11, 269–298.
- Reeves, J., Magee, C., Jackson, C., 2018. Unravelling intrusion-induced forced fold kinematics and ground deformation using 3D seismic reflection data. *Volcanica* 1, 1–17. doi:https://doi.org/10.30909/vol.01.01.0117
- Reusch, A., Loher, M., Bouffard, D., Moernaut, J., Hellmich, F., Anselmetti, F.S., Bernasconi, S.M., Hilbe, M., Kopf, A.J., Lilley, M.D., Meinecke, G., Strasser, M., 2015. Giant lacustrine pockmarks with subaqueous groundwater discharge and subsurface sediment mobilization. *Geophysical Research Letters* 42, 3465–3473. doi:10.1002/2015GL064179
- Riboulot, V., Imbert, P., Cattaneo, A., Voisset, M., 2019. Fluid escape features as relevant players in the enhancement of seafloor stability? *Terra Nova* 1–9. doi:10.1111/ter.12425
- Riboulot, V., Sultan, N., Imbert, P., Ker, S., 2016. Initiation of gas-hydrate pockmark in deep-water Nigeria: Geo-mechanical analysis and modelling. *Earth and Planetary Science Letters* 434, 252–263.
- Ridd, M.F., 1970. Mud volcanoes in New Zealand. *AAPG Bulletin* 54, 601–616.
- Ritger, S., Carson, B., Suess, E., 1987. Methane-derived authigenic carbonates formed by subduction-induced pore-water expulsion along the Oregon/Washington margin. *Geological Society of America Bulletin* 98, 147. doi:10.1130/0016-7606(1987)98<147:MACFBS>2.0.CO;2

- Roddy, D.J., 1977. Large-scale impact and explosion craters-Comparisons of morphological and structural analogs, in: *Impact and Explosion Cratering: Planetary and Terrestrial Implications*. pp. 185–246.
- Rößler, D., 2006. Reconstruction of the Littorina transgression in the Western Baltic Sea. *Marine Science Reports (IOW)* 67, 1–111.
- Rudd, J.W.M., Taylor, C.D., 1980. Methane cycling in aquatic environments. *Adv. Aquatic Microbiol* 2, 77–150.
- Rutherford, S.R., Williams, R.H., 1989. Amplitude-versus-offset variations in gas sands. *Geophysics* 54, 680–688.
- Sahoo, T.R., Browne, G.H., Hill, M.G., 2014. Seismic attribute analysis and depositional elements in the Canterbury Basin, in: *Poster Presented at the Advantage NZ: Geotechnical Petroleum Forum 2014, Wellington New Zealand*.
- Santos, I.R., Burnett, W.C., Dittmar, T., Suryaputra, I.G.N.A., Chanton, J., 2009. Tidal pumping drives nutrient and dissolved organic matter dynamics in a Gulf of Mexico subterranean estuary. *Geochimica et Cosmochimica Acta* 73, 1325–1339. doi:10.1016/j.gca.2008.11.029
- Sauter, E., Laier, T., Andersen, C.E., Dahlgard, H., Schlüter, M., 2001. Sampling of sub-seafloor aquifers by a temporary well for CFC age dating and natural tracer investigations. *Journal of Sea Research* 46, 177–185. doi:10.1016/S1385-1101(01)00080-6
- Sauter, E., Schlüter, M., Sedy, P.L., Fraser, N., Fogt, P., 2003. AUV multi-technique surveying of submarine freshwater seeps-high and ultra-high resolution acoustic and CTD mapping of pockmark sites in Eckernförde Bay, Western Baltic Sea. *Sea Technology* 44, 49–52.
- Schattner, U., Lazar, M., Souza, L.A.P., Ten Brink, U., Mahiques, M.M., 2016. Pockmark asymmetry and seafloor currents in the Santos Basin offshore Brazil. *Geo-Marine Letters* 36, 457–464.
- Schlüter, M., Sauter, E.J., Andersen, C.E., Dahlgard, H., Dando, P.R., 2004. Spatial distribution and budget for submarine groundwater discharge in Eckernförde

- Bay (Western Baltic Sea). *Limnology and Oceanography* 49, 157–167.
- Schmiedel, T., Kjoberg, S., Planke, S., Magee, C., Galland, O., Schofield, N., Jackson, C.A.L., Jerram, D.A., 2017. Mechanisms of overburden deformation associated with the emplacement of the Tulipan sill, mid-Norwegian margin. Interpretation 5, SK23–SK38. doi:10.1190/INT-2016-0155.1
- Schneider von Deimling, J., Hoffmann, J.J.L., 2012. 12PL015 Cruise Report: Multibeam Mapping and Acoustic Water Column Imaging - GEOMAR-Helmholtz centre for ocean research, Kiel.
- Schneider von Deimling, J., Hoffmann, J.J.L., Schröder, J.F., Crutchley, G.J., Gorman, A.R., 2019. FK Littorina L1905 Cruise Report, University of Kiel.
- Schneider von Deimling, J., Ostrovsky, I., Niemann, H., Held, P., Hoffmann, J.J.L., Urban, P., Lohrberg, A., Richner, D., Kunde, T., 2014. R/V Alkor Cruise Report AL447 - University of Kiel.
- Schneider von Deimling, J., Weinrebe, W., Tóth, Z., Fossing, H., Endler, R., Rehder, G., Spieß, V., 2013. A low frequency multibeam assessment: Spatial mapping of shallow gas by enhanced penetration and angular response anomaly. *Marine and Petroleum Geology* 44, 217–222. doi:10.1016/j.marpetgeo.2013.02.013
- Scholten, J., Osvath, I., Pham, M.K., 2013. 226Ra measurements through gamma spectrometric counting of radon progenies: How significant is the loss of radon? *Marine Chemistry* 156, 146–152. doi:10.1016/j.marchem.2013.03.001
- Schüler, F., 1952. Untersuchungen über die Mächtigkeit von Schlickschichten mit Hilfe des Echographen. *Deutsche Hydrographische Zeitschrift* 5, 220–231.
- Schulz, H.D., 2006. Quantification of early diagenesis: dissolved constituents in pore water and signals in the solid phase, in: *Marine Geochemistry*. Springer, pp. 73–124.
- Scott, J.M., Pontesilli, A., Brenna, M., White, J.D.L., Giacalone, E., Palin, J.M., le Roux, P.J., 2020. The Dunedin Volcanic Group and a revised model for Zealandia's alkaline intraplate volcanism. *New Zealand Journal of Geology and Geophysics* 0, 1–20. doi:10.1080/00288306.2019.1707695

- Seager, R., Ting, M., Held, I., Kushnir, Y., Lu, J., Vecchi, G., Huang, H.P., Harnik, N., Leetmaa, A., Lau, N.C., Li, C., Velez, J., Naik, N., 2007. Model Projections of an Imminent Transition to a More Arid Climate in Southwestern North America. *Science* 316, 1181–1184. doi:10.1126/science.1139601
- Seeberg-Elverfeldt, J., Schlüter, M., Feseker, T., Kölling, M., 2005. Rhizon sampling of porewaters near the sediment-water interface of aquatic systems. *Limnology and oceanography: Methods* 3, 361–371.
- Seibold, E., Exon, N., Hartmann, M., Kögler, F.C., Krumm, H., Lutze, G.F., Newton, R.S., Werner, F., 1971. Marine geology of Kiel bay, in: *Sedimentology of Parts of Central Europe, Guidebook, 8th International Sedimentological Congress, Heidelberg*. pp. 209–235.
- Sewell, R.J., 1988. Late Miocene volcanic stratigraphy of central Banks Peninsula, Canterbury, New Zealand. *New Zealand Journal of Geology and Geophysics* 31, 41–64. doi:10.1080/00288306.1988.10417809
- Shaban, A., Khawlie, M., Abdallah, C., Faour, G., 2005. Geologic controls of submarine groundwater discharge: application of remote sensing to north Lebanon. *Environmental Geology* 47, 512–522.
- Shell BP Todd, 1984. Clipper-1, Drilling completion report-Shell BP Todd In: *New Zealand Open-file Petroleum Report 1036*. Crown Minerals, Wellington.
- Shin, H., Santamarina, C.J., Cartwright, J.A., 2008. Contraction-driven shear failure in compacting uncemented sediments. *Geology* 36, 931–934. doi:10.1130/G24951A.1
- Shoulders, S.J., Cartwright, J.A., Huuse, M., 2007. Large-scale conical sandstone intrusions and polygonal fault systems in Tranche 6, Faroe-Shetland Basin. *Marine and Petroleum Geology* 24, 173–188. doi:10.1016/j.marpetgeo.2006.12.001
- Shuey, R.T., 1985. A simplification of the Zoeppritz equations. *Geophysics* 50, 609–614.
- Siegel, J., Person, M., Dugan, B., Cohen, D., Lizarralde, D., Gable, C., 2014. Influence of late Pleistocene glaciations on the hydrogeology of the continental shelf

- offshore Massachusetts, USA. *Geochemistry, Geophysics, Geosystems* 15, 4651–4670. doi:10.1002/2014GC005569
- Sills, G.C., Wheeler, S.J., 1992. The significance of gas for offshore operations. *Continental Shelf Research* 12, 1239–1250. doi:10.1016/0278-4343(92)90083-V
- Silva, A.J., Brandes, H.G., 1998. Geotechnical properties and behavior of high-porosity, organic-rich sediments in Eckernförde Bay, Germany. *Continental shelf research* 18, 1917–1938.
- Simm, R., Bacon, M., 2014. *Seismic Amplitude An Interpreter's Handbook*. Cambridge. doi:10.1017/CB09780511984501
- Smetacek, V., 1985. The annual cycle of Kiel Bight plankton: A long-term analysis. *Estuaries* 8, 145–157.
- Smetacek, V., von Bodungen, B., von Brockel, K., Knoppers, B., Martens, P., Peinert, R., Pollehne, F., Stegmann, P., Zeitzschel, B., 1987. Seasonality of plankton growth and sedimentation. *Seawater—Sediment Interactions in Coastal Waters*. Springer, Berlin 34–56.
- Solheim, A., Elverhøi, A., 1993. Gas-related sea floor craters in the Barents Sea. *Geo-Marine Letters* 13, 235–243. doi:10.1007/BF01207753
- Solomon, E.A., Kastner, M., MacDonald, I.R., Leifer, I., 2009. Considerable methane fluxes to the atmosphere from hydrocarbon seeps in the Gulf of Mexico. *Nature Geoscience* 2, 561–565. doi:10.1038/ngeo574
- Sommer, S., Linke, P., Pfannkuche, O., Schleicher, T., Schneider von Deimling, J., Reitz, A., Haeckel, M., Flögel, S., Hensen, C., 2009. Seabed methane emissions and the habitat of frenulate tubeworms on the Captain Arutyunov mud volcano (Gulf of Cadiz). *Marine Ecology Progress Series* 382, 69–86. doi:10.3354/meps07956
- Steinle, L., Maltby, J., Treude, T., Kock, A., Bange, H.W., Engbersen, N., Zopfi, J., Lehmann, M.F., Niemann, H., 2017. Effects of low oxygen concentrations on aerobic methane oxidation in seasonally hypoxic coastal waters. *Biogeosciences* 14, 1631–1645. doi:10.5194/bg-14-1631-2017

- Stewart, M., Trompeter, V., Van der Raaij, R., 2002. Age and source of Canterbury Plains groundwater, Report No. U02/30. Institute of Geological and Nuclear Sciences, Environment Canterbury.
- Stewart, S.A., 2006. Implications of passive salt diapir kinematics for reservoir segmentation by radial and concentric faults. *Marine and Petroleum Geology* 23, 843–853. doi:10.1016/j.marpetgeo.2006.04.001
- Stewart, S.A., 1999. Seismic interpretation of circular geological structures. *Petroleum Geoscience* 5, 273–285. doi:10.1144/petgeo.5.3.273
- Stieglitz, T., 2005. Submarine groundwater discharge into the near-shore zone of the Great Barrier Reef, Australia. *Marine Pollution Bulletin* 51, 51–59. doi:10.1016/j.marpolbul.2004.10.055
- Stoppa, F., 2006. The Sirente crater, Italy: Impact versus mud volcano origins. *Meteoritics and Planetary Science* 41, 467–477. doi:10.1111/j.1945-5100.2006.tb00474.x
- Stott, L., Davy, B., Shao, J., Coffin, R., Pecher, I., Neil, H., Rose, P., Bialas, J., 2019. CO₂ Release from Pockmarks on the Chatham Rise-Bounty Trough at the Glacial Termination. *Paleoceanography and Paleoclimatology* 1726–1743. doi:10.1029/2019pa003674
- Strogen, D.P., King, P.R., 2014. A new Zealandia-wide seismic horizon naming scheme. *GNS Science Report* 2014/34 20p.
- Strogen, D.P., Seebeck, H., Nicol, A., King, P.R., 2017. Two-phase Cretaceous–Paleocene rifting in the Taranaki Basin region, New Zealand; implications for Gondwana break-up. *Journal of the Geological Society* 174, 929–946.
- Sultan, N., Marsset, B., Ker, S., Marsset, T., Voisset, M., Vernant, A.M., Bayon, G., Cauquil, E., Adamy, J., Colliat, J.L., Drapeau, D., 2010. Hydrate dissolution as a potential mechanism for pockmark formation in the Niger delta. *Journal of Geophysical Research* 115. doi:10.1029/2010JB007453
- Sun, Q., Cartwright, J.A., Wu, S., Chen, D., 2013. 3D seismic interpretation of dissolution pipes in the South China Sea: Genesis by subsurface, fluid induced collapse. *Marine Geology* 337, 171–181. doi:10.1016/j.margeo.2013.03.002

- Sutherland, R., 1999. Cenozoic bending of New Zealand basement terranes and Alpine Fault displacement: a brief review. *New Zealand Journal of Geology and Geophysics* 42, 295–301.
- Sutherland, R., Browne, G.H., 2003. Canterbury basin offers potential on South Island, New Zealand. *Oil and Gas Journal* 101, 45–49.
- Sutton, P., 2003. The Southland Current: A subantarctic current. *New Zealand Journal of Marine and Freshwater Research* 37, 645–652.
doi:10.1080/00288330.2003.9517195
- Szpak, M.T., Monteys, X., O'Reilly, S.S., Lilley, M.K.S., Scott, G.A., Hart, K.M., McCarron, S.G., Kelleher, B.P., 2015. Occurrence, characteristics and formation mechanisms of methane generated micro-pockmarks in Dunmanus Bay, Ireland. *Continental Shelf Research* 103, 45–59.
- Taleb, F., Lemaire, M., Garziglia, S., Marsset, T., Sultan, N., 2020. Seafloor depressions on the Nigerian margin: Seabed morphology and sub-seabed hydrate distribution. *Marine and Petroleum Geology* 114, 104175.
doi:10.1016/j.marpetgeo.2019.104175
- Talukder, A.R., 2012. Review of submarine cold seep plumbing systems: Leakage to seepage and venting. *Terra Nova* 24, 255–272. doi:10.1111/j.1365-3121.2012.01066.x
- Tamborski, J.J., Rogers, A.D., Bokuniewicz, H.J., Cochran, J.K., Young, C.R., 2015. Identification and quantification of diffuse fresh submarine groundwater discharge via airborne thermal infrared remote sensing. *Remote Sensing of Environment* 171, 202–217.
- Tang, D., Jin, G., Jackson, D.R., Williams, K.L., 1994. Analyses of high-frequency bottom and subbottom backscattering for two distinct shallow water environments. *The Journal of the Acoustical Society of America* 96, 2930–2936. doi:10.1121/1.411302
- Taniguchi, M., Burnett, W.C., Cable, J.E., Turner, J. V, 2002. Investigation of submarine groundwater discharge. *Hydrological Processes* 16, 2115–2129.
doi:10.1002/hyp.1145

- Taylor, C.B., Fox, V.J., 1996. An isotopic study of dissolved inorganic carbon in the catchment of the Waimakariri River and deep ground water of the North Canterbury Plains, New Zealand. *Journal of Hydrology* 186, 161–190. doi:10.1016/S0022-1694(96)03027-2
- Treude, T., Krüger, M., Boetius, A., Jørgensen, B.B., 2005. Environmental control on anaerobic oxidation of methane in the gassy sediments of Eckernförde Bay (German Baltic). *Limnology and oceanography* 50, 1771–1786.
- Uruski, C.I., 2010. New Zealand's deepwater frontier. *Marine and Petroleum Geology* 27, 2005–2026. doi:10.1016/j.marpetgeo.2010.05.010
- Uścińowicz, S., 2014. Chapter 7 The Baltic Sea continental shelf. Geological Society, London, *Memoirs* 41, 69–89. doi:10.1144/M41.7
- van Loon, A.J.T., 2010. Sedimentary volcanoes: Overview and implications for the definition of a volcano on Earth, in: Geological Society of America Special Papers, *What Is a Volcano?* Geological Society of America, p. 31.
- Verschuren, M., 1992. An integrated 3D approach to clay tectonic deformation and the development of a new 3D surface modelling method (Doctoral dissertation). University of Gent.
- Viso, R., McCoy, C., Gayes, P.T., Quafisi, D., 2010. Geological controls on submarine groundwater discharge in Long Bay, South Carolina (USA). *Continental Shelf Research* 30, 335–341. doi:10.1016/j.csr.2009.11.014
- Waghorn, K.A., Pecher, I.A., Strachan, L.J., Crutchley, G.J., Bialas, J., Coffin, R., Davy, B., Koch, S., Kroeger, K.F., Papenberg, C., Sarkar, S., 2017. Paleo-fluid expulsion and contouritic drift formation on the Chatham Rise, New Zealand. *Basin Research* 1–15. doi:10.1111/bre.12237
- Watterson, J., Walsh, J., Nicol, A., Nell, P.A.R., Bretan, P.G., 2000. Geometry and origin of a polygonal fault system. *Journal of the Geological Society* 157, 151–162. doi:10.1144/jgs.157.1.151
- Webb, K.E., Hammer, Ø., Lepland, A., Gray, J.S., 2009. Pockmarks in the inner Oslofjord, Norway. *Geo-Marine Letters* 29, 111–124.
- Wefer, G., Balzer, W., von Bodungen, B., Suess, E., 1987. Biogenic carbonates in

- temperate and subtropical environments: production and accumulation, saturation state and stable isotope composition, in: *Seawater-Sediment Interactions in Coastal Waters*. Springer, pp. 263–302.
- Werne, J.P., Haese, R.R., Zitter, T., Aloisi, G., Bouloubassi, I., Heijs, S., Fiala-Médioni, A., Pancost, R.D., Sinninghe Damsté, J.S., de Lange, G., Forney, L.J., Gottschal, J.C., Foucher, J.P., Mascle, J., Woodside, J., 2004. Life at cold seeps: A synthesis of biogeochemical and ecological data from Kazan mud volcano, eastern Mediterranean Sea. *Chemical Geology* 205, 367–390.
doi:10.1016/j.chemgeo.2003.12.031
- Werner, F., 1978. Depressions in mud sediments (Eckernförde Bay, Baltic Sea) related to sub-bottom and currents. *Meyniana* 30, 99–104.
- Werner, F., Erlenkeuser, H., Grafenstein, U. v, McLean, S., Sarnthein, M., Schauer, U., Unsöld, G., Walger, E., Wittstock, R., 1987. Sedimentary records of benthic processes, in: *Seawater-Sediment Interactions in Coastal Waters*. Springer, pp. 162–262.
- Westbrook, G.K., Exley, R., Minshull, T.A., Nouzé, H., Gailler, A., others, 2008. High-resolution 3D seismic investigations of hydrate-bearing fluid-escape chimneys in the Nyegga region of the Vøring plateau, Norway. *Proceedings of the 6th International Conference on Gas Hydrates (ICGH 2008)*, Vancouver, BC, Canada.
- Wever, T.F., Abegg, F., Fiedler, H.M., Fechner, G., Stender, I.H., 1998. Shallow gas in the muddy sediments of Eckernförde Bay, Germany. *Continental Shelf Research* 18, 1715–1739.
- Wever, T.F., Fiedler, H.M., 1995. Variability of acoustic turbidity in Eckernförde Bay (southwest Baltic Sea) related to the annual temperature cycle. *Marine Geology* 125, 21–27. doi:10.1016/0025-3227(95)00054-3
- Wever, T.F., Lühder, R., Voß, H., Knispel, U., 2006. Potential environmental control of free shallow gas in the seafloor of Eckernförde Bay, Germany. *Marine Geology* 225, 1–4. doi:10.1016/j.margeo.2005.08.005
- Weymer, B.A., Wernette, P.A., Everett, M.E., Podthai, P., Jegen, M., Micallef, A., 2019. Combining near-surface electromagnetic methods to characterize the

- hydrogeology of braided alluvial deposits: Canterbury Coast, New Zealand, in: AGU Fall Meeting Abstracts.
- Whiticar, M.J., 2002. Diagenetic relationships of methanogenesis, nutrients, acoustic turbidity, pockmarks and freshwater seepages in Eckernförde Bay. *Marine Geology* 182, 29–53. doi:10.1016/S0025-3227(01)00227-4
- Whiticar, M.J., Werner, F., 1981. Pockmarks: Submarine vents of natural gas or freshwater seeps? *Geo-Marine Letters* 1, 193–199. doi:10.1007/BF02462433
- Wiggins, R., Kenny, G.S., McClure, C.D., 1983. A method for determining and displaying the shear-velocity reflectivities of a geologic formation. European patent application 113944.
- Wilson, I.R., 1985. Galleon-1 well completion report-Shell BP Todd-In: New Zealand Open-file Petroleum Report 1146. Crown Minerals, Wellington.
- Wilson, J., Rocha, C., 2012. Regional scale assessment of Submarine Groundwater Discharge in Ireland combining medium resolution satellite imagery and geochemical tracing techniques. *Remote Sensing of Environment* 119, 21–34. doi:10.1016/j.rse.2011.11.018
- Winterhalter, B., Flodén, T., Ignatius, H., Axberg, S., Niemistö, L., 1981. Geology of the Baltic sea, in: Elsevier Oceanography Series. Elsevier, pp. 1–121.
- Wong, P.P., Losada, I.J., Gattuso, J.P., Hinkel, J., Khattabi, A., McInnes, K.L., Saito, Y., Sallenger, A., 2014. Coastal systems and low-lying areas. *Climate change* 2104, 361–409.
- Wright, I.C., Gamble, J.A., 1999. Southern Kermadec submarine caldera arc volcanoes (SW Pacific): caldera formation by effusive and pyroclastic eruption. *Marine Geology* 161, 207–227.
- Yamamoto, S., Alcauskas, J.B., Crozier, T.E., 1976. Solubility of methane in distilled water and seawater. *Journal of Chemical and Engineering Data* 21, 78–80.
- Zoeppritz, K., 1919. On the reflection and propagation of seismic waves. *Goettinger Nachrichten* 1, 66–84.

Appendix

Appendix A: Cruise reports

For the studies presented I used existing data from previous cruises in combination with newly acquired data during my PhD. I was glad to be able to participate in cruises 17PL124, 19PL410, 19PL377, AL447, L1905. Additionally, I was also able to participate in an R/V Roger Revelle cruise (RR1901/RR1902) and an R/V Tangaroa cruise (TAN1708) which data did not contribute to my thesis.

TAN1703

The R/V Tangaroa cruise TAN1703 was part of the EU funded MARCAN project, a 5-year research project that investigates the role of offshore groundwater in the geomorphic evolution of continental margins. The cruise was investigating meteoric recharge and topographically-driven groundwater flow using seismic, CSEM and hydroacoustic data as well as sediment cores in the Canterbury Basin. During this cruise, an extensive multibeam dataset on the Canterbury Shelf was acquired which revealed pockmarks on the continental shelf. Cruise report: Mountjoy et al. (2017)

TAN1608

Tan1608 was a designated multibeam survey on the Canterbury Slope operated by NIWA. This survey was designed to complement and extend previous bathymetric data from the canyon system offshore Otago, acquired during cruise TAN1209 in 2012. The new data acquired, combined with the archive dataset, results in a bathymetric coverage that encompasses $\sim 40,000$ km² on the eastern

continental slope of New Zealand's South Island. Cruise Report: Mitchell et al. (2016)

EW0001

During R/V Maurice Ewing expedition EW0001 a dense grid of multichannel seismic data were collected from the middle to outer shelf and slope in the Canterbury Basin. This survey was in support of an Ocean Drilling Program (ODP) proposal and was designed to image the Oligocene to Neogene depositional sequences indicative of sea-level fluctuations. Cruise report: (Fulthorpe et al., 2000a)

19PL410

The primary objective of R/V Polaris II cruise 19PL410 was to obtain multibeam backscatter and high-resolution boomer seismic data along a transect perpendicular to the shoreline in the Canterbury Basin. The backscatter data, groundtruthed by sediment samples along the transect and complemented by the boomer seismic data, were used to constrain the lithological environment that is needed to form pockmarks on the Canterbury Shelf. Cruise participants: Jasper Hoffmann, Hamish Bowman, Josiah Lilbourne, Valerie Kwan, Tesia Lin.

18PL377

During R/V Polaris II cruise 18PL377 I acquired high-resolution water-column imaging (WCI) data to test the hypothesis of potential active degassing and pockmark formation on the Canterbury Shelf. Previous WCI results during cruise TAN1703 in this area were inconclusive. Using very short pulse length I assured the highest possible WCI resolution. The multibeam data were complemented by boomer seismic data, to identify potential fluid sources required for pockmark formation. Cruise participants: Jasper Hoffmann, Hamish Bowman, Tayla Ann Hill, Oliver Rees, Lisa Schmidt, Kara Jurgens.

17PL124

The aim of R/V Polaris II cruise 17PL124 was to investigate shallow subsurface fluid migration on the Canterbury Slope. In the northeast of the Waitaki canyon, two shallow bright spots could be identified in the 3D Endurance seismic dataset. The bright spots are situated within the first ~100 ms of the seismic data

directly below numerous seafloor depressions. The aim was to investigate a possible connection between the bright spots, that could indicate free gas below the seafloor, and the seafloor depressions. We collected high-resolution boomer seismic data as well as multibeam data on the Canterbury Slope and in the vicinity of the Waitaki Canyon head. Cruise participants: Jasper Hoffmann, Andrew Gorman, Hamish Bowman, Oliver Rees, Nathanael Chandrakumar, Luke Carrington, Yvonne Caulfield.

AL447

The main objectives of R/V Alkor cruise AL447 were to determine controls on methane seepage in the Baltic Sea. Therefore, different sites were visited around the Baltic Sea, including Eckernförde Bay. Designated water column investigations, as well as bathymetric and subbottom profiler data, were acquired to investigate gas as well as groundwater flux in the bay. Cruise report: Schneider von Deimling et al. (2014)

AL501 & AL527

Alkor cruises AL501 and AL527 were part of the marine geophysical field course of the University of Kiel, investigating the western Baltic Sea. During both cruises bathymetry as well as Innomar subbottom profiler data were acquired in Eckernförde Bay. Cruise reports: Krastel et al. (2019, 2017)

EMB187

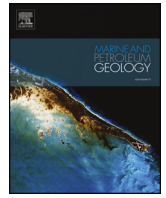
The purpose of R/V Elisabeth Mann Borgese cruise EMB187 was the measurement of R_n and R_d in the water column and the upper sediment to better constrain submarine groundwater discharges (SGD) in Eckernförde Bay. Several Innomar subbottom profiles were acquired to find sites characteristic for SGD. Cruise report: Prien et al. (2018)

L1905

During FK Littorina cruise L1905 we investigated the effects of (SGD) on the seafloor geomorphology and the water column in Eckernförde Bay. The main aim was to collect sediment cores and porewaters to groundtruth hydroacoustic investigations in that area. Cruise report: (Schneider von Deimling et al., 2019)

Appendix B1: Publications

- B1.1 Hoffmann, J.J.L., Gorman, A.R. and Crutchley, G.J., 2019. Seismic evidence for repeated vertical fluid flow through polygonally faulted strata in the Canterbury Basin, New Zealand. *Marine and Petroleum Geology*, 109, pp.317-329.
- B1.2 Hoffmann, J.J.L., Schneider von Deimling, J., Schröder, J.F., Schmidt, M., Held, P., Crutchley, G.J., Scholten, J. and Gorman, A.R., 2020. *Complex eyed pockmarks and submarine groundwater discharge revealed by acoustic data and sediment cores in Eckernförde Bay, SW Baltic Sea*. *Geochemistry, Geophysics, Geosystems*, 21(4), e2019GC008825.
- B1.3 Hoffmann, J., Gorman, A. and Crutchley, G., 2018. Investigation of Possible Shallow Gas Accumulations Associated with Pockmarks on the Otago Slope Southeast of New Zealand. *ASEG Extended Abstracts*, 2018(1), pp.1-7.



Research paper

Seismic evidence for repeated vertical fluid flow through polygonally faulted strata in the Canterbury Basin, New Zealand

Jasper J.L. Hoffmann^{a,*}, Andrew R. Gorman^a, Gareth J. Crutchley^b^a Department of Geology, University of Otago, PO Box 56, Dunedin, 9054, New Zealand^b GNS Science, 1 Fairway Drive, Avalon, Lower Hutt, 5040, New Zealand

ARTICLE INFO

Keywords:

Polygonal faults
 Focused fluid migration
 Pockmarks
 Mud volcano
 Shallow gas
 Chimney

ABSTRACT

Seismic imaging techniques are widely used to determine fluid migration pathways in the subsurface. Understanding the timing and distribution of focused fluid migration pathways is important for assessing reservoir seal quality and hydrocarbon exploration risk, as well as seafloor biogeochemical processes in the case of fluid venting from the seafloor. The frontier Canterbury Basin southeast of New Zealand is well studied, but questions remain regarding the dynamic movement of fluids through the basin. Using 3D seismic data combined with high-resolution boomer seismic data, we characterise focused fluid migration and sediment remobilisation events in the Canterbury Basin. We show how polygonal fault formation and nucleation is affected in the vicinity of vertically ascending fluids and sediments. A cylindrical region devoid of polygonal faulting around the feeder system of a buried sediment volcano points to the possible existence of an axisymmetrical stress field induced by upward migrating fluids and sediments. Sediment remobilisation and intrusions of permeable stringers (i.e. sand injectites) could enable dewatering of their host strata and thereby prevent polygonal faults from nucleating. Amplitude variations with angle (AVA) and a detailed analysis of two tiers of polygonal faults reveal three phases of fluid migration and sediment remobilisation and intrusion through, and into, low permeability sediments. Our integrated conceptual model provides insights into vertical fluid migration mechanisms and the implications for polygonal fault formation.

1. Introduction

Fluid transport through focused flow systems is a widespread phenomenon in sedimentary basins. Fluid migration and accumulation processes play important roles in hydrocarbon exploration, hazard assessment, and environmental conservation (Anka et al., 2012). On the seafloor, circular depressions – often referred to as pockmarks due to their appearance in seafloor bathymetric imagery – can be indicative of underlying fluid migration pathways such as faults, pipes or chimney structures (Berndt et al., 2003; Hovland et al., 2005; Løseth et al., 2011). In some cases, such depressions have been interpreted to result from the removal of sub-seabed material by gas hydrate dissociation and subsequent collapse (Imbert and Ho, 2012; Riboulot et al., 2016; Sultan et al., 2010). The more common process described in the literature is the suspension and removal of seabed material by escaping fluids (King and MacLean, 1970; Mazzini et al., 2016). Pockmarks can form due to episodic dewatering and sediment compaction in sedimentary basins, often in combination with a non-tectonic class of faults, known as polygonal faults (due to their polygonal form in planview).

These faults only form in very fine to fine-grained tiers of sedimentary strata where they alter the bulk permeability of the otherwise low matrix permeability and expel as much as 60 percent water by volume, which is why they are considered a major fluid source (Berndt et al., 2003; Cartwright et al., 2007; Cartwright and Lonergan, 1996; Verschuren, 1992). Pipe structures in the overburden of polygonal fault systems show that polygonal fault systems can act as a long term source for fluid flow (Berndt et al., 2003) as well as pathways for upward fluid migration from deeper strata (Gay et al., 2004). Ho et al. (2016) suggest the lower parts of polygonal faults may behave as fluid conduits while the upper parts of the fault planes appear to be sealed. The polygonal platform may be modified by the underlying morphology as well as by anisotropic stress fields (Ho et al., 2018a).

Sedimentary volcanoes (often classified as mud volcanoes, but also sometimes consisting of coarser-grained, non-cohesive material) are a specific category of natural gas/oil seepage and in general confirm the existence of overpressured hydrocarbon reservoirs in the region (Mazzini and Etiope, 2017; van Loon, 2010). They are an important pathway for degassing deeply buried sediments and represent a

* Corresponding author.

E-mail address: jasper.hoffmann@otago.ac.nz (J.J.L. Hoffmann).<https://doi.org/10.1016/j.marpetgeo.2019.06.025>

Received 14 March 2019; Received in revised form 13 June 2019; Accepted 14 June 2019

Available online 17 June 2019

0264-8172/ © 2019 Elsevier Ltd. All rights reserved.

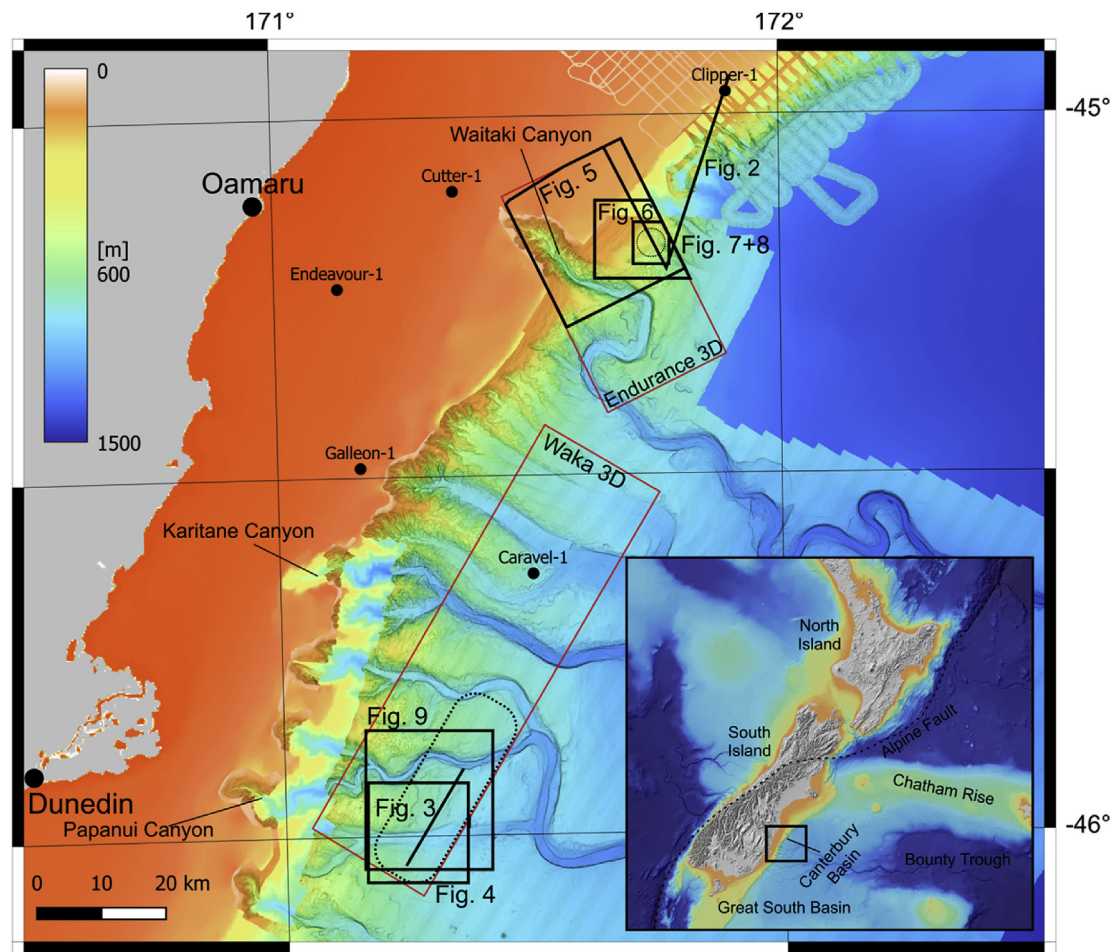


Fig. 1. Bathymetric overview map of the Otago margin working area (Data source: (NIWA 2016, 2012)). The inset map in the lower right shows the location (black box) of the main map. The footprints of two 3D seismic surveys (Waka 3D and Endurance 3D) on the Otago submarine canyon complex are outlined in red (Data source: Anadarko and Origin Energy, 2009; NZOG and Beach Energy, 2013). Buried pockmarks are observed within the dotted black area of the Waka 3D box. (For interpretation of the references to colour in this figure legend, the reader is referred to the Web version of this article.)

significant source of methane in the atmosphere (Dimitrov, 2002). However, in most cases, methane escaping from the seafloor is dissolved and consumed as it rises through the water column (McGinnis et al., 2006) where it has implications for marine biogeochemistry (Leifer and Judd, 2002).

The Canterbury Basin off the southeast coast of New Zealand is the target of on-going commercial petroleum exploration (NZOG, 2018). Six offshore exploration wells (Fig. 1) have been drilled with at least three shows of gas condensates in uncommercial quantities. However, fundamental questions persist regarding sub-surface fluid flow in the basin.

We focus on three-dimensional (3-D) seismic expressions of fluid migration pathways through sedimentary sequences that include several extensive tiers of polygonal faults. Seismic data analysis, particularly in 3-D, is ideally suited to this research because seismic reflectivity and coherency are highly sensitive to both structural deformation and fluid flow processes (Marfurt et al., 1998; Simm and Bacon, 2014). In particular, we examine formation mechanisms of cylindrical faults around a fluid conduit. The aims of this study are: (1) to investigate the nature, and provide a seismic characterisation, of recent and buried fluid migration pathways, (2) to constrain the timing of fluid migration in the Canterbury Basin and (3) to present a conceptual integrated model for the formation of the fluid migration pathways.

2. Geological setting

2.1. Canterbury Basin

The Canterbury Basin, located on the eastern passive continental margin of New Zealand's South Island, covers an area of $\sim 360,000 \text{ km}^2$; it is bounded to the north by the Chatham Rise and in the south by the Great South Basin. The present-day passive continental margin off the Canterbury/Otago coast is characterised by a variable shelf width of 10–90 km. The margin slope in this region is incised by numerous canyons and gullies, especially south of the Waitaki Canyon (Fig. 1).

The margin began to rift from Antarctica at about 105 Ma (Strogen et al., 2017) and is now located $\sim 200 \text{ km}$ to the east of the Alpine Fault (the plate boundary between the Australian and Pacific plates). It has experienced one large-scale tectonically controlled transgressive-regressive cycle during the Cretaceous to Recent, with maximum flooding during the Oligocene (Fulthorpe and Carter, 1989). The tectonically forced sea-level cycle has been overprinted by shorter-term eustatic sea-level changes. The region has been relatively stable tectonically since rifting with faulting only occurring close to shore, mainly associated with local igneous intrusions of late Eocene-Oligocene and Miocene ages (Coombs et al., 1986; Milne et al., 1975).

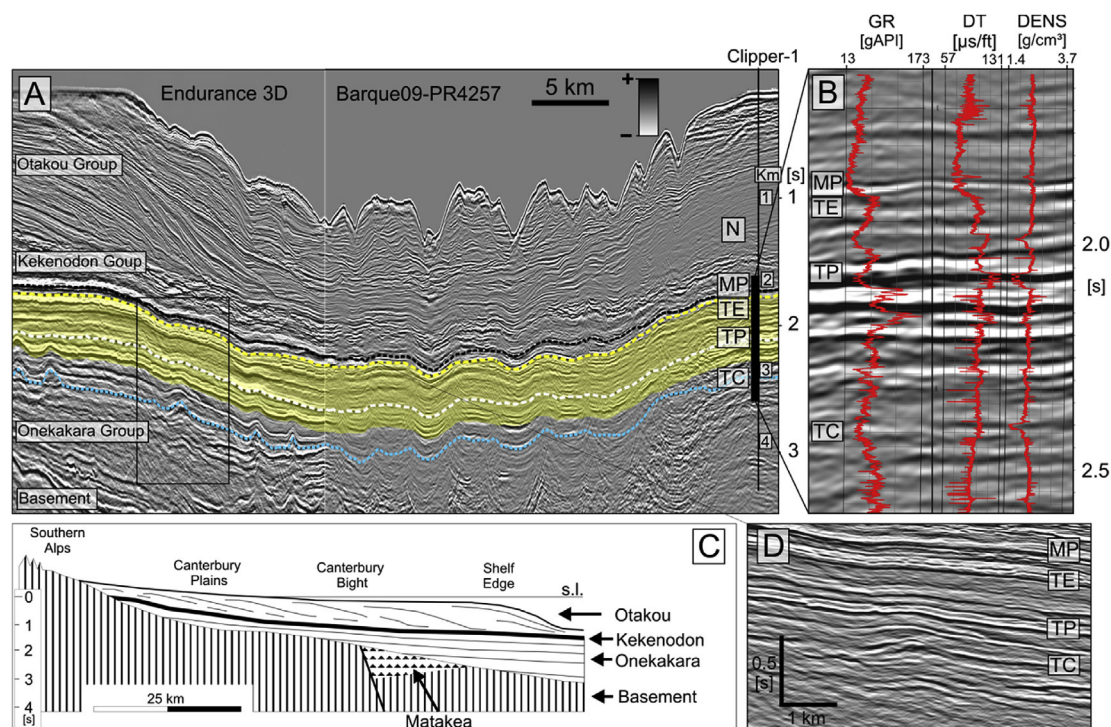


Fig. 2. A) Composite seismic tie line to the Clipper-1 well. Approximate extent of the polygonal faulted tiers are shown in yellow. Neogene (N) Marshall Paraconformity (MP), top Eocene (TE), top Paleocene (TP) and top Cretaceous (TC) are shown as dashed lines. B) Gamma Ray (GR), Sonic (DT) and Density (DENS) logs are shown in the area of interest. C) Schematic cross-section through the Canterbury basin after Fulthorpe and Carter (1989). D) Undisturbed view of the horizons specified. (For interpretation of the references to colour in this figure legend, the reader is referred to the Web version of this article.)

2.2. Stratigraphy

The large-scale transgressive-regressive cycle in the Canterbury Basin has resulted in the deposition of three main stratigraphic units: a transgressive unit (Onekakara Group), a sea-level highstand unit (Kekenodon Group) (Carter, 1988) (Fig. 2).

Post-rift subsidence after the breakup from Antarctica resulted in the initiation of the transgressional phase in the Late Cretaceous that continued until the Oligocene when flooding of the land mass was at a maximum (Fleming, 1962). This mainly terrigenous, transgressive Onekakara Group (late Cretaceous–Oligocene) (Carter, 1985; Fulthorpe et al., 2010) is characterised in seismic reflection data by mainly continuous horizontal reflections of moderate amplitude. In the 3D seismic data, Cretaceous strata onlap onto the basement as moderate to weak amplitude reflections (Fig. 2). Overlying Paleocene and Eocene sediments are well stratified and show at least three intense tiers of polygonal faults that developed in clay-rich mudstone (Fig. 3). At the end of this transgressive phase, reduced terrigenous influx resulted in the deposition of the Amuri Limestone (Fulthorpe et al., 2010). Few of the polygonal faults are observed to penetrate up through the Oligocene Marshall Paraconformity at the top of the Onekakara Group.

The unconformity separates the Onekakara Group from the blanket-like glauconitic and bioclastic sediments of the Kekenodon Group (Late Oligocene–Miocene). The Kekenodon Group is characterised by strong and discontinuous reflections in regions proximal to the emerging landmass to the west, whereas distal reflections are characterised by sub-parallel, horizontal and more consistent amplitudes. Increased sediment supply due to initiation of movement on the plate-bounding Alpine Fault and corresponding uplift of the Southern Alps induced a phase of regression in the region from late Oligocene to early Miocene (Carter and Norris, 1976; Fulthorpe and Carter, 1989). During this phase of regression, the prograding clinoforms of the Otakou Group (Miocene–Recent) were deposited. The Otakou Group mainly consists of

fine quartzose sand and terrigenous siltstone that builds the modern continental shelf (Carter et al., 1990). The clinoforms consist of overlapping and toplapping events indicating erosional and prograding stages.

2.3. Marshall Paraconformity

The Marshall Paraconformity is a regional unconformity in the Canterbury Basin separating the transgressive Onekakara Group from the glauconitic Kekenodon Group. The unconformity is considered to be coeval with the initiation of thermohaline circulation following the separation of Australia and Antarctica ~33.7 Ma (Fulthorpe et al., 2010). It caps the widespread Amuri Limestone and is overlain by greensand and calcarenite limestone (Field et al., 1989).

Lewis and Belliss (1984) noted that the term paraconformity is misleading; the surface of the unconformity is observed in seismic data to be not only conspicuous and complex, but also angular, and therefore does not fit the definition of a paraconformity as introduced by Dunbar and Rodgers (1957) for a biostratigraphic discontinuity (a discontinuity based and evaluated solely on paleontological evidence). However, we still refer to this surface as the Marshall Paraconformity to conform with historical usage.

2.4. Fluid flow and seafloor depressions

Pockmarks are abundant on the slope of the Canterbury Basin where they range in diameter from 20 to 700 m and exhibit crescent forms that are aligned with the north-eastward flowing Southland Current (Hillman et al., 2018). The pockmarks occur in patches that are constrained to the crests between submarine canyons and gullies. Their positions on the seafloor at depths between 500 and 1100 m roughly coincide with shallow areas of the expected gas hydrate stability zone (GHSZ) in this region (Hillman et al., 2015). This approximate coincidence also led to an interpretation that gas hydrate dissociation and

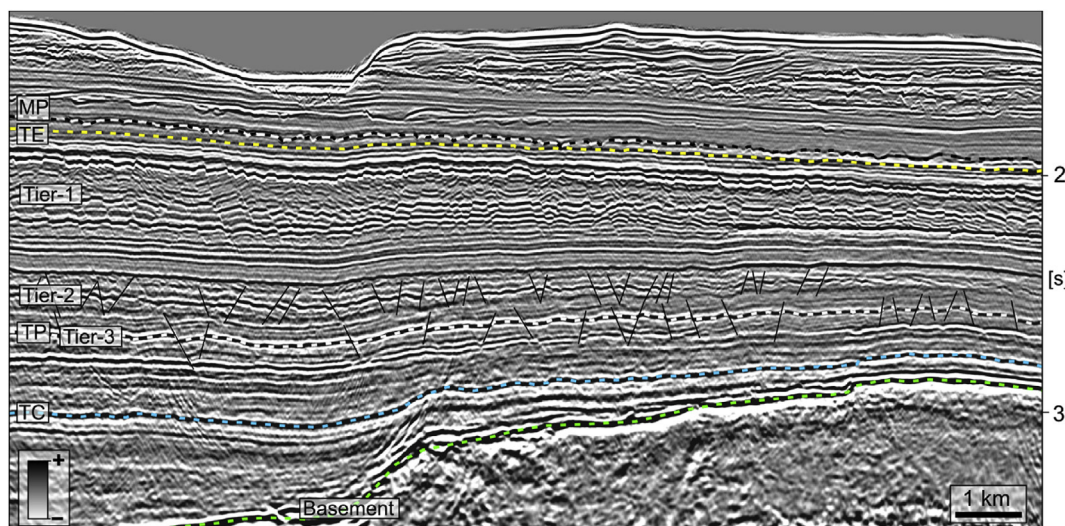


Fig. 3. Overview of the three tiers of polygonal faults within Eocene and Paleocene strata. Key seismic reflectors are annotated and labelled according to the same colour scheme and nomenclature as in Fig. 2. The additional broken green line marks the Basement. (For interpretation of the references to colour in this figure legend, the reader is referred to the Web version of this article.)

resulting venting during glacial-stage sea-level lowstands were responsible for the pockmark formation (Davy et al., 2010). Multibeam and parasound water column investigations in 2012 and 2013 revealed no evidence of active seepage on the seafloor (Bialas et al., 2013; Schneider von Deimling and Hoffmann, 2012). Water and seafloor samples collected in and around the pockmarks show no geochemical evidence of enhanced methane concentrations on the Otago margin (Hillman et al., 2015). Since no indications for shallow hydrocarbons were present, Hillman et al. (2015) concluded that groundwater flux was likely to be the dominant formation process for pockmarks on the Canterbury Basin slope. No active fluid seepage has been reported on the Canterbury Basin slope.

3. Data

Recent exploration efforts by the petroleum industry in this region have involved the collection of two extensive 3D seismic datasets covering the Otago Canyon system (Fig. 1). The 3D datasets cover total areas of 1151 and 680 km² at full fold. One dataset (Waka 3D) is publicly available while the second proprietary seismic dataset (Endurance 3D) was made available for this study. An inline and crossline spacing of 25 × 12.5 m in both datasets allows us to accurately map faults and horizons. Additionally, several CDP-sorted pre-stack 2D lines extracted from the Endurance 3D volume were made available for this study and are used for high-density velocity analysis and amplitude versus angle (AVA) investigations.

The seismic data are complemented by high-resolution multi-channel seismic boomer data in shallow regions. Due to differences in seismic resolution and location, the two 3D seismic datasets show distinct differences in amplitude characteristics and the stratigraphic successions that they image are somewhat different. The three main stratigraphic units in the Canterbury Basin (Onekakara, Kekenodon and Otakou Groups) are readily distinguished in the Endurance 3D seismic dataset which partly covers the shelf and the prograding clinoforms. In contrast, the Waka 3D volume, which is more basinward and further south, does not image the prograding clinoforms but instead covers the channel-levee system on the slope of the margin and the Eocene to basement strata.

3.1. Waka 3D

In 2009, Petroleum Geo-Services (PGS) acquired the Waka 3D

seismic data volume (licence block: PEP38262) using the *M/V Nordic Explorer* with six parallel 5.1 km-long hydrophone streamers and a streamer separation of 100 m. Two Dodera G gun 3090 cu. in arrays at 2000 psi were operated in flip-flop mode. A line spacing of 25 m was achieved. The traces, with a record length of 6 s and a sampling interval of 2 ms, were processed to zero phase, binned using a 12.5 × 25 m grid, and had a pre-stack Kirchhoff time migration applied. In all seismic data shown the phase was rotated by 180° to conform with the Society of Exploration Geophysicists convention where a positive reflection coefficient is represented by a positive amplitude.

3.2. Endurance 3D

The Endurance 3D seismic survey (licence block: PEP52717) was acquired by the licence operator, New Zealand Oil and Gas, contracting the vessel *M/V Polarcus Alima* in 2013. The data were acquired with twelve 8.1 km-long streamers with a separation of 100 m. Two Bolt LLX-LLXT 3480 cu. in arrays were operated in flip-flop mode at 2000 psi. The data were recorded with an 8 s record length and a sample interval of 2 ms and processed on board by ION Geophysical. Amplitudes were preserved during a pre-stack Kirchhoff depth migration. The final bin size is 12.5 × 25 m. For this study, the post-stack dataset is available along with seven pre-stack lines for AVA and velocity analysis.

3.3. Boomer 2D seismic data

We acquired high-resolution boomer seismic data in targeted areas within block PEP52717 using the University of Otago's *R/V Polaris II*. We operated a Ferranti Ocean Research Equipment (ORE) Geopulse sub-bottom profiler source together with a 75 m-long Geometrics MicroEel 24-channel streamer acquisition system. We used GLOBE Claritas® seismic processing software to apply a frequency filter between 100 and 1000 Hz as well as an FK-filter and a Kirchhoff time migration.

4. Methods

The data were loaded into the IHS Markit Kingdom software for visualisation and interpretation. This software also provides algorithms for seismic attribute analysis. The semblance-based coherency attribute highlights lateral changes between adjacent traces and hence was used to detect and map structural discontinuities. Changes in seismic

reflection patterns can be visualised by the energy envelope, which is useful for revealing pronounced acoustic impedance contrasts associated with gas accumulation, changes in depositional environments or sequence boundaries.

A subset of about 200 km of pre-stack CDP sorted 2D seismic data was extracted from the pre-stack time-migrated Endurance 3D volume for additional analyses. We carried out high-density velocity analyses on these lines to refine the shallow velocity model and used the HampsonRussell software to evaluate AVA anomalies.

Velocity analyses based on semblance calculations are a standard procedure undertaken during long-offset seismic processing to determine accurate normal moveout (NMO) corrections and to better constrain migration. This procedure usually involves interactively picking optimal stacking velocities in CDP gathers spaced at regular intervals along a profile and interpolating laterally between picked locations. For the highest spatial resolution, the semblance of every CDP can be picked. We adopted an automated high-density semblance-based velocity analysis scheme – details described by Crutchley et al. (2016) – implemented in the GLOBE Claritas seismic processing software to explore acoustic velocity behaviour in the vicinity of shallow bright spots. We picked semblance along a 2D seismic line extracted from the 3D dataset in 20 ms windows. The 8 km-long streamer provides more-than-sufficient offsets for velocity and AVA studies. Gas charged sands, due to their low impedance and abnormally low Poisson's ratios, embedded into sediments with a higher impedance and 'normal' Poisson's ratio should generally result in a negative reflection coefficient with an increase of reflected P-wave energy with increasing angle of incidence (Class 3 AVA anomalies) (Castagna and Backus, 1993). We used several AVA techniques including AVA gradient analysis, AVA classification by cross-plotting and AVA attribute analysis. The attribute we show here is the product of Intercept (A) and Gradient (B) and therefore positively highlights Class 3 AVA anomalies as well as positive intercept amplitudes with a positive gradient $(-A)*(-B) = +AB = (+A)*(+B)$.

We picked key horizons in the datasets and stratigraphically validated them using Galleon-1, Cutter-1, Endeavour-1 and Clipper-1 exploration wells (Figs. 1 and 2). We picked reflections based on their seismic character (e.g., reflectivity, continuity, dip and stratigraphic framework) and used seismic attributes to identify discontinuities and lithological changes.

5. Results

5.1. Polygonal faults

Three individual polygonally faulted tiers in Paleocene to Oligocene strata are identifiable in the Canterbury Basin seismic data. The uppermost Eocene polygonal faulted tier, "tier-1" extends up to the Marshall Paraconformity with a total thickness of ~400 ms TWT. In the lower Eocene strata, "tier-2" has a thickness of ~100 ms TWT and partly intersects with an upper Paleocene to lowermost Eocene polygonal faulted "tier-3" (Fig. 3). These three faulted tiers are separated by layers of mostly continuously bedded strata that contain only rare faults. The faults of tier-1 show the typical decrease in throw towards the upper and lower boundaries of the tier (Fig. 4). Observed dips range between 20 and 40° measured orthogonal to strike direction and the spacing between faults ranges from 200 to 300 m. The maximum throw is up to 30 m whereas the minimum observable throw is determined by the vertical resolution of the seismic data (~10 m in the Waka 3D and ~20 m in the Endurance 3D seismic datasets). Most faults have a gently listric behaviour, as described elsewhere (Cartwright, 1994a, 2011). The upper extent is generally coincident with the Marshall Paraconformity although some faults are observed to cross the unconformity terminating in a layer of turbidite channel-levee deposits. The data show no evidence of faults continuing up to the seafloor or any direct connection of faults to present day seafloor pockmarks. On the surface

of the Marshall Paraconformity, depressions are observed which often seem to nucleate on the uppermost extent of polygonal fault planes (Fig. 4). The depressions are between 100 and 300 m in diameter and exhibit the same north-east facing oval to crescent shape as modern-day seafloor pockmarks (Hillman et al., 2018). The dip of the maximum similarity seismic attribute highlights strong dips along the Marshall Paraconformity (Fig. 4B). The dips in most pockmarks are steeper along their south-western sides. Seismic reflectivity is higher within the pockmarks compared to surrounding strata. The pockmarks mainly occur in the southern part of the basin.

5.2. Mounded structures associated with radial faults

The polygonal fault systems observed in the seismic data are variably affected by a range of sub-circular mounded structures originating from Cretaceous strata (Fig. 5). The descriptive term "mounded structure" is used here prior to evaluating the formation mechanisms of the features in the discussion. The mounds at the Top Cretaceous reflector show diameters between 1 and 3.5 km and heights ranging from 90 to 350 m. The topographic aspect ratios (height divided by width) are close to 0.1 at the Top Cretaceous horizon and drop down to a mean of 0.056 on the Intra Paleocene horizon. The internal structure of the mounds appears chaotic and Cretaceous sediment layers beneath the mounds are disrupted or deflected upwards (Fig. 5). The mounds mainly affect Cretaceous and Lower Paleocene strata while Upper Paleocene and Eocene sediments seem widely unaffected and mainly overlap onto the flanks of the mounds (Fig. 5A). In two cases though, amplitude anomalies above Mound 7 and Mound 9 are recognised and extend up to the Oligocene Marshall Paraconformity or even the present-day seafloor (Fig. 6, Fig. 8).

In the Paleocene polygonal faulted tier-3, in the proximity of the mounded structures, faults predominantly develop in a radial sense, with fault segments radiating outward from the centre of the mounds over a radius of up to 3 km (highlighted by arrows in Fig. 5C and D). These radial faults are confined to the Paleocene polygonal faulted tier-3. The radial polygonal faults often appear in parallel pairs with a separation of 100–200 m at the intra-paleocene level narrowing towards the base of the tier. This phenomenon of parallel polygonal faults has previously been described and interpreted by Cartwright (2011) as an indication for the high maturity of the polygonal fault system.

5.3. Seismic character of cylindrical faults

Although the upper Eocene tier-1 of polygonal faults is widely unaffected by the mounded structures and extends over a large area of the Canterbury Basin, including both 3D seismic datasets, there is a distinct cylindrical region without polygonal faults within this tier, located above the Cretaceous Mound M7 (Figs. 5B and 6). This cylindrical area has a radius of ~2 km and is bounded by discontinuities as indicated by low similarity values in Fig. 5B. In seismic cross-sections, the cylindrical structure shows amplitude anomalies with enhanced and slightly different reflectivity behaviour in the interior of the cylinder (Fig. 6). Disturbed and disrupted reflections characterise the highly faulted tier-1 surrounding the cylinder. Within the cylinder, reflections abruptly become smoother and more continuous. At the base of the polygonal faulted tier-1, the cylinder becomes slightly narrower and is characterised by low frequencies and high amplitudes starting with a broad negative polarity reflection (Fig. 6A/B). These strong, low-frequency reflections appear to be confined to the lower Eocene strata below the uppermost tier-1 of polygonal faults. The strata surrounding the cylindrical Lower Eocene anomalies are mainly characterised by weak to very weak seismic amplitudes.

While the cylindrical column of anomalies is bounded by faults in the polygonal faulted tier-1, the low-frequency amplitude anomalies below do not show any structural boundaries. The cylindrical anomalies are centred on the vertical axis of the Cretaceous mounded structure,

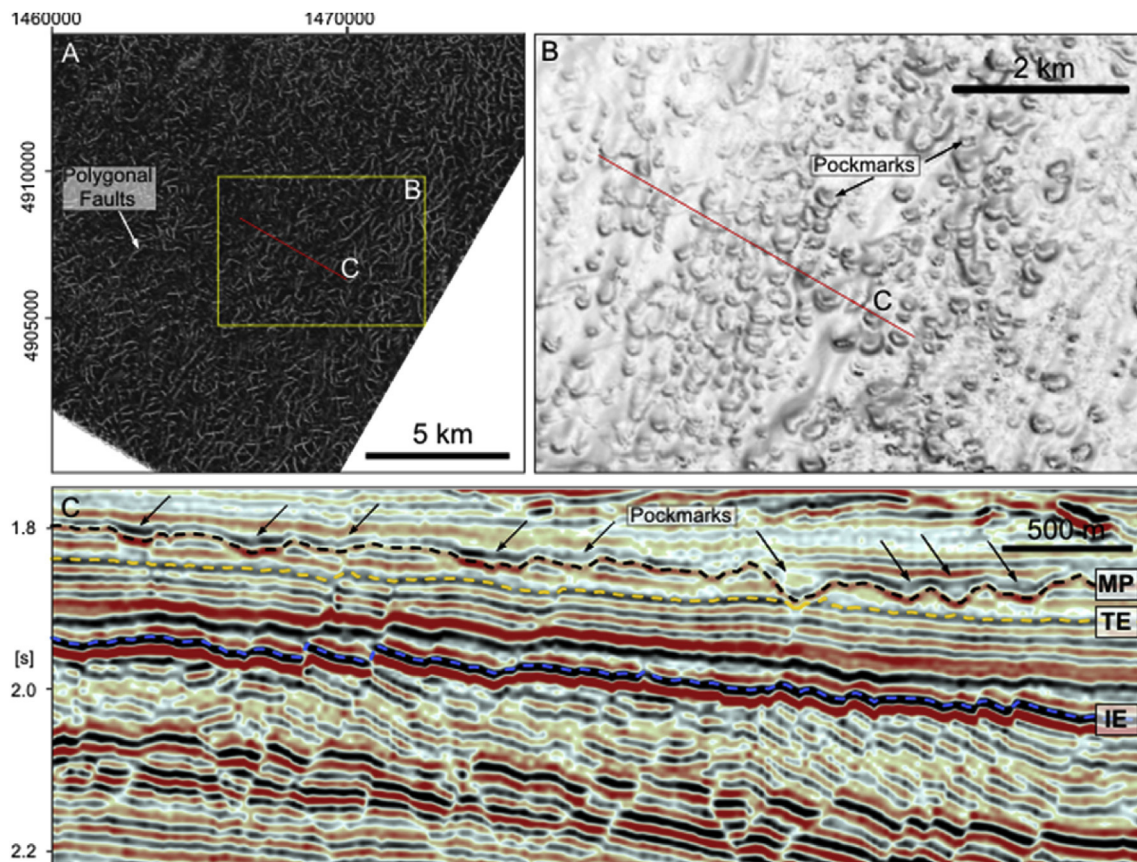


Fig. 4. A) Horizon slice of the similarity seismic attribute extracted along the broken blue horizon in C. Light colours indicate low similarity values and are therefore indicative of discontinuities. B) Horizon slice of the “dip of maximum similarity” seismic attribute along the black horizon (MP: Marshall Paraconformity) marked in C. Darker colours indicate steeper dips along the horizon. C) Seismic section through a polygonal fault system and buried pockmark field (see Fig. 1 for line location). (For interpretation of the references to colour in this figure legend, the reader is referred to the Web version of this article.)

denoted here as Mound M7. Reflections above Mound M7 are convex, but continuous, and are not disrupted by onlapping (Fig. 6A/B) as is observed with the other mounded structures (Fig. 5A).

A vertical stack of upward-bent reflections marks the centre of the cylindrical faults in the polygonal fault system (Fig. 6B). These form a connection from Mound M7 to an irregular, ~100 m high and 500 m wide, elevated region that can be mapped on the Marshall Paraconformity (Fig. 6C). This elevated zone/mound is surrounded by a crater-like morphological expression ~4 km in diameter (Fig. 6C). The semblance based high-density velocity analysis we conducted does not reveal a distinct velocity variation within or around the cylindrical anomaly. Also, no indications of cylindrical faults, other discontinuities or pulled-up reflections are observed in the strata above the Marshall Paraconformity in this region.

In Fig. 7B, sediment thicknesses between two Eocene horizons (red and yellow, Fig. 7D) show drastically decreased sediment volumes within the cylindrical anomaly compared to the surrounding strata. In contrast, younger stratigraphic units within the cylinder (between the red and turquoise horizons in Fig. 7D) appear to be thicker than the corresponding horizons outside (Fig. 7A).

5.4. Shallow bright spots/chimneys

In the crest of a gully to the northeast of the Waitaki Canyon, shallow bright spots exhibit a strong phase reversal and are underlain by a curtain of acoustic suppression (Fig. 8). Detailed high-frequency boomer seismic surveying, which targeted the bright spots, also reveals a zone of reduced amplitudes beneath shallow high-amplitude reflections (Fig. 8D). The boomer seismic data reveal that the bright spots are

located only a few tens of metres below the present-day seafloor. The summation of energy in the upper 100 m of the seafloor shows the distribution of shallow bright spots in blue colours in Fig. 8C.

The 3D industry seismic data reveal a near vertical zone of slightly reduced seismic amplitudes that connects one of the mounded structures (Mound M9) to the shallow bright spots (Fig. 8A/B). Red colours in Fig. 8C indicate low reflection energy values extracted in a 1 km thick window above the Marshall Paraconformity, while green colours represent higher values. The circular red region in Fig. 8C, therefore, represents a sub-vertical, cylindrical low energy zone that connects Mound M9 to the shallow bright spots. This sub-vertical low energy cylinder is well imaged in the AVA section where it is characterised by an AVA product close to zero (Fig. 8A). This very steeply basinward-dipping reduced amplitude zone is the result of small AVA intercept values rather than small AVA gradients. While an acoustic curtain and pulled down reflections are visible in the seismic amplitude data up to 400 ms below the bright spots, the corridor of low AVA product extends downward roughly 3 s and terminates at the Cretaceous stratigraphic level at Mound M9. AVA analysis of the shallow bright spots beneath the seafloor reveals Class 3 AVA behaviour (increasing negative amplitudes with angle) resulting in a positive anomaly in the AVA attribute.

6. Discussion

6.1. Formation mechanisms of the cylindrical anomaly

Upward-bent or pulled-up reflections are common phenomena in seismic data. They are often attributed to increased velocities in areas of

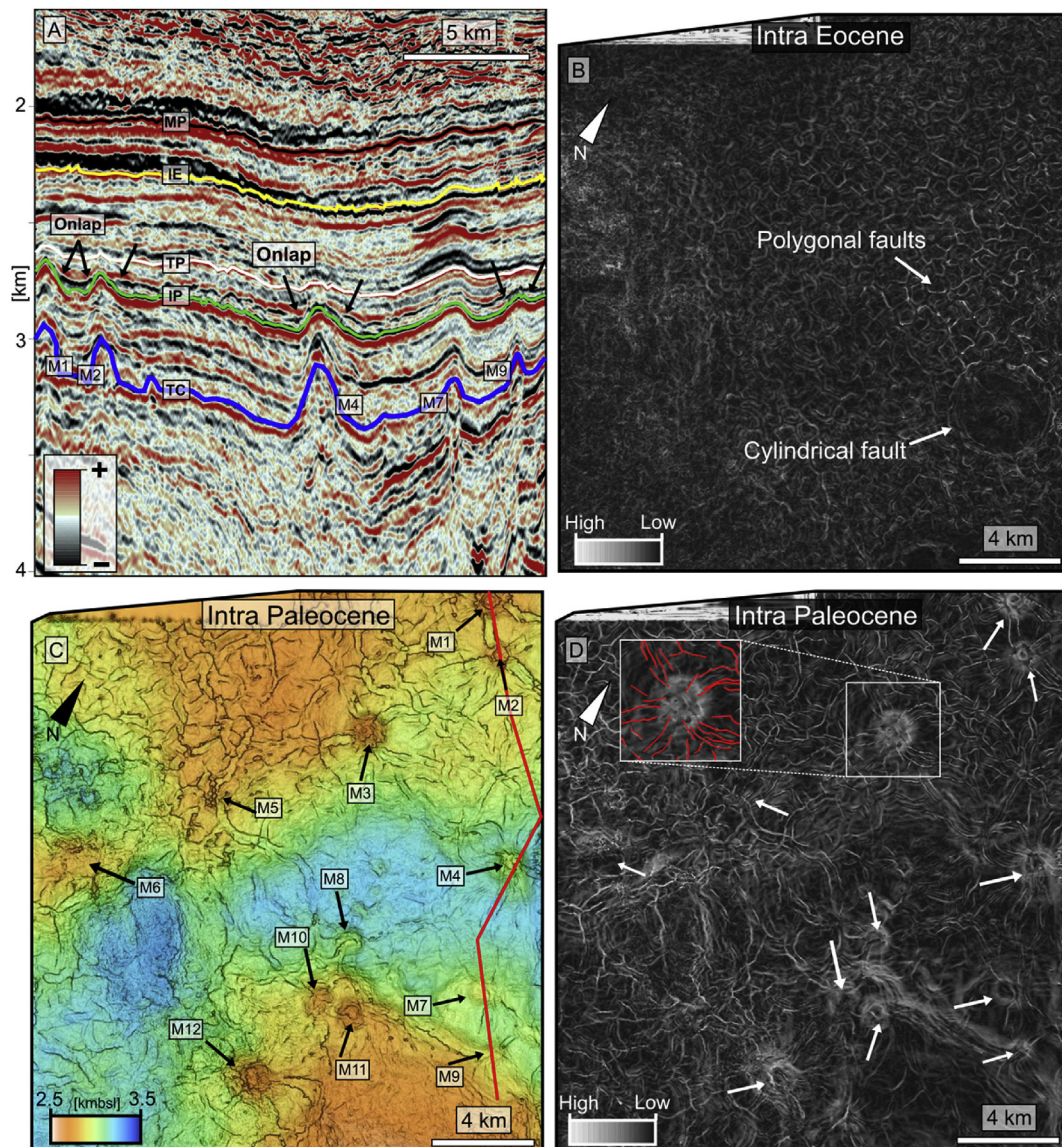


Fig. 5. A) Seismic cross-section through mounded structures originating from Cretaceous strata. Upper Paleocene strata onlap onto the mounds. B) The dip of maximum similarity attribute extracted along the Intra Eocene horizon highlights polygonal as well as cylindrical faults. C) The surface of the Intra Paleocene horizon highlighting mounded structures with associated radial faults. The red line is the arbitrary seismic line shown in (A). D) The dip of maximum similarity attribute extracted along the Intra Paleocene horizon highlights polygonal and radial faults striking away from the mounds. Note: Each map (B, C and D) covers an identical areal extent and is plotted at the same scale. (For interpretation of the references to colour in this figure legend, the reader is referred to the Web version of this article.)

enhanced gas hydrate concentrations or authigenic carbonate cement within fluid conduits (Hustoft et al., 2010). Pulled-up reflections in this sense are an artefact of seismic imaging that is caused by erroneous seismic velocities (in the conduits) used for processing the data. By contrast, fluids ascending vertically due to overpressured sequences can also hydraulically fracture the overburden and cause up-warped reflections through physical disruption of the strata (Karstens and Berndt, 2015; Løseth et al., 2011).

The up-warped reflections we observe in the centre of the cylindrical amplitude anomaly above the mounded structure M7 show no indications of enhanced velocities in our semblance based velocity analysis. As such, we can be confident that they represent real upward bending of sedimentary layers rather than being an artefact of seismic imaging. Due to the similar seismic expression to structures observed by Berndt (2005), Berndt et al. (2003), Gay et al. (2012), Karstens and Berndt (2015) or Løseth et al. (2011), we interpret that the up-bending represents a structural conduit for upward migrating fluids. The

location of the crater-like circular expression on the surface of the Marshall Paraconformity above the fluid conduit (Fig. 6) suggests an intrinsic link between the conduit and the circular feature.

Sediment volcanoes exhibit a wide variety of morphologies on land, at the seabed and in buried surfaces (Mazzini and Etiope, 2017; van Loon, 2010). They are the surface expression of a three-phase discharge (sediments, liquids, and gas) related to gravitational instability and hydrocarbon producing systems (Etiope and Martinelli, 2009). Onshore analogues of crater-like mud volcano morphologies sourced from hydrocarbon bearing basins have previously been described by Mazzini and Etiope (2017) and Stoppa (2006). The crater like morphology on the Marshall Paraconformity clearly indicates extruded and discharged sediments onto the unconformity with the feeding system indicated by the upward-bent reflections. We therefore interpret the intrinsic link between the conduit and the crater-like impression to indicate some type of sediment volcanism. The decreased and increased thicknesses of two stratigraphic intervals within the cylinder compared to its

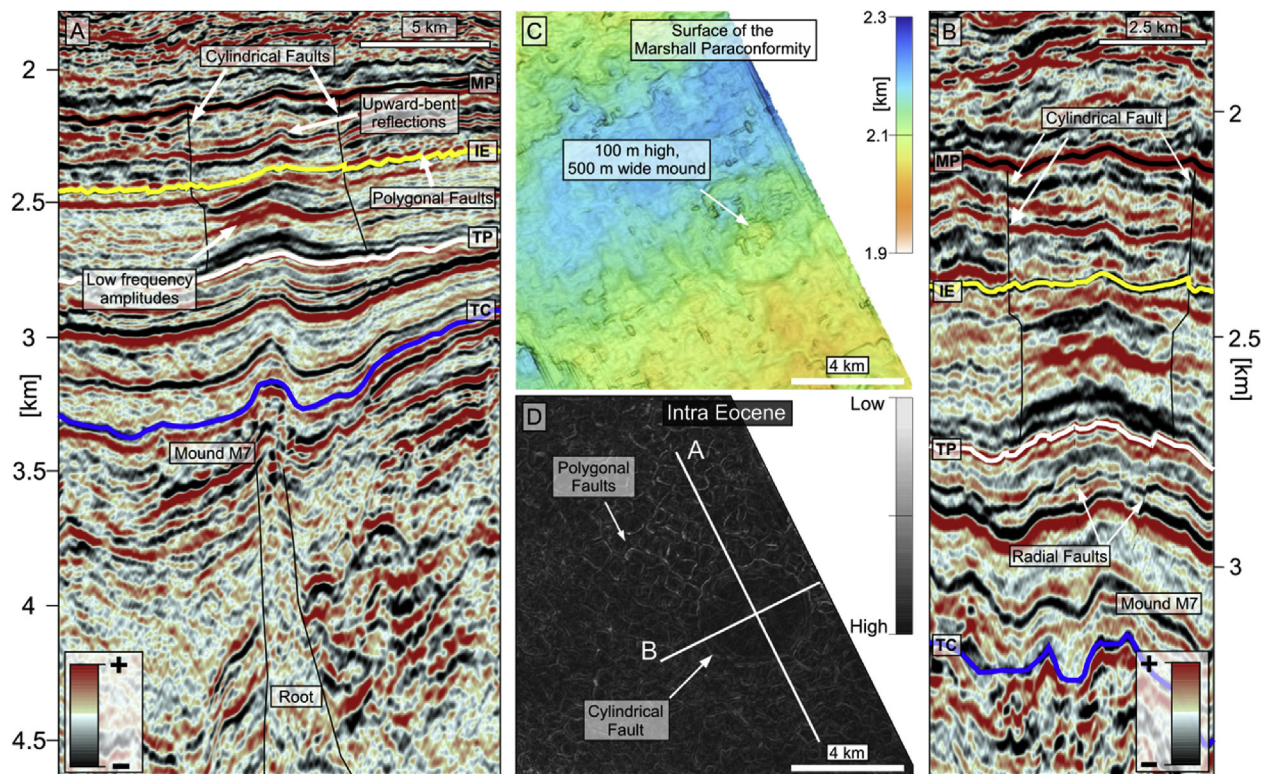


Fig. 6. Map view and seismic cross-sections of the cylindrical feature. **A/B)** Seismic inline and crossline through the cylindrical faults. Low-frequency amplitude anomalies appear in lower Eocene strata below the polygonal faulted tier-1. Cylindrical faults form in the upper Eocene polygonal faulted tier-1. **C)** Depth map of the Marshall Paraconformity (MP-black horizon in A and B). **D)** The similarity attribute extracted along the Intra Eocene (IE-yellow) horizon shown in (A) and (B). Light colours indicate low similarity values and are therefore indicative of discontinuities. (For interpretation of the references to colour in this figure legend, the reader is referred to the Web version of this article.)

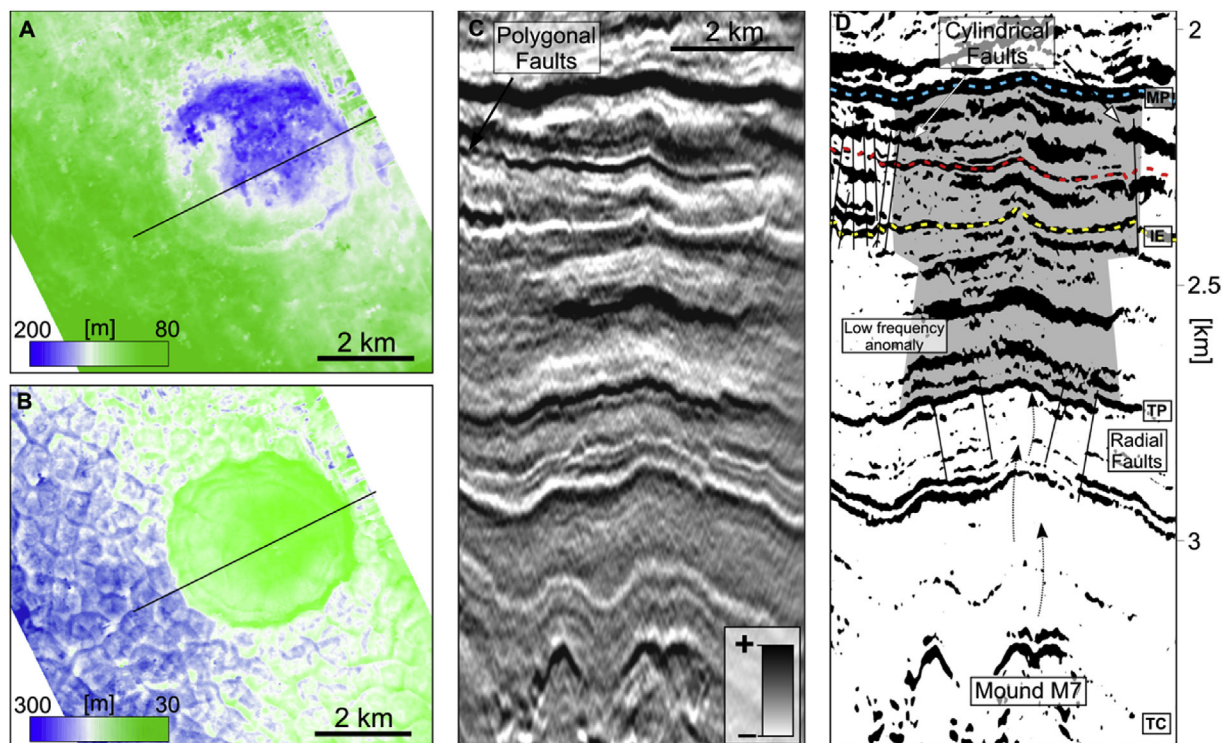


Fig. 7. **A)** Layer thickness between turquoise and red horizons in D. **B)** Layer thickness between red and yellow horizons in D. **C)** Seismic crossline through the cylindrical anomaly, with interpretation in D. **D)** Black and white image of the energy envelope. Gray shaded area shows a cylindrical feature with cylindrical faults in the upper Eocene tier-1 of polygonal faults and low frequency amplitude anomalies below. Radial faults spread out below the cylindrical feature, and above Mound M7. MP-Marshall Paraconformity (blue), IE-Intra Eocene (green), TP-Top Paleocene, TC-Top Cretaceous. (For interpretation of the references to colour in this figure legend, the reader is referred to the Web version of this article.)

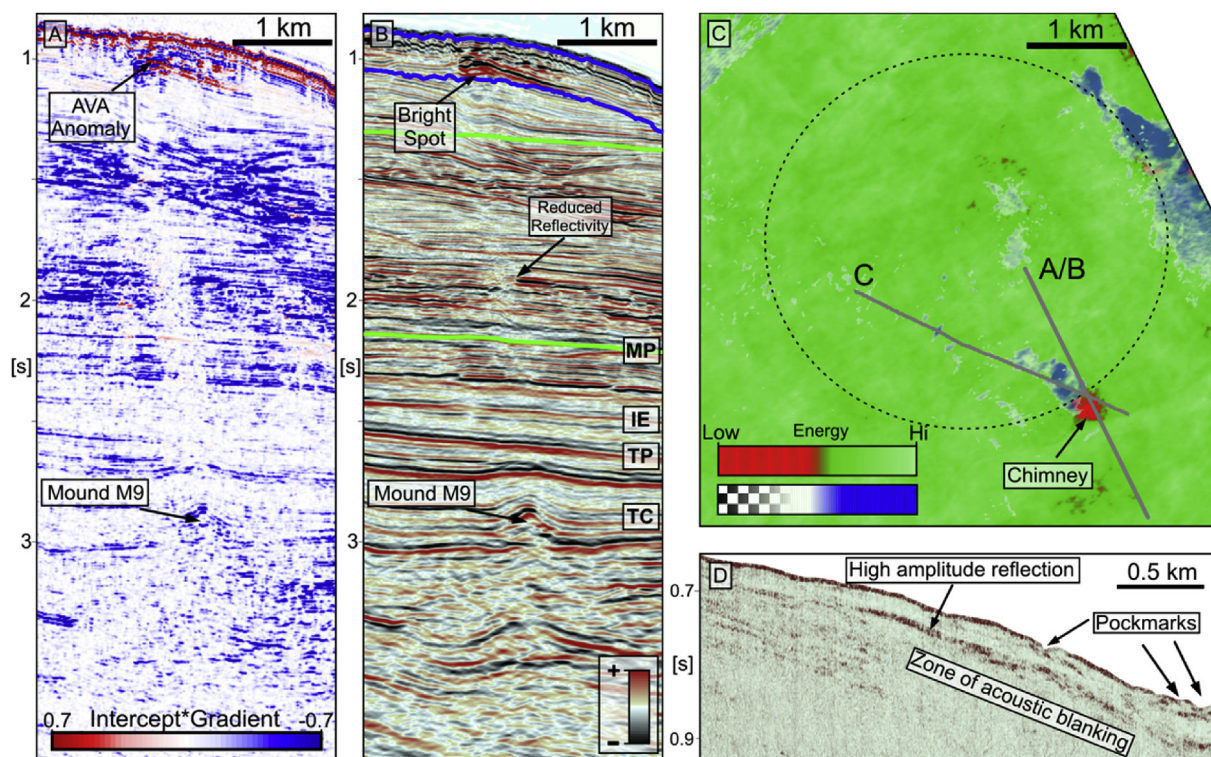


Fig. 8. A) AVA-Product (Intercept x Gradient) of the seismic section in B. Shallow bright spots show a distinct AVA anomaly with a subvertical zone of low AVA-Products connecting the bright spot to Mound M9. B) Seismic section showing the bright spot and slightly reduced reflectivity below. D) Map view around bright spots. Blue colours indicate high bulk energy in the uppermost 100 m beneath the seafloor (between blue horizons in B). Red/Green colours represent high/low bulk energy summations (respectively) between the green horizons. The dashed line indicates the location of cylindrical faults deeper beneath Mound M9. C) High-resolution boomer seismic data across the bright spot shown in (A) and (B). A high amplitude reflection and an acoustically transparent zone below are visible. (For interpretation of the references to colour in this figure legend, the reader is referred to the Web version of this article.)

surrounding (Fig. 7A and B) suggest remobilisation and removal of sediment from the deeper sequence and intrusion of the sediment into the shallower sequence.

The source of the deposited sediments above Mound M7 is difficult to assess and could be from either the Cretaceous stratigraphic level beneath Mound M7 or partly from younger stratigraphic levels (Fig. 7A and B). The fluids and overpressure necessary to transport the solid phase in sedimentary volcanoes in general, similarly can be sourced from different stratigraphic levels (Planke et al., 2003). With the Barque prospect in close proximity and in a proven petroleum system (Sahoo et al., 2015), overpressure generation and fluid availability to feed a sedimentary volcano seem likely and we therefore interpret the cylinder to have formed in response to upward migrating fluids and sediments.

6.2. Cylindrical and radial faults

Curved and listric faults are not uncommon in polygonal fault systems. Cartwright (2011) suggested a lithological effect on fault curvature and noted that biosiliceous tiers tend most often to create listric faults. Circular patterns (in planview) within polygonal faulted tiers have been reported above and around morphological depressions such as pockmarks (Ho et al., 2018b, 2013; Morgan et al., 2015). Concentric extensional faults are described in the literature in various geological settings, e.g., around collapsing salt diapirs (Stewart, 2006), in glaciers (Malthe-Sørensen et al., 1999), volcanic and mining-related settings (Branney, 1995) and in polygonal fault systems developing due to an anisotropic stress field above buried pockmarks (Ho et al., 2013; Morgan et al., 2015). Concentric reverse fault patterns have only rarely been described since they pose a “space problem”; they have been described in the literature around rapid and forceful intrusions (Galland

et al., 2009; Quatrehomme and İşcan, 1998).

Concentric normal fault patterns associated with fluid flow have previously been reported around mud volcanoes in Azerbaijan (Davies and Stewart, 2005; Planke et al., 2003). While Planke et al. (2003) describe a circular subsidence fault pattern with a radial distance of about 100 m dipping towards the centre, Davies and Stewart (2005) report on concentric faults similar to the ones observed here in the polygonal fault system dipping away from the central feeder system over distances of several kilometres. They attribute their existence to shear stress at the base of the mud volcano due to lateral compaction of the edifice muds. We don't observe a large mud volcanic edifice and the cylindrical faults are confined to the polygonal fault system. This suggests a compactional origin due to differential compaction and dewatering mechanisms within tier-1 rather than shear stress-related mechanisms.

Gay et al. (2012) imaged a cone-shaped amplitude anomaly around a fluid conduit in seismic data and inferred, through sandbox models, that it represents a zone of sediment deformation by upward migrating fluids. This would imply a different stress field within the cylinder that surrounds the pipe, which would affect pore pressure and therefore sediment compaction. We assume the strong low-frequency reflections beneath the Intra Eocene horizon (Fig. 6) to be fluids expelled by the sediment volcano feeder system which accumulated beneath the low permeability tier-1 containing the polygonal faults. This cylindrical accumulation could be the reason for an axisymmetrical stress field within the cylinder in the upper Eocene tier-1, rather than a conical shaped anomaly like that described by Gay et al. (2004).

While concentric faults are mainly associated with subsidence, radial faults generally occur in regions of doming (Hansen et al., 2005; Stewart, 2006). We assume the radial fault patterns we observe (Fig. 5) to result from an anisotropic stress field induced by Cretaceous

sediment intrusions into Paleocene sediments. This is mainly indicated by onlapping reflectors onto the seismically chaotic mounded structures (Fig. 5). Hansen et al. (2005) described similar buried mounded structures with radial fault patterns within an overlying polygonal fault system in the Vøring Basin on the Norwegian continental shelf. Due to the similar seismic expression, the same aspect ratios, and the analogous influence on the surrounding polygonal fault system to what Hansen et al. (2005) described, we assume a similar formation mechanism by intruding sediments and a resulting anisotropic stress field surrounding the mounds.

6.3. Lack of polygonal faults within the cylindrical feature

It is intriguing that although the upper Eocene polygonal fault system extends over the entire basin, no polygonal faults have formed within a ~2 km radial distance of the central fluid conduit around Mound M7. Horizontal, continuous and mainly undisturbed reflections within the cylindrical structure suggest that polygonal faults never nucleated within this body (i.e., ruling out a reworking, overprinting or healing of faults in this zone).

Despite two decades of research on polygonal fault nucleation and development the processes leading to shear failure are still widely debated and mechanisms like density inversion (Henriet et al., 1991; Watterson et al., 2000), overpressure collapse (Cartwright, 1994b), volumetric contraction (Cartwright and Lonergan, 1996), syneresis (Cartwright and Dewhurst, 1998; Dewhurst et al., 1999), low coefficient of friction (Gouly, 2001), particle scale contraction (Shin et al., 2008) or diagenetically induced shear failure (Cartwright, 2011) have been proposed. Since all mechanisms include sediment compaction and episodic fluid expulsion of very-fine to fine-grained tiers, a local difference in sediment composition (i.e. grain size) or burial history (compaction) could be invoked to explain the absence of polygonal fault nucleation within this cylinder. We cannot envisage any feasible geological process that would result in a local, cylinder-shaped change in depositional lithology or burial history. Compaction, however, can also be influenced by local pore fluid pressure and sediment composition could have changed by remobilisation and intruding sediments.

The differential stress field that would be expected within the cylindrical feature (discussed in Section 6.2 with respect to the study of Gay et al. (2012)) could have had important implications for pore fluid pressure and sediment compaction, thereby influencing polygonal fault development. Over-pressured fluids migrating upwards through the plumbing system of the sediment volcano could have introduced increased pore fluid pressure around the feeder system. This would reduce the effective stress of the sediment and therefore effect compaction, contraction and diagenesis of the material. Since these are the main driving forces for all polygonal fault formation mechanisms described in the literature, it seems likely that a local change in compaction history and effective stress could affect polygonal fault nucleation. In this case, we interpret that the cylindrical pattern surrounding the fluid pipe would mark the radial limits of where a pipe-induced increase in pore pressure was no longer strong enough to prevent polygonal faults from propagating which could explain the perfectly circular planform.

Alternatively, a change in lithology due to intruding coarser grained material e.g. intruding sandy sediments into the fine-grained sedimentary sequences is known to prevent polygonal faults from nucleating (Cartwright, 2011; Cartwright et al., 2003). Sand intrusions often exhibit conical and saucer shaped geometries, especially when intruding pervasive polygonal fault systems (Bureau et al., 2013; Hurst et al., 2003; Monnier et al., 2014; Shoulders et al., 2007) and are mainly characterised by high amplitude anomalies, a highly disrupted top and base and often chaotic internal reflections (Bureau et al., 2013; Hurst et al., 2003; Hurst and Cartwright, 2005). Although we do not observe these characteristics, it is possible that thin (sub-seismic scale) permeable stringers (i.e. sand injectites) could intrude the surrounding of the

sediment volcano feeder pipe. Such permeable stringers would enable dewatering of their host strata. In the upper Eocene polygonal faulted tier-1 localized dewatering in this way could prevent polygonal fault nucleation. Fig. 7 clearly indicates remobilisation and intrusion of sediments into this tier. An increased volume of coarser grained material intruding tier-1 could have also changed the bulk lithology to a degree that it was no longer prone to polygonal fault formation.

The higher amplitudes and lower frequency of strata within the cylinder below polygonal fault tier-1 (Fig. 6A and B) indicate a change in physical properties within this zone. We interpret this as being due to the presence of some amount of free gas within the cylinder, which would contribute to both an increase in amplitude and a decrease in frequency. Again, thin gas charged sand stringers might cause the low-frequency, high amplitude reflections in the cylinder below tier-1 (Fig. 6). Since the anomalous high-amplitude reflections cannot be directly correlated to horizons surrounding the cylinder we assume accumulation of some amount of free gas below the polygonal fault tier-1 and horizontal radial migration.

Within the tier-1 horizons are slightly offset by polygonal and cylindrical faults but can often be traced throughout the 3-D survey and through the cylinder. This indicates deposition of sediments within the cylinder was contemporaneous to its surrounding and prior to vertically migrating sediments and fluids.

6.4. Recent fluid migration

Although a distinct low-velocity zone around the bright spots is not obvious, the amplitude reversal, the acoustic curtain and especially the connection to deeper strata and the distinct class 3 AVA anomaly suggest that the shallow bright spots represent free gas (Fig. 8).

The 300-m-wide near-vertical zone of reduced AVA attribute connects the shallow gas to Mound M9 at about 3 s TWT (Fig. 8A). We do not interpret the blanked-out zone to be an imaging artefact (e.g., the high reflection coefficient of shallow gas causing a zone of “acoustic turbidity” or a “seismic curtain” beneath) since it is not vertically aligned beneath the shallow gas but is rather offset slightly basinward (Fig. 8B). Importantly, we note that the blanked-out zone is also visible in far angle stacks (32–41°) where the shallow gas can be under-shot to avoid any vertical imaging artefacts (Supplement 1). We, therefore, interpret the feature to be a geological conduit (or “chimney”) that focuses fluid flow. Mound M9 appears to be the root of the chimney. Since Mound M9 shows no distinct differences to adjacent mounds at depth we assume that it must have recently reactivated to create the chimney. The migrated seismic section shows mainly continuous reflections with no indications of sediment modification or deformation in or around the chimney, at the resolution of these data (Fig. 8B). The presented data therefore suggest that active sediment remobilisation of Cretaceous sediment eased during the Paleocene below Mound M9. Paleocene to Eocene strata in this area mainly consists of fine-grained material with high porosities but low permeabilities (Blanke, 2015). Since no faults are visible, we assume capillary invasion by gas and small-scale fracturing (sub-seismic scale) to be the most likely process for chimney formation.

6.5. Timing of fluid migration

Polygonal faults, in general, form during the early burial history of their host sediments (Cartwright et al., 2007; Cartwright and Dewhurst, 1998; Chenrai and Huuse, 2017). Pockmark formation above polygonal fault systems due to porewater expulsion and sediment compaction would therefore be expected to be contemporaneous with the faulting (Berndt et al., 2003; Gay et al., 2004; Gay and Berndt, 2007; Gouly, 2008). In some cases, pipes or chimneys form within or above polygonal fault systems, channelling and episodically releasing fluids to form pockmarks (Berndt et al., 2003; Gay and Berndt, 2007; Ho et al., 2018a). In these cases pockmarks can also form asynchronous to

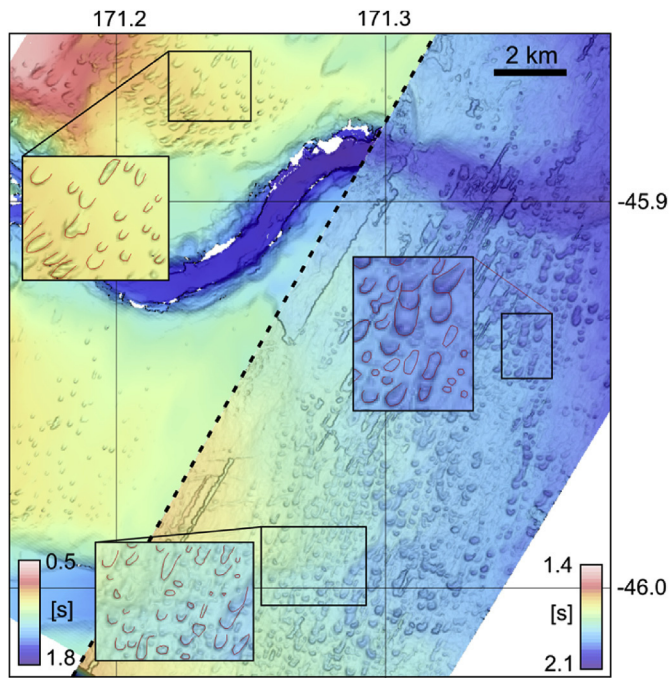


Fig. 9. Comparison between present-day seafloor pockmarks (left of dotted line) and buried pockmarks (right of dotted line) both, mapped in the Waka 3D dataset at different stratigraphic levels but in close spatial proximity.

polygonal faults. However, no such pipes are observed above or within the tiers of polygonal faulting in this dataset. Although there seem to be several types of interaction between polygonal fault and pockmark formation, the location and extension of polygonal faults beneath and up to the Marshall Paraconformity suggests nucleation and growth prior to or during the formation of the Marshall Paraconformity.

Hillman et al. (2018) reported on the modification of present-day seafloor depressions by submarine currents on the Canterbury slope. Due to their analogous expression in shape and size and their spatial proximity (Fig. 9) we assume similar currents to be responsible for the northward facing elongated shape of the buried pockmarks in this study. Higher amplitudes in the seafloor craters are probably due to the removal of fine-grained material by seeping fluids leaving only coarse-grained highly reflective material or due to authigenic carbonate precipitation.

Our results show that Cretaceous sediment intrusions push up the lower Paleocene strata, creating mounded structures. Onlapping strata indicate a mid-Paleocene age of formation for most of the intrusions. Only Mound M7 seems to deflect Eocene and Oligocene sediments, indicating a later stage of formation.

The lack of any seismic evidence of fluid flow above the Marshall Paraconformity in the vicinity of anomalous Mound M7 suggests that fluid flow activity associated with Mound M7 has not occurred during the Neogene. In contrast, our results suggest relatively recent activity in the chimney above Mound M9. We assume that the feeder system beneath Mound M7 was sealed off and that the overpressured Cretaceous sequences beneath the level of the mounds switched to Mound M9, resulting in the establishment of a new chimney system (Fig. 10).

The radial and polygonal faults in the Paleocene tier-3 probably formed during or shortly after the up-doming of Cretaceous mud-pillows and laccoliths, as also suggested by Hansen et al. (2005). The polygonal and cylindrical faults in the upper Eocene tier-1 suggest that fluid actively migrated and altered the stress field during polygonal fault nucleation. This suggests that the sediment volcano formed prior to or simultaneously with the polygonal faults. Since polygonal faults, in general, form during the early burial history of their host and the mud volcano edifice forms on the upper boundary of the polygonal

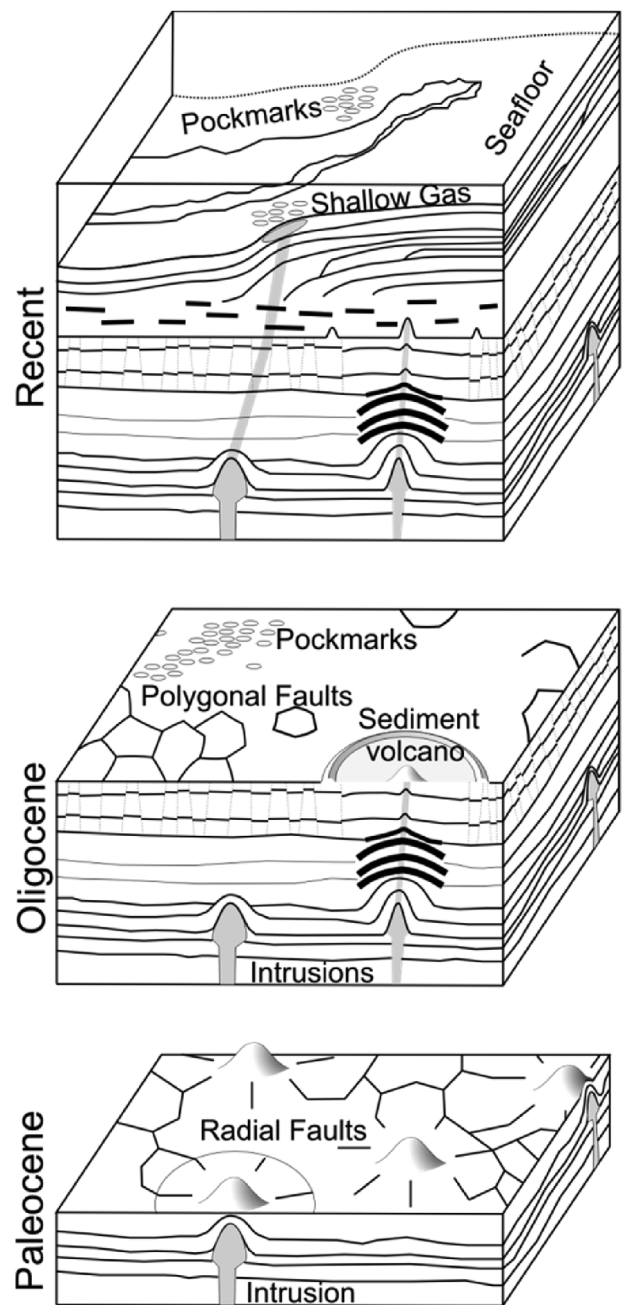


Fig. 10. Schematic summary of mud and fluid migration in the Canterbury Basin. Paleocene mud intrusions are followed by Oligocene Mud volcanism and polygonal faults. Recent fluid migration from a reactivated sediment intrusion reaches all the way to the present-day seafloor.

faults (Marshall Paraconformity) a simultaneous formation seems likely.

7. Conclusions

Three fluid migration events imaged in the seismic data point to the existence of recent and past sediment migration and gas emissions in the Canterbury Basin, originating from Cretaceous sediments. Due to the difference in timing, the events show very different structural effects on the overburden sediment.

Shallow gas, manifesting itself in bright spots in the seismic data, represents a recent focused fluid migration event sourced from the same stratigraphic level as the sediment volcano. Due to the more lithified

sediments at this stage, overburden sediment appears to be less deformed by the migrating fluids compared to the conduit feeding the sediment volcano.

Cretaceous intrusions into Paleocene strata indicate widespread sediment remobilisation in the Canterbury Basin during the Paleocene. We have imaged the plumbing system of an ancient sediment volcano that expelled material onto the surface of the Marshall Paraconformity. Reduced sediment thicknesses around the feeder system indicate that the Paleocene/Eocene sediment that hosts the plumbing system probably provided additional material that ascended and was intruded back into other (shallower) sedimentary formations. The sediment volcano plumbing system likely formed prior to or simultaneously with the upper Eocene polygonal fault system. Pockmarks on the same buried surface where sediments were extruded indicate additional fluid expulsion from another source, potentially the polygonal fault system. Present day seafloor depressions as well as buried pockmarks could not be related to any hydrocarbon seepage and should therefore not be used as hydrocarbon proxies in this case.

The lack of polygonal faults within a cylindrical feature around the fluid conduit (over a radial distance of 2 km) is a striking observation which could be explained by different processes;

- 1) increased pore pressure and decreased effective stress around the sediment volcano feeder pipe resulted in a different compaction history compared to the surrounding strata.
- 2) permeable, thin (sub-seismic scale) stringers were intruded into the fine grained material of polygonal fault tier-1. These permeable stringers supported dewatering of the tier-1 and therefore changed the compaction history.
- 3) remobilised coarser grained material extruded outward from the feeder pipe and changed the lithology within a cylindrical area sufficiently to prevent polygonal fault nucleation.

Declarations of interest

None.

Acknowledgements

We gratefully acknowledge New Zealand Oil and Gas (NZOG), in particular Bernice Herd, for the provision of seismic data and their ongoing efforts, comments and contributions. We thank Patrice Imbert (Total) and Marzia Rovere (ISMAR) for their thorough reviews which significantly improved this paper. We additionally thank Anadarko NZ Ltd, Origin Energy, and the National Institute of Water and Atmospheric Research (NIWA) for the provision of data used during this research. This study was funded by New Zealand's Ministry of Business, Innovation and Employment (MBIE) as part of the GNS Science-led programme "Understanding petroleum source rocks, fluids, and plumbing systems in New Zealand basins: a critical basis for future oil and gas discoveries" (Contract C05X1507). Thanks also to the crew of the RV *Polaris II* for their help and support during data acquisition. Seismic processing and analysis were undertaken through academic licences for GLOBE Claritas, CGG's HampsonRussell and IHS Markit's Kingdom software. Jasper Hoffmann is supported by a University of Otago PhD scholarship.

Appendix A. Supplementary data

Supplementary data to this article can be found online at <https://doi.org/10.1016/j.marpetgeo.2019.06.025>.

References

Anka, Z., Berndt, C., Gay, A., 2012. Hydrocarbon leakage through focused fluid flow systems in continental margins. *Mar. Geol.* 334, 1–3. <https://doi.org/10.1016/j.marpetgeo.2012.10.012>.

- Berndt, C., 2005. Focused fluid flow in passive continental margins. *Philos. Trans. A Math. Phys. Eng. Sci.* 363, 2855–2871. <https://doi.org/10.1098/rsta.2005.1666>.
- Berndt, C., Bünn, S., Mienert, J., 2003. Polygonal fault systems on the mid-Norwegian margin: a long-term source for fluid flow. *Subsurf. Sediment Mobil. Geol. Soc. Lond. Spec. Publ.* 216, 283–290. <https://doi.org/10.1144/GSL.SP.2003.216.01.18>.
- Bialas, J., Klauke, L., Mögeltönder, J., 2013. RV SONNE Fahrtbericht/Cruise Report SO226-CHIRMP CHatham Rise Methane Pockmarks. 07.01–06.02. 2013/Auckland–Lyttelton, 07.02.–01.03. 2013/Lyttelton–Wellington.
- Blanke, S.J., 2015. Caravel-1: lessons learned in the deepwater Canterbury basin. In: International Conference and Exhibition, Melbourne, Australia 13–16 September 2015. Society of Exploration Geophysicists and American Association of Petroleum Geologists, pp. 519.
- Branney, M.J., 1995. Downsag and extension at calderas: new perspectives on collapse geometries from ice-melt, mining, and volcanic subsidence. *Bull. Volcanol.* 57, 303–318. <https://doi.org/10.1007/BF00301290>.
- Bureau, D., Mourgues, R., Cartwright, J.A., Foschi, M., Abdelmalak, M.M., 2013. Characterisation of interactions between a pre-existing polygonal fault system and sandstone intrusions and the determination of paleo-stresses in the Faroe-Shetland basin. *J. Struct. Geol.* 46, 186–199. <https://doi.org/10.1016/j.jsg.2012.09.003>.
- Carter, L., Carter, R.M., Nelson, C.S., Fulthorpe, C.S., Neil, H.L., 1990. Evolution of pliocene to recent abyssal sediment waves on bounty channel levees, New Zealand. *Mar. Geol.* 95, 97–109. [https://doi.org/10.1016/0025-3227\(90\)90043-J](https://doi.org/10.1016/0025-3227(90)90043-J).
- Carter, R.M., 1988. Post-breakup stratigraphy of the kaikoura synthem (cretaceous-cenozoic), continental margin, southeastern New Zealand. *N. Z. J. Geol. Geophys.* 31, 405–429. <https://doi.org/10.1080/00288306.1988.10422141>.
- Carter, R.M., 1985. The mid-oligocene Marshall paraconformity, New Zealand: coincidence with global eustatic sea-level fall or rise? *J. Geol.* 93, 359–371.
- Carter, R.M., Norris, R.J., 1976. Cainozoic history of southern New Zealand: an accord between geological observations and plate-tectonic predictions. *Earth Planet. Sci. Lett.* 31, 85–94. [https://doi.org/10.1016/0012-821X\(76\)90099-6](https://doi.org/10.1016/0012-821X(76)90099-6).
- Cartwright, J.A., 2011. Diagenetically induced shear failure of fine-grained sediments and the development of polygonal fault systems. *Mar. Pet. Geol.* 28, 1593–1610. <https://doi.org/10.1016/j.marpetgeo.2011.06.004>.
- Cartwright, J.A., 1994a. Episodic basin-wide fluid expulsion from geopressed sahle sequences in the North sea basin. *Geology* 22 (5), 447–450.
- Cartwright, J.A., 1994b. Episodic basin-wide hydrofracturing of overpressured early cenozoic mudrock sequences in the north sea basin. *Mar. Pet. Geol.* 11, 587–607. [https://doi.org/10.1016/0264-8172\(94\)90070-1](https://doi.org/10.1016/0264-8172(94)90070-1).
- Cartwright, J.A., Dewhurst, D.N., 1998. Layer-bound compaction faults in fine-grained sediments. *Geol. Soc. Am. Bull.* 110, 1242–1257.
- Cartwright, J.A., Huuse, M., Aplin, A., 2007. Seal bypass systems. *Am. Assoc. Pet. Geol. Bull.* 91, 1141–1166. <https://doi.org/10.1306/04090705181>.
- Cartwright, J.A., James, D., Bolton, A., 2003. The genesis of polygonal fault systems: a review. *Geol. Soc. Lond. Spec. Publ.* 216, 223–243.
- Cartwright, J.A., Lonergan, L., 1996. Volumetric contraction during the compaction of mudrocks: a mechanism for the development of regional-scale polygonal fault systems. *Basin Res.* 8, 183–193. <https://doi.org/10.1046/j.1365-2117.1996.01536.x>.
- Castagna, J.P., Backus, M.M., 1993. Offset-dependent Reflectivity—Theory and Practice of AVO Analysis. Society of Exploration Geophysicists.
- Chenrai, P., Huuse, M., 2017. Pockmark formation by porewater expulsion during rapid progradation in the offshore Taranaki Basin, New Zealand. *Mar. Pet. Geol.* 82, 399–413. <https://doi.org/10.1016/j.marpetgeo.2017.02.017>.
- Coombs, D.S., Cas, R.A., Kawachi, Y., Landis, C.A., McDonough, W.F., Reay, A., 1986. Cenozoic volcanism in north, east and central Otago. *R. Soc. N. Z. Bull.* 23, 278–312.
- Crutchley, G.J., Maslen, G., Pecher, I.A., Mountjoy, J.J., 2016. High-resolution seismic velocity analysis as a tool for exploring gas hydrate systems: an example from New Zealand's southern Hikurangi margin. *Interpretation* 4, 1–12.
- Davies, R.J., Stewart, S.A., 2005. Emplacement of giant mud volcanoes in the South Caspian Basin: 3D seismic reflection imaging of their root zones. *J. Geol. Soc. Lond.* 162, 1–4.
- Davy, B., Pecher, I., Wood, R., Carter, L., Gohl, K., 2010. Gas escape features off New Zealand: evidence of massive release of methane from hydrates. *Geophys. Res. Lett.* 37, 1–5. <https://doi.org/10.1029/2010GL045184>.
- Dewhurst, D.N., Cartwright, J.A., Lonergan, L., 1999. The development of polygonal fault systems by syneresis of colloidal sediments. *Mar. Pet. Geol.* 16, 793–810. [https://doi.org/10.1016/S0264-8172\(99\)00035-5](https://doi.org/10.1016/S0264-8172(99)00035-5).
- Dimitrov, L.I., 2002. Mud volcanoes—the most important pathway for degassing deeply buried sediments. *Earth Sci. Rev.* 59, 49–76.
- Dunbar, C.O., Rodgers, J., 1957. *Principles of Stratigraphy*.
- Etiopie, G., Martinelli, G., 2009. "Pieve Santo Stefano" is not a mud volcano: comment on "Structural controls on a carbon dioxide-driven mud volcano field in the Northern Apennines" (by Bonini, 2009). *J. Struct. Geol.* 31, 1270–1271. <https://doi.org/10.1016/j.jsg.2009.06.009>.
- Field, B.D., Browne, G.H., Davy, B.W., 1989. Cretaceous and Cenozoic sedimentary basins and geological evolution of the Canterbury region, South Island, New Zealand. *N. Z. Geol. Survey* 2, 1–94.
- Fleming, C.A., 1962. New Zealand biogeography: a paleontologist's approach. *Timaru Her. Print* 10, 54–107.
- Fulthorpe, C.S., Carter, R.M., 1989. Test of seismic sequence methodology on a Southern Hemisphere passive margin: the Canterbury Basin, New Zealand. *Mar. Pet. Geol.* 6, 348–359. [https://doi.org/10.1016/0264-8172\(89\)90031-7](https://doi.org/10.1016/0264-8172(89)90031-7).
- Fulthorpe, C.S., Hoyanagi, K., Blum, P., Guérin, G., Slagle, A.L., Blair, S.A., Browne, G.H., Carter, R.M., Ciobanu, M.C., Claypool, G.E., Crundwell, M.P., Dinarès-Turell, J., Ding, X., George, S.C., Hepp, D.A., Jaeger, J., Kawagata, S., Kemp, D.B., Kim, Y.G., Kominz, M.A., Lever, H., Lipp, J.S., Marsaglia, K.M., McHugh, C.M., Murakoshi, N., Ohi, T.,

- Pea, L., Richaud, M., Suto, I., Tanabe, S., Tinto, K.J., Uramoto, G., Yoshimura, T., 2010. Integrated ocean drilling program expedition 317 preliminary report canterbury basin sea level global and local controls on continental margin stratigraphy. *Integr. Ocean Drill. Progr. Prelim. Rep.* 1–133. <https://doi.org/10.2204/ioldp.pr.317.2010>.
- Galland, O., Planke, S., Neumann, E.R., Malthé-Sørenssen, A., 2009. Experimental modelling of shallow magma emplacement: application to saucer-shaped intrusions. *Earth Planet. Sci. Lett.* 277, 373–383. <https://doi.org/10.1016/j.epsl.2008.11.003>.
- Gay, A., Berndt, C., 2007. Cessation/reactivation of polygonal faulting and effects on fluid flow in the Vøring Basin, Norwegian Margin. *J. Geol. Soc. Lond.* 164, 129–141.
- Gay, A., Lopez, M., Cochonat, P., Sermondadaz, G., 2004. Polygonal faults-furrows system related to early stages of compaction-Upper Miocene to present sediments of the Lower Congo Basin. *Basin Res.* 16, 101–116. <https://doi.org/10.1111/j.1365-2117.2003.00224.x>.
- Gay, A., Mourgues, R., Berndt, C., Bureau, D., Planke, S., Laurent, D., Gautier, S., Lauer, C., Loggia, D., 2012. Anatomy of a fluid pipe in the Norway Basin: initiation, propagation and 3D shape. *Mar. Geol.* 332–334, 75–88. <https://doi.org/10.1016/j.margeo.2012.08.010>.
- Goult, N.R., 2008. Geomechanics of polygonal fault systems: a review. *Pet. Geosci.* 14, 389–397. <https://doi.org/10.1144/1354-079308-781>.
- Goult, N.R., 2001. Mechanics of layer-bound polygonal faulting in fine-grained sediments. *J. Geol. Soc. Lond.* 159, 239–246.
- Hansen, J.P.V., Cartwright, J.A., Huuse, M., Clausen, O.R., 2005. 3D seismic expression of fluid migration and mud remobilization on the Gjallar Ridge, offshore mid-Norway. *Basin Res.* 17, 123–139. <https://doi.org/10.1111/j.1365-2117.2005.00257.x>.
- Henriet, J.P., De Batist, M., Verschuren, M., 1991. Early fracturing of Palaeogene clays, southernmost North Sea: relevance to mechanisms of primary hydrocarbon migration. *Gener. Accumul. Prod. Eur. Hydrocarb.* 1, 217–227.
- Hillman, J.I.T., Gorman, A.R., Pecher, I.A., 2015. Geostatistical analysis of seafloor depressions on the southeast margin of New Zealand's South Island - investigating the impact of dynamic near seafloor processes on geomorphology. *Mar. Geol.* 360, 70–83. <https://doi.org/10.1016/j.margeo.2014.11.016>.
- Hillman, J.I.T., Klauke, I., Pecher, I.A., Gorman, A.R., Schneider von Deimling, J., Bialas, J., 2018. The influence of submarine currents associated with the Subtropical Front upon seafloor depression morphologies on the eastern passive margin of south island, New Zealand. *N. Z. J. Geol. Geophys.* 0, 1–14. <https://doi.org/10.1080/00288306.2018.1434801>.
- Ho, S., Carruthers, D., Imbert, P., 2016. Insights into the permeability of polygonal faults from their intersection geometries with Linear Chimneys: a case study from the Lower Congo Basin. *Carnets Géol.* 16 (2), 17–26 Madrid.
- Ho, S., Carruthers, D., Imbert, P., Cartwright, J., 2013. Spatial variations in geometries of polygonal faults due to stress perturbations & interplay with fluid venting features. In: 75th EAGE Conf. Exhib. London, <https://doi.org/10.3997/2214-4609.20131054>.
- Ho, S., Hovland, M., Blouet, J., Wetzel, A., Imbert, P., Carruthers, D., 2018a. Formation of linear planform chimneys controlled by preferential hydrocarbon leakage and anisotropic stresses in faulted fine-grained sediments, offshore Angola. *Solid Earth* 9, 1437–1468. <https://doi.org/10.5194/se-9-1437-2018>.
- Ho, S., Imbert, P., Hovland, M., Wetzel, A., Philippe, J., Daniel, B., 2018b. Downslope-shifting pockmarks: interplay between hydrocarbon leakage, sedimentation, currents and slope's topography. *Int. J. Earth Sci.* 107, 2907–2929. <https://doi.org/10.1007/s00531-018-1635-5>.
- Hovland, M., Svensen, H., Forsberg, C.F., Johansen, H., Fichler, C., Fosså, J.H., Jonsson, R., Rueslåtten, H., 2005. Complex pockmarks with carbonate-ridges off mid-Norway: products of sediment degassing. *Mar. Geol.* 218, 191–206. <https://doi.org/10.1016/j.margeo.2005.04.005>.
- Hurst, A., Cartwright, J.A., 2005. Sand injectites: an emerging global play in deep-water clastic environments. In: *Petroleum Geology: North-West Europe and Global Perspectives—Proceedings of the 6th Petroleum Geology Conference*, pp. 133–144. <https://doi.org/10.1144/0060133>.
- Hurst, A., Cartwright, J.A., Huuse, M., Jonk, R., Schwab, A., Duranti, D., Cronin, B., 2003. Significance of large-scale sand injectites as long-term fluid conduits: evidence from seismic data. *Geofluids* 3, 263–274. <https://doi.org/10.1046/j.1468-8123.2003.00066.x>.
- Hustoft, S., Bünnz, S., Mienert, J., 2010. Three-dimensional seismic analysis of the morphology and spatial distribution of chimneys beneath the Nyegga pockmark field, offshore mid-Norway. *Basin Res.* 22, 465–480. <https://doi.org/10.1111/j.1365-2117.2010.00486.x>.
- Imbert, P., Ho, S., 2012. Seismic-scale funnel-shaped collapse features from the paleocene – Eocene of the north west shelf of Australia. *Mar. Geol.* 332–334, 198–221. <https://doi.org/10.1016/j.margeo.2012.10.010>.
- Karstens, J., Berndt, C., 2015. Seismic chimneys in the Southern Viking Graben – implications for palaeo fluid migration and overpressure evolution. *Earth Planet. Sci. Lett.* 412, 88–100. <https://doi.org/10.1016/j.epsl.2014.12.017>.
- King, L.H., MacLean, B., 1970. Pockmarks on the scotian shelf. *Geol. Soc. Am. Bull.* 81, 3141–3148.
- Leifer, I., Judd, A.G., 2002. Oceanic methane layers: the hydrocarbon seep bubble deposition hypothesis. *Terra Nova* 14, 417–424.
- Lewis, D.W., Belliss, S.E., 1984. Mid tertiary unconformities in the Waitaki subdivision, north Otago. *J. R. Soc. N. Z.* 14, 251–276. <https://doi.org/10.1080/03036758.1984.10426303>.
- Løseth, H., Wensaas, L., Arntsen, B., Hanken, N.M., Basire, C., Graue, K., 2011. 1000 M long gas blow-out pipes. *Mar. Pet. Geol.* 28, 1040–1060. <https://doi.org/10.1016/j.margeo.2010.10.001>.
- Malthé-Sørenssen, A., Walmann, T., Jamtveit, B., Feder, J., Jossang, T., 1999. Simulation and characterization of fracture patterns in glaciers. *J. Geophys. Res. Solid Earth* 104.
- Marfurt, K.J., Kirilin, R.L., Farmer, S.L., Bahorich, M.S., 1998. 3-D seismic attributes using a semblance-based coherency algorithm. *Geophysics* 63, 1150. <https://doi.org/10.1190/1.1444415>.
- Mazzini, A., Etiope, G., 2017. Mud volcanism: an updated review. *Earth Sci. Rev.* 168, 81–112. <https://doi.org/10.1016/j.earscirev.2017.03.001>.
- Mazzini, A., Svensen, H.H., Planke, S., Forsberg, C.F., Tjelta, T.I., 2016. Pockmarks and methanogenic carbonates above the giant Troll gas field in the Norwegian North Sea. *Mar. Geol.* 373, 26–38. <https://doi.org/10.1016/j.margeo.2015.12.012>.
- McGinnis, D.F., Greinert, J., Artemov, Y., Beaubien, S.E., Wüest, A., 2006. Fate of rising methane bubbles in stratified waters: how much methane reaches the atmosphere? *J. Geophys. Res. Ocean* 111, 1–15. <https://doi.org/10.1029/2005JC003183>.
- Milne, A.D., Simpson, C., Threadgold, P., 1975. Well completion report resolution, for BP, shell, total canterbury service limited. *N. Z. Geol. Surv Unpubl. Open-file Petrol Rep. No.* 648.
- Monnier, D., Imbert, P., Gay, A., Mourgues, R., Lopez, M., 2014. Review Pliocene Sand Injectites from a Submarine Lobe Fringe during Hydrocarbon Migration and Salt Diapirism: a Seismic Example from the Lower Congo Basin. pp. 1–19. <https://doi.org/10.1111/gf.12057>.
- Morgan, D.A., Cartwright, J.A., Imbert, P., 2015. Perturbation of polygonal fault propagation by buried pockmarks and the implications for the development of polygonal fault systems. *Mar. Pet. Geol.* 65, 157–171. <https://doi.org/10.1016/j.margeo.2015.03.024>.
- NZOG, 2018. *New Zealand Oil & Gas Ltd: Activities. Report 1–4*.
- Planke, S., Svensen, H., Hovland, M., Banks, D.A., Jamtveit, B., 2003. Mud and fluid migration in active mud volcanoes in Azerbaijan. *Geo Mar. Lett.* 23, 258–267. <https://doi.org/10.1007/s00367-003-0152-z>.
- Quatrehomme, G., İşcan, M.Y., 1998. Analysis of beveling in gunshot entrance wounds. *Forensic Sci. Int.* 93, 45–60. [https://doi.org/10.1016/S0379-0738\(98\)00030-9](https://doi.org/10.1016/S0379-0738(98)00030-9).
- Riboulot, V., Sultan, N., Imbert, P., Ker, S., 2016. Initiation of gas-hydrate pockmark in deep-water Nigeria: Geo-mechanical analysis and modelling. *Earth Planet. Sci. Lett.* 434, 252–263.
- Sahoo, T.R., Kroeger, K.F., Thrasher, G., Munday, S., Mingard, H., Cozens, N., Hill, M., 2015. Facies distribution and impact on petroleum migration in the Canterbury basin, New Zealand. *East Aust. Basins Symp. Publ. Proc.* 187–202. <https://doi.org/10.1190/ice2015-2148698>.
- Schneider von Deimling, J., Hoffmann, J.J.L., 2012. 12PL015 Cruise Report: Multibeam Mapping and Acoustic Water Column Imaging.
- Shin, H., Santamarina, C.J., Cartwright, J.A., 2008. Contraction-driven shear failure in compacting uncemented sediments. *Geology* 36, 931–934. <https://doi.org/10.1130/G24951A.1>.
- Shoulders, S.J., Cartwright, J.A., Huuse, M., 2007. Large-scale conical sandstone intrusions and polygonal fault systems in Tranche 6, Faroe-Shetland Basin. *Mar. Pet. Geol.* 24, 173–188. <https://doi.org/10.1016/j.margeo.2006.12.001>.
- Simm, R., Bacon, M., 2014. Seismic Amplitude an Interpreter's Handbook. <https://doi.org/10.1017/CBO9780511984501>.
- Stewart, S.A., 2006. Implications of passive salt diapir kinematics for reservoir segmentation by radial and concentric faults. *Mar. Pet. Geol.* 23, 843–853. <https://doi.org/10.1016/j.margeo.2006.04.001>.
- Stoppa, F., 2006. The Sirente crater, Italy: impact versus mud volcano origins. *Meteorit. Planet. Sci.* 41, 467–477. <https://doi.org/10.1111/j.1945-5100.2006.tb00474.x>.
- Strogen, D.P., Seebeck, H., Nicol, A., King, P.R., 2017. Two-phase cretaceous–paleocene rifting in the taranaki basin region, New Zealand; implications for gondwana breakup. *J. Geol. Soc. Lond.* 174, 929–946.
- Sultan, N., Marsset, B., Ker, S., Marsset, T., Voisset, M., Vernant, A.M., Bayon, G., Cauquil, E., Adamy, J., Colliat, J.L., Drapeau, D., 2010. Hydrate dissolution as a potential mechanism for pockmark formation in the Niger delta. *J. Geophys. Res.* 115. <https://doi.org/10.1029/2010JB007453>.
- van Loon, A.J.T., 2010. Sedimentary volcanoes: overview and implications for the definition of a volcano on Earth. *What is a volcano?* 470, 31.
- Verschuren, M., 1992. *An Integrated 3D Approach to Clay Tectonic Deformation and the Development of a New 3D Surface Modelling Method (Doctoral Dissertation)*.
- Watterson, J., Walsh, J., Nicol, A., Nell, P.A.R., Bretan, P.G., 2000. Geometry and origin of a polygonal fault system. *J. Geol. Soc. Lond.* 157, 151–162. <https://doi.org/10.1144/jgs.157.1.151>.

RESEARCH ARTICLE

10.1029/2019GC008825

Key Points:

- We present a new form of eyed pockmarks caused by shallow gas
- We establish acoustic indicators for submarine groundwater discharge associated with gas

Supporting Information:

- Supporting Information S1
- Table S1
- Figure S1

Correspondence to:

 J. J. L. Hoffmann,
jasper.hoffmann@otago.ac.nz

Citation:








Hoffmann, J. J. L., Schneider von Deimling, J., Schröder, J. F., Schmidt, M., Held, P., Crutchley, G. J., et al. (2020). Complex eyed pockmarks and submarine groundwater discharge revealed by acoustic data and sediment cores in Eckernförde Bay, SW Baltic Sea. *Geochemistry, Geophysics, Geosystems*, 21, e2019GC008825. <https://doi.org/10.1029/2019GC008825>

Received 13 NOV 2019

Accepted 19 MAR 2020

Accepted article online 26 MAR 2020

Complex Eyed Pockmarks and Submarine Groundwater Discharge Revealed by Acoustic Data and Sediment Cores in Eckernförde Bay, SW Baltic Sea

 J. J. L. Hoffmann¹ , J. Schneider von Deimling² , J. F. Schröder² , M. Schmidt³ , P. Held² , G. J. Crutchley³ , J. Scholten², and A. R. Gorman¹ 
¹Department of Geology, University of Otago, Dunedin, New Zealand, ²Institute of Geosciences, University of Kiel, Kiel, Germany, ³GEOMAR Helmholtz Centre for Ocean Research Kiel, Kiel, Germany

Abstract Submarine groundwater discharge into coastal areas is a common global phenomenon and is rapidly gaining scientific interest due to its influence on marine ecology, the coastal sedimentary environment, and its potential as a future freshwater resource. We conducted an integrated study of hydroacoustic surveys combined with geochemical pore water and water column investigations at a well-known groundwater seep site in Eckernförde Bay (Germany). We aim to better constrain the effects of shallow gas and submarine groundwater discharge on high-frequency multibeam backscatter data and to present acoustic indications for submarine groundwater discharge. Our high-quality hydroacoustic data reveal hitherto unknown internal structures within the pockmarks in Eckernförde Bay. Using precisely positioned sediment core samples, our hydroacoustic-geochemical approach can differentiate intrapockmark regimes that were formerly assigned to pockmarks of a different nature. We demonstrate that high-frequency multibeam data, in particular the backscatter signals, can be used to detect shallow free gas in areas of enhanced groundwater advection in muddy sediments. Intriguingly, our data reveal relatively small (typically <15 m across) pockmarks within the much larger, previously mapped pockmarks. The small pockmarks, which we refer to as “intrapockmarks,” have formed due to the localized ascent of gas and groundwater; they manifest themselves as a new type of “eyed” pockmarks, revealed by their acoustic backscatter pattern. Our data suggest that, in organic-rich muddy sediments, morphological lows combined with a strong multibeam backscatter signal can be indicative of free shallow gas and subsequent advective groundwater flow.

Plain Language Summary Groundwater that seeps out of the ocean floor is a common global phenomenon. Marine ecosystems are highly dependent on nutrient supply from land, and recent studies have suggested that groundwater seeping out of the seafloor supplies even more nutrients to the world's oceans than rivers do. Also, nearshore freshwater springs have been used as a source of drinking water for decades and large offshore groundwater reserves in continental shelves can potentially prevent future freshwater shortages. We use echo sounding methods to search for indications for submarine groundwater. The methods enable us to carry out detailed investigations of intriguing seafloor depressions (i.e., “pockmarks”). Our accurate measurements give new insights into the morphology and characterization of the Eckernförde Bay pockmarks and reveal a new type of pockmark that is related to seeping groundwater. In the muddy sediment of Eckernförde Bay, methane gas forms in the sediments due to microbial decomposition of biomass. In areas of enhanced groundwater advection, this methane gas is brought closer to the seafloor, where pockmarks form and where we can detect the gas with our sonar system. Given the abundant global distribution of muddy gaseous sediments, our findings have important implications for the future detection of offshore groundwater systems.

1. Introduction

Escalating water demand in coastal areas and the nature and dynamics of interconnected onshore and offshore aquifers have significantly increased scientific interest in submarine groundwater discharge (SGD) over recent decades. SGD often carries large amounts of nutrients into the sea with diverse implications for the coastal ecosystems and environments (Lecher et al., 2016; Moore, 2010). Cho et al. (2018)

estimated that the global nutrient flux into the oceans through SGD even exceeds riverine inputs. Future climate change and, in particular, an expected increased frequency of global droughts (IPCC, 2014; Seager et al., 2007) have provided traction to research into offshore groundwater reserves as a possible source of potable and agricultural water (Berndt & Micallef, 2019). Therefore, cost- and time-effective detection and characterization of submarine groundwater systems, the dynamics of their discharge, and their temporal and spatial variation are crucial for a potential exploitation in the future.

Numerous methods have been used to detect and quantify SGD (Burnett et al., 2006) including optical systems (Karpen et al., 2004); geochemical water column investigations of tracers like the natural radionuclides radium and radon (Burnett & Dulaiova, 2003; Moore, 1996; Moore et al., 2008; Scholten et al., 2013), dissolved silicon (Oehler et al., 2019), methane, and chloride (Dulaiova et al., 2010; Schlüter et al., 2004); remote sensing (Shaban et al., 2005; Tamborski et al., 2015; Wilson & Rocha, 2012); and direct investigations using cores and different types of seepage meters (Bugna et al., 1996; Burnett & Dulaiova, 2003; Cable et al., 1997; Sauter et al., 2001). Only a few geophysical methods, like geoelectric (Stieglitz, 2005; Viso et al., 2010), controlled source electromagnetic (Gustafson et al., 2019; Müller et al., 2011), or autonomous underwater vehicle investigations (Sauter et al., 2003) have been used to explore SGD. Other hydroacoustic studies often postulate SGD solely based on geomorphological characteristics but without any geochemical verification (e.g., Goff, 2019; Hillman et al., 2015; Jakobsson et al., 2020).

Submarine hydrocarbon seeps likewise attract much interest because of the specific microenvironments they create at the seafloor (Berndt, 2005; Judd & Hovland, 2009) and their influence on slope stability (Chapron et al., 2004; Riboulot et al., 2019), representing a risk to infrastructure (Cayocca et al., 2001; Mulder & Chochonat, 1996). Since they often emit methane, a potent greenhouse gas, they can contribute to climate change and exacerbate symptoms of global warming like ocean acidification and oxygen depletion in the oceans (Biastoch et al., 2011; Borges et al., 2016; Leifer et al., 2006; Lohrberg et al., 2020; Solomon et al., 2009).

In Eckernförde Bay, sulfate reduction is the dominant process for organic carbon degradation in the upper ~30 cm below the seafloor before the sulfate is depleted (Maltby et al., 2018). Below the sulfate-methane transition zone (SMTZ), methanogenesis leads to methane oversaturation and gas formation in the organic-rich mud, resulting in widespread acoustic turbidity zones (Figure 1). Several pockmarks form along the coastlines as well as in the central part of Eckernförde around Mittelgrund as a result of gas and submarine groundwater seepage (Bussmann & Suess, 1998; Jensen et al., 2002; Kaleris et al., 2002; Müller et al., 2011; Patiris et al., 2018; Schlüter et al., 2004; Whiticar, 2002). We define a pockmark according to Judd and Hovland (2009) as a seafloor depression of erosive nature with an eroding agent that comes from beneath the seabed. In Eckernförde Bay questions remain regarding the fluid contributions to pockmark formation as well as the different pockmark classifications given by different authors (Albert et al., 1998; Whiticar, 2002). Although numerous research cruises and international research projects (e.g., Coastal Benthic Boundary Layer [CBBL] and Submarine Groundwater Fluxes and Transport Processes from Methane-Rich Coastal Sedimentary Environment [Sub-GATE]) have investigated the geological, geomechanical, geochemical, and geophysical background of the pockmarks and their host sediments, the internal pockmark geomorphology is still poorly constrained. Sidescan and multibeam data published by Sauter et al. (2003) and Schlüter et al. (2004) show the delineation and depth of the pockmarks but are unable to reveal their internal structure and morphology.

In this paper, we investigate the geomorphological expressions of SGD and gas escape as well as the subbottom characteristics within the pockmarks in Eckernförde Bay. We conducted hydroacoustic surveys using multifrequency single beam, multibeam, and subbottom profiler data in 2014, 2017, 2018, and 2019 and ground truth observations from these data with pore water geochemistry from 13 sediment cores as well as conductivity, temperature, and depth (CTD) casts and transects of the water column. This high-frequency (up to 400 kHz) study, on the one hand, provides very high resolution bathymetry enabling us to acquire targeted and accurately positioned sediment cores for pore water analysis and ground truthing. On the other hand, the high frequency has limited but significant seafloor penetration and therefore provides subsurface information. We investigate a new type of pockmark associated with SGD in gaseous mud. Hovland et al. (2002) described complex unit and eyed pockmarks, but a combination of them has not been reported previously. Our aim is to improve the characterization of pockmarks forming by SGD

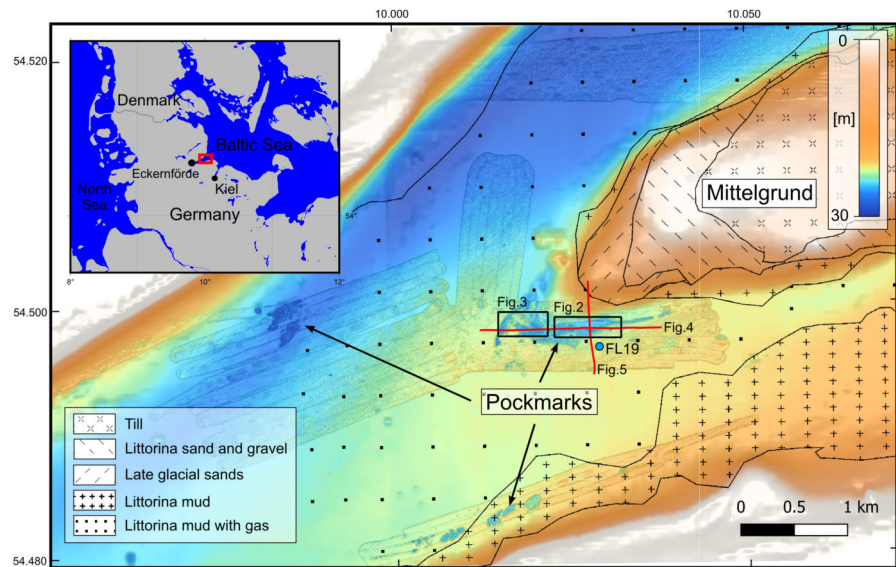


Figure 1. Overview bathymetric map of Eckernförde Bay with geological surface sediments overlaid, as described by Jensen et al. (2002). High-resolution bathymetry from Cruise AL447 (2014) overlays the regional bathymetry kindly provided by the Federal Marine Hydrographic agency. The sediment background core FL19 is indicated by the blue dot.

and gas and to determine possible acoustic indications for groundwater discharge in regions of organic-rich gaseous mud.

2. Geological Setting

The 17 km long and 3 km wide Eckernförde Bay is located in the western Baltic Sea and was mainly shaped during the end of the Weichselian glaciation about 13,000 yr BP. The mouth of Eckernförde Bay is divided into a deeper northern entrance and a shallower southern channel by a morainal sill called Mittelgrund (Figure 1). Sediment grain size distribution in Eckernförde Bay gradually decreases with increasing water depth (Seibold et al., 1971; Werner et al., 1987). The sediments are mainly derived from the retreating till cliffs surrounding the bay with a minor amount contributed by the abrasion of Mittelgrund (Healy & Wefer, 1980; Healy & Werner, 1987).

Mean sedimentation rates in the central basin of 4.2 and 3.9 mm/yr were reported by Balzer et al. (1987) and Nittrouer et al. (1998), respectively; however, Milkert and Werner (1997) and Balzer et al. (1987) show that strong temporal fluctuations occur with sedimentation rates of up to 10 mm/yr. In the inner part of Eckernförde Bay, high Corg accumulation rates originate mainly from marine plankton and macroalgal sources (Balzer, 1984; Koegler, 1967). The high organic matter content (between 4% and 5%) of surface sediments together with seasonally hypoxic bottom water leads to strong anoxic conditions, a rapid decrease of sulfate, and the onset of methanogenesis in the sediment within a few centimeters below the seafloor (Maltby et al., 2018; Steinle et al., 2017; Treude et al., 2005; Whiticar, 2002). Sediments below 20–22 m water depths consist mainly of Holocene mud deposited after the Littorina transgression (<8,000 yr BP; Röbller, 2006) with gaseous (i.e., methane) sediments of microbial origin below ~0.5–3 m (Martens et al., 1999; Schüller, 1952; Wever et al., 1998, 2006; Whiticar & Werner, 1981). This interstitial gas results in the characteristic acoustic turbidity zone (first described as the “Becken Effect” by Hinz et al. (1971)) commonly found in many shallow seas and lakes.

Although the bay is only minimally affected by tides, strong surface currents and sea level changes can occur due to wind forcing, storm surges, and the effect of seiches (Dietrich, 1951; Khandriche et al., 1987; Orsi et al., 1996). Bottom currents of up to 55 cm/s, 4 m above the seafloor, have been reported to follow storm surges (Geyer, 1964). The water column in Eckernförde Bay is generally well stratified with pycnoclines

forming due to strong variations of salinity and temperature, caused by the inflow of salty North Sea waters underneath the fresher and warmer surface water (Bange et al., 2011). This stratification becomes less pronounced over winter when cold surface waters and storms mix the entire water column (Smetacek, 1985; Smetacek et al., 1987).

Several aquifers have been attributed to supply groundwater into the bay. Bussmann and Suess (1998) and Wever et al. (1998) attributed the origin of this groundwater to the major Miocene lignite sand aquifer which reaches a thickness of 100–130 m on the southern side of the bay in ~100 m depth and is hydraulically connected to shallower aquifers (Marczinek & Piotrowski, 2002). These shallower 10–15 m thick Pleistocene sand aquifers occur between two till units (Jensen et al., 2002). In the coastal area south of the bay, another few meters thick late Pleistocene to Holocene sand aquifer is sealed by late glacial clays, glaciolacustrine silts, and till. Jensen et al. (2002) and Whitticar (2002) concluded that SGD into the Eckernförde Bay is related to marginal areas where the late glacial seal is thinned and the Holocene mud coverage is weak enough to be penetrated by artesian groundwater.

3. Data

3.1. Multibeam Echo Sounder

The multibeam echo sounder (MBES) data used in this study were repeat surveys of the pockmarks carried out over a 4.5 yr period. The data were acquired on R/V *Alkor* and R/V *Littorina* during three surveys in October–November 2014 (cruise AL447), August 2017 (cruise AL501), and May 2019 (cruise L1905). Three different MBES systems were used during variable weather conditions resulting in grids with different resolutions.

For cruise AL447 in 2014, an EM2040c system was installed on R/V *Alkor* with a 200–400 kHz transducer combined with a CodaOctopus F180 motion sensor. During the 2017 AL501 cruise, a Norbit Wideband Multibeam System (iWBMS) with integrated motion sensor was operated at 400 kHz. For cruise L1905 in 2019 we used a 180 kHz Seabeam 1000 system. More specific information on the MBES data acquisition can be found in the corresponding cruise reports (Krastel et al., 2017; Schneider von Deimling, 2014, 2019). The data were assessed, calibrated, and cleaned using software packages including MBSsystems, QPS Qimera/Fledermaus, and Hypack/Hysweep. We acquired sound velocity profiles in regular intervals which were assigned to the data during postprocessing with respect to their time of acquisition. Tidal corrections were applied using the tidal gauge in Eckernförde with reference to NHN, DHHN92.

The final processed data have horizontal resolutions of up to 0.5 m and decimeter-scale vertical resolutions enabling the imaging of 3–15 cm deep trawl marks. The backscatter amplitude data were corrected for the variation with grazing angle. We ensured the highest possible resolution by using the raw backscatter time series data for each footprint (snippets) where available and compensated for the angle of incidence using reference grids.

3.2. Subbottom Profiler

Subbottom profiler data were acquired with the R/V *Alkor* and R/V *Elisabeth Mann Borgese* in late October 2014 (cruise AL447), the beginning of July 2018 (cruise EMB187), and August 2018 (cruise AL514). We used the parametric Innomar SES-2000 medium system creating secondary peak frequencies between 4 and 15 kHz. For cruises AL447, AL514, and EMB187, we used 4, 4, and 6 kHz, respectively. The data were converted into SEG-Y format and further processed and interpreted using the IHS Markit Kingdom software packages.

3.3. Sediment Cores

During the L1905 cruise in May 2019, we used a Frahm-Lot (100 cm core liner, diameter of 10 cm; MBT GmbH-MacArtney Germany) to collect a total of 13 sediment cores with sediment recovery between 20 and 60 cm.

For pore water sampling, the plastic liner was predrilled along the side with diameters of 2.5 and 8 mm, respectively, then drill holes were closed with adhesive stripes, to insert syringes or Rhizons directly after core recovery. After retrieval of sediment cores on deck, 3 ml of sediment was subsampled by inserting

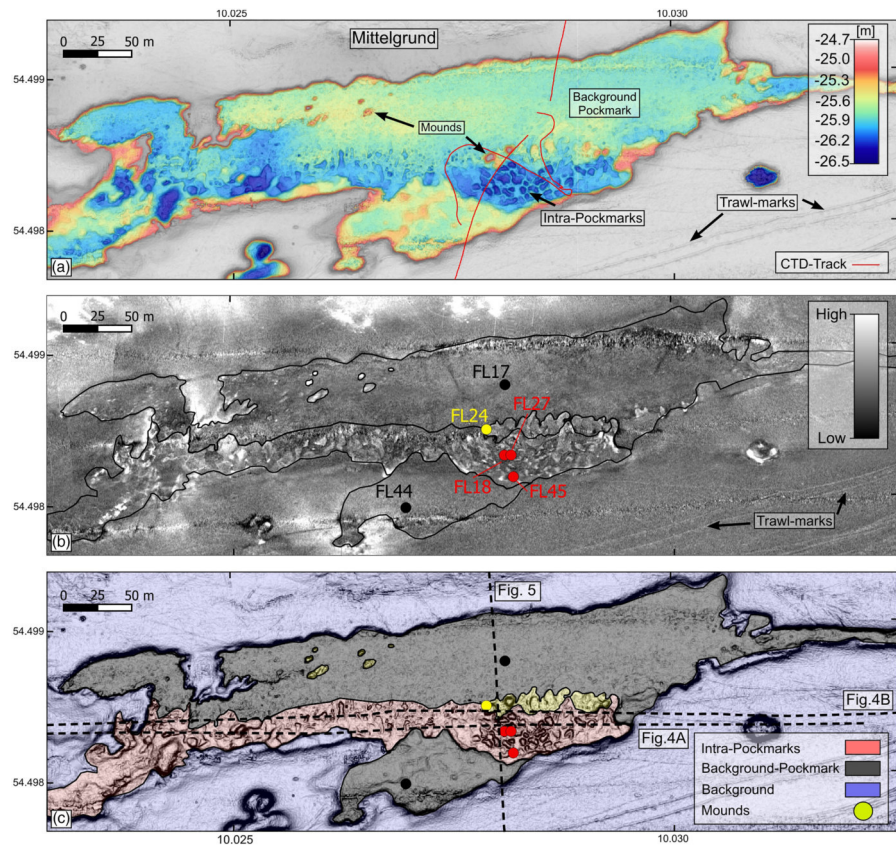


Figure 2. Bathymetric overview of the eastern Mittelgrund pockmark (data from cruise AL447 in October 2014). (a) Bathymetric map highlighting the large-scale eastern Mittelgrund pockmark (colored region) and its internal intrapockmark and background pockmark regime. Example mounds are also labeled, and the red line shows the towed CTD tracks. (b) Corrected (300 kHz) backscatter image showing the high-amplitude responses of the intrapockmarks. Colored dots show core locations, and the black lines delineate the classification regime shown in (c). (c) Slope map overlaid with pockmark classification (semitransparent colors) as described in the text. Dashed lines show the location of the subbottom profiler data displayed in Figures 4 and 5, and colored dots show core locations.

plastic syringes in a 2–4 cm interval into the predrilled holes. The sampled sediment from each syringe was pushed into a 20 ml headspace vial containing 9 ml of saturated NaCl solution (Sommer et al., 2009). Headspace vials were crimped with rubber stopper and aluminum cap and stored for gas chromatographic analysis at GEOMAR. Headspace gas (100 μ l) was injected into a Shimadzu gas chromatograph (GC-2014, flame ionization detector, carrier gas: He 5.0; HayeSepTM Q 80/100 column, column length: 2 m; column diameter: 1/8 in.). The detection limit for CH₄ was 0.1 ppmV. Precision was about 4% (2σ).

Pore water was sampled on board in 1–4 cm intervals by Rhizon extraction (Rhizosphere Research Products; e.g., Seeberg-Elverfeldt et al., 2005) for subsequent sulfate and chloride ion concentration determinations onshore. The ion concentrations were analyzed at GEOMAR by using ion chromatography (Metrohm IC761; conductivity detector, eluent: Na₂CO₃/NaHCO₃, column: Metrosep A Supp 5 100/4.0) with a precision of about 2% (2σ) determined with International Association for the Physical Sciences of the Oceans (IAPSO) seawater standard. Porosity of sediment was determined from about 10–15 g of wet sediment samples, weighted before and after freeze drying.

Methane solubility calculations have been performed for bottom water conditions (water depth = 26 m, temperature = 15 °C, and salinity = 20 (~312 mmol/L chloride)) according to Yamamoto et al. (1976).

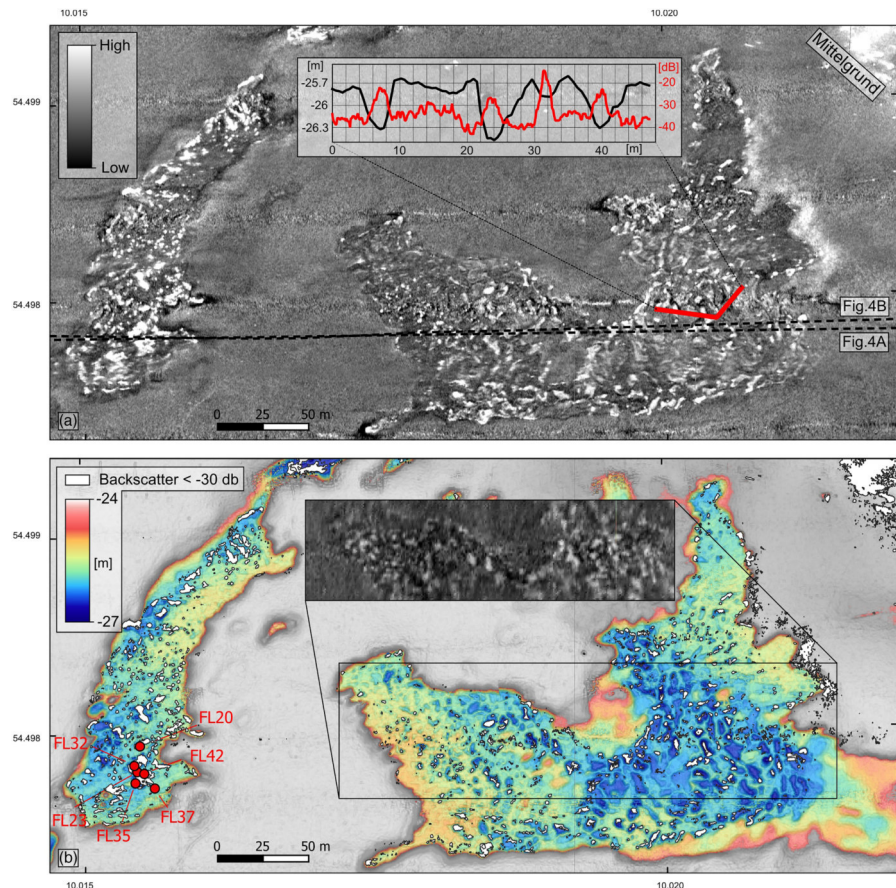


Figure 3. (a) A 300 kHz backscatter image of the western Mittelgrund pockmark showing the patchy strong backscatter strength of the intrapockmarks (Cruise AL447, October 2014). Inset graph shows the clear inverse correlation between relative backscatter strength (dB) and seafloor elevation (m). (b) Bathymetry of the pockmark with strong backscatter values (< -30 dB) overlain in white. Inset shows the 180 kHz backscatter image of cruise L1905, May 2019.

To maximize the accuracy of positioning of the vessel and the cores, we used a Stonex S9i GNSS receiver with Real Time Kinematic corrections received from the ascos (AXIO-NET GmbH) satellite reference service resulting in centimeter-scale accuracy at the receiver. Positioning of onboard coring equipment and cable deployment resulted in meter-scale accuracy for the core position (indicated by 5 m diameter circles in Figures 2 and 3).

3.4. EK60

During cruise AL447 (October 2014) and AL514 (August 2018), the fix mounted Kongsberg EK60 fishery echosounder was operated at multiple frequencies at 38, 70, 120, and 200 kHz for gas bubble detection and to identify potential anomalies associated with SGD. The four frequencies were calibrated with copper spheres in the beginning of the cruise. Pulse length and power were constant throughout the cruise.

3.5. CTD

During R/V *Littorina* Cruise L1905, we acquired three CTD water column profiles with two towed transects using a Sea and Sun CTD. For the transects the CTD was towed ~ 1 m above the seafloor.

4. Results

4.1. Bathymetry

The high-resolution bathymetry data south of Mittelgrund show the internal morphology of the targeted pockmarks in a water depth of ~ 25 m (Figures 2 and 3). The pockmarks show a mean elevation difference

of ~1.8 m compared to the surrounding area. They are elongated features and align around Mittelgrund, with widths of up to 200 m and lengths of over 1 km. The seafloor morphology within the pockmarks is highly variable. In some areas, we observe a smooth and relatively flat seafloor, while other regions show a highly uneven surface with anomalous mounds and depressions. These depressions within the pockmarks—which we hereafter refer to as “intrapockmarks”—mainly occur on the side furthest from Mittelgrund. The smoother areas—which we hereafter refer to as “background pockmark”—mainly occur on the side closest to Mittelgrund, although patches of smoother pockmark seafloor are also observed beyond the intrapockmarks further from Mittelgrund.

We divide the pockmark area southwest of Mittelgrund into three different regimes based on bathymetric morphology and their acoustic character. In Figure 2c we distinguish between (1) background (blue), (2) background pockmark (black), and (3) intrapockmark (red). The background regime describes the area outside the pockmarks (i.e., beyond both background pockmark and intrapockmark) which is morphologically characterized by a smooth surface with several 3–15 cm deep trawl marks, especially to the southeast and west of the pockmark area. Within the pockmarks, the background pockmark regime makes up most of the eastern Mittelgrund pockmark area (~70%; see Figure 2) and shows a remarkably even surface. The intrapockmark regime on the contrary shows a highly uneven surface, with depressions (intrapockmarks) of various sizes and shapes, from circular to very complex forms. They show diameters between a couple of meters and ~30 m with a vertical relief that ranges from decimeter scales up to 1 m. The intrapockmark regime shows a high pockmark density with depressions occurring close to each other without much space between them. The different regimes are in some places divided and in other places intersected and interrupted by several circular to elliptical anomalous mounded structures with heights of up to 50 cm. The various data resolutions and data qualities of the multibeam surveys permitted a comparison of the bathymetry over the 4.5-yr time period. Our visual inspection and differencing of the grids revealed no significant bathymetric changes over the course of the sampling period.

4.2. Backscatter

By thorough inspection of the geolocated multibeam snippet backscattering strength, we found a good correlation to the morphological data (Figures 2 and 3). Outside the pockmarks, in the background regime, we generally find low backscattering strength (averaging -36 dB) with slightly enhanced amplitudes (~ -30 dB) within the trawl marks in the southeast and west (Figure 2b). North and northeast of the pockmarks are areas of very strong backscatter that correspond to the Mittelgrund late glacial sands.

Within the pockmarks, the background pockmark area does not show any elevated backscatter signals (< -30 dB) and is characterized by a rather consistent and homogeneous response (Figure 2b). The intrapockmark areas on the other hand exhibit highly variable acoustic responses that vary from very strong (< -20 dB) to very low (> -40 dB) signal strength (Figure 2b). This relationship can also clearly be seen in backscatter data from the western Mittelgrund pockmark (Figure 3a). The strong backscatter values appear in patches and correlate with the bathymetric lows of the individual intrapockmarks (Figure 3a). Nearly all individual intrapockmarks show increased backscatter strength, with the strongest responses (< -30 dB) shown in white in Figure 3b. Backscatter values similar in strength to those of the late glacial sands of Mittelgrund (~ -20 dB) are observed in several of the intrapockmarks.

Although the data quality from the three surveys varies due to different equipment and weather conditions, the patchy backscatter pattern of the intrapockmarks remains obvious across all data sets.

4.3. Subbottom Profiling

The subbottom profiler data show the characteristic shallow gas front of Eckernförde Bay with the acoustic turbidity zone below (Figure 4) as observed by Hinz et al. (1971). The depth beneath the seafloor of the free gas front varies significantly over time. During the early July 2018 measurement campaign, the average depth of free gas in the background regime was ~70 cm, while in October 2014 gas occurrences at a depth of ~40 cm were observed, in accordance with reports by Wever et al. (1998). In July 2018 (Figure 4a), the acoustic manifestations of shallow gas accumulations in the background regime appear as condensed regions of high reflectivity with sharply delineated tops. In October 2014 (Figure 4b), by contrast, where the gas accumulations occur closer to the seafloor, they have a less condensed and more distributed acoustic manifestation. In the intrapockmark regime, we observe similar changes over time, although they do not

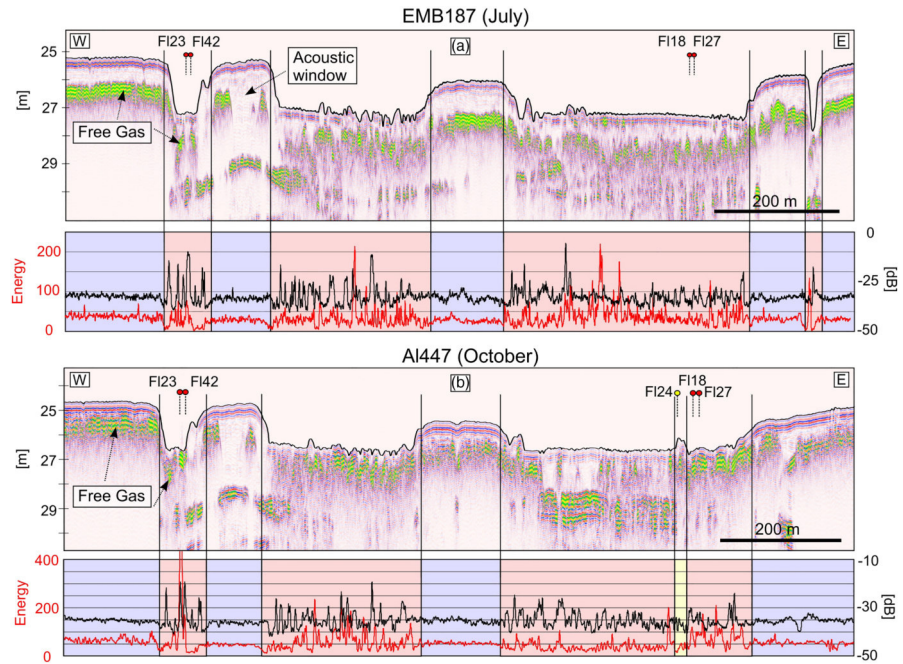


Figure 4. Innomar subbottom profiler data across the Mittelgrund pockmarks, with the energy extracted from the upper 50 cm beneath the seafloor in red and the along-track multibeam backscatter in black (in the accompanying plots). (a) Profile acquired during July 2018. (b) Profile acquired during October 2014 (locations in Figures 1–3). Sediment core locations along the profile are marked by labeled dots. Semitransparent colors in the dots and behind the energy plots are representative of different seafloor classifications as defined in Figure 2c.

seem to be as pronounced as the temporal changes observed outside of the pockmarks (in the background regime). High-amplitude reflections occur in the uppermost 50 cm throughout the data sets in the intrapockmark regime.

Outside of the pockmarks, in the background area, the free gas manifestation shows strong horizontally continuous amplitudes with occasional regions where the gas front is absent or occurs at greater depths (Figure 4), previously described by Albert et al. (1998) as acoustic windows. Within the pockmarks, free gas appears closer to the seafloor but the gas front is less continuous and the reflected acoustic energy is more

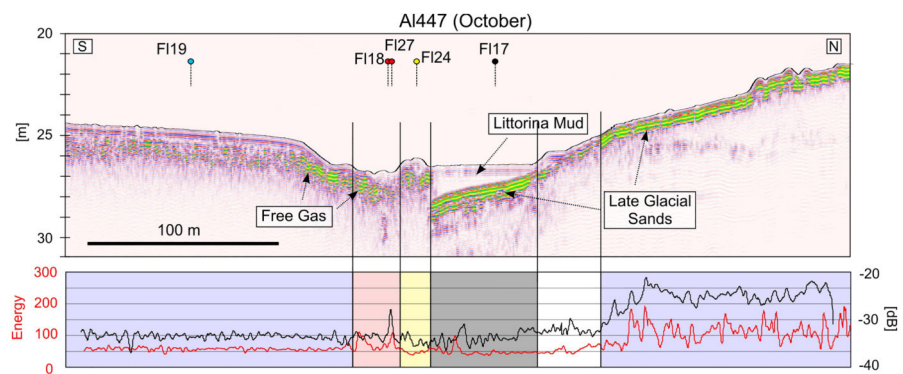


Figure 5. (top) North-south profile through the pockmarks covering Mittelgrund in the north and the inner bay in the south. Location of the profile is given in Figures 1 and 2. (bottom) The energy extracted from the upper 50 cm beneath the seafloor is displayed in red and the along-track multibeam backscatter in black. Sediment core locations along the profile are marked by labeled dots. Semitransparent colors in the dots and behind the energy plots are representative of different seafloor classifications as defined in Figure 2c.

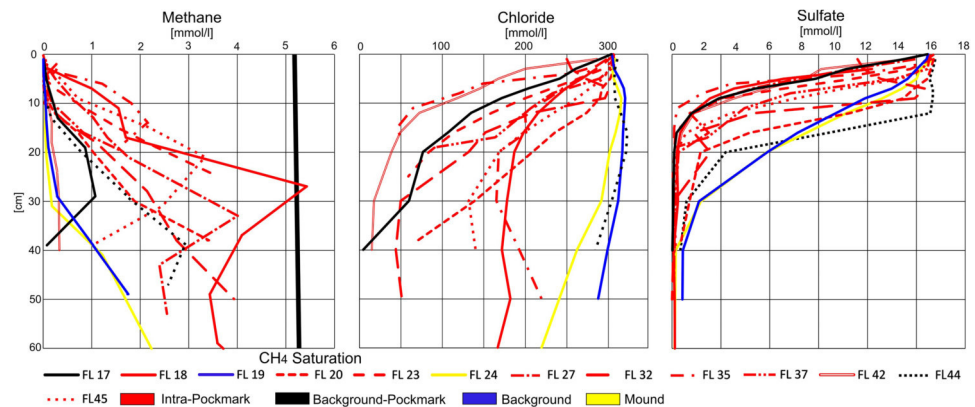


Figure 6. Pore water methane, chloride, and sulfate concentrations in all sediment cores collected, color coded by regime.

distributed over a wider depth interval (Figures 4 and 5). Several patches, indicating free gas, occur close to the seafloor.

We extracted the reflected acoustic energy within a 50 cm window below the seafloor by computing the envelope of each trace and subsequently summing the envelope within that window (Figures 4 and 5). The sum of energy shows strongly elevated energy levels at shallow subseafloor depths within the intrapockmark regime compared to the background pockmark and background regimes.

The background pockmark area, delineated in gray in Figure 5, shows a very weak seafloor reflection and no internal reflections above a layered high-amplitude southward dipping unit. This unit extends from the surface of Mittelgrund in the north beneath the pockmarks and is commonly referred to as the late glacial sands (Jensen et al., 2002). High energies in the 50 cm below the seafloor are observed in the north of the profile shown in Figure 5 around Mittelgrund, where the late glacial sands crop out at the seafloor and create a rough and hummocky morphology. This late glacial sand unit is only visible in the northern part of the pockmark area (in the background pockmark regime). Distal from Mittelgrund, in the intrapockmark regime, free gas occurs close to the seafloor, limiting the acoustic penetration. The transparent unit above the late glacial sands in the background pockmark region shows no signs of free gas and low to moderate reflection energy in the subbottom profiler as well as in the backscatter data.

4.4. Sediment Cores

We obtained sediment cores, 20–60 cm in length, from all three acoustically distinguishable regimes (Figures 2, 3, and 6). All sediment cores consisted of a dark gray to black muddy lithology with a variable centimeter-scale brown fluffy layer on top. The water content of the mud throughout the cores was extremely high, with porosities averaging 93% in the upper centimeters as previously reported by Silva and Brandes (1998). More than 50% of the attempts to recover a sediment core on deck failed due to discharge of the soft, unconsolidated, weak, and water-saturated mud, resulting in loss of the core before sampling could take place.

Pore water geochemistry profiles, that is, methane, chloride, and sulfate concentration versus depth from these cores, are shown in Figure 6 and Table S1. No distinct differences in porosity or other sediment properties were observed in the cores. The background core (FL19, Figures 1, 5, and 6) shows no enhanced methane concentrations in the uppermost 30 cm and an increase of methane to ~2 mM below 50 cm. Sulfate in the core decreases between sediment surface and 30 cm depth (SMTZ) from about 16 mM down to below ~2 mM, while the chloride concentration in the pore water is more or less constant with depth at about 290–320 mM.

The cores collected in the background pockmark area show a higher SMTZ located at about 10 cm below sediment surface; however, maximum methane concentrations below this depth are about 1 mM, which



Figure 7. Voids in the sediment cores containing free gas immediately after core recovery (core FL18).

is well below the methane solubility at this depth (i.e., 5.18–5.27 mM; Figure 6). No free gas voids were observed in the background and background pockmark sediment after core recovery on deck. Core FL17 in the background pockmark regime shows one of the strongest gradients in sulfate decrease, while core FL44 displays one of the lowest. Chlorinity profiles vary in the background pockmark area. While the northernmost core FL17 shows a strong decrease with depth to ~5 mM of chloride, the southernmost core FL44 shows chloride variability similar to the background core FL19.

With core FL24, we targeted one of the mound structures where only minor pore water freshening with depth is observed. The sulfate and methane concentration profiles of FL24 are comparable to background core FL19 (Figure 6).

In the intrapockmark regime, all cores show a strong groundwater influence from below. Pore water chloride concentrations of less than 100 mM (~30% of the bottom water concentration) were measured at about 10 cm (Figure 6). These low chloride values are accompanied by high methane concentrations of up to 2 mM at 10 cm and strong methane concentration gradients with depth. The SMTZ occurs between ~5 and 15 cm in the intrapockmark regime, and methane concentrations of up to 5.42 mM were measured in core FL18 at about 30 cm (Figure 6). As bubble formation even under in situ pressure conditions is anticipated based on the measured methane concentration, the scattered methane concentration measured below 30 cm is probably related to strong degas-

ing effects on deck. Indeed, several cores from this region showed evidence of free gas bubbles beneath ~10 cm, when they came to the surface (Figure 7). This includes core FL42, which for an unknown reason does not show enhanced dissolved CH_4 pore water concentrations higher than 0.3 mM. We attribute this lack of methane to degassing during core acquisition and unfortunately too long storage time on deck until sampling (Abegg & Anderson, 1997; Wever et al., 1998).

4.5. CTD

We conducted three CTD casts with two towed transects in different regions of Eckernförde Bay. The location of the towed CTD transect is shown in Figure 1a. All of the casts and transects show low saline surface water of $S \sim 14$ (~218 mmol/L chloride) with an increasing salinity to ~20 (~312 mmol/L chloride) in the bottom water, as characteristic for the Baltic Sea (Bange et al., 2011; Lennartz et al., 2014). Although we managed to tow the CTD as close as ~1 m above the seafloor, none of the CTD casts or transects showed any groundwater influence on the water column, neither within nor outside of the pockmarks.

5. Discussion

5.1. Characterization of Eckernförde Bay Pockmarks

Albert et al. (1998) have noted that pockmarks closer to the coast of Eckernförde Bay appear to be a different type altogether than those around Mittelgrund. This was based on the observation of low methane and low chloride concentrations, as measured by Whiticar and Werner (1981) and later by Whiticar (2002) in the Mittelgrund pockmarks, compared to high methane concentrations in pockmarks closer to the coast.

Our high-frequency multibeam approach enabled us to collect targeted sediment cores with a meter-scale accuracy. These new data suggest a classification of the pockmarks into different regimes rather than separating the coastal and Mittelgrund pockmarks into different types based on different eroding agents from below. Depending on core location, even within the same pockmark, methane and chloride concentrations can vary significantly (Figure 6). While the background regime shows no influence of

groundwater, a comparatively deep SMTZ, and only a moderate positive methane gradient below the SMTZ, the cores from within the pockmarks are variable. In the northern background pockmark regime low methane concentrations correlate with a thin organic-rich Littorina mud cover above the late glacial sands (Figure 5). The subbottom profiler data show no signs of free gas or internal reflections in this area. We observe a moderate methane concentration gradient below the SMTZ with maximum methane concentrations well below the solubility of methane in pore water (core FL17, Figure 6). The even seafloor of the background pockmark area therefore corresponds to high groundwater influence with low methane concentrations. The background pockmark sulfate profile of core 44 shows anomalously high concentrations of sulfate compared to the other cores, down to 12 cm. The high sulfate is accompanied by moderate methane concentrations and high chloride concentrations indicating limited groundwater influence. The sigmoidal shape of the sulfate concentration profile below 12 cm indicates a nonsteady state of anaerobic microbial methane oxidation related to sulfate reduction during the respective season (Schulz, 2006). Although the porosity of this core is not anomalous compared to other cores, a high permeability and effective exchange of pore water with bottom water at the top of the core could be the cause. The background pockmark regime therefore varies in sulfate and chloride according to the location of the core, the thickness of the Littorina mud cover, and the influence of ascending groundwater.

In the intrapockmark regime, the mud reaches thicknesses of more than 1 m above the late glacial sands and the SMTZ is shifted to shallower depths compared to the background pockmark. Free gas occurs very close to the seafloor as seen in the subbottom profiler data as well as in the sediment cores, and the elevated methane concentrations are reaching oversaturation at depth (e.g., FL27, Figure 6). Although Jensen et al. (2002) reported that the late glacial sands extend over the entire Eckernförde basin, we cannot resolve this southward dipping unit outside the background pockmark area due to the acoustic turbidity where free gas is present. All the cores in this morphologically rough intrapockmark region show a strong groundwater influence with high methane concentrations and a shallow SMTZ.

5.2. Formation and Modification Processes of the Intrapockmarks

The formation of the Eckernförde pockmarks has been debated for decades. Bottom currents (Werner, 1978), military activities (Edgerton et al., 1966), gas seepage (Fabian & Roese, 1962), and groundwater seepage (Khandriche & Werner, 1995; Whiticar & Werner, 1981) have all been proposed as formation mechanisms since their discovery by Edgerton et al. (1966). It is now widely accepted that episodic artesian groundwater springs, in combination with bottom currents, erode the pockmarks (Bussmann & Suess, 1998; Jensen et al., 2002; Kaleris et al., 2002; Müller et al., 2011; Patiris et al., 2018; Schlüter et al., 2004; Whiticar, 2002). The newly observed (this study) eyed intrapockmarks in Eckernförde Bay seem to host both high methane and low chloride concentrations. Albert et al. (1998) proposed that the Eckernförde pockmarks act as morphological sinks for organic material and therefore could enhance methanogenesis close to the sediment-water interface. Khandriche and Werner (1995) suggested that the erosion of the pockmarks, once initiated, leads to a positive feedback mechanism since deeper sediment layers with a higher gas content are exposed to water currents. Since the depth of the gas front varies within the sediments by tens of centimeters (magnitudes higher than accumulation or erosion rates) due to seasonal variations and short-term weather conditions, we assume that the high gas content close to the seafloor within the pockmarks is the result of groundwater seepage rather than erosion. The high gas content combined with the low chlorinity very close to the seafloor induces sediment instabilities and a reduction in shear strength (Sills & Wheeler, 1992) which consequently make sediments more easily erodible. In areas where only minor gas concentrations were measured in the pockmarks (background pockmark area), we find an even and flat seafloor morphology, whereas in areas with strong methane gradients (intrapockmark area), we observe a scoured surface which likely indicates lower shear strength and additional erosion. Since we did not observe any indications for seafloor scouring by bottom currents (e.g., elongation, preferred orientation, or azimuthal variations in slope of the intrapockmarks), we propose that the abnormally shallow gas (which forms due to SGD; see section 5.3) and the episodic release of groundwater are the main drivers of intrapockmark formation. We suggest that the free gas changes the geotechnical properties, (e.g. reduces the shear strength (Sills & Wheeler, 1992)), meaning that even weak groundwater discharge phases erode the very fine

sediments. The background pockmark, on the other hand, shows no indications for elevated methane concentrations, and we therefore presume that its morphology is the sole result of groundwater discharge during strong discharge phases.

5.3. Enhanced Backscatter Signals of Intrapockmarks

High backscatter at the bottom of pockmarks, as we observed in Eckernförde Bays intrapockmarks, is a common phenomenon (Dandapath et al., 2010; Hovland et al., 2002; Judd & Hovland, 2009; Loncke et al., 2004). Seeping fluids frequently result in authigenic carbonate precipitation due to the microbially driven anaerobic oxidation of methane once methane enters the SMTZ (e.g., Boetius et al., 2000; Ritger et al., 1987). These carbonates are often associated with high-amplitude, positive polarity reflections and a high backscatter signal in pockmarks (Böttner et al., 2019; Dandapath et al., 2010; Ho et al., 2012; Judd & Hovland, 2009). Similarly, the suspension of fine-grained material due to fluid escape, leaving the coarser-grained material behind as well as enhancing biological activity due to seeping fluids (skeleton remains, dead and living shells, etc.), can create a strong impedance contrast and a rougher surface area and therefore results in strong backscatter values in pockmarks (Hovland, 1989; Hovland et al., 2002; Reusch et al., 2015). These pockmarks containing highly reflective objects at their centers have commonly been described as “eyed” pockmarks (Hovland et al., 2002).

In Eckernförde Bay, the carbonate concentration in the sediment is extremely low (<2%) due to undersaturation in bottom waters (Lewy, 1975; Wefer et al., 1987), ruling out carbonate precipitation as a plausible cause of high backscatter. Also, the pockmark area, which was well sampled over recent decades, shows a surface sedimentary composition that consists of homogeneous Holocene mud without a significant amount of coarser-grained material (section 4.4, Jensen et al., 2002; Martens et al., 1999; Schlüter et al., 2004; Whiticar, 2002). Similar to carbonate, gas-bearing sediments induce a strong impedance contrast to the surrounding water-saturated sediments which creates a strong (albeit negative polarity) reflection. Beneath the intrapockmarks, the closely spaced subbottom profiler data show that the shallow gas front occurs closer to the seafloor and becomes patchier compared to the surrounding regions. This is highlighted by the sum of acoustic energy extracted within a 50 cm window beneath the seafloor (Figure 4). The upper 50 cm includes the strong reflections associated with the shallow gas in the intrapockmark regime (see CH₄ saturation in Figure 6) while excluding the reflections associated with deeper gas in the background. Additionally, the sediment cores collected within the intrapockmarks show elevated methane concentrations compared to the background pockmark and background cores. In several sediment cores recovered on deck, we visually detected free gas bubbles ~10 cm beneath the sediment-water interface (Figure 7). Moreover, measured methane concentrations of the intrapockmark regime are comparable to the solubility limit of methane at in situ pressure, temperature, and salinity conditions (Figure 6). This, together with the good correlation of multibeam backscatter strength and subbottom profiler reflectivity shown in Figures 4 and 5, suggests that the elevated backscatter results from free shallow gas within the sediment at depth of ~10–20 cm.

Tang et al. (1994) reported that backscatter from a 40 kHz benthic acoustic measurement system results from gas voids about 1 m beneath the seafloor in Eckernförde Bay. In a geologically very similar environment to Eckernförde Bay, Schneider von Deimling et al. (2013) showed how a 12 kHz multibeam system can be used to map shallow gas in up to 12 m sediments depth, while a 95 kHz system detected the sediment-water interface. Our results indicate that, in the soft muddy sediments of Eckernförde Bay (with low attenuation coefficients of ~0.1–0.2 dB m⁻¹ kHz⁻¹; Jackson & Richardson, 2007), even the 400 kHz systems penetrate the upper few decimeters of the seafloor, and volume scattering provides information on subsurface sediment properties (in this case, partially gas saturated sediment). A large-scale seafloor backscatter classification approach in Eckernförde Bay by Alevizos et al. (2018) classified parts of the Mittelgrund pockmarks to consist of sand with small amounts of gravel due to the elevated backscatter signals in the pockmarks. The intrapockmarks indeed exhibit exceptionally high backscatter values with signal strengths comparable to the backscatter of the late glacial sands of Mittelgrund. However, no substantial amount of sand or gravel has been reported from sediment cores or grabs in this region and the automated seafloor classification likely incorrectly identified the free gas as sand.

The depth of the shallow gas front in Eckernförde Bay changes over time on a short-term (effective pressure dependent) and seasonal (water temperature dependent) basis (Treude et al., 2005; Wever et al., 1998, 2006). On a seasonal basis, the bottom waters have highest temperatures around October–November with lowest bottom water temperatures during March–April (Lennartz et al., 2014). While a decrease in water temperature increases the solubility of methane, a temperature increase reduces the solubility and therefore increases the amount of free gas bubbles. The free gas front is therefore expected to be deepest during March–April and shallowest between October and November (Wever et al., 1998). We observe this phenomenon in our subbottom data where the EMB187 line (acquired on 7 July 2018) shows a free gas front around 70 cm below the seafloor in the background area compared to ~40 cm below the seafloor in the AL447 data (acquired on 22 October 2014).

Although the different multibeam systems used for acquisition were not calibrated for the target strength (i.e., pockmark backscatter cannot be directly compared), the backscatter distribution pattern of the intrapockmarks seems to be unaffected by seasonal variations and show the same strong patchy backscatter character throughout all three data sets (22 October, 8 September, and 16 May). This suggests that free shallow gas constantly resides in the uppermost decimeters within the intrapockmark regime and affects multibeam backscatter systems with 180, 300, and 400 kHz to a similar degree. This is supported by strong amplitudes close to the seafloor–water interface in all subbottom profiler data (Figure 4). We suggest that this phenomenon results mainly from the ascending groundwater, which is thought to intensify the upward migration of dissolved as well as free methane gas (Khandriche & Werner, 1995), thereby increasing gas concentrations closer to the seafloor. Moreover, as sulfate is rapidly depleted in pore water by ascending groundwater (Figure 6), the SMTZ is uplifted closer to the seafloor and thus the depths where methanogenesis would lead to oversaturation. Therefore, gas bubble formation is uplifted and free gas occurs closer to the seafloor in areas of SGD.

5.4. Acoustic Indicators for Groundwater

One aim of this study was to find hydroacoustic indications for SGD in the water column or the seafloor. Khandriche and Werner (1995), as well as Bussmann and Suess (1998), reported decreased salinities in the water column down to $S = 2.9$ (~45 mmol/L chloride) near the bottom of a pockmark, indicating a strong groundwater outflow during their surveying. However, repeated dedicated water column analysis of multibeam water column imaging data and Simrad EK60 single beam data over several years revealed no indications of groundwater influence on the water column above the pockmark sites. We could observe several small gas seeps and single gas bubbles in the acoustic water column data though (Figure S1). Horizontal, locally continuous pycnoclines observed in the EK60 data do not seem to be affected by fluid seepage above the pockmarks (Figure S1). This agrees with findings from Bussmann and Suess (1998) who reported that the water column stability was not affected by less dense groundwater at the base of the pockmarks. The lack of observed acoustic reflections from discharging groundwater may indicate a quiescence phase during our sampling periods. Our sediment pore water chloride profiles (collected May 2019) and also published chloride records from Albert et al. (1998), Bussmann et al. (1999), Müller et al. (2011), or Schlüter et al. (2004) indicate that mixing of low saline groundwater with seawater already occurs in the upper sediments preventing the low saline groundwater from seeping out. In Eckernförde Bay the discharge rate is highly variable since groundwater discharges episodically (Bussmann & Suess, 1998; Schlüter et al., 2004). Unfortunately, no long-term seepage meters were available during our surveys. Even during a strong groundwater outflow event, like observed by Khandriche and Werner (1995) or Bussmann and Suess (1998), strong mixing between fresh and saltwater could occur, resulting in a gradual transition of acoustic impedances between the two water bodies which prevents the development of a reflection at their interface. We therefore used a different attempt to find acoustic indications for SGD by analyzing the seafloor morphology and backscatter characteristics.

In general, the sediment cores we collected in Eckernförde Bay show a strong relation between methane concentrations and groundwater. Only in core FL17, low chloride pore waters occur close to the sediment surface, but no enhanced methane concentrations were observed; nor do we find acoustic indications for free gas in the background pockmark area. We attribute this to the relatively thin organic-rich sediment

cover above the late glacial sands of Mittelgrund which are dipping south beneath the pockmark (Figure 5). The thickness of organic-rich *Littorina* mud covering the sands increases with distance from Mittelgrund, and once the *Littorina* mud reaches thicknesses of more than ~1 m, free gas occurs in the sediments.

With this one exception, all pore water profiles show increased methane concentrations where chloride concentrations are low. In previous studies, Bugna et al. (1996) and Dulaiova et al. (2010) used elevated methane concentrations in groundwater as a tracer for SGD. Ascending groundwater is not only often already enriched in dissolved methane but also suppresses sulfate mixing into the sediment and therefore increases the amount of metabolizable organic carbon reaching the methanogenic zone, allowing gas to form closer to the seafloor (Albert et al., 1998; Dulaiova et al., 2010). Albert et al. (1998) modeled the influence of different groundwater fluxes on methane concentrations in Eckernförde Bay and showed how an increased groundwater flux can lead to enhanced methane concentrations close to the seafloor when assuming a higher input of metabolizable organic material into morphological sinks like pockmarks. As discussed earlier, we acoustically detected and highly accurately located the free gas phase in the muddy sediments of Eckernförde Bay. The free gas phase and therefore the high backscatter in the pockmarks directly correlate with low chloride concentrations. We therefore assume that in areas with sufficient organic material and methanogenesis, acoustic investigations can provide indications for groundwater seepage. Since Fleischer et al. (2001) showed how globally abundant gaseous muds are in coastal waters and shallow adjacent seas, our approach will have significant implications for future efforts to detect and characterize SGD.

6. Conclusions

Using high-resolution acoustic data in combination with 13 precisely located sediment cores, we reveal the nature of different pockmark classifications made by previous authors in Eckernförde Bay. We propose a classification of the pockmarks into different regimes according to their morphological and backscatter characteristics rather than differentiating them into different types based exclusively on the pore water geochemistry. We discovered a new form of eyed intrapockmarks with enhanced backscatter signals at their bases which is neither caused by authigenic carbonates nor by a change in seafloor material but rather by shallow gas occurring close to the seafloor. This implies that even when using high frequencies, significant signal penetration and volume scattering need to be considered and seabed classification methods must take this into account. We assume that SGD (1) enhances upward migration of dissolved and free methane gas bubbles to the seafloor and (2) enhances methanogenesis close to the seafloor due to decreased sulfate concentrations in groundwater. This leads to an extremely shallow, consistent, and more stable gas front within the intrapockmarks, less affected by temperature changes than the surrounding area. We suggest that this consistent shallow gas alters the geotechnical properties of the unconsolidated sediments making them more easily erodible by the discharging groundwater than the surrounding sediments. The intrapockmarks are therefore a manifestation of groundwater flow that mobilizes free gas, which in turn promotes sediment weaknesses and subsequent erosion. Recognizing this process is important for understanding how pockmarks can be caused by SGD and why they occur where they do. Ultimately, this will help in identifying and characterizing offshore groundwater systems which may become important sources of fresh water in the future.

We showed that high-frequency multibeam data can be used to detect shallow gas within the sediment in regions of SGD. The seafloor morphology combined with backscatter data can, therefore, be used to obtain indications for potential groundwater seepage in organic-rich, gaseous, and muddy sediments. Since shallow gas in muddy sediments is a common global phenomenon, our study highlights the importance of investigating how SGD and shallow gas interact close to the seafloor. We showcase that even at 400 kHz frequency, backscattering strength is significantly increased by subsurface volume scattering from shallow gas. Our study also highlights the potential for shallow gas to confuse bathymetric depth and backscatter interpretations, in addition to studies dealing with lower frequencies (e.g., Gaida et al., 2019; Schneider von Deimling et al., 2013). In particular, we show that high-resolution hydroacoustic surveys followed by targeted coring can be used to identify specific locations of SGD and provide new insight into how SGD influences seafloor geochemistry and morphology. Our knowledge on the

occurrence of SGD in deeper basins and oceans is limited (Post et al., 2013) because of the lack of suitable detection techniques. The methodology we presented describes a possible way to survey SGD associated with methane release and can be used elsewhere around the world to improve the identification and characterization of SGD.

Acknowledgments

We are thankful for onboard coring and sediment sampling assistance by M. Ippach. Laboratory chemical analyses were conducted by A. Bodenbinder, A. Bleyer, and B. Domeyer. Thanks also to Ercan Erkul and the crew of the R/V *Littorina*, R/V *Alkor*, and R/V *Elisabeth Mann Borgese* for their help and support during data acquisition. Hoffmann thanks the marine geophysics and hydroacoustics working group of the University of Kiel for their sustained support. Access to the pore water geochemistry, subbottom profiler, and MBES data is available through Pangaea data repository (<https://doi.pangaea.de/10.1594/PANGAEA.912274>). This work resulted from the BONUS ECOMAP and BONUS SEAMOUNT projects, supported by BONUS (art. 185), funded jointly by the EU and the Federal Ministry of Education and Research of Germany (BMBF, Grant 03F0771B), the National Centre for Research and Development of Poland (NCBR), and the Innovation Fund Denmark (Innovationsfonden). Additional funding was provided by New Zealand's Ministry of Business, Innovation and Employment (MBIE) as part of the GNS Science-led program "Understanding petroleum source rocks, fluids, and plumbing systems in New Zealand basins: A critical basis for future oil and gas discoveries" (Contract C05X1507). We gratefully acknowledge the German Academic Exchange Service (DAAD) for providing a short-term research grant to Hoffmann (Funding program: 57440917). Data processing and analysis were undertaken through academic licenses for QPS Qimera, Fledermaus, and IHS Markit's Kingdom software. Hoffmann is supported by the University of Otago PhD scholarship.

References

- Abegg, F., & Anderson, A. L. (1997). The acoustic turbid layer in muddy sediments of Eckernförde Bay, Western Baltic: Methane concentration, saturation and bubble characteristics. *Marine Geology*, *137*(1–2), 137–147. [https://doi.org/10.1016/S0025-3227\(96\)00084-9](https://doi.org/10.1016/S0025-3227(96)00084-9)
- Albert, D. B., Martens, C. S., & Alperin, M. J. (1998). Biogeochemical processes controlling methane in gassy coastal sediments—Part 2: Groundwater flow control of acoustic turbidity in Eckernförde Bay sediments. *Continental Shelf Research*, *18*(14–15), 1771–1793. [https://doi.org/10.1016/S0278-4343\(98\)00057-0](https://doi.org/10.1016/S0278-4343(98)00057-0)
- Alevizos, E., Snellen, M., Simons, D., Siemes, K., & Greinert, J. (2018). Multi-angle backscatter classification and sub-bottom profiling for improved seafloor characterization. *Marine Geophysical Research*, *39*(1–2), 289–306. <https://doi.org/10.1007/s11001-017-9325-4>
- Balzer, W. (1984). Organic matter degradation and biogenic element cycling in a nearshore sediment (Kiel Bight) 1. *Limnology and Oceanography*, *29*(6), 1231–1246. <https://doi.org/10.4319/lo.1984.29.6.1231>
- Balzer, W., Erlenkeuser, H., Hartmann, M., Müller, P. J., & Pollehn, F. (1987). Diagenesis and exchange processes at the benthic boundary. In *Seawater-sediment interactions in coastal waters* (Chap. 4, pp. 111–161). Berlin, Heidelberg: Springer. <https://doi.org/10.1029/LN013p0111>
- Bange, H. W., Hansen, H. P., Malien, F., Laß, K., Dale, A. W., Karstensen, J., et al. (2011). Boknis Eck time series station (SW Baltic Sea): Measurements from 1957 to 2010. *LOICZ Inprint*, *2011*(1), 16–22.
- Berndt, C. (2005). Focused fluid flow in passive continental margins. *Philosophical Transactions of the Royal Society A: Mathematical, Physical and Engineering Sciences*, *363*(1837), 2855–2871. <https://doi.org/10.1098/rsta.2005.1666>
- Berndt, C., & Micallef, A. (2019). Could offshore groundwater rescue coastal cities? *Nature*, *574*(7776), 36. <https://doi.org/10.1038/d41586-019-02924-7>
- Biaostoch, A., Treude, T., Rüpke, L. H., Riebesell, U., Roth, C., Burwicz, E. B., et al. (2011). Rising Arctic Ocean temperatures cause gas hydrate destabilization and ocean acidification. *Geophysical Research Letters*, *38*(8). <https://doi.org/10.1029/2011GL047222>
- Boetius, A., Ravensschlag, K., Schubert, C. J., Rickert, D., Widdel, F., Gieseke, A., et al. (2000). A marine microbial consortium apparently mediating anaerobic oxidation of methane. *Nature*, *407*(6804), 623–626. <https://doi.org/10.1038/35036572>
- Borges, A. V., Champenois, W., Gypens, N., Delille, B., & Harlay, J. (2016). Massive marine methane emissions from near-shore shallow coastal areas. *Scientific Reports*, *6*(1), 27908. <https://doi.org/10.1038/srep27908>
- Böttner, C., Berndt, C., Reinardy, B. T. I., Geersen, J., Karstensen, J., Bull, J. M., et al. (2019). Pockmarks in the Witch Ground Basin, central North Sea. *Geochemistry, Geophysics, Geosystems*, *20*(4), 1698–1719. <https://doi.org/10.1029/2018GC008068>
- Bugna, G. C., Chanton, J. P., Cable, J. E., Burnett, W. C., & Cable, P. H. (1996). The importance of groundwater discharge to the methane budgets of nearshore and continental shelf waters of the northeastern Gulf of Mexico. *Geochimica et Cosmochimica Acta*, *60*(23), 4735–4746. [https://doi.org/10.1016/S0016-7037\(96\)00290-6](https://doi.org/10.1016/S0016-7037(96)00290-6)
- Burnett, W. C., Aggarwal, P. K., Aureli, A., Bokuniewicz, H., Cable, J. E., Charette, M. A., et al. (2006). Quantifying submarine groundwater discharge in the coastal zone via multiple methods. *Science of the Total Environment*, *367*(2–3), 498–543. <https://doi.org/10.1016/j.scitotenv.2006.05.009>
- Burnett, W. C., & Dulaiova, H. (2003). Estimating the dynamics of groundwater input into the coastal zone via continuous radon-222 measurements. *Journal of Environmental Radioactivity*, *69*(1–2), 21–35. [https://doi.org/10.1016/S0265-931X\(03\)00084-5](https://doi.org/10.1016/S0265-931X(03)00084-5)
- Bussmann, I., Dando, P., Niven, S., & Suess, E. (1999). Groundwater seepage in the marine environment: Role for mass flux and bacterial activity. *Marine Ecology Progress Series*, *178*(1), 169–177. <https://doi.org/10.3354/meps178169>
- Bussmann, I., & Suess, E. (1998). Groundwater seepage in Eckernförde Bay (western Baltic Sea): Effect on methane and salinity distribution of the water column. *Continental Shelf Research*, *18*(14–15), 1795–1806. [https://doi.org/10.1016/S0278-4343\(98\)00058-2](https://doi.org/10.1016/S0278-4343(98)00058-2)
- Cable, J. E., Burnett, W. C., & Chanton, J. P. (1997). Magnitude and variations of groundwater seepage along a Florida marine shoreline. *Biogeochemistry*, *38*(2), 189–205. <https://doi.org/10.1023/A:1005756528516>
- Cayocca, F., Sultan, N., Cochonat, P., & Bourillet, J. F. (2001). Evaluation of the risk of marine slope instability: A pseudo-3D approach for application to large areas. *Marine Georesources and Geotechnology*, *19*(2), 107–133. <https://doi.org/10.1080/10641190109353807>
- Chapron, E., Van Rensbergen, P., De Batist, M., Beck, C., & Henriot, J. P. (2004). Fluid-escape features as a precursor of a large sub-lacustrine sediment slide in Lake Le Bourget, NW Alps, France. *Terra Nova*, *16*(5), 305–311. <https://doi.org/10.1111/j.1365-3121.2004.00566.x>
- Cho, H.-M., Kim, G., Kwon, E. Y., Moosdorf, N., Garcia-Orellana, J., & Santos, I. R. (2018). Radium tracing nutrient inputs through submarine groundwater discharge in the global ocean. *Scientific Reports*, *8*(1), 2439. <https://doi.org/10.1038/s41598-018-20806-2>
- Dandapath, S., Chakraborty, B., Karisiddaiah, S. M., Menezes, A., Ranade, G., Fernandes, W., et al. (2010). Morphology of pockmarks along the western continental margin of India: Employing multibeam bathymetry and backscatter data. *Marine and Petroleum Geology*, *27*(10), 2107–2117. <https://doi.org/10.1016/j.marpetgeo.2010.09.005>
- Dietrich, G. (1951). Oberflächenströmungen im Kattegat, im Sund und in der Beltsee. *Deutsche Hydrografische Zeitschrift*, *4*(4–6), 129–150. <https://doi.org/10.1007/BF02019555>
- Dulaiova, H., Camilli, R., Henderson, P. B., & Charette, M. A. (2010). Coupled radon, methane and nitrate sensors for large-scale assessment of groundwater discharge and non-point source pollution to coastal waters. *Journal of Environmental Radioactivity*, *101*(7), 553–563. <https://doi.org/10.1016/j.jenvrad.2009.12.004>
- Edgerton, H. E., Seibold, E., Vollbrecht, K., & Werner, F. (1966). Morphologische Untersuchungen am Mittelgrund (Eckernförde Bucht, westliche Ostsee). *Meyniana*, *16*, 37–50.
- Fabian, H. S., & Roese, K. L. (1962). Das Erdölfeld Schwedeneck. *Erdöl-Zeitschrift*, *78*, 283–294.
- Fleischer, P., Orsi, T. H., Richardson, M. D., & Anderson, A. L. (2001). Distribution of free gas in marine sediments: A global overview. *Geo-Marine Letters*, *21*(2), 103–122. <https://doi.org/10.1007/s003670100072>

- Gaida, T. C., Mohammadloo, T. H., Snellen, M., & Simons, D. G. (2019). Mapping the seabed and shallow subsurface with multi-frequency multibeam echosounders. *Remote Sensing*, *12*(1), 52. <https://doi.org/10.3390/rs12010052>
- Geyer, D. (1964). Eigenschwingungen und Erneuerung des Wasser in der Eckernförder Bucht unter besonderer Berücksichtigung der Sturmflut vom 5.-6. Dezember 1961. *Kieler Meeresforschungen*, *21*, 33–54.
- Goff, J. A. (2019). Modern and fossil pockmarks in the New England mud patch: Implications for submarine groundwater discharge on the middle shelf. *Geophysical Research Letters*, *46*(21), 12213–12220. <https://doi.org/10.1029/2019GL084881>
- Gustafson, C., Key, K., & Evans, R. L. (2019). Aquifer systems extending far offshore on the U.S. Atlantic margin. *Scientific Reports*, *9*(1), 8709. <https://doi.org/10.1038/s41598-019-44611-7>
- Healy, T., & Wefer, G. (1980). The efficacy of submarine abrasion vs. cliff retreat as a supplier of marine sediment in the Kieler Bucht, western Baltic. *Meyniana*, *32*, 89–96.
- Healy, T., & Werner, F. (1987). Sediment budget for a semi-enclosed sea in a near-homogeneous lithology: Example of Kieler Bucht, western Baltic. *Senckenbergiana Maritima*, *19*(3–4), 195–222.
- Hillman, J. I. T., Gorman, A. R., & Pecher, I. A. (2015). Geostatistical analysis of seafloor depressions on the southeast margin of New Zealand's South Island—Investigating the impact of dynamic near seafloor processes on geomorphology. *Marine Geology*, *360*, 70–83. <https://doi.org/10.1016/j.margeo.2014.11.016>
- Hinz, K., Kögler, F. C., Richter, I., & Seibold, E. (1971). Reflexionsseismische Untersuchungen mit einer pneumatischen Schallquelle und einem Sedimentecholot in der westlichen Ostsee. *Meyniana*, *21*, 17–24.
- Ho, S., Cartwright, J. A., & Imbert, P. (2012). Vertical evolution of fluid venting structures in relation to gas flux, in the Neogene-Quaternary of the Lower Congo Basin, offshore Angola. *Marine Geology*, *332–334*, 40–55. <https://doi.org/10.1016/j.margeo.2012.08.011>
- Hovland, M. (1989). The formation of pockmarks and their potential influence on offshore construction. *Quarterly Journal of Engineering Geology*, *22*(2), 131–138. <https://doi.org/10.1144/GSL.QJEG.1989.022.02.04>
- Hovland, M., Gardner, J. V., & Judd, A. G. (2002). The significance of pockmarks to understanding fluid flow processes and geohazards. *Geofluids*, *2*(2), 127–136. <https://doi.org/10.1046/j.1468-8123.2002.00028.x>
- IPCC (2014). In Core Writing Team, R. K. Pachauri, & L. A. Meyer (Eds.), *Climate change 2014: Synthesis report. Contribution of Working Groups I, II and III to the Fifth Assessment Report of the Intergovernmental Panel on Climate Change*, (p. 151). Geneva, Switzerland: IPCC.
- Jackson, D., & Richardson, M. (2007). High-frequency seafloor acoustics. Springer Science & Business Media.
- Jakobsson, M., O'Regan, M., Mörth, C.-M., Stranne, C., Weidner, E., Hansson, J., et al. (2020). Potential links between Baltic Sea submarine terraces and groundwater seeping. *Earth Surface Dynamics*, *8*(1), 1–15. <https://doi.org/10.5194/esurf-8-1-2020>
- Jensen, J. B., Kuijpers, A., Bennike, O., Laier, T., & Werner, F. (2002). New geological aspects for freshwater seepage and formation in Eckernförde Bay, western Baltic. *Continental Shelf Research*, *22*(15), 2159–2173. [https://doi.org/10.1016/S0278-4343\(02\)00076-6](https://doi.org/10.1016/S0278-4343(02)00076-6)
- Judd, A., & Hovland, M. (2009). *Seabed fluid flow: The impact on geology, biology and the marine environment*. Cambridge: Cambridge University Press.
- Kaleris, V., Lagas, G., Marczynek, S., & Piotrowski, J. a. (2002). Modeling submarine groundwater discharge: An example from the western Baltic Sea. *Journal of Hydrology*, *265*(1–4), 76–99. [https://doi.org/10.1016/S0022-1694\(02\)00093-8](https://doi.org/10.1016/S0022-1694(02)00093-8)
- Karpen, V., Thomsen, L., & Suess, E. (2004). A new 'schlieren' technique application for fluid flow visualization at cold seep sites. *Marine Geology*, *204*(1–2), 145–159. [https://doi.org/10.1016/S0025-3227\(03\)00370-0](https://doi.org/10.1016/S0025-3227(03)00370-0)
- Khandriche, A., & Werner, F. (1995). Freshwater induced pockmarks in Bay of Eckernförde, western Baltic. *Proceedings of the Third Marine Geological Conference "The Baltic"*, *2*(149), 155–164.
- Khandriche, A., Werner, F., & Erlenkeuser, H. (1987). Auswirkungen der Oststürme vom Winter 1978/79 auf die Sedimentation im Schlickbereich der Eckernförder Bucht (Westliche Ostsee). *Meyniana*, *38*, 125–151.
- Koegler, F. C. (1967). *Geotechnical properties of recent marine sediments from the Arabian Sea and the Baltic Sea*, (pp. 170–176). Urbana, IL: Marine Geotechnique. University of Chicago Press.
- Krastel, S., Berndt, C., & Schneider von Deimling, J. (2017). Cruise report R/V Alkor, Cruise No: AL501.
- Lecher, A. L., Chien, C.-T., & Paytan, A. (2016). Submarine groundwater discharge as a source of nutrients to the North Pacific and Arctic coastal ocean. *Marine Chemistry*, *186*, 167–177. <https://doi.org/10.1016/j.marchem.2016.09.008>
- Leifer, I., Luyendyk, B. P., Boles, J., & Clark, J. F. (2006). Natural marine seepage blowout: Contribution to atmospheric methane. *Global Biogeochemical Cycles*, *20*(3). <https://doi.org/10.1029/2005GB002668>
- Lennartz, S. T., Lehmann, A., Herrford, J., Malien, F., Hansen, H.-P., Biester, H., & Bange, H. W. (2014). Long-term trends at the Boknis Eck time series station (Baltic Sea), 1957–2013: Does climate change counteract the decline in eutrophication? *Biogeosciences*, *11*(22), 6323–6339. <https://doi.org/10.5194/bg-11-6323-2014>
- Lewy, Z. (1975). Early diagenesis of calcareous skeletons in the Baltic Sea, Western Germany. *Meyniana*, *27*, 29–33.
- Lohrberg, A., Schmale, O., Ostrovsky, I., Niemann, H., Held, P., & Schneider von Deimling, J. (2020). Discovery and quantification of a widespread methane ebullition event in a coastal inlet (Baltic Sea) using a novel sonar strategy. *Scientific Reports*, *10*, 1–13. <https://doi.org/10.1038/s41598-020-60283-0>
- Loncke, L., Mascle, J., & Fanil Scientific Parties (2004). Mud volcanoes, gas chimneys, pockmarks and mounds in the Nile deep-sea fan (Eastern Mediterranean): Geophysical evidences. *Marine and Petroleum Geology*, *21*(6), 669–689. <https://doi.org/10.1016/j.margeo.2004.02.004>
- Maltby, J., Steinle, L., Löscher, C. R., Bange, H. W., Fischer, M. A., Schmidt, M., & Treude, T. (2018). Microbial methanogenesis in the sulfate-reducing zone of sediments in the Eckernförde Bay, SW Baltic Sea. *Biogeosciences*, *15*(1), 137–157. <https://doi.org/10.5194/bg-15-137-2018>
- Marczynek, S., & Piotrowski, J. A. (2002). Grundwasserströmung und-beschaffenheit im Einzugsgebiet der Eckernförder Bucht, Schleswig-Holstein. *Grundwasser*, *7*(2), 101–110. <https://doi.org/10.1007/s007670200015>
- Martens, C. S., Albert, D. B., & Alperin, M. J. (1999). Stable isotope tracing of anaerobic methane oxidation in the gassy sediments of Eckernförde Bay, German Baltic Sea. *American Journal of Science*, *299*(7–9), 589–610. <https://doi.org/10.2475/ajs.299.7-9.589>
- Milkert, D., & Werner, F. (1997). Formation and distribution of storm layers in western Baltic Sea muds. *Oceanographic Literature Review*, *4*(44), 326.
- Moore, W. S. (1996). Large groundwater inputs to coastal waters revealed by ²²⁶Ra enrichments. *Nature*, *380*(6575), 612–614. <https://doi.org/10.1038/380612a0>
- Moore, W. S. (2010). The effect of submarine groundwater discharge on the ocean. *Annual Review of Marine Science*, *2*(1), 59–88. <https://doi.org/10.1146/annurev-marine-120308-081019>
- Moore, W. S., Sarmiento, J. L., & Key, R. M. (2008). Submarine groundwater discharge revealed by ²²⁶Ra distribution in the upper Atlantic Ocean. *Nature Geoscience*, *1*(5), 309–311. <https://doi.org/10.1038/ngeo183>

- Mulder, T., & Chochonat, P. (1996). Classification of offshore mass movements. *Journal of Sedimentary Research*, 66(1), 43–57.
- Müller, H., von Dobeneck, T., Nehmiz, W., & Hamer, K. (2011). Near-surface electromagnetic, rock magnetic, and geochemical fingerprinting of submarine freshwater seepage at Eckernförde Bay (SW Baltic Sea). *Geo-Marine Letters*, 31(2), 123–140. <https://doi.org/10.1007/s00367-010-0220-0>
- Nittrouer, C. A., Lopez, G. R., Donelson Wright, L., Bentley, S. J., D'Andrea, A. F., Friedrichs, C. T., et al. (1998). Oceanographic processes and the preservation of sedimentary structure in Eckernförde Bay, Baltic Sea. *Continental Shelf Research*, 18(14–15), 1689–1714. [https://doi.org/10.1016/S0278-4343\(98\)00054-5](https://doi.org/10.1016/S0278-4343(98)00054-5)
- Oehler, T., Tamborski, J., Rahman, S., Moosdorf, N., Ahrens, J., Mori, C., et al. (2019). DSI as a tracer for submarine groundwater discharge. *Frontiers in Marine Science*, 6, 563. <https://doi.org/10.3389/fmars.2019.00563>
- Orsi, T. H., Werner, F., Milkert, D., Anderson, A. L., & Bryant, W. R. (1996). Environmental overview of Eckernförde Bay, northern Germany. *Geo-Marine Letters*, 16(3), 140–147. <https://doi.org/10.1007/BF01204501>
- Patiris, D. L., Tsabaris, C., Schmidt, M., Karageorgis, A. P., Prospathopoulos, A. M., Alexakis, S., & Linke, P. (2018). Mobile underwater in situ gamma-ray spectroscopy to localize groundwater emanation from pockmarks in the Eckernförde Bay, Germany. *Applied Radiation and Isotopes*, 140(August), 305–313. <https://doi.org/10.1016/j.apradiso.2018.07.037>
- Post, V. E. A., Groen, J., Kooi, H., Person, M., Ge, S., & Edmunds, W. M. (2013). Offshore fresh groundwater reserves as a global phenomenon. *Nature*, 504(7478), 71–78. <https://doi.org/10.1038/nature12858>
- Reusch, A., Loher, M., Bouffard, D., Moernaut, J., Hellmich, F., Anselmetti, F. S., et al. (2015). Giant lacustrine pockmarks with subaqueous groundwater discharge and subsurface sediment mobilization. *Geophysical Research Letters*, 42(9), 3465–3473. <https://doi.org/10.1002/2015GL064179>
- Riboulot, V., Imbert, P., Cattaneo, A., & Voisset, M. (2019). Fluid escape features as relevant players in the enhancement of seafloor stability? *Terra Nova*, (July), 1–9. <https://doi.org/10.1111/ter.12425>
- Ritger, S., Carson, B., & Suess, E. (1987). Methane-derived authigenic carbonates formed by subduction-induced pore-water expulsion along the Oregon/Washington margin. *Geological Society of America Bulletin*, 98, 147. [https://doi.org/10.1130/0016-7606\(1987\)98<147:MACFBS>2.0.CO;2](https://doi.org/10.1130/0016-7606(1987)98<147:MACFBS>2.0.CO;2)
- Rößler, D. (2006). Reconstruction of the *Littorina* transgression in the western Baltic Sea. *Marine Science Reports (IOW)*, 67, 1–111.
- Sauter, E., Laier, T., Andersen, C. E., Dahlgard, H., & Schlüter, M. (2001). Sampling of sub-seafloor aquifers by a temporary well for CFC age dating and natural tracer investigations. *Journal of Sea Research*, 46(2), 177–185. [https://doi.org/10.1016/S1385-1101\(01\)00080-6](https://doi.org/10.1016/S1385-1101(01)00080-6)
- Sauter, E., Schlüter, M., Sedyn, P. L., Fraser, N., & Fogt, P. (2003). AUV multi-technique surveying of submarine freshwater seeps-high and ultra-high resolution acoustic and CTD mapping of pockmark sites in Eckernförde Bay, western Baltic Sea. *Sea Technology*, 44(3), 49–52.
- Schlüter, M., Sauter, E. J., Andersen, C. E., Dahlgard, H., & Dando, P. R. (2004). Spatial distribution and budget for submarine groundwater discharge in Eckernförde Bay (western Baltic Sea). *Limnology and Oceanography*, 49(1), 157–167. <https://doi.org/10.4319/lo.2004.49.1.0157>
- Schneider von Deimling, J. (2014). R/V *Alkor* cruise report AL447.
- Schneider von Deimling, J. (2019). Cruise report RV *Littorina*, Cruise No.: L19/05. Christian-Albrechts-Universität zu Kiel.
- Schneider von Deimling, J., Weinrebe, W., Tóth, Z., Fossing, H., Endler, R., Rehder, G., & Spieß, V. (2013). A low frequency multibeam assessment: Spatial mapping of shallow gas by enhanced penetration and angular response anomaly. *Marine and Petroleum Geology*, 44, 217–222. <https://doi.org/10.1016/j.marpetgeo.2013.02.013>
- Scholten, J. C., Osvath, I., & Pham, M. K. (2013). ²²⁶Ra measurements through gamma spectrometric counting of radon progenies: How significant is the loss of radon? *Marine Chemistry*, 156, 146–152. <https://doi.org/10.1016/j.marchem.2013.03.001>
- Schüler, F. (1952). Untersuchungen über die Mächtigkeit von Schlichschichten mit Hilfe des Echographen. *Deutsche Hydrographische Zeitschrift*, 5(5–6), 220–231. <https://doi.org/10.1007/BF02019284>
- Seager, R., Ting, M., Held, I., Kushnir, Y., Lu, J., Vecchi, G., et al. (2007). Model projections of an imminent transition to a more arid climate in southwestern North America. *Science*, 316(5828), 1181–1184. <https://doi.org/10.1126/science.1139601>
- Seeberg-Elverfeldt, J., Schlüter, M., Feseker, T., & Kölling, M. (2005). Rhizon sampling of porewaters near the sediment-water interface of aquatic systems. *Limnology and Oceanography: Methods*, 3(8), 361–371.
- Seibold, E., Exon, N., Hartmann, M., Kögler, F.-C., Krumm, H., Lutze, G. F., et al. (1971). Marine geology of Kiel bay. In *Sedimentology of Parts of Central Europe, Guidebook, 8th International Sedimentological Congress, Heidelberg* (pp. 209–235).
- Shaban, A., Khawlie, M., Abdallah, C., & Faour, G. (2005). Geologic controls of submarine groundwater discharge: Application of remote sensing to north Lebanon. *Environmental Geology*, 47(4), 512–522. <https://doi.org/10.1007/s00254-004-1172-3>
- Sills, G. C., & Wheeler, S. J. (1992). The significance of gas for offshore operations. *Continental Shelf Research*, 12(10), 1239–1250. [https://doi.org/10.1016/0278-4343\(92\)90083-V](https://doi.org/10.1016/0278-4343(92)90083-V)
- Silva, A. J., & Brandes, H. G. (1998). Geotechnical properties and behavior of high-porosity, organic-rich sediments in Eckernförde Bay, Germany. *Continental Shelf Research*, 18(14–15), 1917–1938. [https://doi.org/10.1016/S0278-4343\(98\)00063-6](https://doi.org/10.1016/S0278-4343(98)00063-6)
- Smetacek, V. (1985). The annual cycle of Kiel Bight plankton: A long-term analysis. *Estuaries*, 8(2), 145–157. <https://doi.org/10.2307/1351864>
- Smetacek, V., von Bodungen, B., von Brockel, K., Knoppers, B., Martens, P., Peinert, R., et al. (1987). Seasonality of plankton growth and sedimentation. In *Seawater-sediment interactions in coastal waters*, (pp. 34–56). Berlin: Springer.
- Solomon, E. A., Kastner, M., MacDonald, I. R., & Leifer, I. (2009). Considerable methane fluxes to the atmosphere from hydrocarbon seeps in the Gulf of Mexico. *Nature Geoscience*, 2(8), 561–565. <https://doi.org/10.1038/ngeo574>
- Sommer, S., Linke, P., Pfannkuche, O., Schleicher, T., Schneider von Deimling, J., Reitz, A., et al. (2009). Seabed methane emissions and the habitat of frenulate tubeworms on the Captain Arutyunov mud volcano (Gulf of Cadiz). *Marine Ecology Progress Series*, 382, 69–86. <https://doi.org/10.3354/meps07956>
- Steinle, L., Maltby, J., Treude, T., Kock, A., Bange, H. W., Engbersen, N., et al. (2017). Effects of low oxygen concentrations on aerobic methane oxidation in seasonally hypoxic coastal waters. *Biogeosciences*, 14(6), 1631–1645. <https://doi.org/10.5194/bg-14-1631-2017>
- Stieglitz, T. (2005). Submarine groundwater discharge into the near-shore zone of the Great Barrier Reef, Australia. *Marine Pollution Bulletin*, 51(1–4), 51–59. <https://doi.org/10.1016/j.marpolbul.2004.10.055>
- Tamborski, J. J., Rogers, A. D., Bokuniewicz, H. J., Cochran, J. K., & Young, C. R. (2015). Identification and quantification of diffuse fresh submarine groundwater discharge via airborne thermal infrared remote sensing. *Remote Sensing of Environment*, 171, 202–217. <https://doi.org/10.1016/j.rse.2015.10.010>
- Tang, D., Jin, G., Jackson, D. R., & Williams, K. L. (1994). Analyses of high-frequency bottom and subbottom backscattering for two distinct shallow water environments. *The Journal of the Acoustical Society of America*, 96(5), 2930–2936. <https://doi.org/10.1121/1.411302>

- Treude, T., Krüger, M., Boetius, A., & Jørgensen, B. B. (2005). Environmental control on anaerobic oxidation of methane in the gassy sediments of Eckernförde Bay (German Baltic). *Limnology and Oceanography*, 50(6), 1771–1786. <https://doi.org/10.4319/lo.2005.50.6.1771>
- Viso, R., McCoy, C., Gayes, P., & Quafisi, D. (2010). Geological controls on submarine groundwater discharge in Long Bay, South Carolina (USA). *Continental Shelf Research*, 30(3-4), 335–341. <https://doi.org/10.1016/j.csr.2009.11.014>
- Wefer, G., Balzer, W., Bodungen, B. V., & Suess, E. (1987). Biogenic carbonates in temperate and subtropical environments: Production and accumulation, saturation state and stable isotope composition. In *Seawater-sediment interactions in coastal waters* (pp. 263–302). Berlin, Heidelberg: Springer.
- Werner, F. (1978). Depressions in mud sediments (Eckernförde Bay, Baltic Sea) related to sub-bottom and currents. *Meyniana*, 30, 99–104.
- Werner, F., Erlenkeuser, H., Grafenstein, U. V., McLean, S., Sarnthein, M., Schauer, U., et al. (1987). Sedimentary records of benthic processes. In *Seawater-sediment interactions in coastal waters* (pp. 162–262). Berlin, Heidelberg: Springer.
- Wever, T. F., Abegg, F., Fiedler, H. M., Fechner, G., & Stender, I. H. (1998). Shallow gas in the muddy sediments of Eckernförde Bay, Germany. *Continental Shelf Research*, 18(14-15), 1715–1739. [https://doi.org/10.1016/S0278-4343\(98\)00055-7](https://doi.org/10.1016/S0278-4343(98)00055-7)
- Wever, T. F., Lühder, R., Voß, H., & Knispel, U. (2006). Potential environmental control of free shallow gas in the seafloor of Eckernförde Bay, Germany. *Marine Geology*, 225(1–4), 1–4. <https://doi.org/10.1016/j.margeo.2005.08.005>
- Whiticar, M. J. (2002). Diagenetic relationships of methanogenesis, nutrients, acoustic turbidity, pockmarks and freshwater seepages in Eckernförde Bay. *Marine Geology*, 182(1–2), 29–53. [https://doi.org/10.1016/S0025-3227\(01\)00227-4](https://doi.org/10.1016/S0025-3227(01)00227-4)
- Whiticar, M. J., & Werner, F. (1981). Pockmarks: Submarine vents of natural gas or freshwater seeps? *Geo-Marine Letters*, 1(3–4), 193–199. <https://doi.org/10.1007/BF02462433>
- Wilson, J., & Rocha, C. (2012). Regional scale assessment of submarine groundwater discharge in Ireland combining medium resolution satellite imagery and geochemical tracing techniques. *Remote Sensing of Environment*, 119, 21–34. <https://doi.org/10.1016/j.rse.2011.11.018>
- Yamamoto, S., Alcauskas, J. B., & Crozier, T. E. (1976). Solubility of methane in distilled water and seawater. *Journal of Chemical and Engineering Data*, 21(1), 78–80. <https://doi.org/10.1021/je60068a029>

Appendix B2: Conference presentations

- 2020 Hoffmann, J., Schneider von Deimling, J., Schröder, J.F., Schmidt, M., Held, P., Crutchley, G.J., Scholten, J. and Gorman, A.R.; (2020) *Complex eyed pockmarks associated with submarine groundwater discharge in gaseous muddy sediments Eckernförde Bay, SW Baltic Sea*, EGU Geophysical Research Abstracts (Vol. 22)
- 2019 Hoffmann, J; Gorman, A; Crutchley, G; Micallef, A; Mountjoy, J & Averses, T; (2019) *Pockmark formation and modification processes on the Canterbury Shelf, New Zealand*; EGU Geophysical Research Abstracts (Vol. 21)
- 2019 Hoffmann, J; Schneider von Deimling, J; Schröder, J; Schmidt, M; Scholten, J; Crutchley, G & Gorman, A; (2018) *Complex eyed pockmarks associated with submarine groundwater discharge in gaseous muddy sediments, Eckernförde Bay, SW Baltic Sea*. Geoscience Society of New Zealand Annual Conference (Hamilton)
- 2018 Hoffmann, J; Gorman, A; Crutchley, G; Micallef, A; Mountjoy, J & Averses, T; (2018) *Pockmark formation, modification and fluid seepage on the Canterbury Shelf*; Geoscience Society of New Zealand Annual Conference (Napier)
- 2018 Hoffmann, J., Gorman, A., & Crutchley, G. (2018). *Interaction of fluid migration structures with polygonal faults imaged by 3D seismic data in the Canterbury Basin (New Zealand)*. EGU General Assembly Conference Abstracts (Vol. 20)
- 2018 Hoffmann, J., Gorman, A., & Crutchley, G. (2018). *Investigation of Possible Shallow Gas Accumulations Associated with Pockmarks on the Otago Slope Southeast of New Zealand*. Australasian Exploration Geoscience Conference (Sydney)
- 2017 Hoffmann, J., Gorman, A., & Crutchley, G. (2017) *Seismic investigations of fluid flow related structures on the south Canterbury Shelf and Slope, New Zealand* Geoscience Society of New Zealand Annual Conference (Auckland)
- 2017 Hoffmann, J., Gorman, A., & Crutchley, G. (2017) *Seismic investigations of fluid flow related structures on the south Canterbury Shelf and slope*, New Zealand Petroleum Geoscience Workshop (Wellington)